

AES/TG/07-27

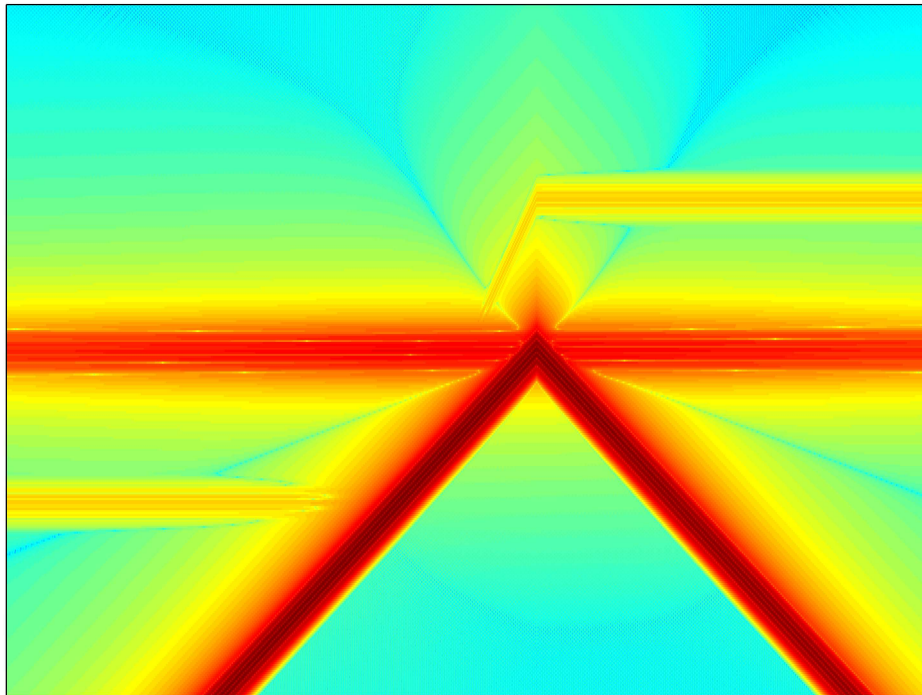
# Simulation of Interferometric Seismo- electric Green's Function Recovery

For the SH-TE propagation mode

August 2007

Sjoerd A.L. de Ridder

---





Title : **Simulation of Interferometric Seismoelectric Green's  
Function Recovery;**  
For the SH-TE propagation mode

Author : **Sjoerd A.L. de Ridder, B.Sc.**

Date : August 2007  
Professor : prof.dr.ir. C.P.A. Wapenaar  
Supervisor : dr.ir. E.C. Slob  
TA Report number : AES/TG/07-27

Postal Address : Section of Earth Sciences  
Department of Applied Earth Sciences  
The Netherlands

Telephone : (31) 15 2786134  
(31) 15 2781328 (secretary)

Telefax : (31) 15 2781189  
Electronic-mail : [salderidder@gmail.com](mailto:salderidder@gmail.com)

Copyright © 2007 Section for Applied Geophysics and Petrophysics

*All rights reserved.*

*No parts of this publication may be reproduced.*

*Stored in a retrieval system, or transmitted.*

*In any form or by any means, electronic,  
mechanical, photocopying, recording, or otherwise,  
without the prior written permission of the  
Section for Applied Geophysics and Petrophysics.*



# **Simulation of Interferometric Seismoelectric Green's Function Recovery**

**For the SH-TE propagation mode**

MASTER OF SCIENCE THESIS

A thesis submitted to the Department of Geotechnology at Delft University of Technology in partial fulfillment of the requirements for the degree of Master of Science in Applied Earth Sciences

Sjoerd A.L. de Ridder

August 2007



---

# Abstract

A recent novel technique known as seismic interferometry makes use of seismic ‘noise’ to reconstruct a Green’s function between two receivers by crosscorrelation. This technique can be applied for example in permanent subsurface monitoring using passive seismics or the creation of virtual sources on positions where only recordings were made. The aim of this thesis is to derive and understand equations for seismoelectric interferometry.

The first part of this thesis focusses on a the calculation of SH-TE seismoelectrical responses in a 2D horizontally stratified earth. We decompose the two-way wave equation for SH-TE waves into upgoing and downgoing waves which we relate through a reflectivity formulation. The reflectivity formulation is based upon reflection matrices only, even though we can simulate both reflection and transmission experiments. We solve the SH-TE seismoelectric system in a 1D homogeneous world.

In the second part of this thesis we derive interferometric Green’s function representations from reciprocity theorems that relate two different states in one domain. Interferometric Green’s function representations express the Green’s function between two receivers as a function of crosscorrelations of responses of sources throughout a domain and on it’s boundary. We cast the seismoelectric system in a general diffusion, flow and wave equation and define a Green’s matrix for all different field and source types. Using this formulation we derive a source-receiver reciprocity relation for the Green’s matrix from the convolution type reciprocity theorem. The correlation type reciprocity theorem for the Green’s matrix is modified using source-receiver reciprocity to obtain the interferometric Green’s function representation.

We study the SH-TE seismoelectrical interferometric representation 1D and 2D in homogeneous media. A seismoelectric interferometric representation was written to recover the causal response of the particle velocity at position B due to a electrical current source at position A, as a function of cross correlations of electric field recordings at A and particle velocity recordings at B. Provided there exists a dense coverage of sources in the domain and on it’s boundary, the representation was validated in both 1D and 2D.

Approximations to the interferometric representation are investigated by studying the contributions of parts of the domain and boundary integrals. It was found that a dominant spurious event resides in the separate contributions of the domain and boundary integrals,

that destructively interferes when both contributions are combined. The role of different source types in the interferometric representation was studied. In a homogeneous medium the measured events have propagated either as an electromagnetic wave or as a shear wave. The dominant contribution to the reconstruction of an electromagnetic event is by electromagnetic sources. Similarly, can the reconstructed shear wave event be attributed mainly due to seismic sources. In a medium with low electromagnetic and shear wave losses we could ignore the domain integral, this will result in amplitude errors and we will suffer from spurious events.

---

# Acknowledgments

This thesis would never be complete without acknowledging Evert Slob. He has been of great support, both technically and mentally, he is a better adviser than any graduate student could ever wish for. I would like to thank professor Kees Wapenaar for suggesting the subject of seismoelectric interferometry, it has been both challenging and interesting. I am greatfull that both Kees and Evert expressed their confidence in me by suggesting this topic. Professor Roel Snieder at the Colorado School of Mines hosted me for a month's visit to the Center of Wave Phenomena. There was not a day that passed without a discussion with Roel or one of the students that made my visit worth while. Thanks to all CWP's students and faculty, especially Kurang, Fan, Steve and Gabi, it was great to see old friends and make new ones. I thank my committee, professor Hans Bruining, Deyan Dragonov and Christiaan Schoemaker, for their many suggestions for improvement of this manuscript.

During six years of study, I made many friends with whom I share memories that I deeply cherish. Jelmer, Gerson, Ilse, Babet, Floris, Koen, Mara, Menne, Robert, Cheryl, Wouter, and many more. I can only say that it is my dearest wish, that in 10 years time we we'll be sharing even more happy memories. Tonnie, Anela en Niels, my homies from Huize Barabas, made me feel at home in Utrecht. Thanks to them I knew Utrecht was about more than just the geo-world. I would like to thank my Peruvian friend Raul, together we worked through the Delft curriculum that we both found new, chaotic and difficult. Thanks to my geophysics friends in Delft; Raul, Joost, Elmer, Nihed, Christiaan, Karel, and more. I had a great time, not in the least during the DOGS drinks and the EAGE conferences.

Thanks to my friends Merijn and Marijn, our path's parted but friendship remains. When we meet it feels like it was only yesterday that we graduated from high school. My oldest friends Jelle and Gody, have always been there for me. Lastly and most importantly, the two people whom I never forget what they mean to me; thank you Mom and Dad, for your support, encouragement and example.

Sjoerd de Ridder  
Delft, August 2007.



---

# Table of Contents

<b>Abstract</b>	<b>iii</b>
<b>Acknowledgments</b>	<b>v</b>
<b>List of Symbols</b>	<b>xiii</b>
<b>1 Introduction</b>	<b>1</b>
1-1 Motivation . . . . .	1
1-2 Seismoelectric Phenomena . . . . .	2
1-3 Interferometric Green's function recovery . . . . .	2
1-4 Outline of this thesis . . . . .	2
1-5 Notations and definitions . . . . .	3
1-5-1 Fourier transformations . . . . .	4
1-5-2 Transposed and adjointed operators . . . . .	5
<b>2 Seismoelectric system of equations</b>	<b>7</b>
2-1 Pride's seismoelectric system of equations . . . . .	7
2-1-1 The coupling coefficient . . . . .	8
2-1-2 Equations of motion . . . . .	9
2-1-3 Isotropic frequency-independent elastic parameters . . . . .	10
2-1-4 Electromagnetic equations . . . . .	10
2-1-5 Isotropic frequency-independent electromagnetic parameters . . . . .	11
2-2 General diffusion, flow and wave equation . . . . .	12
2-2-1 Symmetry properties of the general diffusion, flow and wave equation . . . . .	14
2-3 Boundary conditions . . . . .	14
2-3-1 Boundary conditions at the pressure-free surface . . . . .	15

<b>I</b>	<b>SH-TE Seismoelectrical Modeling in 2D</b>	<b>17</b>
<b>3</b>	<b>The seismoelectric two- and one-way wave equations</b>	<b>19</b>
3-1	Two-way wave equation . . . . .	20
3-1-1	Symmetry properties of the two-way system matrix . . . . .	23
3-2	Decoupling of the SH-TE and P-SV-TM systems . . . . .	23
3-3	One-way wave equation . . . . .	25
3-3-1	Homogeneous source-free subdomain . . . . .	26
3-3-2	Symmetry properties of the one-way system matrix . . . . .	27
3-4	Seismoelectric decomposition for the SH-TE system . . . . .	27
3-5	The seismoelectric system in vacuum . . . . .	29
3-5-1	Diagonalization in a homogeneous source-free subdomain . . . . .	29
<b>4</b>	<b>Seismoelectric modeling using reflection formalism.</b>	<b>31</b>
4-1	Local and global reflection matrices . . . . .	31
4-2	Calculation of global reflection matrices . . . . .	33
4-3	Homogeneous bounded subdomain with sources . . . . .	35
4-4	Determination of the wave fields outside the source layer . . . . .	36
4-5	Scattering matrix against a pressure-free surface . . . . .	37
4-6	Seismoelectric modeling scheme . . . . .	38
<b>5</b>	<b>Examples of seismoelectric simulations in 2D</b>	<b>39</b>
5-1	Numerical implementation . . . . .	39
5-1-1	Discrete Fourier transformations . . . . .	39
5-1-2	Causality trick . . . . .	41
5-2	Medium parameters for medium type A and B . . . . .	42
5-2-1	Reflection matrices . . . . .	44
5-3	Reflection and transmission experiments . . . . .	46
<b>II</b>	<b>Interferometric Seismoelectric Green's Function Recovery</b>	<b>53</b>
<b>6</b>	<b>Theory of interferometric Green's function recovery</b>	<b>55</b>
6-1	Matrix vector representation of the divergence theorem of Gauss . . . . .	55
6-2	Reciprocity theorem of the convolution type . . . . .	57
6-2-1	Source-receiver reciprocity . . . . .	57
6-3	Reciprocity theorem of the correlation type . . . . .	58
6-4	Interferometric Green's function representations in 3D . . . . .	59
6-5	Interferometric Green's function representations in 2D and 1D . . . . .	60

<b>7 SH-TE interferometric Green's function representations in 1D and 2D</b>	<b>63</b>
7-1 SH-TE seismoelectric coupling in 1D . . . . .	63
7-2 Convolution-type reciprocity theorem for SH-TE in 1D . . . . .	64
7-3 Correlation-type reciprocity theorem for SH-TE in 1D . . . . .	65
7-4 Seismoelectric interferometric Green's function recovery in 1D . . . . .	66
7-4-1 Interferometric representation in medium type A and B . . . . .	67
7-4-2 Relation between the two retrieved Green's function matrices . . . . .	67
7-5 SH-TE seismoelectric coupling in 2D . . . . .	68
7-6 Convolution-type reciprocity theorem for SH-TE in 2D . . . . .	69
7-7 Correlation-type reciprocity theorem for SH-TE in 2D . . . . .	70
7-8 Seismoelectric interferometric Green's function recovery in 2D . . . . .	71
7-8-1 Interferometric representation in medium type A and B . . . . .	73
7-8-2 Relation between the two retrieved Green's function matrices . . . . .	73
<b>8 Simulation of interferometric seismoelectric Green's function recovery</b>	<b>75</b>
8-1 1D Seismoelectric interferometry in homogeneous media. . . . .	75
8-1-1 Results in medium type A . . . . .	76
8-1-2 Results in medium type B . . . . .	78
8-1-3 Middle Riemann sum . . . . .	80
8-2 Dissecting the 1D interferometric representation . . . . .	80
8-2-1 Main contributions of the interferometric representation. . . . .	81
8-2-2 Correlation gather of the domain integral . . . . .	85
8-2-3 Alternative boundary positions . . . . .	86
8-3 2D Seismoelectric interferometry in a homogeneous medium . . . . .	88
<b>9 Discussion and conclusions</b>	<b>97</b>
9-1 Forward modeling in 2D . . . . .	97
9-2 Seismoelectric interferometric Green's function representation . . . . .	97
9-3 Numerical evaluation of the Seismoelectric interferometric Green's function representation . . . . .	98
9-4 Domain versus boundary integral . . . . .	98
9-4-1 Main contributions to the retrieved result . . . . .	99
9-4-2 Stationary phases . . . . .	100
9-5 2D versus 1D . . . . .	101
9-6 Conclusions . . . . .	101
<b>References</b>	<b>103</b>
<b>A Derivation of the seismoelectric two-way wave equation</b>	<b>107</b>

---

<b>B SH-TE Decomposition</b>	<b>113</b>
B-1 Velocities . . . . .	113
B-2 Non-zero eigenvalues . . . . .	114
B-3 Eigenvectors of SH-TE system . . . . .	116
B-3-1 Stability of the scaling terms . . . . .	118
B-4 The decoupled SH-TE systems . . . . .	118
B-4-1 Decoupled SH waves in porous media . . . . .	118
B-4-2 Decoupled TE waves in vacuum . . . . .	120
<b>C SH-TE general diffusion, flow and wave equation in 2D and 1D</b>	<b>123</b>
C-1 SH-TE general diffusion, flow and wave equation in 2D . . . . .	123
C-2 SH-TE general diffusion, flow and wave equation in 1D . . . . .	125
C-3 Solution to the 1D SH-TE seismoelectric system in a homogeneous domain . . . . .	125
C-3-1 Green's matrix for the 1D SH-TE system . . . . .	126

---

## List of Figures

2-1	Interface between two media. . . . .	14
4-1	Annotations in a layered medium. . . . .	32
4-2	Calculation scheme of the responses of a source buried in a layered medium. . . . .	38
5-1	Wrapping effects in (a) and the results of applying the causality trick in (b). . . . .	41
5-2	Exponentials in the causality trick. . . . .	42
5-3	Real and imaginary parts of the seismoelectrical wave velocities. . . . .	43
5-4	Loss functions of the SH-TE system. . . . .	43
5-5	Reflection matrix, from layer type A against B. . . . .	44
5-6	Reflection matrix, from layer type B against A. . . . .	45
5-7	Pressure-free surface scattering matrix, from layer type A against vacuum. . . . .	45
5-8	Experiment geometry of a transmission experiment in a homogeneous medium. . . . .	47
5-9	Transmission experiment in a homogeneous medium: $f_2 \rightarrow E_2$ . . . . .	47
5-10	Transmission experiment in a homogeneous medium: $-J_2^{s,e} \rightarrow v_2^s$ . . . . .	48
5-11	Experiment geometry of a reflection experiment above an aquifer. . . . .	49
5-12	Reflection experiment above an aquifer. . . . .	49
5-13	Experiment geometry of a transmission experiment in an aquifer. . . . .	51
5-14	Transmission experiment in an aquifer. . . . .	51
6-1	Scalar field $a(\mathbf{x})$ in domain $\mathbb{D}$ bounded by $\partial\mathbb{D}$ . . . . .	56
6-2	Matrix field $\{\mathbf{a} \mathbf{b}^t\}(\mathbf{x})$ in domain $\mathbb{D}$ bounded by $\partial\mathbb{D}$ . . . . .	57
6-3	The character of two physical states for the convolution type reciprocity theorem. . . . .	57
6-4	The character of two physical states for the correlation-type reciprocity theorem. . . . .	58
6-5	Geometry for the 3D interferometric Green's function representation. . . . .	59
6-6	Geometry for the 1D interferometric Green's function representation. . . . .	60

8-1	Symmetric position of receivers and boundary points for 1D interferometry. . . . .	76
8-2	Exact and retrieved superposition of $G^{v,J^e}(t)$ and $G^{E,f}(-t)$ in medium type A. . .	76
8-3	Separate contributions of the domain integral and the boundary points. . . . .	77
8-4	Exact and retrieved superposition of $G^{v,J^e}(t)$ and $G^{E,f}(-t)$ in medium type B. . .	79
8-5	Separate contributions of the domain integral and the boundary points. . . . .	79
8-6	Recovered signal using alternative sample densities of the Riemann sum. . . . .	80
8-7	Different segments of the domain integral in the 1D interferometric geometry. . .	81
8-8	The separate contributions of the sources at $x_{3;1}$ and the sources at $x_{3;2}$ . . . . .	82
8-9	The contributions of the three segments of the domain integral. . . . .	82
8-10	Contributions from the different crosscorrelation terms at the boundary point $x_{3;1}$ . .	83
8-11	Contributions from the different crosscorrelation terms at the boundary point $x_{3;2}$ . .	84
8-12	Contributions from the different crosscorrelations in the domain integral. . . . .	84
8-13	Correlation gather for seismoelectric interferometry in a 1D homogeneous medium. .	85
8-14	Logarithm of the absolute value of the correlation gather in Figure 8-13. . . . .	86
8-15	Alternative position of receivers and boundary points for 1D interferometry. . . . .	87
8-16	Reconstructed signal using two alternative positions of the boundary points. . . . .	87
8-17	Geometry for a 2D seismoelectric interferometric experiment. . . . .	88
8-18	Exact and retrieved superposition of $G^{v,J^e}(t)$ and $G^{E,f}(-t)$ in 2D. . . . .	89
8-19	Separate contributions of the domain and boundary integrals. . . . .	90
8-20	Source contributions with depth to the recovered signal. . . . .	90
8-21	A close look at the time window $t = \pm 0.1$ seconds of Figure 8-20. . . . .	91
8-22	Source contributions with horizontal distance to the recovered signal. . . . .	91
8-23	A close look at the time window $t = \pm 0.1$ seconds of Figure 8-22. . . . .	92
8-24	Correlation gather of a horizontal line of sources at $x_3 = 150.5$ meter. . . . .	94
8-25	Correlation gather of a horizontal line of sources at $x_3 = 449.5$ meter. . . . .	94
8-26	Correlation gather of a vertical line of sources at $x_1 = -800$ meter. . . . .	95
8-27	Correlation gather of a vertical line of sources at $x_1 = -600$ meter. . . . .	95
8-28	Correlation gather of a vertical line of sources at $x_1 = -400$ meter. . . . .	96
B-1	The numerical behavior of the $\hat{\xi}$ scaling terms in the SH-TE eigenvectors. . . . .	119

---

## List of Symbols

$\mathbf{E}$	: Bulk-averaged electric field strength	$[\text{V m}^{-1}]$	2-1-4
$\mathbf{H}$	: Bulk-averaged magnetic field strength	$[\text{A m}^{-1}]$	2-1-4
$\mathbf{v}^s$	: Phase-averaged solid particle velocity	$[\text{m s}^{-1}]$	2-1-2
$\mathbf{v}^f$	: Phase-averaged fluid particle velocity	$[\text{m s}^{-1}]$	2-1-2
$\mathbf{w}$	: Bulk-averaged Biot filtration velocity	$[\text{m s}^{-1}]$	2-1-2
$\boldsymbol{\tau}^b$	: Bulk-averaged stress	$[\text{N m}^{-2}]$	2-1-2
$p^f$	: Phase-averaged fluid pressure	$[\text{N m}^{-2}]$	2-1-2
$\mathbf{J}^{s,e}$	: Density of external electric current source	$[\text{A m}^{-2}]$	2-1-4
$\mathbf{J}^{s,m}$	: Density of external magnetic current source	$[\text{kg s}^{-3}\text{A}^{-1}]$	2-1-4
$\mathbf{f}^f$	: Density of external force applied to fluid phase	$[\text{N m}^{-3}]$	2-1-2
$\mathbf{f}^b$	: Density of external force applied to the bulk	$[\text{N m}^{-3}]$	2-1-2
$\mathbf{h}^b$	: Density of external deformation rate on the bulk	$[\text{s}^{-1}]$	2-1-2
$q^i$	: Density of volume injection rate in fluid phase	$[\text{s}^{-1}]$	2-1-2
$\rho^f$	: Density of the fluid phase	$[\text{kg m}^{-3}]$	2-1-2
$\rho^s$	: Density of the solid phase	$[\text{kg m}^{-3}]$	2-1-2
$\rho^b$	: Density of the bulk	$[\text{kg m}^{-3}]$	2-1-2
$K^f$	: Bulk modulus of fluid phase	$[\text{N m}^{-2}]$	2-1-3
$K^s$	: Bulk modulus of solid phase	$[\text{N m}^{-2}]$	2-1-3
$K^{fr}$	: Bulk modulus of the framework of grains	$[\text{N m}^{-2}]$	2-1-3
$K_G$	: Grassman's bulk modulus	$[\text{N m}^{-2}]$	2-1-3
$N$	: Shear modulus of the framework of grains	$[\text{N m}^{-2}]$	2-1-3
$\mathbf{c}$	: Stiffness parameter of the porous solid	$[\text{N m}^{-2}]$	2-1-3
$M$	: Stiffness parameter of the porous solid	$[\text{N m}^{-2}]$	2-1-3
$\mathbf{d}$	: Stiffness parameter of the porous solid	$[\text{N m}^{-2}]$	2-1-3
$\rho^E$	: Effective fluid density	$[\text{kg m}^{-3}\text{s}^{-1}]$	2-1-2
$\rho^c$	: Effective bulk density	$[\text{kg m}^{-3}]$	2-1-2
$\mathcal{L}$	: Dynamic seismoelectric coupling coefficient	$[\text{m}^2\text{s V}^{-1}]$	2-1-1

$\mathcal{L}_0$	: Static seismoelectric coupling coefficient	$[\text{m}^2 \text{s V}^{-1}]$	2-1-1
$\alpha_\infty$	: Tortuosity	$[-]$	2-1-1
$\Lambda$	: Volume to surface ration of porous material	$[\text{m}]$	2-1-1
$\phi$	: Porosity as a volume fraction	$[-]$	2-1-1
$m$	: Similarity parameter for porous media	$[-]$	2-1-1
$\eta$	: Pore fluid viscosity	$[\text{N s m}^{-2}]$	2-1-1
$\delta^\eta$	: Viscous skin depth	$[\text{m}]$	2-1-5
$\mathbf{k}$	: Dynamic permeability	$[\text{m}^2]$	2-1-1
$k_0$	: Static permeability	$[\text{m}^2]$	2-1-1
$d^l$	: Debye length	$[\text{m}]$	2-1-1
$\omega_c$	: Critical frequency	$[\text{Radians}]$	2-1-1
$\zeta$	: Zeta potential of the double layer	$[\text{V}]$	2-1-1
$C$	: Electrolyte concentration in the pore fluid	$[\text{mol liter}^{-1}]$	2-1-1
$\mathcal{N}_l$	: Bulk ionic concentration of species $l$	$[\text{mol liter}^{-1}]$	2-1-1
$z_l$	: Ion valency of ion species $l$	$[-]$	2-1-1
$b_l$	: Ion Mobility of ion species $l$	$[\text{m s}^{-1} \text{N}^{-1}]$	2-1-5
$e$	: Elementary charge ( $1.60217733 \cdot 10^{-19}$ )	$[\text{C}]$	2-1-1
$\mathcal{N}_A$	: Avogadro's Number ( $6.022 \cdot 10^{23}$ )	$[-]$	2-1-1
$k_b$	: Boltzmann constant ( $1.380658 \cdot 10^{-23}$ )	$[\text{J K}^{-1}]$	2-1-1
$T$	: Temperature	$[\text{K}]$	2-1-1
$P_0$	: Parameter in osmotic conductivity	$[-]$	2-1-5
$\epsilon$	: Bulk dielectric permittivity	$[\text{F m}^{-1}]$	2-1-5
$\mu$	: Bulk magnetic permeability	$[\text{H m}^{-1}]$	2-1-5
$\sigma^e$	: Bulk electric conductivity	$[\text{S m}^{-1}]$	2-1-5
$\sigma^m$	: Bulk magnetic conductivity	$[(\text{S m})^{-1}]$	2-1-5
$\epsilon_0$	: Dielectric permittivity of the vacuum ( $8.854 \cdot 10^{-12}$ )	$[\text{F m}^{-1}]$	2-1-5
$\epsilon_r^f$	: Relative dielectric permittivity of the fluid phase	$[-]$	2-1-5
$\epsilon_r^s$	: Relative dielectric permittivity of the solid phase	$[-]$	2-1-5
$\mu_0$	: Magnetic permeability of the vacuum ( $4\pi \cdot 10^{-7}$ )	$[\text{H m}^{-1}]$	2-1-5
$\sigma^f$	: Conductivity of the fluid phase	$[\text{S m}^{-1}]$	2-1-5
$\sigma_{em}$	: Double layer electron migration conductivity	$[\text{S m}^{-1}]$	2-1-5
$\sigma_{os}$	: Osmotic conductivity of the streaming current	$[\text{S m}^{-1}]$	2-1-5
$\epsilon$	: Effective electrical permittivity	$[\text{F m}^{-1}]$	3-1
$\sigma$	: Effective electrical conductivity	$[\text{S m}^{-1}]$	3-1
$\epsilon_{\mathcal{L}}$	: Effective electrical permittivity including coupling	$[\text{F m}^{-1}]$	3-1
$\sigma_{\mathcal{L}}$	: Effective electrical conductivity including coupling	$[\text{S m}^{-1}]$	2-2

---

# Chapter 1

---

## Introduction

### 1-1 Motivation

This thesis was sparked by the publication of a generalized theory for Greens function retrieval by crosscorrelation [Wapenaar et al., 2006] for arbitrary diffusion, flow and wave systems. Thus predicting the possibility of retrieving a seismoelectric Green's function by crosscorrelating the measurements of the particle velocity at a receiver station A with the measurements of the electrical field at a receiver station B. This thesis aims to derive and validate the interferometric seismoelectric Green's function representation to understand what seismic and electromagnetic background noise is needed for the interferometry to deliver the desired seismoelectric response.

Conventional geophysical techniques aim to obtain a image of the subsurface. Although they succeed in obtaining an image of a wide range of subsurface properties, they provide very little information on hydraulic permeability. Which has been the motivation to perform seismoelectric surveys for many authors, who obtained different levels of success. This thesis provides an alternative way to obtain the seismoelectric response, using alternative positions of the source, or using the natural seismic and electromagnetic sources in the subsurface. Using this method, we could benefit from a better signal to noise ratio by simply recording for a longer time period. But we likely suffer from a imperfect source distribution. Understanding the seismoelectric interferometric representation Green's function representation is a key step in the development of experiments of seismoelectric interferometry.

The seismoelectric system of Pride [1994] combines Biot's theory of wave propagation through saturated porous media with Maxwell's equations for the electromagnetic fields. Seismoelectric interferometry is an extreme application of Greens function retrieval by crosscorrelation. proper understanding of the seismoelectric interferometric Green's function representation will increase our understanding of the boundary conditions for Greens function retrieval by crosscorrelation.

## 1-2 Seismoelectric Phenomena

The first reported observation of seismoelectric phenomena was in 1936 by R.R. Thompson in the first issue of *Geophysics*. Thompson [1936, 1939], reported on electrical conductivity changes upon the passing of a seismic wave. Shortly afterward, Ivanov [1939] reported on the measurement of a electromagnetic field on the passing of a seismic wave, which later became known as the co-seismic electrical field. Frenkel [1944] was the first to attempt to provide a theoretical framework for seismoelectric phenomena. A major corner stone for the derivation of seismoelectric theory for porous saturated media was given by Biot's his theory for wave propagation in saturated porous media, [Biot, 1956], [Biot, 1956]. It was until 1994 that S.R. Pride derived a self-consistent system that describes seismoelectric wave phenomena in saturated porous media. Pride [1994] combined Biot's theory of wave propagation through saturated porous media with Maxwell's equations for the electromagnetic fields.

## 1-3 Interferometric Green's function recovery

The principle for Greens function retrieval by crosscorrelation was first derived by Claerbout [1968], who showed that the reflection response of a horizontally layered medium can be synthesized from the autocorrelation of its transmission response. Only little was reported on the subject until Weaver and Lobkis [Weaver and Lobkis, 2002] showed how the Green's function emerges in the cross-correlation of diffuse wave-fields. The conjecture of Claerbout that his relation holds for any arbitrary medium in 3D was confirmed by Wapenaar [2004], who derived the interferometry relation from reciprocity theorems. The derivation from reciprocity theorems does not require the wave-field to be diffusive. Another derivation is based upon stationary phase [Snieder, 2004b], showing that certain sources are more important than other sources. Recent work has shown that the derivation from reciprocity theorems holds for for situations where time-reversal invariance does not hold, as for electromagnetic waves in conducting media [Slob et al., 2007], acoustic waves in attenuating media [Snieder, 2007], or general scalar diffusion phenomena [Snieder, 2006]. Theses developments eventually lead to the derivation of interferometric Green's function representations for arbitrary diffusion, flow and wave phenomena, [Wapenaar et al., 2006], predicting relations for seismoelectric interferometry.

## 1-4 Outline of this thesis

In Chapter 2 we introduce the seismoelectric system of equations and compile them into a general matrix-vector equation. In the first chapter of Part I we provide the seismoelectric two-way wave equation together with composition and decomposition matrices to decompose the SH-TE fields into up and down going waves. A reflection formalism is derived in Chapter 4 that can be used to compute the responses of sources buried in layered media. Several examples of these simulations are given in Chapter 5. Part II focuses on interferometric Green's function representations and a numerical study of seismoelectric interferometric Green's function representations. The general theory is introduced in Chapter 6, written in an abstract formulation using the general matrix-vector equation that was introduced in Chapter 2. In

Chapter 7 we expand interferometric Green's function representations for the SH-TE seismoelectric system in 1D and 2D. The anatomy of these representations is studied in Chapter 8, we focused on understanding the complications that arise from ignoring several contributions in these representations. A discussion and conclusions follow in Chapter 9.

## 1-5 Notations and definitions

In this thesis, we use a large number of variables and parameters in addition to multiple general vector-matrix equations for the seismoelectric system of equations. Therefore it is important to use some general notation conventions.

A position in space is denoted by a triplet of Cartesian coordinates. The position vector is denoted by  $\mathbf{x}$  and the vector elements contain the coordinates of the point in space,  $\mathbf{x} = (x_1, x_2, x_3)^t$ , defined in a right-handed coordinate system and  $^t$  means matrix transposition (see Section 1-5-2 below), we use  $\mathbf{x}_H$  for the horizontal coordinates  $x_1$  and  $x_2$ . Spatial derivatives are denoted by  $\partial_i$ , in which the subscript  $i$  specifies the coordinate,  $x_i$  with respect to which the partial differentiation is taken. The time coordinate is denoted by  $t$  and  $\partial_t$  means temporal differentiation.

A vector can be written as  $\mathbf{v} = v_k \mathbf{i}_k$ , where the summation convention applies to the repeated subscript  $k$  and where  $\mathbf{i}_k$  is a unit base vector of the Cartesian reference frame and the subscript  $k$  indicates one of the three base vector directions. Hence,  $v_1$  is the  $\mathbf{i}_1$  component of the vector  $\mathbf{v}$ .

Possible additional super- and subscripts are added to denote, for example, a state in reciprocity theorems (A or B), medium phases, when used above a field or source quantity, or symbols that are added for differentiation between previously defined variables and parameters. We have the  $x_1$  component of the particle velocity in the solid in state A as  $v_{1,A}^s$ . A underlined variable or matrix denotes a slightly alternative definition from its original version, for example in the system matrices  $\mathbf{A}$  and  $\underline{\mathbf{A}}$  in Section 2-2 and in the source terms  $\underline{f}_2$  and  $\underline{J}_2^e$  defined in Section 7-1 and Appendix B.

We use lower case Latin symbols for variables, except for the electric and magnetic fields where we use the capital letters E and H. Matrices and vectors are written in boldface, where the context separates between matrices and vectors. Some special vectors are denoted by Greek boldface symbols. Operators (matrices) are written in calligraphic script and so are the matrices that are derived from operators by Fourier transforms, although strictly in the Fourier domain they are no longer operators. An exception is the composition operator  $\mathbf{L}$ , this is to discriminate from the seismoelectric coupling coefficient  $\mathcal{L}$ .

The Einstein summation convention is used and applies to repeated subscripts, that denote the elements of a vector or matrix. Lower-case Latin subscripts take on the values 1, 2 and 3, while lower-case Greek subscripts take on the values 1 and 2. Hence

$$\partial_i w_i \quad \text{stands for} \quad \sum_{i=1}^3 \partial_i w_i, \quad (1-1)$$

which is the *divergence* of  $\mathbf{w}$ .

Some exceptions have been made in Chapter 4, where we use  $z$  as the vertical coordinate. And we do not perform Einstein summation convention over the subscript  $n$  that denotes the layer number and the subscript  $w$  that denotes wave type. Some tricky definitions are those of the stiffness parameter  $\mathbf{d}$ , that is denoted in roman-case if used in the isotropic case where  $d_{ij} = d\delta_{ij}$ . This is to discriminate from the notion of an infinitesimal small step size,  $d$ , in an integration variable.

### 1-5-1 Fourier transformations

We use the following definition for the temporal Fourier transformation

$$\mathcal{F}^t\{f(\mathbf{x}, t)\} = \hat{f}(\mathbf{x}, \omega) = \int_{-\infty}^{\infty} f(\mathbf{x}, t)e^{-i\omega t} dt, \quad (1-2)$$

where  $\omega$  is angular frequency,  $t$  is time, and  $i = \sqrt{-1}$  is the imaginary unit. The frequency domain function  $\hat{f}(\mathbf{x}, \omega)$  is the temporal Fourier transform of the time domain function  $f(\mathbf{x}, t)$ . The inverse temporal Fourier transform is,

$$(\mathcal{F}^t)^{-1}\{\hat{f}(\mathbf{x}, \omega)\} = f(\mathbf{x}, t) = \frac{1}{2\pi} \int_{-\infty}^{\infty} \hat{f}(\mathbf{x}, \omega)e^{i\omega t} d\omega. \quad (1-3)$$

Note that  $\partial_t$  after temporal Fourier transformation is replaced by  $i\omega$ , assuming zero initial conditions. We use the following definition for the spatial Fourier transformation,

$$\mathcal{F}^s\{f(x_1, x_2, x_3, t)\} = \check{f}(k_1, x_2, x_3, t) = \int_{-\infty}^{\infty} f(x_1, x_2, x_3, t)e^{ik_1 x_1} dx_1, \quad (1-4)$$

where  $k$  is a wavenumber,  $x$  is a spatial coordinate, and  $f(x_1, x_2, x_3, t)$  is the time domain function that is transformed to the wavenumber domain function  $\check{f}(k_1, x_2, x_3, t)$ . Note the different choice of sign in the exponential of the temporal Fourier transformation. The inverse spatial Fourier transformation,

$$(\mathcal{F}^s)^{-1}\{\check{f}(k_1, x_2, x_3, t)\} = f(x_1, x_2, x_3, t) = \frac{1}{2\pi} \int_{-\infty}^{\infty} \check{f}(k_1, x_3, t)e^{-ik_1 x_1} dk_1. \quad (1-5)$$

The spatial Fourier transformation can repetitively be applied to each spatial coordinate  $(\mathcal{F}^s)^3\{f(x_1, x_2, x_3, t)\} = \check{\check{\check{f}}}(\mathbf{k}, t)$ . A spatial derivative with respect to the coordinate  $x_i$ ,  $\partial_i$  is after spatial Fourier transformation replaced by  $-ik_i$ . In Chapter 2 we transform our space time domain functions to the space frequency domain. In Chapter 3, after dropping the  $x_2$  dependence we perform another Fourier transformation and go to the horizontal-wavenumber frequency domain  $(\mathcal{F}^{t,s})^2\{f(x_1, x_3, t)\} = \tilde{f}(k_1, x_3, \omega)$ . The interferometric relations of Part II of the thesis are all derived in the space frequency domain.

In our calculations we only use positive frequencies and make use of relation 1-6, stating that for real functions of  $t$  we can rewrite the Fourier transformation over the positive frequencies only [Bracewell, 2000],

$$f(\mathbf{x}, t) = \frac{1}{2\pi} \int_{-\infty}^{\infty} \hat{f}(\mathbf{x}, \omega)e^{i\omega t} d\omega = \mathcal{R} \left( \frac{1}{\pi} \int_0^{\infty} \hat{f}(\mathbf{x}, \omega)e^{i\omega t} d\omega \right). \quad (1-6)$$

For a discussion on how we discretise the Fourier transformations and some additional aspects of how we implement this in our calculations, see Sections 5-1-1 and 5-1-2.

### 1-5-2 Transposed and adjointed operators

Throughout the thesis we make a formal separation between scalar functions and operator functions, or more general between matrices containing algebraic factors and matrices containing operators. We use a lower-case superscript  $t$  to denote simple matrix transposition, while we use an upper-case superscript  $T$  to denote operator matrix transposition. If we denote a complex conjugation for a scalar function or elements of a matrix we use an astrich  $*$ . When we transpose a matrix and take the complex conjugate of its elements, we use a superscript  $H$  and name it the Hermitian. When we mean complex conjugation and operator matrix transposition we use a superscript  $\dagger$ , and name it the adjoint. In what follows we introduce the transposed and adjoint of an operator (matrix).

For two vector functions  $\mathbf{f}(\mathbf{x}_H)$  and  $\mathbf{g}(\mathbf{x}_H)$  of the horizontal coordinates  $\mathbf{x}_H$  we define the bilinear form as

$$\langle \mathbf{f}, \mathbf{g} \rangle_b = \int_{\mathbb{S}} \mathbf{f}^T(\mathbf{x}_H) \mathbf{g}(\mathbf{x}_H) d^2 \mathbf{x}_H, \quad (1-7)$$

and the sesquilinear form as

$$\langle \mathbf{f}, \mathbf{g} \rangle_s = \int_{\mathbb{S}} \mathbf{f}^\dagger(\mathbf{x}_H) \mathbf{g}(\mathbf{x}_H) d^2 \mathbf{x}_H. \quad (1-8)$$

Consider an operator matrix  $\mathbf{u}$ , we introduce the transposed operator matrix  $\mathbf{u}^T$  via

$$\langle \mathbf{u}\mathbf{f}, \mathbf{g} \rangle_b = \langle \mathbf{f}, \mathbf{u}^T \mathbf{g} \rangle_b \quad (1-9)$$

and the adjoint operator matrix  $\mathbf{u}^\dagger$  via

$$\langle \mathbf{u}\mathbf{f}, \mathbf{g} \rangle_s = \langle \mathbf{f}, \mathbf{u}^\dagger \mathbf{g} \rangle_s. \quad (1-10)$$

Definitions 1-7 and 1-8 are through an integration over the complete horizontal coordinates, hence transposed and adjoint operators are not defined for an operator acting on the time or vertical-space coordinates. An operator matrix is called *symmetric* when it obeys

$$\mathbf{u}^T = \mathbf{u} \quad (1-11)$$

and it is *self-adjoint* when

$$\mathbf{u}^\dagger = \mathbf{u}. \quad (1-12)$$

For an operator matrix

$$\mathbf{u} = \begin{pmatrix} u_{11} & u_{12} \\ u_{21} & u_{22} \end{pmatrix}, \quad (1-13)$$

it follows from relation 1-9 above that

$$\mathbf{u}^T = \begin{pmatrix} u_{11}^T & u_{21}^T \\ u_{12}^T & u_{22}^T \end{pmatrix}. \quad (1-14)$$

Thus  $\mathbf{u}^T$  is a transposed matrix, containing transposed operators. Through definition 1-10, we have for the adjoint operator matrix  $\mathbf{u}^\dagger$ ,

$$\mathbf{u}^\dagger = \begin{pmatrix} (u_{11}^T)^* & (u_{21}^T)^* \\ (u_{12}^T)^* & (u_{22}^T)^* \end{pmatrix} = (\mathbf{u}^T)^*. \quad (1-15)$$

Note that the use of  $T$  on a matrix that does not contain operators is equal to the use of  $t$ , and similarly for  $\dagger$  and  $H$ .



# Seismoelectric system of equations

In this Chapter the seismoelectric equations are presented and a general diffusion, flow and wave equation is presented that captures these equations in 22 by 22 matrices. At the end the boundary conditions used to solve the system of equations are presented for source-free interfaces and for a source level in a homogeneous subdomain.

The equations in this Chapter are applicable for 3D seismoelectric wavefields in inhomogeneous anisotropic porous media. Nevertheless, some parameters are only specified for isotropic media. We use the boundary conditions in Part I to derive a scattering formalism that we use for seismoelectric modeling in isotropic horizontally-stratified media. And we use the general diffusion, flow and wave equation in Part II to derive reciprocity relations and interferometric Green's function representations for seismoelectric waves.

## 2-1 Pride's seismoelectric system of equations

In this Section we introduce the seismoelectric system of equations as derived by [Pride \[1994\]](#). Pride derived the system starting from Maxwell's equations for the electromagnetic field and Biot's equations of elastodynamic waves in porous media. He performed volume averaging of the governing equations in a porous medium with coupling through an electric double layer system around the grains. The final form of the equations take the form of Biot's equations linearly coupled with Maxwell's equations through a coupling coefficient  $\mathcal{L}$ .

The system of Pride has been derived making numerous assumptions. The most important ones are summarized here. The fluid is assumed to be an ideal electrolyte. Both the solid grains and all the macroscopic constitutive laws are assumed to be isotropic. In the literature it is generally assumed that this assumption can be relaxed to include anisotropic macroscopic constitutive parameters. The frequency dependency of the dynamic permeability and the coupling coefficient are smooth functions and postulated between continuous current and  $f_\infty$ . Under the assumptions that at the pore and grain scale the dielectric constant of the grains is much smaller than that of the electrolyte and the thickness of the double layer is much smaller than the radii of the curvature of the solid grains, all wave induced diffusion effects are

ignored. Scattering at the pore and grain scale is not accounted for, so the highest frequency of mechanic waves that can be considered is in the order of  $10^6$  Hz. No piezoelectric effects are considered and Lorentz currents are neglected. Only linear disturbances are considered.

### 2-1-1 The coupling coefficient

The coupling coefficient  $\hat{\mathcal{L}}$  is given in the frequency domain by

$$\hat{\mathcal{L}} = \mathcal{L}_0 \left[ 1 + i \frac{\omega}{\omega_c} \frac{m}{4} \left( 1 - 2 \frac{d^l}{\Lambda} \right)^2 \left( 1 - d^l \sqrt{\frac{i\omega\rho^f}{\eta}} \right)^2 \right]^{-\frac{1}{2}}, \quad (2-1)$$

where the static coupling coefficient  $\mathcal{L}_0$  is defined as

$$\mathcal{L}_0 = -\frac{\phi}{\alpha_\infty} \frac{\epsilon_0 \epsilon^f \zeta}{\eta} \left( 1 - 2 \frac{d^l}{\Lambda} \right). \quad (2-2)$$

The coupling coefficient is a frequency dependent function of tortuosity  $\alpha_\infty$ , volume-to-surface ratio of a porous material  $\Lambda$ , fluid relative dielectric permittivity  $\epsilon_r^f$ , dielectric permittivity in vacuum  $\epsilon_0$ , pore fluid viscosity  $\eta$ , Debye length  $d^l$ , critical frequency  $\omega_c$ , the density of the fluid phase  $\rho^f$  and the zeta potential of the double layer  $\zeta$ . [Pride and Morgan \[1991\]](#) have collected the datasets of previous researchers who determined the streaming potential, or zeta potential, in quartz systems and found

$$\zeta = 8 \cdot 10^{-3} + 26 \cdot 10^{-3} \log_{10} C, \quad (2-3)$$

where  $C$  is the electrolyte concentration in the pore fluid. The assumption that we consider the fluid to be an ideal electrolyte restricts  $10^{-6} < C < 10^0$  [mol/liter]. The Debye length is the characteristic length of the region of influence of the charge of mobile carriers. For an electrolyte containing  $L$  ion species, the Debye length  $d^l$  is given by

$$\frac{1}{(d^l)^2} = \sum_{i=1}^L \frac{(ez_i)^2 \mathcal{N}_i}{\epsilon_0 \epsilon^f k_b T}, \quad (2-4)$$

where  $\mathcal{N}_i$  is the bulk-ionic concentration of species  $i$ ,  $z_i$  are the ion valences,  $e$  is the elementary charge,  $k_b$  is the Boltzmann constant and  $T$  is the temperature, we use  $T = 323K$ . The bulk ionic concentration of ion species  $i$  is calculated using

$$\mathcal{N}_i = 10^3 C \mathcal{N}_A \text{abs}(z'_i), \quad (2-5)$$

where  $z'_i$  is the valency of the conjugate ion. The critical frequency separates low-frequency viscous flow and high-frequency inertial flow, and is defined as

$$\omega_c = \frac{\phi \eta}{\alpha_\infty k_0 \rho_f}, \quad (2-6)$$

where  $k_0$  is the static permeability in  $[m^2]$ , and  $\phi$  is the porosity as a volume fraction [-]. This gives us a total of three pore geometry parameters  $\alpha_\infty$ ,  $\Lambda$  and  $k_0$  that characterize the porous

material. A parameter, derived from those, is the similarity parameter  $m$  [Johnson et al., 1987]

$$m = \frac{\phi \Lambda^2}{\alpha_\infty k_0}. \quad (2-7)$$

Under the assumption that there exists only one scaling function for all porous media,  $m$  has been fixed to  $m = 8$  [Johnson, 1989]. We use a Carmen-Kozeny relationship which relates the static permeability  $k_0$  to the porosity  $\phi$  cubed, which is representative for clean Fontainebleau sandstones [Bourbié et al., 1987],

$$k_0 = 2 \cdot 10^{-11} \phi^3. \quad (2-8)$$

The tortuosity  $\alpha_\infty$  remains the last free pore geometry parameter. In the general anisotropic case the coupling coefficient is a tensor. Onsager reciprocity is satisfied under the thin double layer assumption [Pride, 1994] and we have  $\mathcal{L} = \mathcal{L}^t$ . This means that the coupling coefficient in Biot's equations is equal to the coupling coefficient in Maxwell's equations.

### 2-1-2 Equations of motion

In Pride's system, the equations of motion are Biot's equations of motion in porous media including a coupling term to the electric field. For an arbitrary inhomogeneous anisotropic medium they are given by

$$i\omega \hat{\rho}^b \hat{\mathbf{v}}^s + i\omega \hat{\rho}^f \hat{\mathbf{w}} - \partial_j \hat{\boldsymbol{\tau}}_j^b = \hat{\mathbf{f}}^b, \quad (2-9)$$

$$i\omega \hat{\rho}^f \hat{\mathbf{v}}^s + \eta \hat{\mathbf{k}}^{-1} (\hat{\mathbf{w}} - \hat{\mathcal{L}} \hat{\mathbf{E}}) + \nabla \hat{p}^f = \hat{\mathbf{f}}^f, \quad (2-10)$$

where  $\hat{\mathbf{w}}$  is the Biot filtration velocity  $\hat{\mathbf{w}} = \phi(\hat{\mathbf{v}}^f - \hat{\mathbf{v}}^s)$ ,  $\hat{\mathbf{v}}^s$  and  $\hat{\mathbf{v}}^f$  are the averaged solid and fluid particle velocities,  $\hat{\mathbf{E}}$  is the averaged electric field strength,  $\hat{\boldsymbol{\tau}}^b$  the averaged bulk stress and  $\hat{p}^f$  is the averaged pressure in the fluid. The source terms  $\hat{\mathbf{f}}^f$  and  $\hat{\mathbf{f}}^b$  are the volume densities of external force applied to the fluid phase and bulk phase, respectively. The constitutive parameters  $\hat{\rho}^f$ ,  $\hat{\rho}^s$  and  $\hat{\rho}^b$  are anisotropic frequency-dependent density tensors, and we have  $\hat{\rho}^b = (1 - \phi) \hat{\rho}^s + \phi \hat{\rho}^f$ . We assume that  $\hat{\rho}^f = \{\hat{\rho}^f\}^t$  and  $\hat{\rho}^s = \{\hat{\rho}^s\}^t$ . Which is, for example, the case when the anisotropy is the result of parallel fine layering at a scale much smaller than the wavelength [Schoenberg and Sen, 1983]. The complex frequency-dependent tensor  $\hat{\mathbf{k}}$  is the dynamic permeability tensor of the porous material, with  $\hat{\mathbf{k}} = \{\hat{\mathbf{k}}\}^t$ . The stress-strain relations read

$$-i\omega \hat{\boldsymbol{\tau}}_j^b + \hat{\mathbf{c}}_{jl} \partial_l \hat{\mathbf{v}}^s + \hat{\mathbf{d}}_j \nabla^t \hat{\mathbf{w}} = \hat{\mathbf{c}}_{jl} \hat{\mathbf{h}}_l^b + \hat{\mathbf{d}}_j \hat{q}^i, \quad (2-11)$$

$$i\omega \hat{p}^f + \hat{\mathbf{d}}_l^t \partial_l \hat{\mathbf{v}}^s + \hat{M} \nabla^t \hat{\mathbf{w}} = \hat{\mathbf{d}}_l^t \hat{\mathbf{h}}_l^b + \hat{M} \hat{q}^i, \quad (2-12)$$

where  $\hat{\mathbf{h}}^b$  is the density of external deformation rate on the bulk and  $\hat{q}^i$  is the density of volume injection rate in the fluid phase,  $\mathbf{0}$  is a  $3 \times 1$  vector of zeros. Our notation has

$$\hat{\boldsymbol{\tau}}_j^b = \begin{pmatrix} \hat{\tau}_{1j}^b \\ \hat{\tau}_{2j}^b \\ \hat{\tau}_{3j}^b \end{pmatrix}, \quad \hat{\mathbf{h}}_j = \begin{pmatrix} \hat{h}_{1j}^b \\ \hat{h}_{2j}^b \\ \hat{h}_{3j}^b \end{pmatrix}, \quad \hat{\mathbf{d}}_j = \begin{pmatrix} \hat{d}_{1j} \\ \hat{d}_{2j} \\ \hat{d}_{3j} \end{pmatrix} \text{ and} \quad (2-13)$$

$$\hat{\mathbf{c}}_{jl} = \begin{pmatrix} \hat{c}_{1j1l} & \hat{c}_{1j2l} & \hat{c}_{1j3l} \\ \hat{c}_{2j1l} & \hat{c}_{2j2l} & \hat{c}_{2j3l} \\ \hat{c}_{3j1l} & \hat{c}_{3j2l} & \hat{c}_{3j3l} \end{pmatrix}. \quad (2-14)$$

with  $\hat{\tau}^b = \{\hat{\tau}^b\}^t$  and  $\hat{\mathbf{h}}^b = \{\hat{\mathbf{h}}^b\}^t$ . The stiffness parameters of the porous solid are  $\hat{M}$ ,  $\hat{\mathbf{d}} = \{\hat{\mathbf{d}}\}^t$  and  $\hat{c}_{ijkl} = \hat{c}_{jikl} = \hat{c}_{ijlk} = \hat{c}_{klij}$ .

### 2-1-3 Isotropic frequency-independent elastic parameters

In this thesis we assume the elastic media parameters to be isotropic. We also assume certain elastic parameters to be frequency independent. For the frequency-dependent dynamic permeability we assume  $\hat{k}_{ij} = \delta_{ij}\hat{k}$ , with

$$\hat{k} = k_0 \left[ \left( 1 + i \frac{\omega}{\omega_c} \frac{4}{m} \right)^{\frac{1}{2}} + i \frac{\omega}{\omega_c} \right]^{-1}, \quad (2-15)$$

where the static permeability  $k_0$  is given in equation 2-8. The frequency-independent stiffness tensors are  $d_{ij} = \delta_{ij}d$  and

$$c_{ijkl} = V\delta_{ij}\delta_{kl} + N(\delta_{ik}\delta_{jl} + \delta_{il}\delta_{jk}) \quad (2-16)$$

where

$$V = \left( K_G - \frac{2}{3}N \right). \quad (2-17)$$

The frequency-independent shear modulus of the framework of grains,  $N$ , is the shear modulus as if the fluid is absent. According to Pride [1994] the frequency-independent elastic parameters  $K_G$ ,  $d$  and  $M$  are given by,

$$K_G = \frac{K^{fr} + \phi K^f + (1 + \phi) K^s \Delta}{1 + \Delta}, \quad (2-18)$$

$$d = \frac{K^f + K^s \Delta}{1 + \Delta}, \quad (2-19)$$

$$M = \frac{1}{\phi} \frac{K^f}{1 + \Delta}, \quad (2-20)$$

$$\Delta = \frac{K^f}{\phi (K^s)^2} \left( (1 - \phi) K^s - K^{fr} \right). \quad (2-21)$$

where  $K^s$ ,  $K^f$  and  $K^{fr}$  are the frequency-independent compression moduli of the solid, fluid and the framework of the grains, respectively. We also assume isotropic and frequency-independent densities,  $\hat{\rho}_{ij}^f = \delta_{ij}\rho^f$ ,  $\hat{\rho}_{ij}^s = \delta_{ij}\rho^s$  and thus  $\hat{\rho}_{ij}^b = \delta_{ij}\rho^b$ .

### 2-1-4 Electromagnetic equations

The other half of Pride's system are given by Maxwell's equations with a coupling coefficient to Biot's equation of motion in porous media. For an arbitrary inhomogeneous anisotropic

medium Maxwell's equations are given by

$$i\omega\epsilon\hat{\mathbf{E}} + \hat{\mathbf{J}}^e - \nabla \times \hat{\mathbf{H}} = -\hat{\mathbf{J}}^{s,e}, \quad (2-22)$$

$$i\omega\mu\hat{\mathbf{H}} + \hat{\mathbf{J}}^m + \nabla \times \hat{\mathbf{E}} = -\hat{\mathbf{J}}^{s,m}, \quad (2-23)$$

with the electric and magnetic current densities given by

$$\hat{\mathbf{J}}^e = \left( \hat{\sigma}^e - \eta\hat{\mathcal{L}}\hat{\mathbf{k}}^{-1}\hat{\mathcal{L}} \right) \hat{\mathbf{E}} + \eta\hat{\mathcal{L}}\hat{\mathbf{k}}^{-1}\hat{\mathbf{w}}, \quad (2-24)$$

$$\hat{\mathbf{J}}^m = \hat{\sigma}^m\hat{\mathbf{H}}, \quad (2-25)$$

where  $\mathbf{E}$  and  $\mathbf{H}$  are the averaged electric and magnetic field strengths,  $\hat{\mathbf{J}}^{s,e}$  and  $\hat{\mathbf{J}}^{s,m}$  are the external electric and magnetic current source densities. The constitutive parameters  $\hat{\sigma}^e$  and  $\hat{\sigma}^m$  are the frequency-dependent electric and magnetic conductivities,  $\epsilon$  and  $\mu$  are real-valued frequency-independent dielectric permittivity and magnetic permeability. We have  $\hat{\sigma}^e = \{\hat{\sigma}^e\}^t$ ,  $\hat{\sigma}^m = \{\hat{\sigma}^m\}^t$ ,  $\epsilon = \{\epsilon\}^t$  and  $\mu = \{\mu\}^t$ . Note that all possible relaxation mechanisms are captured in the electric and magnetic conductivity tensors.

### 2-1-5 Isotropic frequency-independent electromagnetic parameters

We assume the electromagnetic media parameters to be isotropic. The choice for frequency-independent dielectric permittivity and magnetic permeability does not imply any loss of generality, because all relaxation mechanisms are captured in the frequency-dependent electrical conductivity and magnetic permeability. We have  $\hat{\sigma}_{ij}^e = \hat{\sigma}^e\delta_{ij}$ ,  $\hat{\sigma}_{ij}^m = \delta_{ij}\hat{\sigma}^m$ ,  $\epsilon_{ij} = \delta_{ij}\epsilon$  and  $\mu_{ij} = \delta_{ij}\mu$ . We neglect magnetic relaxation losses,  $\hat{\sigma}^m = 0$ , and approximate the magnetic permeability of the subsurface by the permeability of vacuum  $\mu_0$ . We have

$$\mu = \mu_0. \quad (2-26)$$

We calculate the dielectric permittivity according to [Pride \[1994\]](#)

$$\epsilon = \epsilon_0 \left( \frac{\phi}{\alpha_\infty} (\epsilon_r^f - \epsilon_r^s) + \epsilon_r^s \right), \quad (2-27)$$

where  $\epsilon_0$  and  $\mu_0$  are the electric permittivity and magnetic permeability of the vacuum. And  $\epsilon_r^f$  and  $\epsilon_r^s$  are the fluid and solid relative dielectric constants. The electrical conductivity is composed from the frequency-independent pore-fluid conductivity  $\sigma^f$ , the frequency-independent double layer electron migration conductivity  $\sigma_{em}$  and the frequency-dependent osmotic conductivity of the streaming current  $\hat{\sigma}_{os}$ . From [Pride \[1994\]](#) we have

$$\hat{\sigma}^e = \frac{\phi\sigma^f}{\alpha_\infty} \left( 1 + \frac{2(\sigma_{em} + \hat{\sigma}_{os})}{\sigma^f\Lambda} \right), \quad (2-28)$$

where we use,

$$\sigma^f = \sum_{i=1}^L (ez_i)^2 b_i \mathcal{N}_i, \quad (2-29)$$

$$\sigma_{em} \approx 2d_l \sum_{i=1}^L (ez_i)^2 b_i \mathcal{N}_i \left[ \exp\left(-\frac{ez_i\zeta}{2k_b T}\right) - 1 \right], \quad (2-30)$$

$$\hat{\sigma}_{os} = \frac{(\epsilon_0\epsilon^f)^2 \zeta^2}{2d^l\eta} P_0 \left( 1 - \frac{2}{P_0} \frac{d^l}{\delta\eta} \right)^{-1}, \quad (2-31)$$

where  $b_i$  are the ion-mobilities and the dimensionless parameter  $P_0$  is defined as

$$P_0 = \frac{8k_b T \{d^l\}^2}{\epsilon_0 \epsilon^f \zeta^2} \sum_{i=1}^L \mathcal{N}_i \left[ \exp\left(-\frac{e z_i \zeta}{2k_b T}\right) - 1 \right], \quad (2-32)$$

and the viscous skin depth  $\delta^\eta$  is defined as

$$\delta^\eta = \sqrt{\frac{\eta}{i\omega\rho^f}}. \quad (2-33)$$

## 2-2 General diffusion, flow and wave equation

Following [Wapenaar and Fokkema \[2004\]](#) we capture the seismoelectric system in a general diffusion, flow and wave equation. For non-flowing media this equation reads in the frequency domain as

$$i\omega\hat{\mathbf{A}}\hat{\mathbf{u}} + \hat{\mathbf{B}}\hat{\mathbf{u}} + \mathbf{D}_x\hat{\mathbf{u}} = \hat{\mathbf{s}}, \quad (2-34)$$

where  $\hat{\mathbf{u}}$  is a vector containing space and frequency-dependent field quantities,  $\hat{\mathbf{s}}$  is a vector containing the source functions,  $\hat{\mathbf{A}}$  and  $\hat{\mathbf{B}}$  are matrices containing space-dependent material parameters, and  $\mathbf{D}_x$  is a matrix containing the spatial differential operators. The  $i\omega$  factor in the first term is the frequency representation of a temporal derivative.

The matrices  $\hat{\mathbf{A}}$ ,  $\hat{\mathbf{B}}$ ,  $\mathbf{D}_x$  the field vector  $\hat{\mathbf{u}}$  and the source vector  $\hat{\mathbf{s}}$  can be defined such that the system represents diffusion processes, acoustic wave propagation, momentum transport, elastodynamic wave propagation, electromagnetic wave propagation or coupled elastodynamic and electromagnetic wave propagation in porous solids. The different systems have different sizes, the seismoelectric system consists of 22 by 22 matrices and 22 by 1 field and source vectors.

Substituting the electromagnetic constitutive relations [2-24](#) and [2-25](#) into Maxwell's equations [2-22](#), [2-23](#) yields,

$$i\omega\epsilon\hat{\mathbf{E}} + \left(\hat{\boldsymbol{\sigma}}^e - \eta\hat{\mathcal{L}}\hat{\mathbf{k}}^{-1}\hat{\mathcal{L}}\right)\hat{\mathbf{E}} + \hat{\mathcal{L}}\eta\hat{\mathbf{k}}^{-1}\hat{\mathbf{w}} - \nabla \times \hat{\mathbf{H}} = -\hat{\mathbf{J}}^{\text{s},e}, \quad (2-35)$$

$$i\omega\mu\hat{\mathbf{H}} + \hat{\boldsymbol{\sigma}}^m\hat{\mathbf{H}} + \nabla \times \hat{\mathbf{E}} = -\hat{\mathbf{J}}^{\text{s},m}. \quad (2-36)$$

We define a conductivity that includes the contribution of the coupling coefficient as  $\hat{\boldsymbol{\sigma}}_{\mathcal{L}}^e = \hat{\boldsymbol{\sigma}}^e - \eta\hat{\mathcal{L}}\hat{\mathbf{k}}^{-1}\hat{\mathcal{L}}$ . Equations [2-9](#), [2-10](#), [2-11](#), [2-12](#), [2-35](#), [2-36](#) can now be combined to fit into the following form of the general diffusion, flow and wave equation

$$i\omega\hat{\mathbf{A}}\hat{\mathbf{u}} + \hat{\mathbf{B}}\hat{\mathbf{u}} + \hat{\mathbf{C}}\mathbf{D}_x\hat{\mathbf{u}} = \hat{\mathbf{C}}\hat{\mathbf{s}} \quad (2-37)$$

where

$$\hat{\mathbf{u}}^t = \left( \hat{\mathbf{E}}^t, \hat{\mathbf{H}}^t, \{\hat{\mathbf{v}}^s\}^t, -\{\hat{\boldsymbol{\tau}}_1^b\}^t, -\{\hat{\boldsymbol{\tau}}_2^b\}^t, -\{\hat{\boldsymbol{\tau}}_3^b\}^t, \mathbf{w}, \hat{p}^f \right), \quad (2-38)$$

$$\hat{\mathbf{s}}^t = \left( -\{\hat{\mathbf{J}}^{\text{s},e}\}^t, -\{\hat{\mathbf{J}}^{\text{s},m}\}^t, \{\hat{\mathbf{f}}^b\}^t, \{\hat{\mathbf{h}}_1^b\}^t, \{\hat{\mathbf{h}}_2^b\}^t, \{\hat{\mathbf{h}}_3^b\}^t, \{\hat{\mathbf{f}}^f\}^t, \hat{q}^i \right). \quad (2-39)$$

The matrices  $\bar{\mathbf{A}}$ ,  $\bar{\mathbf{B}}$ ,  $\mathbf{C}$ ,  $\mathbf{D}_x$  are defined as

$$\hat{\mathbf{A}} = \begin{pmatrix} \epsilon & \mathbf{O} & \mathbf{O} & \mathbf{O} & \mathbf{O} & \mathbf{O} & \mathbf{O} & \mathbf{O} \\ \mathbf{O} & \mu & \mathbf{O} & \mathbf{O} & \mathbf{O} & \mathbf{O} & \mathbf{O} & \mathbf{O} \\ \mathbf{O} & \mathbf{O} & \hat{\rho}^b & \mathbf{O} & \mathbf{O} & \mathbf{O} & \hat{\rho}^f & \mathbf{0} \\ \mathbf{O} & \mathbf{O} & \mathbf{O} & \mathbf{I} & \mathbf{O} & \mathbf{O} & \mathbf{O} & \mathbf{0} \\ \mathbf{O} & \mathbf{O} & \mathbf{O} & \mathbf{O} & \mathbf{I} & \mathbf{O} & \mathbf{O} & \mathbf{0} \\ \mathbf{O} & \mathbf{O} & \mathbf{O} & \mathbf{O} & \mathbf{O} & \mathbf{I} & \mathbf{O} & \mathbf{0} \\ \mathbf{O} & \mathbf{O} & \{\hat{\rho}^f\}^t & \mathbf{O} & \mathbf{O} & \mathbf{O} & \mathbf{O} & \mathbf{0} \\ \mathbf{0}^t & \mathbf{0}^t & \mathbf{0}^t & \mathbf{0}^t & \mathbf{0}^t & \mathbf{0}^t & \mathbf{0}^t & 1 \end{pmatrix}, \quad (2-40)$$

$$\hat{\mathbf{B}} = \begin{pmatrix} \hat{\sigma}_{\mathcal{L}}^e & \mathbf{O} & \mathbf{O} & \mathbf{O} & \mathbf{O} & \mathbf{O} & \eta \hat{\mathcal{L}} \hat{\mathbf{k}}^{-1} & \mathbf{0} \\ \mathbf{O} & \hat{\sigma}^m & \mathbf{O} & \mathbf{O} & \mathbf{O} & \mathbf{O} & \mathbf{O} & \mathbf{0} \\ \mathbf{O} & \mathbf{O} & \mathbf{O} & \mathbf{O} & \mathbf{O} & \mathbf{O} & \mathbf{O} & \mathbf{0} \\ \mathbf{O} & \mathbf{O} & \mathbf{O} & \mathbf{O} & \mathbf{O} & \mathbf{O} & \mathbf{O} & \mathbf{0} \\ \mathbf{O} & \mathbf{O} & \mathbf{O} & \mathbf{O} & \mathbf{O} & \mathbf{O} & \mathbf{O} & \mathbf{0} \\ \mathbf{O} & \mathbf{O} & \mathbf{O} & \mathbf{O} & \mathbf{O} & \mathbf{O} & \mathbf{O} & \mathbf{0} \\ -\{\eta \hat{\mathcal{L}} \hat{\mathbf{k}}^{-1}\}^t & \mathbf{O} & \mathbf{O} & \mathbf{O} & \mathbf{O} & \mathbf{O} & \eta \hat{\mathbf{k}}^{-1} & \mathbf{0} \\ \mathbf{0}^t & \mathbf{0}^t & \mathbf{0}^t & \mathbf{0}^t & \mathbf{0}^t & \mathbf{0}^t & \mathbf{0}^t & 0 \end{pmatrix}, \quad (2-41)$$

$$\hat{\mathbf{C}} = \begin{pmatrix} \mathbf{I} & \mathbf{O} & \mathbf{O} & \mathbf{O} & \mathbf{O} & \mathbf{O} & \mathbf{O} & \mathbf{0} \\ \mathbf{O} & \mathbf{I} & \mathbf{O} & \mathbf{O} & \mathbf{O} & \mathbf{O} & \mathbf{O} & \mathbf{0} \\ \mathbf{O} & \mathbf{O} & \mathbf{I} & \mathbf{O} & \mathbf{O} & \mathbf{O} & \mathbf{O} & \mathbf{0} \\ \mathbf{O} & \mathbf{O} & \mathbf{O} & \hat{c}_{11} & \hat{c}_{12} & \hat{c}_{13} & \mathbf{O} & \hat{d}_1 \\ \mathbf{O} & \mathbf{O} & \mathbf{O} & \hat{c}_{21} & \hat{c}_{22} & \hat{c}_{23} & \mathbf{O} & \hat{d}_2 \\ \mathbf{O} & \mathbf{O} & \mathbf{O} & \hat{c}_{31} & \hat{c}_{32} & \hat{c}_{33} & \mathbf{O} & \hat{d}_3 \\ \mathbf{O} & \mathbf{O} & \mathbf{O} & \mathbf{O} & \mathbf{O} & \mathbf{O} & \mathbf{I} & \mathbf{0} \\ \mathbf{0}^t & \mathbf{0}^t & \mathbf{0}^t & \hat{d}_1^t & \hat{d}_2^t & \hat{d}_3^t & \mathbf{0}^t & \hat{M} \end{pmatrix}, \quad (2-42)$$

$$\mathbf{D}_x = \begin{pmatrix} \mathbf{O} & \mathbf{D}_0^t & \mathbf{O} & \mathbf{O} & \mathbf{O} & \mathbf{O} & \mathbf{O} & \mathbf{0} \\ \mathbf{D}_0 & \mathbf{O} & \mathbf{O} & \mathbf{O} & \mathbf{O} & \mathbf{O} & \mathbf{O} & \mathbf{0} \\ \mathbf{O} & \mathbf{O} & \mathbf{O} & \mathbf{D}_1 & \mathbf{D}_2 & \mathbf{D}_3 & \mathbf{O} & \mathbf{0} \\ \mathbf{O} & \mathbf{O} & \mathbf{D}_1 & \mathbf{O} & \mathbf{O} & \mathbf{O} & \mathbf{O} & \mathbf{0} \\ \mathbf{O} & \mathbf{O} & \mathbf{D}_2 & \mathbf{O} & \mathbf{O} & \mathbf{O} & \mathbf{O} & \mathbf{0} \\ \mathbf{O} & \mathbf{O} & \mathbf{D}_3 & \mathbf{O} & \mathbf{O} & \mathbf{O} & \mathbf{O} & \mathbf{0} \\ \mathbf{O} & \mathbf{O} & \mathbf{O} & \mathbf{O} & \mathbf{O} & \mathbf{O} & \mathbf{O} & \nabla \\ \mathbf{0}^t & \mathbf{0}^t & \mathbf{0}^t & \mathbf{0}^t & \mathbf{0}^t & \mathbf{0}^t & \nabla^t & 0 \end{pmatrix}. \quad (2-43)$$

Where

$$\mathbf{D}_0 = \begin{pmatrix} 0 & -\partial_3 & \partial_2 \\ \partial_3 & 0 & -\partial_1 \\ -\partial_2 & \partial_1 & 0 \end{pmatrix}, \quad \mathbf{D}_j = \begin{pmatrix} \partial_j & 0 & 0 \\ 0 & \partial_j & 0 \\ 0 & 0 & \partial_j \end{pmatrix} \text{ and } \nabla = \begin{pmatrix} \partial_1 \\ \partial_2 \\ \partial_3 \end{pmatrix} \quad (2-44)$$

The empty parts of these matrices are filled by appropriately sized null matrices  $\mathbf{O}$  and null vectors  $\mathbf{0}$ . Finally, to match equation 2-37 to equation 2-34, we define  $\hat{\mathbf{A}} = \hat{\mathbf{C}}^{-1} \hat{\mathbf{A}}$  and  $\hat{\mathbf{B}} = \hat{\mathbf{C}}^{-1} \hat{\mathbf{B}}$ .

### 2-2-1 Symmetry properties of the general diffusion, flow and wave equation

The matrices in the general diffusion, flow and wave equation obey symmetry relations. Using transposition symmetry of the material parameters in matrices  $\hat{\mathbf{A}}$  and  $\hat{\mathbf{B}}$  discussed in previous Sections, we find

$$\mathbf{K}_0 \hat{\mathbf{A}}^t \mathbf{K}_0 = \hat{\mathbf{A}} \quad \text{and} \quad \mathbf{K}_0 \hat{\mathbf{B}}^t \mathbf{K}_0 = \hat{\mathbf{B}}, \quad (2-45)$$

where  $\mathbf{K}_0$  is defined by

$$\mathbf{K}_0 = \text{diag}(-1, 1, 1, -1, -1, -1, 1, -1). \quad (2-46)$$

The matrix  $\mathbf{D}_x$  containing spatial derivative operators obeys

$$\mathbf{K}_0 \mathbf{D}_x \mathbf{K}_0 = -\mathbf{D}_x = -\mathbf{D}_x^t. \quad (2-47)$$

## 2-3 Boundary conditions

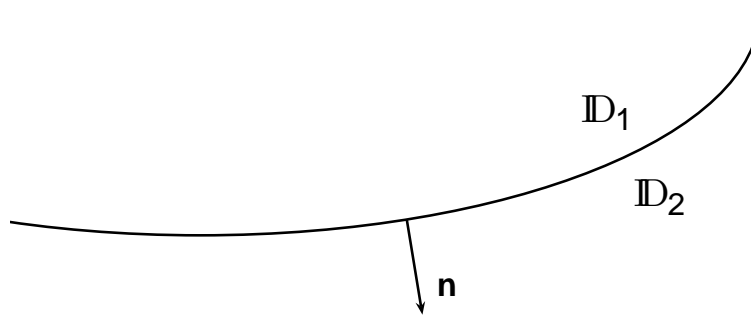


**Figure 2-1:** Perfectly welded interface with normal vector  $\mathbf{n}$  between two media  $\mathbb{D}_1$  and  $\mathbb{D}_2$  with different medium properties.

At interfaces where the medium parameters change, we need boundary conditions to solve for the fields at either side of the medium, see Figure 2-3. In general, an interface can be non-perfect or contain sources. For simplicity we treat two cases, a perfectly welded source free interface and a source level in a homogeneous subdomain. For the boundary conditions across a source-free interface we have the open-pore boundary conditions from [Deresiewicz and Skalak \[1963\]](#). In the time domain we have

Normal and shear stresses in the bulk,	$\tau_3^b$ ,	are continuous.
Normal stress in the fluid phase,	$p^f$ ,	is continuous.
Normal and horizontal velocities in the solid,	$\mathbf{v}^s$ ,	are continuous.
Normal component of filtration velocity,	$w_3$ ,	is continuous.
Tangential electric field,	$\mathbf{E}_0$ ,	is continuous.
Tangential magnetic field,	$\mathbf{H}_0$ ,	is continuous.

All these quantities are contained in the field vector  $\mathbf{q}$ , given by

$$\mathbf{q}^t = \left( -\left(\tau_3^b\right)^t, p^f, \left(\mathbf{E}_0\right)^t, \left(\mathbf{v}^s\right)^t, w_3, \left(\mathbf{H}_0\right)^t \right), \quad (2-48)$$

where

$$\boldsymbol{\tau}_3^b = \begin{pmatrix} \tau_{13}^b \\ \tau_{23}^b \\ \tau_{33}^b \end{pmatrix}, \mathbf{v}^s = \begin{pmatrix} v_1^s \\ v_2^s \\ v_3^s \end{pmatrix}, \mathbf{E}_0 = \begin{pmatrix} E_1 \\ E_2 \end{pmatrix}, \mathbf{H}_0 = \begin{pmatrix} H_2 \\ -H_1 \end{pmatrix} \quad (2-49)$$

We see in Chapter 3, how the components of this vector are decomposed in upgoing and downgoing waves. In Chapter 4 how we make use of these boundary conditions to derive our scattering formalism. The boundary condition on the field vector  $\mathbf{q}$  for source free interfaces at  $x_{3,n}$  between upper medium  $n$  and lower medium  $n + 1$  can be written as,

$$\lim_{x_3 \downarrow x_{3,n}} \mathbf{q}_{\{n+1\}}(x_3) - \lim_{x_3 \uparrow x_{3,n}} \mathbf{q}_{\{n\}}(x_3) = \mathbf{0}. \quad (2-50)$$

Across a level  $x_{3,s}$  containing sources, the field vector  $\mathbf{q}$  does not remain continuous, but instead experiences a jump. The jump condition is defined by the source vector  $\mathbf{d}$ , from below the source level  $\mathbf{q}^b$  to above the source level  $\mathbf{q}^a$ ,

$$\lim_{x_3 \downarrow x_{3,s}} \mathbf{q}^b(x_3) - \lim_{x_3 \uparrow x_{3,s}} \mathbf{q}^a(x_3) = \mathbf{d}(x_{3,s}). \quad (2-51)$$

The source vector  $\mathbf{d}$  is defined in chapter 3.

### 2-3-1 Boundary conditions at the pressure-free surface

We use vacuum to approximate air in simulations containing the earth's surface. In vacuum the normal and shear stresses are zero. To solve for the scattering matrix of a porous medium against vacuum, see Section 4-5, we need a special set of boundary conditions. There are no seismic waves and only electromagnetic waves propagate across the pressure-free surface and in vacuum. At the pressure-free surface we have

Normal and shear stresses in the bulk,	$\boldsymbol{\tau}_3^b$ ,	are zero.
Normal stress in the fluid phase,	$p^f$ ,	is zero.
Tangential electric field,	$\mathbf{E}_0$ ,	is continuous.
Tangential magnetic field,	$\mathbf{H}_0$ ,	is continuous.



**Part I**

**SH-TE Seismoelectrical Modeling in  
2D**



# The seismoelectric two- and one-way wave equations

In this chapter the seismoelectric one- and two-way wave equations are introduced. We consider horizontally, piecewise homogeneous, layered isotropic media. In those media the two-way wave equation can be rearranged into two independent modes of propagation. In the SH-TE mode, the horizontally polarized shear waves couple to the transverse polarized electrical fields. In the P-SV-TM mode, the pressure waves and vertically polarized shear waves are coupled to the transverse polarized magnetic fields. The two-way wave equation equates the vertical variations of the continuous field quantities in  $\hat{\mathbf{q}}$ , as a function of the horizontal derivatives, contained in  $\hat{\mathcal{A}}$ , of the continuous field quantities and a source vector  $\hat{\mathbf{d}}$ . In the frequency domain the two-way wave equation is given by

$$\partial_3 \hat{\mathbf{q}} = \hat{\mathcal{A}} \hat{\mathbf{q}} + \hat{\mathbf{d}}. \quad (3-1)$$

The one-way wave equation contains the field quantities of the two-way wave equation decomposed into upgoing and downgoing waves. The wave vector  $\tilde{\mathbf{p}}$  contains upgoing and downgoing waves, the matrix  $\tilde{\mathcal{B}}$  contains the eigenvalues of  $\tilde{\mathcal{A}}$  and connects the upgoing and downgoing waves. The sources are contained in the one-way source vector  $\tilde{\mathbf{b}}$ . In the horizontal wavenumber-frequency domain the one-way wave equation is given by

$$\partial_3 \tilde{\mathbf{p}} = \tilde{\mathcal{B}} \tilde{\mathbf{p}} + \tilde{\mathbf{b}}. \quad (3-2)$$

We derive the decomposition matrix  $\tilde{\mathbf{L}}^{-1}$  and the composition matrix  $\tilde{\mathbf{L}}$  for the SH-TE mode of propagation in the horizontal-wavenumber frequency domain. We further derive one-way wave extrapolators in a homogeneous subdomain by diagonalizing the matrix  $\tilde{\mathcal{A}}$ . At the end of this chapter we consider the electromagnetic system in vacuum. We connect upgoing and downgoing waves through a reflection formalism in Chapter 4.

### 3-1 Two-way wave equation

We rearrange the seismoelectric system of equations given in Chapter 2 such that we express the vertical derivatives as a function of the horizontal derivatives. To this purpose we eliminate the field quantities that are not continuous over a source-free interface. According to Section 2-3 we capture  $-\tau_{13}^b, -\tau_{23}^b, -\tau_{33}^b, p, E_1, E_2, v_1^s, v_2^s, v_3^s, w_3, H_2, -H_1$  in the field vector  $\mathbf{q}$ . The complete derivation for a isotropic medium starting from the equations of motion 2-9, 2-10, the stress-strain relations 2-11, 2-12 and the electromagnetic equations 2-22 and 2-23, is given in Appendix A.

We define the effective electric permittivity  $\hat{\epsilon} = \epsilon + \frac{1}{i\omega}\hat{\sigma}^e$  and the effective magnetic permeability  $\hat{\mu} = \mu + \frac{1}{i\omega}\hat{\sigma}^m = \mu_0$ . We also include the coupling coefficient in the effective electric permittivity  $\hat{\epsilon}_{\mathcal{L}} = \hat{\epsilon} - \hat{\rho}_E \hat{\mathcal{L}}^2$ . We define the effective fluid density  $\hat{\rho}^E = \frac{\eta}{i\omega k}$  and a complex density  $\hat{\rho}^c = \rho^b - \frac{(\rho^f)^2}{\hat{\rho}^E}$ .

We find the seismoelectric two-way wave equation

$$\partial_3 \hat{\mathbf{q}} = \hat{\mathcal{A}} \hat{\mathbf{q}} + \hat{\mathbf{d}}. \quad (3-3)$$

The field vector  $\hat{\mathbf{q}}$  and the source vector  $\hat{\mathbf{d}}$  are defined as

$$\hat{\mathbf{q}} = \begin{pmatrix} -\hat{\tau}_3^b \\ \hat{p} \\ \hat{\mathbf{E}}_0 \\ \hat{\mathbf{v}}^s \\ \hat{w}_3 \\ \hat{\mathbf{H}}_0 \end{pmatrix} \quad \text{and} \quad \hat{\mathbf{d}} = \begin{pmatrix} \hat{\mathbf{f}}^b - i\omega\rho^f \frac{k}{\eta} \hat{\boldsymbol{\delta}}_\alpha \hat{f}_\alpha^f + \frac{1}{i\omega} \partial_\alpha \mathbf{R}_{\alpha\beta} \hat{\mathbf{h}}_\beta^b \\ \hat{f}_3^f - \frac{1}{i\omega \hat{\epsilon}_{\mathcal{L}}} \hat{\mathcal{L}} \frac{\eta}{k} \hat{J}_3^{\text{s},e} \\ -\hat{\mathbf{J}}_0^{\text{s},m} - \begin{pmatrix} \partial_1 \\ \partial_2 \end{pmatrix} \frac{1}{i\omega \hat{\epsilon}_{\mathcal{L}}} \hat{J}_3^{\text{s},e} \\ \hat{\mathbf{h}}_3^b + \mathbf{e}_{33}^{-1} \mathbf{e}_{3\alpha} \hat{\mathbf{h}}_\alpha^b \\ -\partial_\beta \frac{k}{\eta} \hat{f}_\beta^f + \frac{d}{M} \mathbf{r}_\beta^t \hat{\mathbf{h}}_\beta + \hat{\mathbf{q}}^i \\ -\hat{\mathbf{J}}_0^{\text{s},e} - \hat{\mathcal{L}} \boldsymbol{\gamma}_\alpha \hat{f}_\alpha^f - \begin{pmatrix} \partial_2 \\ -\partial_1 \end{pmatrix} \frac{1}{i\omega \mu_0} \hat{J}_3^{\text{s},m} \end{pmatrix}. \quad (3-4)$$

In  $\hat{\mathbf{d}}$ ,

$$(\mathbf{e}_{jl})_{kl} = \mathbf{e}_{ijkl} = S \delta_{ij} \delta_{kl} + N (\delta_{ik} \delta_{jl} + \delta_{il} \delta_{jk}), \quad (3-5)$$

in which

$$S = K_G - \frac{2}{3}N - \frac{d^2}{M} \quad (3-6)$$

and we define

$$\mathbf{R}_{\alpha\beta} = \mathbf{e}_{\alpha\beta} - \mathbf{e}_{\alpha 3} \mathbf{e}_{33}^{-1} \mathbf{e}_{3\beta}, \quad (3-7)$$

$$\mathbf{r}_\alpha = \boldsymbol{\delta}_\alpha - \mathbf{e}_{\alpha 3} \mathbf{e}_{33}^{-1} \boldsymbol{\delta}_3. \quad (3-8)$$

The vectors  $\hat{\mathbf{J}}_0^{\text{s},e}$ ,  $\hat{\mathbf{J}}_0^{\text{s},m}$ ,  $\boldsymbol{\delta}_i$  and  $\boldsymbol{\gamma}_i$  are given by

$$\hat{\mathbf{J}}_0^{\text{s},e} = \begin{pmatrix} \hat{J}_1^{\text{s},e} \\ \hat{J}_2^{\text{s},e} \end{pmatrix}, \quad \hat{\mathbf{J}}_0^{\text{s},m} = \begin{pmatrix} \hat{J}_2^{\text{s},m} \\ -\hat{J}_1^{\text{s},m} \end{pmatrix}, \quad \boldsymbol{\delta}_i = \begin{pmatrix} \delta_{1i} \\ \delta_{2i} \\ \delta_{3i} \end{pmatrix}, \quad \boldsymbol{\gamma}_i = \begin{pmatrix} \delta_{1i} \\ \delta_{2i} \end{pmatrix}. \quad (3-9)$$

We have eliminated the fields  $\boldsymbol{\tau}_1^b, \boldsymbol{\tau}_2^b, \mathbf{E}_3, \mathbf{H}_3, w_1$  and  $w_2$ . The source quantities  $J_3^{s,e}, J_3^{s,m}, f_1^f, f_2^f, \hat{\mathbf{h}}_1$  and  $\hat{\mathbf{h}}_2$  are still contained in the source vector  $\mathbf{d}$ . The eliminated field quantities can simply be calculated from quantities in  $\mathbf{q}$  according to,

$$\hat{E}_3 = \frac{1}{i\omega\epsilon_{\mathcal{L}}} \left( \partial_2 \hat{H}_1 - \partial_1 \hat{H}_2 - \hat{\mathcal{L}} \frac{\eta}{k} \hat{w}_3 - \hat{J}_3^{s,e} \right), \quad (3-10)$$

$$\hat{H}_3 = \frac{1}{i\omega\mu_0} \left( \partial_2 \hat{E}_1 - \partial_1 \hat{E}_2 - \hat{J}_3^{s,m} \right), \quad (3-11)$$

$$\hat{w}_1 = \frac{k}{\eta} \left( \hat{f}_1^f - \partial_1 \hat{p}^f - i\omega\rho^f \hat{v}_1^s \right) + \hat{\mathcal{L}} \hat{E}_1, \quad (3-12)$$

$$\hat{w}_2 = \frac{k}{\eta} \left( \hat{f}_2^f - \partial_2 \hat{p}^f - i\omega\rho^f \hat{v}_2^s \right) + \hat{\mathcal{L}} \hat{E}_2, \quad (3-13)$$

$$-\hat{\boldsymbol{\tau}}_1^b = \frac{1}{i\omega} \left( \mathbf{e}_{1l} \mathbf{h}_l^b + i\omega \frac{d}{M} \delta_1 \hat{p}^f - \mathbf{e}_{1l} \partial_l \hat{\mathbf{v}}^s \right), \quad (3-14)$$

$$-\hat{\boldsymbol{\tau}}_2^b = \frac{1}{i\omega} \left( \mathbf{e}_{2l} \mathbf{h}_l^b + i\omega \frac{d}{M} \delta_2 \hat{p}^f - \mathbf{e}_{2l} \partial_l \hat{\mathbf{v}}^s \right). \quad (3-15)$$

The matrix  $\hat{\mathcal{A}}$  is composed as

$$\hat{\mathcal{A}} = \begin{pmatrix} \hat{\mathcal{A}}_{11} & \hat{\mathcal{A}}_{12} \\ \hat{\mathcal{A}}_{21} & \hat{\mathcal{A}}_{22} \end{pmatrix}, \quad (3-16)$$

where after substitution of equations A-34 - A-53 we find,

$$\hat{\mathcal{A}}_{11} = \begin{pmatrix} 0 & 0 & -\partial_1 \left( \frac{S}{K_c} \cdot \right) & \frac{\rho^f}{\hat{\rho}^E} \partial_1 - \partial_1 \left( \frac{2dN}{MK_c} \cdot \right) & -i\omega\rho^f \hat{\mathcal{L}} & 0 \\ 0 & 0 & -\partial_2 \left( \frac{S}{K_c} \cdot \right) & \frac{\rho^f}{\hat{\rho}^E} \partial_2 - \partial_2 \left( \frac{2dN}{MK_c} \cdot \right) & 0 & -i\omega\rho^f \hat{\mathcal{L}} \\ -\partial_1 & -\partial_2 & 0 & 0 & 0 & 0 \\ 0 & 0 & 0 & 0 & 0 & 0 \\ 0 & 0 & 0 & 0 & 0 & 0 \\ 0 & 0 & 0 & 0 & 0 & 0 \end{pmatrix}, \quad (3-17)$$

$$\hat{\mathcal{A}}_{12} = \begin{pmatrix} -i\omega\hat{\rho}^c + \frac{1}{i\omega}(\partial_1(\nu_1\partial_1\cdot) + \partial_2(N\partial_2\cdot)) \\ \frac{1}{i\omega}(\partial_2(\nu_2\partial_1\cdot) + \partial_1(N\partial_2\cdot)) \\ 0 \\ 0 \\ 0 \\ 0 \end{pmatrix} \quad (3-18)$$

$$\begin{pmatrix} \frac{1}{i\omega}(\partial_2(N\partial_1\cdot) + \partial_1(\nu_2\partial_2\cdot)) & 0 \\ -i\omega\hat{\rho}^c + \frac{1}{i\omega}(\partial_1(N\partial_1\cdot) + \partial_2(\nu_1\partial_2\cdot)) & 0 \\ 0 & -i\omega\rho^b \\ 0 & -i\omega\rho^f \\ 0 & 0 \\ 0 & 0 \end{pmatrix} \quad (3-19)$$

$$\begin{pmatrix} 0 & 0 & 0 \\ 0 & 0 & 0 \\ -i\omega\rho^f & 0 & 0 \\ -i\omega\hat{\rho}^E \left(1 + \frac{\hat{\rho}^E}{\hat{\varepsilon}_L} \hat{\mathcal{L}}^2\right) & \frac{\hat{\rho}^E}{\hat{\varepsilon}_L} \hat{\mathcal{L}}\partial_1 & \frac{\hat{\rho}^E}{\hat{\varepsilon}_L} \partial_2 \\ -\partial_1 \left(\frac{\hat{\rho}^E}{\hat{\varepsilon}_L} \hat{\mathcal{L}}\cdot\right) & -i\omega\mu_0 + \frac{1}{i\omega} \partial_1 \left(\frac{1}{\hat{\varepsilon}_L} \partial_1\cdot\right) & \frac{1}{i\omega} \partial_1 \left(\frac{1}{\hat{\varepsilon}_L} \partial_2\cdot\right) \\ -\partial_2 \left(\frac{\hat{\rho}^E}{\hat{\varepsilon}_L} \hat{\mathcal{L}}\cdot\right) & \frac{1}{i\omega} \partial_2 \left(\frac{1}{\hat{\varepsilon}_L} \partial_1\cdot\right) & -i\omega\mu_0 + \frac{1}{i\omega} \partial_2 \left(\frac{1}{\hat{\varepsilon}_L} \partial_2\cdot\right) \end{pmatrix}, \quad (3-20)$$

$$\hat{\mathcal{A}}_{21} = \begin{pmatrix} -\frac{i\omega}{N} & 0 & 0 & 0 \\ 0 & -\frac{i\omega}{N} & 0 & 0 \\ 0 & 0 & -\frac{i\omega}{K_c} & \frac{i\omega d}{MK_c} \\ 0 & 0 & \frac{i\omega d}{MK_c} & -i\omega \left(\frac{d^2}{M^2 K_c} + \frac{1}{M}\right) + \partial_\beta \left(\frac{1}{i\omega\hat{\rho}^E} \partial_\beta\cdot\right) \\ 0 & 0 & 0 & \hat{\mathcal{L}}\partial_1 \\ 0 & 0 & 0 & \hat{\mathcal{L}}\partial_2 \end{pmatrix} \quad (3-21)$$

$$\begin{pmatrix} 0 & 0 \\ 0 & 0 \\ 0 & 0 \\ -\partial_1(\hat{\mathcal{L}}\cdot) & -\partial_2(\hat{\mathcal{L}}\cdot) \\ -i\omega\hat{\varepsilon} + \frac{1}{i\omega} \partial_2 \left(\frac{1}{\mu_0} \partial_2\cdot\right) & -\frac{1}{i\omega} \partial_2 \left(\frac{1}{\mu_0} \partial_1\cdot\right) \\ -\frac{1}{i\omega} \partial_1 \left(\frac{1}{\mu_0} \partial_2\cdot\right) & -i\omega\hat{\varepsilon} + \frac{1}{i\omega} \partial_1 \left(\frac{1}{\mu_0} \partial_1\cdot\right) \end{pmatrix}, \quad (3-22)$$

$$\hat{\mathcal{A}}_{22} = \begin{pmatrix} 0 & 0 & 0 & -\partial_1 & 0 & 0 \\ 0 & 0 & 0 & -\partial_2 & 0 & 0 \\ -\left(\frac{S}{K_c}\right)\partial_1 & -\left(\frac{S}{K_c}\right)\partial_2 & 0 & 0 & 0 & 0 \\ \partial_1\left(\frac{\rho^f}{\hat{\rho}^E}\right) - \frac{2dN}{MK_c}\partial_1 & \partial_2\left(\frac{\rho^f}{\hat{\rho}^E}\right) - \frac{2dN}{MK_c}\partial_2 & 0 & 0 & 0 & 0 \\ i\omega\rho^f\hat{\mathcal{L}} & 0 & 0 & 0 & 0 & 0 \\ 0 & i\omega\rho^f\hat{\mathcal{L}} & 0 & 0 & 0 & 0 \end{pmatrix}, \quad (3-23)$$

where

$$\nu_1 = 4N \left( \frac{S+N}{K_c} \right), \quad (3-24)$$

$$\nu_2 = 2N \left( \frac{S}{K_c} \right) \quad \text{and} \quad (3-25)$$

$$K_c = S + 2N. \quad (3-26)$$

### 3-1-1 Symmetry properties of the two-way system matrix

The matrix  $\hat{\mathcal{A}}$  obeys similar symmetry properties as the matrices  $\hat{\mathbf{A}}$ ,  $\hat{\mathbf{B}}$  and  $\hat{\mathbf{D}}_{\mathbf{x}}$  in the general diffusion, flow and wave equation of Section 2-2. The matrix  $\hat{\mathcal{A}}$  obeys [Wapenaar, 1996]

$$\hat{\mathcal{A}}^T \mathbf{N}_0 = -\mathbf{N}_0 \hat{\mathcal{A}} \quad \text{and} \quad \hat{\mathcal{A}}^\dagger \mathbf{M}_0 = -\mathbf{M}_0 \hat{\mathcal{A}}^*. \quad (3-27)$$

The time domain equivalent of the medium state  $\hat{\mathcal{A}}^*$  is a medium with time-reversed medium parameters, i.e., a lossy medium becomes effectual. The matrices  $\mathbf{N}_0$  and  $\mathbf{M}_0$  are given by

$$\mathbf{N}_0 = \begin{pmatrix} \mathbf{O} & \mathbf{I}_n \\ -\mathbf{I}_n & \mathbf{O} \end{pmatrix} \quad \text{and} \quad \mathbf{M}_0 = \begin{pmatrix} \mathbf{O} & \mathbf{I}_n \\ \mathbf{I}_n & \mathbf{O} \end{pmatrix}, \quad (3-28)$$

where  $\mathbf{I}_n$  is the identity matrix of size  $n$ . For the seismoelectric matrix given in Section 3-1 we have  $n = 6$ . The SH-TE system of Section 3-4 has  $n = 2$  and the separate TE and SH systems each have  $n = 1$ .

## 3-2 Decoupling of the SH-TE and P-SV-TM systems

In a stratified earth there are two independent modes of propagation. The system can be decoupled by using a cylindrical coordinate transformation [White and Zhou, 2006], or to define line sources. Interferometric Green's function recovery requires source coverage over large volumes and surfaces. Therefore we define line sources in the  $x_2$  direction. This sets all derivatives with respect to  $x_2$  to zero,  $\partial_2 = 0$ . With that, we rearrange the matrix  $\hat{\mathcal{A}}$  such that it decouples into a block diagonal matrix of two sub matrices,

$$\partial_3 \hat{\mathbf{q}} = \hat{\mathcal{A}} \hat{\mathbf{q}} + \hat{\mathbf{d}}, \quad (3-29)$$

where

$$\hat{\mathcal{A}} = \begin{pmatrix} \hat{\mathcal{A}}_{shte} & \mathbf{O} \\ \mathbf{O} & \hat{\mathcal{A}}_{psvtm} \end{pmatrix}, \quad \hat{\mathbf{q}} = \begin{pmatrix} \hat{\mathbf{q}}_{shte} \\ \hat{\mathbf{q}}_{psvtm} \end{pmatrix} \quad \text{and} \quad \hat{\mathbf{d}} = \begin{pmatrix} \hat{\mathbf{d}}_{shte} \\ \hat{\mathbf{d}}_{psvtm} \end{pmatrix}. \quad (3-30)$$

We choose the order in the field vectors  $\hat{\mathbf{q}}_{shte}$  and  $\hat{\mathbf{q}}_{psvtm}$  such that they represent the original order in the field vector  $\hat{\mathbf{q}}$ . In that way, the sub matrices  $\hat{\mathcal{A}}_{shte}$  and  $\hat{\mathcal{A}}_{psvtm}$  exhibit the same symmetry properties of the original matrix  $\hat{\mathcal{A}}$ . Alternative arrangements can be chosen [Haartsen, 1995], [Haartsen and Pride, 1997], [van der Burg, 2002], [Shaw, 2004], [White and Zhou, 2006], such that the sub matrices  $\hat{\mathcal{A}}_{shte}$  and  $\hat{\mathcal{A}}_{psvtm}$  become anti-diagonal. This simplifies the linear algebra methods that are employed to decompose into upgoing and downgoing waves [Ursin, 1983], but we show in Appendix B that this is not strictly necessary.

We find

$$\hat{\mathbf{q}}_{shte} = \left( -\hat{\tau}_{23}^b, \hat{E}_2, \hat{v}_2^s, -\hat{H}_1 \right)^t, \quad (3-31)$$

$$\hat{\mathbf{q}}_{psvtm} = \left( -\hat{\tau}_{13}^b, -\hat{\tau}_{33}^b, \hat{p}, \hat{E}_1, \hat{v}_1^s, \hat{v}_3^s, \hat{w}_3, \hat{H}_2 \right), \quad (3-32)$$

$$\hat{\mathcal{A}}_{shte} = \begin{pmatrix} 0 & -i\omega\rho^f\hat{\mathcal{L}} & -i\omega\hat{\rho}^c + \frac{1}{i\omega}(\partial_1(N\partial_1\cdot)) & 0 \\ 0 & 0 & 0 & -i\omega\mu_0 \\ -i\omega\frac{1}{N} & 0 & 0 & 0 \\ 0 & -i\omega\hat{\varepsilon} + \frac{1}{i\omega}\left(\partial_1\left(\frac{1}{\mu_0}\partial_1\cdot\right)\right) & i\omega\rho^f\hat{\mathcal{L}} & 0 \end{pmatrix}, \quad (3-33)$$

$$\hat{\mathcal{A}}_{psvtm} = \begin{pmatrix} 0 & -\partial_1\left(\frac{S}{K_c}\cdot\right) & \frac{\hat{\rho}^f}{\hat{\rho}^E}\partial_1 - \partial_1\left(\frac{2dN}{MK_c}\cdot\right) & -i\omega\rho^f\hat{\mathcal{L}} \\ -\partial_1 & 0 & 0 & 0 \\ 0 & 0 & 0 & 0 \\ 0 & 0 & 0 & 0 \\ -i\omega\frac{1}{N} & 0 & 0 & 0 \\ 0 & -i\omega\frac{1}{K_c} & i\omega\frac{d}{MK_c} & 0 \\ 0 & i\omega\frac{d}{MK_c} & -i\omega\left(\frac{d^2}{M^2K_c} + \frac{1}{M}\right) + \partial_1\left(\frac{1}{i\omega\hat{\rho}^E}\partial_1\cdot\right) & -\partial_1(\hat{\mathcal{L}}\cdot) \\ 0 & 0 & 0 & 0 \\ -i\omega\hat{\rho}^c + \frac{1}{i\omega}(\partial_1(\nu_1\partial_1\cdot)) & 0 & 0 & 0 \\ 0 & -i\omega\rho^b & -i\omega\rho^f & 0 \\ 0 & -i\omega\rho^f & -i\omega\hat{\rho}^E\left(1 + \frac{\hat{\rho}^E}{\hat{\varepsilon}_L}\hat{\mathcal{L}}^2\right) & \frac{\hat{\rho}^E}{\hat{\varepsilon}_L}\hat{\mathcal{L}}\partial_1 \\ 0 & 0 & -\partial_1\left(\frac{\hat{\rho}^E}{\hat{\varepsilon}_L}\hat{\mathcal{L}}\cdot\right) & -i\omega\mu_0 + \frac{1}{i\omega}\partial_1\left(\frac{1}{\hat{\varepsilon}_L}\partial_1\cdot\right) \\ 0 & -\partial_1 & 0 & 0 \\ -\frac{S}{K_c}\partial_1 & 0 & 0 & 0 \\ \partial_1\left(\frac{\rho^f}{\hat{\rho}^E}\cdot\right) - \frac{2dN}{MK_c}\partial_1 & 0 & 0 & 0 \\ 0 & 0 & 0 & 0 \end{pmatrix}. \quad (3-34)$$

The decoupled source vectors are given by

$$\hat{\mathbf{d}}_{shte} = \begin{pmatrix} \hat{f}_2^b - \frac{\rho^f}{\hat{\rho}^E}\hat{f}_2^f - \frac{1}{i\omega}\partial_1N\left(\hat{h}_{12} + \hat{h}_{21}\right) \\ \hat{J}_1^{s,m} \\ \hat{h}_{23} + \hat{h}_{32} \\ -\hat{J}_2^{s,e} - \hat{\mathcal{L}}\hat{f}_2^f + \partial_1\frac{1}{i\omega\mu_0}\hat{J}_3^{s,m} \end{pmatrix} \quad (3-35)$$

and

$$\hat{\mathbf{d}}_{psvtm} = \begin{pmatrix} \hat{f}_1^b - \frac{\rho^f}{\hat{\rho}^E} \hat{f}_1^f - \frac{1}{i\omega} \partial_1 \left( 2N\hat{h}_{11} + \left( S - \frac{S^2}{K_c} \right) (\hat{h}_{11} + \hat{h}_{22}) \right) \\ \hat{f}_3^b - \frac{\rho^f}{\hat{\rho}^E} \hat{f}_3^f \\ \hat{f}_3^f - \frac{\hat{\rho}^E}{\hat{\epsilon}_L} \hat{\mathcal{L}} \hat{J}_3^{s,e} \\ - \hat{J}_2^{s,m} - \partial_1 \frac{1}{i\omega \hat{\epsilon}_L} \hat{J}_3^{s,e} \\ \hat{h}_{31} + \hat{h}_{13} \\ \hat{h}_{33} + \left( \frac{S}{K_c} \right) (\hat{h}_{11} + \hat{h}_{22}) \\ \hat{q}^i - \partial_1 \frac{1}{i\omega \hat{\rho}^E} \hat{f}_1^f \\ - \hat{J}_1^{s,e} - \hat{\mathcal{L}} \hat{f}_1^f \end{pmatrix}. \quad (3-36)$$

In the remaining of Part I we only consider the SH-TE mode, therefore by default we refer to the SH-TE system when we omit the subscript *shte* in the matrix  $\hat{\mathbf{A}}$ , field vector  $\hat{\mathbf{q}}$  and source vector  $\hat{\mathbf{d}}$ .

### 3-3 One-way wave equation

We give a short summary of one-way wave theory, for a more thorough treatment, see Wapenaar and Berkhout [1989]. Starting from the two-way wave equation 3-1 in the horizontal-wavenumber frequency domain (see Section 1-5-1), we diagonalize the system matrix  $\hat{\mathbf{A}}$  3-37. Matrix  $\tilde{\mathbf{L}}$  is a matrix whose columns are the eigenvectors of the system matrix  $\hat{\mathbf{A}}$ , the diagonal matrix  $\tilde{\mathcal{H}}$  contains the eigenvalues of the system,

$$\tilde{\mathcal{H}} = \tilde{\mathbf{L}}^{-1} \hat{\mathbf{A}} \tilde{\mathbf{L}}. \quad (3-37)$$

The field vector  $\tilde{\mathbf{q}}$  transforms into the vector  $\hat{\mathbf{p}}$ , upon multiplication by  $\tilde{\mathbf{L}}^{-1}$ . Similarly the source vector  $\tilde{\mathbf{d}}$  transforms into the vector  $\tilde{\mathbf{b}}$ . We have

$$\tilde{\mathbf{d}} = \tilde{\mathbf{L}} \tilde{\mathbf{b}} \quad \text{and} \quad \tilde{\mathbf{q}} = \tilde{\mathbf{L}} \hat{\mathbf{p}}. \quad (3-38)$$

Inserting equations 3-38 and 3-37 into the two-way wave equation 3-1 we obtain

$$\partial_3 \tilde{\mathbf{p}} = \tilde{\mathcal{B}} \tilde{\mathbf{p}} + \tilde{\mathbf{b}}, \quad (3-39)$$

with the one-way first order differential operator

$$\tilde{\mathcal{B}} = \tilde{\mathcal{H}} - \tilde{\mathbf{L}}^{-1} \partial_3 \tilde{\mathbf{L}}. \quad (3-40)$$

The general solution of equation 3-39 reads [Wapenaar and Berkhout, 1989]

$$\tilde{\mathbf{p}}(x_3) = \tilde{\mathcal{W}}(x_3, x_{3,0}) \tilde{\mathbf{p}}(x_{3,0}) + \int_{x_{3,0}}^{x_3} \tilde{\mathcal{W}}(x_3, x'_3) \tilde{\mathbf{b}}(x'_3) dx'_3, \quad (3-41)$$

where  $\tilde{\mathcal{W}}(x_3, x_{3,0})$  is defined by

$$\tilde{\mathcal{W}}(x_3, x_{3,0}) = \sum_{m=0}^{\infty} \frac{(x_3 - x_{3,0})^m}{m!} \tilde{\mathcal{B}}_m(x_{3,0}) \quad (3-42)$$

and  $\tilde{\mathcal{C}}_m$  is recursively defined as

$$\tilde{\mathcal{B}}_{m+1}(x_{3,0}) = \partial_3 \tilde{\mathcal{B}}_m(x_3) \Big|_{x_{3,0}} + \tilde{\mathcal{B}}_m(x_{3,0}) \tilde{\mathcal{B}}_1(x_{3,0}), \quad (3-43)$$

where

$$\tilde{\mathcal{B}}_0(x_{3,0}) = \mathbf{I}. \quad (3-44)$$

### 3-3-1 Homogeneous source-free subdomain

For the special case of a homogeneous source-free subdomain, the solution to equation 3-39 greatly simplifies. We can see that the vertical derivatives in equations 3-39, 3-43 and the source terms in equations 3-39, 3-41 disappear. We find

$$\partial_3 \tilde{\mathbf{p}} = \tilde{\mathcal{H}} \tilde{\mathbf{p}}, \quad (3-45)$$

with solution

$$\tilde{\mathbf{p}}(x_3) = \tilde{\mathcal{W}}(x_3, x_{3,0}) \tilde{\mathbf{p}}(x_{3,0}). \quad (3-46)$$

The matrix  $\tilde{\mathcal{W}}$  extrapolates the one-way wave fields in  $\tilde{\mathbf{p}}$  from depth  $x_{3,0}$  to  $x_3$ . This is only valid in homogeneous source-free subdomains.

For  $\tilde{\mathcal{C}}_m(x_{3,0})$  in equation 3-42 we find that equation 3-43 simplifies to  $\tilde{\mathcal{C}}_{m+1} = \tilde{\mathcal{C}}_m \tilde{\mathcal{C}}_1$ , or  $\tilde{\mathcal{C}}_m = \tilde{\mathcal{C}}_1^m = \tilde{\mathcal{H}}^m$ . With this simplification of  $\tilde{\mathcal{C}}_m$ , we may represent  $\tilde{\mathcal{W}}(x_3, x_{3,0})$  in equation 3-46 symbolically as

$$\tilde{\mathcal{W}}(x_3, x_{3,0}) = \exp \left\{ \tilde{\mathcal{H}}(x_3 - x_{3,0}) \right\}. \quad (3-47)$$

We show below that due to our choice of the structure of matrix  $\tilde{\mathbf{L}}$ , the eigenvalue matrix  $\tilde{\mathcal{H}}$  has a structure

$$\tilde{\mathcal{H}} = \begin{pmatrix} \tilde{\mathcal{H}}^+ & 0 \\ 0 & \tilde{\mathcal{H}}^- \end{pmatrix}, \quad (3-48)$$

where  $\tilde{\mathcal{H}}^- = -\tilde{\mathcal{H}}^+$ . Hence the wavefield extrapolator matrix  $\tilde{\mathcal{W}}$  has a similar form

$$\tilde{\mathcal{W}} = \begin{pmatrix} \tilde{\mathcal{W}}^+ & 0 \\ 0 & \tilde{\mathcal{W}}^- \end{pmatrix}. \quad (3-49)$$

We can see that according to 3-47 and 3-48 we have

$$\tilde{\mathcal{W}}(z_2, z_1) = \left( \tilde{\mathcal{W}}(z_1, z_2) \right)^{-1}. \quad (3-50)$$

We now see how the matrix  $\tilde{\mathbf{L}}^{-1}$  decomposes the two-way field quantities into upgoing and downgoing waves, therefore we refer to the matrix  $\tilde{\mathbf{L}}$  and  $\tilde{\mathbf{L}}^{-1}$  as the composition and decomposition matrices respectively. The one-way wave and source vectors are written as

$$\tilde{\mathbf{p}} = \begin{pmatrix} \tilde{\mathbf{p}}^+ \\ \tilde{\mathbf{p}}^- \end{pmatrix} \quad \text{and} \quad \tilde{\mathbf{b}} = \begin{pmatrix} \tilde{\mathbf{b}}^+ \\ \tilde{\mathbf{b}}^- \end{pmatrix}. \quad (3-51)$$

### 3-3-2 Symmetry properties of the one-way system matrix

We do not perform flux normalization on our decomposition matrices, but choose a velocity normalization or electric field normalization instead. However, in homogeneous subdomains, the one-way system matrix  $\tilde{\mathbf{B}}$  still obeys a very similar symmetry relation as the two-way system matrix,

$$\tilde{\mathbf{B}}^T \mathbf{N}_0 = -\mathbf{N}_0 \tilde{\mathbf{B}} \quad \text{and} \quad \tilde{\mathbf{B}}^\dagger \mathbf{J}_0 = -\mathbf{J}_0 \tilde{\mathbf{B}}^*. \quad (3-52)$$

Where the matrices  $\mathbf{N}_0$  and  $\mathbf{J}_0$  are given by

$$\mathbf{N}_0 = \begin{pmatrix} \mathbf{O} & \mathbf{I}_n \\ -\mathbf{I}_n & \mathbf{O} \end{pmatrix} \quad \text{and} \quad \mathbf{J}_0 = \begin{pmatrix} \mathbf{I}_n & \mathbf{O} \\ \mathbf{O} & -\mathbf{I}_n \end{pmatrix}, \quad (3-53)$$

where  $\mathbf{I}_n$  is the identity matrix of size  $n$ . For the seismoelectric matrix given in Section 3-1 we have  $n = 6$ . The SH-TE system of Section 3-4 has  $n = 2$  and the separate TE and SH systems each have  $n = 1$ . The symmetry properties given in equations 3-52 are symmetry properties of the operator  $\tilde{\mathcal{H}} = \sqrt{\frac{\omega^2}{\hat{c}^2} - k_1^2}$ . These are discussed by Wapenaar [1996] and Grimbergen et al. [1998]. The time-reversed operator  $\tilde{\mathcal{H}}^*$  is given by a time-reversed propagation velocity  $\hat{c}^*$ , defined in the time domain in a medium with adjoint medium parameters.

## 3-4 Seismoelectric decomposition for the SH-TE system

In Section 3-2 we derived the system matrix  $\tilde{\mathcal{A}}$  for the SH-TE coupling mode, see matrix 3-33. In the horizontal-wavenumber frequency domain  $\tilde{\mathcal{A}}_{sh\text{te}}$  is given by

$$\tilde{\mathcal{A}} = \begin{pmatrix} 0 & -i\omega\rho^f\hat{\mathcal{L}} & -i\omega\hat{\rho}^c + \frac{ik_1^2}{\omega}N & 0 \\ 0 & 0 & 0 & -i\omega\mu_0 \\ -i\omega\frac{1}{N} & 0 & 0 & 0 \\ 0 & -i\omega\hat{\varepsilon} + \frac{ik_1^2}{\omega}\frac{1}{\mu_0} & i\omega\rho^f\hat{\mathcal{L}} & 0 \end{pmatrix}. \quad (3-54)$$

The solutions to the eigenvalue problem are contained on the diagonal of  $\mathcal{H}$ . In Appendix B we derive the wave velocities, the eigenvalues and eigenvectors of matrix  $\tilde{\mathcal{A}}$ . Horizontally propagating waves have zero vertical slowness and follow from the trivial solution of the eigenvalue problem. There are 4 roots to the zero-eigenvalue problem,

$$\frac{2}{\hat{c}^2} = \frac{\hat{\rho}^c}{N} + \hat{\varepsilon}\mu_0 \pm \sqrt{\left(\frac{\hat{\rho}^c}{N} - \hat{\varepsilon}\mu_0\right)^2 - 4\frac{\mu_0}{N}\left(\rho^f\hat{\mathcal{L}}\right)^2}. \quad (3-55)$$

The plus sign is associated with the velocity of the SH-wave,  $\hat{c}_{sh}$ , and the minus sign with the velocity of the TE wave,  $\hat{c}_{te}$ , as can be seen when the coupling coefficient is set to zero,  $\hat{\mathcal{L}} = 0$ .

In Appendix B-2 we derive the non-zero eigenvalues of the seismoelectric SH-TE system. There are 4 non-zero solutions to the eigenvalue problem that represent plane wave solutions each propagating with a non-zero vertical slowness as eigenvalue. All four non-zero eigenvalues have the form of  $i\tilde{\mathcal{H}}_w^\pm = \mp i\tilde{\mathcal{H}}_w$ , with  $\tilde{\mathcal{H}}_w = \sqrt{\frac{\omega^2}{\hat{c}_w^2} - k_1^2}$ , where  $\hat{c}_w$  is the velocity of either a

shear horizontal ( $w = sh$ ) or an transverse electric wave ( $w = te$ ). We have to choose the branch of the square root such that propagating waves decay. The real part of the exponentials in equation 3-47 need to be negative for propagating waves. Thus we choose  $\Im\left\{\sqrt{\frac{\omega^2}{\hat{c}_w^2} - k_1^2}\right\} \leq 0$ . We find for the eigenvalue matrix,

$$\tilde{\mathcal{H}} = \begin{pmatrix} i\tilde{\mathcal{H}}_{sh}^+ & 0 & 0 & 0 \\ 0 & i\tilde{\mathcal{H}}_{te}^+ & 0 & 0 \\ 0 & 0 & i\tilde{\mathcal{H}}_{sh}^- & 0 \\ 0 & 0 & 0 & i\tilde{\mathcal{H}}_{te}^- \end{pmatrix}. \quad (3-56)$$

The arrangement follows from our eigenvector arrangement in the matrix  $\tilde{\mathbf{L}}$  and is chosen such that we decompose our two-way wave fields into shear waves and electric waves, respectively, downgoing and upgoing.

For a general eigenvalue  $i\tilde{\mathcal{H}}_w^\pm$  we find a general eigenvector  $\tilde{\mathbf{a}}_w^\pm$

$$\tilde{\mathbf{a}}_w^\pm = \begin{pmatrix} \pm \frac{\tilde{\mathcal{H}}_w}{\omega} N \\ \hat{\xi}_w \\ 1 \\ \pm \frac{\tilde{\mathcal{H}}_w}{\omega} \frac{1}{\mu_0} \hat{\xi}_w \end{pmatrix}, \quad (3-57)$$

with

$$\hat{\xi}_{sh} = \frac{\mu_0 \rho^f \hat{\mathcal{L}}}{(\hat{\epsilon} \mu_0 - \frac{1}{\hat{c}_{sh}^2})} \quad \text{and} \quad \hat{\xi}_{te} = \frac{(\frac{N}{\hat{c}_{te}^2} - \hat{\rho}^c)}{\hat{\rho}^f \hat{\mathcal{L}}}. \quad (3-58)$$

We arrange the eigenvectors into  $\tilde{\mathbf{L}}$  as  $\tilde{\mathbf{L}} = (\tilde{\mathbf{a}}_{sh}^+, \tilde{\mathbf{a}}_{te}^+, \tilde{\mathbf{a}}_{sh}^-, \tilde{\mathbf{a}}_{te}^-)$ . With that, the composition matrix is given by

$$\tilde{\mathbf{L}} = \begin{pmatrix} \frac{\tilde{\mathcal{H}}_{sh} N}{\omega} & \frac{\tilde{\mathcal{H}}_{te} N}{\omega} & -\frac{\tilde{\mathcal{H}}_{sh} N}{\omega} & -\frac{\tilde{\mathcal{H}}_{te} N}{\omega} \\ \hat{\xi}_{sh} & \hat{\xi}_{te} & \hat{\xi}_{sh} & \hat{\xi}_{te} \\ 1 & 1 & 1 & 1 \\ \frac{\tilde{\mathcal{H}}_{sh}}{\omega} \frac{1}{\mu_0} \hat{\xi}_{sh} & \frac{\tilde{\mathcal{H}}_{te}}{\omega} \frac{1}{\mu_0} \hat{\xi}_{te} & -\frac{\tilde{\mathcal{H}}_{sh}}{\omega} \frac{1}{\mu_0} \hat{\xi}_{sh} & -\frac{\tilde{\mathcal{H}}_{te}}{\omega} \frac{1}{\mu_0} \hat{\xi}_{te} \end{pmatrix}. \quad (3-59)$$

The decomposition matrix is found inverting equation 3-59,

$$\tilde{\mathbf{L}}^{-1} = \frac{1}{2(\hat{\xi}_{sh} - \hat{\xi}_{te})} \begin{pmatrix} -\frac{\omega}{\tilde{\mathcal{H}}_{sh}} \frac{\hat{\xi}_{te}}{N} & 1 & -\hat{\xi}_{te} & \frac{\omega}{\tilde{\mathcal{H}}_{sh}} \mu_0 \\ \frac{\omega}{\tilde{\mathcal{H}}_{te}} \frac{\hat{\xi}_{sh}}{N} & -1 & \hat{\xi}_{sh} & -\frac{\omega}{\tilde{\mathcal{H}}_{te}} \mu_0 \\ \frac{\omega}{\tilde{\mathcal{H}}_{sh}} \frac{\hat{\xi}_{te}}{N} & 1 & -\hat{\xi}_{te} & -\frac{\omega}{\tilde{\mathcal{H}}_{sh}} \mu_0 \\ -\frac{\omega}{\tilde{\mathcal{H}}_{te}} \frac{\hat{\xi}_{sh}}{N} & -1 & \hat{\xi}_{sh} & \frac{\omega}{\tilde{\mathcal{H}}_{te}} \mu_0 \end{pmatrix}. \quad (3-60)$$

The decomposition matrix is normalized to the particle velocity  $\tilde{v}_2^s$ . Alternative normalizations, for example power-flux normalization, are discussed by Haartsen [1995]. One-way reciprocity theorems would require power-flux normalization [Wapenaar, 1996] because the one-way formalism has to be energy conservative for reciprocity to hold. We use reciprocity relations based upon the two-way field quantities in  $\tilde{\mathbf{u}}$  and  $\tilde{\mathbf{q}}$  so the normalization of  $\tilde{\mathbf{L}}$  is arbitrary.

The one-way wave vector and one-way source vector are given as

$$\tilde{\mathbf{p}} = \begin{pmatrix} \tilde{p}_{sh}^+ \\ \tilde{p}_{te}^+ \\ \tilde{p}_{sh}^- \\ \tilde{p}_{te}^- \end{pmatrix} \quad \text{and} \quad \tilde{\mathbf{b}} = \begin{pmatrix} \tilde{b}_{sh}^+ \\ \tilde{b}_{te}^+ \\ \tilde{b}_{sh}^- \\ \tilde{b}_{te}^- \end{pmatrix}. \quad (3-61)$$

For the wavefield extrapolator matrix  $\tilde{\mathcal{W}}$  in a homogeneous source-free subdomain we find

$$\tilde{\mathcal{W}}(x_3, x_{3,0}) = \begin{pmatrix} e^{i\tilde{\mathcal{H}}_{sh}^+(x_3-x_{3,0})} & 0 & 0 & 0 \\ 0 & e^{i\tilde{\mathcal{H}}_{te}^+(x_3-x_{3,0})} & 0 & 0 \\ 0 & 0 & e^{i\tilde{\mathcal{H}}_{sh}^-(x_3-x_{3,0})} & 0 \\ 0 & 0 & 0 & e^{i\tilde{\mathcal{H}}_{te}^-(x_3-x_{3,0})} \end{pmatrix}. \quad (3-62)$$

### 3-5 The seismoelectric system in vacuum

The air cannot sustain shear stresses and we neglect pressures. There is no linear seismoelectric coupling in the air and we approximate air by vacuum. The dielectric permittivity is  $\hat{\epsilon} = \epsilon_0$ . There are only two equations left that represent the TE waves in vacuum. The matrix  $\tilde{\mathcal{A}}$  reduces to a  $2 \times 2$  matrix, see Appendix B-4-2. We have the two-way wave equation of the TE system in vacuum as

$$\tilde{\mathbf{q}} = \tilde{\mathcal{A}}\tilde{\mathbf{q}} + \tilde{\mathbf{d}}, \quad (3-63)$$

with

$$\hat{\mathcal{A}} = \begin{pmatrix} 0 & -i\omega\mu_0 \\ -i\omega\epsilon_0 + \frac{ik_1^2}{\omega} \frac{1}{\mu_0} & 0 \end{pmatrix}, \quad (3-64)$$

$$\tilde{\mathbf{q}} = \begin{pmatrix} \tilde{E}_2 \\ -\tilde{H}_1 \end{pmatrix} \quad \text{and} \quad \tilde{\mathbf{d}} = \begin{pmatrix} \tilde{J}_1^{s,m} \\ -\tilde{J}_2^{s,e} \end{pmatrix}. \quad (3-65)$$

#### 3-5-1 Diagonalization in a homogeneous source-free subdomain

We diagonalize the system matrix 3-64 in a homogeneous source-free subdomain

$$\tilde{\mathcal{H}} = \tilde{\mathbf{L}}^{-1} \tilde{\mathcal{A}} \tilde{\mathbf{L}}. \quad (3-66)$$

The zero-eigenvalue problem confirms the velocity of electromagnetic waves

$$\hat{c}_0^2 = \frac{1}{\epsilon_0\mu_0}. \quad (3-67)$$

For the non-zero eigenvalues we find

$$\tilde{\mathcal{H}} = \begin{pmatrix} i\tilde{\mathcal{H}}^+ & 0 \\ 0 & i\tilde{\mathcal{H}}^- \end{pmatrix}. \quad (3-68)$$

The general eigenvalue  $i\tilde{\mathcal{H}}^\pm = \mp i\tilde{\mathcal{H}}$  with  $\tilde{\mathcal{H}} = \sqrt{\frac{\omega^2}{\tilde{\epsilon}_0^2} - k_1^2}$  corresponds to a general eigenvector  $\mathbf{a}^\pm$  given as

$$\tilde{\mathbf{a}}^\pm = \begin{pmatrix} 1 \\ \pm \frac{\tilde{\mathcal{H}}}{\omega} \frac{1}{\mu_0} \end{pmatrix}, \quad (3-69)$$

which has been normalized to the electrical field in the  $x_2$  direction. The different normalization of the eigenvectors in vacuum and in the porous medium is of no consequences as long as we work with composed field quantities. All normalizations are captured in the reflection and transmission relationships as derived in Chapter 4.

For the composition and decomposition matrices  $\tilde{\mathbf{L}}$  and  $\tilde{\mathbf{L}}^{-1}$  of the TE system in vacuum we again choose  $\tilde{\mathbf{L}} = (\tilde{\mathbf{a}}^+, \tilde{\mathbf{a}}^-)$  and find

$$\tilde{\mathbf{L}} = \begin{pmatrix} 1 & 1 \\ \frac{\tilde{\mathcal{H}}}{\omega} \frac{1}{\mu_0} & -\frac{\tilde{\mathcal{H}}}{\omega} \frac{1}{\mu_0} \end{pmatrix} \quad \text{and} \quad \tilde{\mathbf{L}}^{-1} = \frac{1}{2} \begin{pmatrix} 1 & \frac{\omega}{\tilde{\mathcal{H}}} \frac{1}{\mu_0} \\ 1 & -\frac{\omega}{\tilde{\mathcal{H}}} \frac{1}{\mu_0} \end{pmatrix}. \quad (3-70)$$

Application of  $\tilde{\mathbf{L}}^{-1}$  on the field vector  $\tilde{\mathbf{q}}$  and source vector  $\tilde{\mathbf{d}}$ , leads to

$$\tilde{\mathbf{p}} = \begin{pmatrix} \tilde{p}^+ \\ \tilde{p}^- \end{pmatrix} \quad \text{and} \quad \tilde{\mathbf{b}} = \begin{pmatrix} \tilde{b}^+ \\ \tilde{b}^- \end{pmatrix} \quad (3-71)$$

In a homogeneous source-free subdomain we can extrapolate upgoing or downgoing wave-fields with the wavefield extrapolator

$$\tilde{\mathcal{W}}(x_3, x_{3,0}) = \begin{pmatrix} e^{i\tilde{\mathcal{H}}^+(x_3-x_{3,0})} & 0 \\ 0 & e^{i\tilde{\mathcal{H}}^-(x_3-x_{3,0})} \end{pmatrix}. \quad (3-72)$$

# Seismoelectric modeling using reflection formalism.

In this chapter we introduce a reflection formalism for simulation of reflection and transmission experiments in horizontally stratified media. We start by defining local and global reflection matrices and show how the global reflection matrices can be calculated from the local medium parameters. Then we provide a general description of the relationship between upgoing and downgoing waves in a homogeneous, but bounded, subdomain with a source. We also show how the field can be propagated to a neighboring bounded source-free subdomain. In these descriptions we only use medium parameters, local and global reflection matrices, thereby avoiding the use of transmission matrices. The first to give the procedure for the scalar global reflection coefficient of a three layer medium was [Airy \[1833\]](#), this was later written in matrix form. To our knowledge we are the first to extend this procedure to calculate the response of a source buried inside a stack of layers. Examples of seismoelectric responses calculated with the equations derived in this chapter are provided in [Chapter 5](#).

We use a right handed Cartesian coordinate system with  $z$  axis positive downward. Subdomains are labeled  $\mathbb{D}_n$ , with  $n$  denoting the layer number. A subdomain  $\mathbb{D}_n$  is bounded below by interface labeled  $n$ , with  $z$  coordinate  $z_n$ . The upper half-space is vacuum, this subdomain has label  $\mathbb{D}_0$ , the associated pressure-free surface has  $z$  coordinate  $z_0$ . The lower half-space is numbered  $\mathbb{D}_N$ . See [Figure 4-1](#). All derivations are performed in the horizontal wavenumber frequency domain.

### 4-1 Local and global reflection matrices

Our reflection formalism is based upon the use of reflection matrices. The local downgoing reflection matrix of interface  $n$  at depth  $z_n$ , below layer  $n$  and above layer  $n$  is defined as,

$$\tilde{\mathbf{p}}_n^-(z_n) = \tilde{\mathbf{r}}_n^+(z_n)\tilde{\mathbf{p}}_n^+(z_n). \quad (4-1)$$

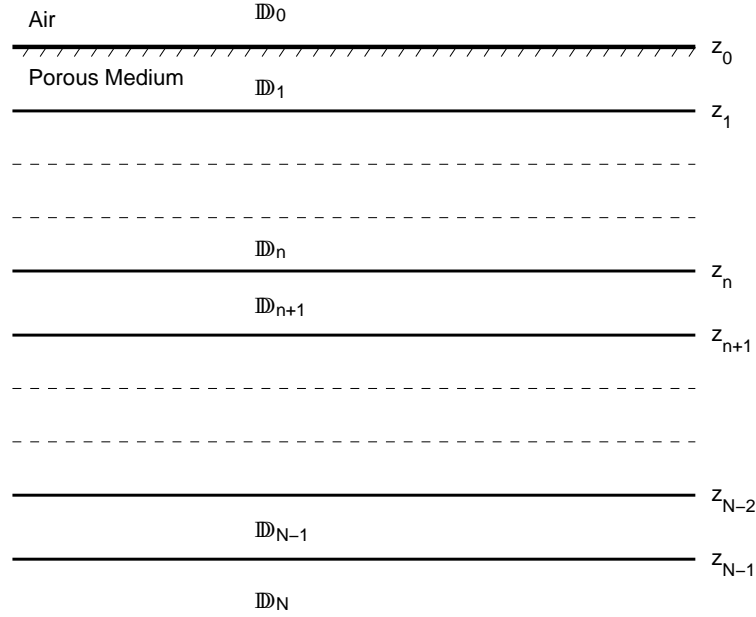


**Figure 4-1:** Layer and interface annotations: Subdomains are labeled  $\mathbb{D}_n$ , with  $n$  denoting the layer number. A subdomain  $\mathbb{D}_n$  is bounded below by interface labeled  $n$ , with  $z$  coordinate  $z_n$ . The upper half-space is vacuum, this subdomain has label  $\mathbb{D}_0$ , the associated pressure-free surface has  $z$  coordinate  $z_0$ . The lower half-space is numbered  $\mathbb{D}_N$ .

The local upgoing reflection matrix of interface  $n - 1$  at depth  $z_{n-1}$ , below layer  $n - 1$  and above layer  $n + 1$  is defined as,

$$\tilde{\mathbf{p}}_n^+(z_{n-1}) = \tilde{\mathbf{r}}_n^-(z_{n-1})\tilde{\mathbf{p}}_n^-(z_{n-1}). \quad (4-2)$$

The  $z$  dependence of the reflection matrices is explicitly mentioned, because these reflection matrices can be extrapolated in homogeneous source-free subdomains to different depth levels where they still connect the same upgoing and downgoing waves. The local reflection matrices strictly only account for one reflection at one interface.

We define a global reflection matrix that accounts for all multiple scattering behind the locally reflecting interface. For the global downgoing reflection matrix we have,

$$\tilde{\mathbf{p}}_n^-(z_n) = \tilde{\mathbf{R}}_n^+(z_n)\tilde{\mathbf{p}}_n^+(z_n), \quad (4-3)$$

and for the global upgoing reflection matrix

$$\tilde{\mathbf{p}}_n^+(z_{n-1}) = \tilde{\mathbf{R}}_n^-(z_{n-1})\tilde{\mathbf{p}}_n^-(z_{n-1}). \quad (4-4)$$

It is important to note that these global reflection matrices include all multiple reflections of the incoming wave. Not included are waves coming from sources below or above the level at which the global downgoing or upgoing reflection matrix is defined. Also excluded are secondary incoming waves. For example, incoming waves that have been reflected by the global downgoing or upgoing reflection matrix defined at a certain reference depth level and that are reflected above or below that certain depth level to return at the reference depth level.

However, all phenomena can be included in the calculations if we follow a certain scheme as outlined in Section 4-6.

In homogeneous source-free subdomains we can extrapolate local or global reflection matrices away from the interface using the extrapolators as defined in equation 3-49. For the incident and reflected wave-fields in the global downgoing reflection matrix 4-3 we have,

$$\tilde{\mathbf{p}}_n^-(z) = \tilde{\mathcal{W}}^-(z, z_n)\tilde{\mathbf{p}}_n^-(z_n), \quad (4-5)$$

$$\tilde{\mathbf{p}}_n^+(z) = \tilde{\mathcal{W}}^+(z, z_n)\tilde{\mathbf{p}}_n^+(z_n). \quad (4-6)$$

Substituting equations 4-5 and 4-6 into equation 4-3 we have

$$\tilde{\mathcal{W}}^-(z, z_n)\tilde{\mathbf{p}}_n^-(z) = \tilde{\mathbf{R}}_n^+(z_n)\tilde{\mathcal{W}}^+(z, z_n)\tilde{\mathbf{p}}_n^+(z). \quad (4-7)$$

We rewrite equation 4-7 making use of the symmetry property of the wavefield extrapolator in equation 3-50, as

$$\tilde{\mathbf{p}}_n^-(z) = \tilde{\mathcal{W}}^+(z_n, z)\tilde{\mathbf{R}}_n^+(z_n)\tilde{\mathcal{W}}^+(z_n, z)\tilde{\mathbf{p}}_n^+(z). \quad (4-8)$$

We recognize that we have for  $\mathbf{R}_n$  at a depth  $z$  in homogeneous subdomain  $\mathbb{D}_n$ ,

$$\tilde{\mathbf{R}}_n^+(z) = \tilde{\mathcal{W}}^+(z_n, z)\tilde{\mathbf{R}}_n^+(z_n)\tilde{\mathcal{W}}^+(z_n, z). \quad (4-9)$$

The result in equation 4-9 shows how a downgoing reflection matrix can be extrapolated in a homogeneous subdomain. For the upgoing reflection matrix in the same layer we can follow a similar derivation and find,

$$\tilde{\mathbf{R}}_n^-(z) = \tilde{\mathcal{W}}^-(z_{n-1}, z)\tilde{\mathbf{R}}_n^-(z_{n-1})\tilde{\mathcal{W}}^-(z_{n-1}, z). \quad (4-10)$$

## 4-2 Calculation of global reflection matrices

We need to calculate the global reflection matrices from the medium parameters in regions outside the layer with the source. To this aim we write the boundary conditions from Section 2-3 of an interface  $n$ ,

$$\lim_{z \downarrow z_n} \tilde{\mathbf{q}}_{n+1}(z) - \lim_{z \uparrow z_n} \tilde{\mathbf{q}}_n(z) = \mathbf{0}. \quad (4-11)$$

The layer  $n + 1$  does not contain a source, thus evaluating the limits we can write,

$$\tilde{\mathbf{q}}_n(z_n) = \tilde{\mathbf{q}}_{n+1}(z_n), \quad (4-12)$$

we substitute  $\tilde{\mathbf{q}}_n = \tilde{\mathbf{L}}\tilde{\mathbf{p}}_n$  and find,

$$\tilde{\mathbf{L}}_n\tilde{\mathbf{p}}_n(z_n) = \tilde{\mathbf{L}}_{n+1}\tilde{\mathbf{p}}_{n+1}(z_n). \quad (4-13)$$

We split the composition matrix  $\tilde{\mathbf{L}}$  into the columns that multiply into  $\tilde{\mathbf{p}}^+$  and that multiply into  $\tilde{\mathbf{p}}^-$  according to,

$$\tilde{\mathbf{L}}_n\tilde{\mathbf{p}}_n(z_n) = \tilde{\mathbf{L}}_n^+\tilde{\mathbf{p}}_n^+(z_n) + \tilde{\mathbf{L}}_n^-\tilde{\mathbf{p}}_n^-(z_n). \quad (4-14)$$

With the definitions of the columns in  $\tilde{\mathbf{L}}$  for the SH-TE system given by the general eigenvector  $\tilde{\mathbf{a}}_n^\pm$  in Section 3-4 we have,

$$\tilde{\mathbf{L}}^+ = (\tilde{\mathbf{a}}_{sh}^+, \tilde{\mathbf{a}}_{te}^+), \quad (4-15)$$

$$\tilde{\mathbf{L}}^- = (\tilde{\mathbf{a}}_{sh}^-, \tilde{\mathbf{a}}_{te}^-). \quad (4-16)$$

The next modification is to rearrange the components of the general eigenvector  $\tilde{\mathbf{a}}_n^\pm$  such that the first two do not change sign for upgoing or downgoing waves and the last two do change their sign,

$$\tilde{\mathbf{a}}^\pm = \begin{pmatrix} \tilde{\mathbf{a}}' \\ \tilde{\mathbf{a}}''^\pm \end{pmatrix}. \quad (4-17)$$

For the SH-TE system we have,

$$\tilde{\mathbf{a}}^\pm = \begin{pmatrix} \tilde{a}_3 \\ \tilde{a}_1 \\ \tilde{a}_2^\pm \\ \tilde{a}_4^\pm \end{pmatrix}. \quad (4-18)$$

These modifications define a composition operator written as,

$$\tilde{\mathbf{L}} = \begin{pmatrix} \tilde{\mathbf{L}}'^+ & \tilde{\mathbf{L}}'^- \\ \tilde{\mathbf{L}}''^+ & \tilde{\mathbf{L}}''^- \end{pmatrix} = \begin{pmatrix} \tilde{\mathbf{L}}'^+ & \tilde{\mathbf{L}}'^+ \\ \tilde{\mathbf{L}}''^+ & -\tilde{\mathbf{L}}''^+ \end{pmatrix}. \quad (4-19)$$

We can omit the superscript  $+$  in the right-hand side of equation 4-19. Implementing this rearrangement into equation 4-13 gives,

$$\tilde{\mathbf{L}}'_n \tilde{\mathbf{p}}_n^+(z_n) + \tilde{\mathbf{L}}'_n \tilde{\mathbf{p}}_n^-(z_n) = \tilde{\mathbf{L}}'_{n+1} \tilde{\mathbf{p}}_{n+1}^+(z_n) + \tilde{\mathbf{L}}'_{n+1} \tilde{\mathbf{p}}_{n+1}^-(z_n), \quad (4-20)$$

$$\tilde{\mathbf{L}}''_n \tilde{\mathbf{p}}_n^+(z_n) - \tilde{\mathbf{L}}''_n \tilde{\mathbf{p}}_n^-(z_n) = \tilde{\mathbf{L}}''_{n+1} \tilde{\mathbf{p}}_{n+1}^+(z_n) - \tilde{\mathbf{L}}''_{n+1} \tilde{\mathbf{p}}_{n+1}^-(z_n). \quad (4-21)$$

Using the definition of the global reflection matrix 4-3 we have,

$$\tilde{\mathbf{p}}_n^-(z_n) = \tilde{\mathbf{R}}_n^+(z_n) \tilde{\mathbf{p}}_n^+(z_n), \quad (4-22)$$

$$\tilde{\mathbf{p}}_{n+1}^-(z_n) = \tilde{\mathbf{R}}_{n+1}^+(z_n) \tilde{\mathbf{p}}_{n+1}^+(z_n), \quad (4-23)$$

substituting 4-22 and 4-23 into equations 4-20 and 4-21 gives,

$$\tilde{\mathbf{L}}'_n \left( \mathbf{I} + \tilde{\mathbf{R}}_n^+(z_n) \right) \tilde{\mathbf{p}}_n^+(z_n) = \tilde{\mathbf{L}}'_{n+1} \left( \mathbf{I} + \tilde{\mathbf{R}}_{n+1}^+(z_n) \right), \quad (4-24)$$

$$\tilde{\mathbf{L}}''_n \left( \mathbf{I} - \tilde{\mathbf{R}}_n^+(z_n) \right) \tilde{\mathbf{p}}_n^+(z_n) = \tilde{\mathbf{L}}''_{n+1} \left( \mathbf{I} - \tilde{\mathbf{R}}_{n+1}^+(z_n) \right). \quad (4-25)$$

Now we can solve for  $\tilde{\mathbf{R}}_n^+(z_n)$  as a function of  $\tilde{\mathbf{R}}_{n+1}^+(z_n)$ . We find,

$$\tilde{\mathbf{R}}_n^+(z_n) = \left[ \left( \tilde{\mathbf{L}}'_n - \tilde{\mathbf{L}}''_n \right) + \left( \tilde{\mathbf{L}}'_n + \tilde{\mathbf{L}}''_n \right) \tilde{\mathbf{R}}_{n+1}^+(z_n) \right] \left[ \left( \tilde{\mathbf{L}}'_n + \tilde{\mathbf{L}}''_n \right) + \left( \tilde{\mathbf{L}}'_n - \tilde{\mathbf{L}}''_n \right) \tilde{\mathbf{R}}_{n+1}^+(z_n) \right]^{-1}, \quad (4-26)$$

where we defined,

$$\tilde{\mathbf{L}}'_n = \left[ \tilde{\mathbf{L}}'_n \right]^{-1} \tilde{\mathbf{L}}'_{n+1}, \quad (4-27)$$

$$\tilde{\mathbf{L}}''_n = \left[ \tilde{\mathbf{L}}''_n \right]^{-1} \tilde{\mathbf{L}}''_{n+1}. \quad (4-28)$$

Note that we have,

$$\tilde{\mathbf{R}}_{n+1}^+(z_n) = \tilde{\mathcal{W}}^+(z_{n+1}, z_n) \tilde{\mathbf{R}}_{n+1}^+(z_{n+1}) \tilde{\mathcal{W}}^+(z_{n+1}, z_n). \quad (4-29)$$

Equation 4-26 is a matrix form of the equation given by Fokkema and Ziolkowski [1987]. With equation 4-26 we can calculate the downgoing global reflection matrix in any layer starting from the bottom interface  $N - 1$ , where  $\tilde{\mathbf{R}}_N^+(z_N) = \mathbf{0}$ . In that case equation 4-26 reduces to an expression for a local reflection matrix of interface  $n$ ,

$$\tilde{\mathbf{r}}_n^+ = \left[ \tilde{\mathbf{L}}_n' - \tilde{\mathbf{L}}_n'' \right] \left[ \tilde{\mathbf{L}}_n' + \tilde{\mathbf{L}}_n'' \right]^{-1}. \quad (4-30)$$

Equation 4-26 can be cast such that we recognise the local reflection matrix, like in the scalar version given by Fokkema and Ziolkowski [1987], we can write,

$$\tilde{\mathbf{R}}_n^+(z_n) = \left[ \tilde{\mathbf{r}}_n^+(z_n) + (\tilde{\mathbf{L}}_n' + \tilde{\mathbf{L}}_n'') \tilde{\mathbf{R}}_{n+1}^+ (\tilde{\mathbf{L}}_n' + \tilde{\mathbf{L}}_n'')^{-1} \right] \left[ \mathbf{I} + (\tilde{\mathbf{L}}_n' - \tilde{\mathbf{L}}_n'') \tilde{\mathbf{R}}_{n+1}^+ (\tilde{\mathbf{L}}_n' + \tilde{\mathbf{L}}_n'')^{-1} \right]^{-1}. \quad (4-31)$$

To calculate the upgoing global reflection matrix, we simply switch the geometry vertically and start our recursion formula with the local upgoing reflection matrix of the pressure-free surface.

### 4-3 Homogeneous bounded subdomain with sources

In a homogeneous layer  $n$  we have a source at source level  $z_s$ , which does not coincide with the interfaces bounding the layer. We need to distinguish between the wave fields above the source level with superscript  $a$  and below the source level with superscript  $b$ . The upper bounding interface is at  $z = z_{n-1}$  and the lower bounding interface at  $z = z_n$ .

From the boundary condition equation 2-51 in Section 2-3 we have,

$$\lim_{z \downarrow z_s} \tilde{\mathbf{q}}_n^b(z) - \lim_{z \uparrow z_s} \tilde{\mathbf{q}}_n^a(z) = \tilde{\mathbf{d}}(z_s). \quad (4-32)$$

If we now apply the decomposition operator  $\tilde{\mathbf{L}}_n$  to the two-way fields in equation 4-32, we find the jump condition in one-way wave quantities. Substitute  $\tilde{\mathbf{q}}_n = \tilde{\mathbf{L}}_n \tilde{\mathbf{p}}_n$  and  $\tilde{\mathbf{d}} = \tilde{\mathbf{L}}_n \tilde{\mathbf{b}}$  into 4-32 and evaluate at the limits. We arrive at,

$$\tilde{\mathbf{L}}_n \tilde{\mathbf{p}}_n^b(z_s) - \tilde{\mathbf{L}}_n \tilde{\mathbf{p}}_n^a(z_s) = \tilde{\mathbf{L}}_n \tilde{\mathbf{b}}(z_s). \quad (4-33)$$

If we divide  $\tilde{\mathbf{L}}_n$  out of the equation, we arrive at two relationships between  $\tilde{\mathbf{p}}_n^{a,+}$ ,  $\tilde{\mathbf{p}}_n^{a,-}$ ,  $\tilde{\mathbf{p}}_n^{b,+}$  and  $\tilde{\mathbf{p}}_n^{b,-}$  as a function of the decomposed source terms  $\tilde{\mathbf{b}}^+$  and  $\tilde{\mathbf{b}}^-$  at  $z_s$ ,

$$\tilde{\mathbf{p}}_n^{b,+}(z_s) = \tilde{\mathbf{p}}_n^{a,+}(z_s) + \tilde{\mathbf{b}}^+(z_s), \quad (4-34)$$

$$\tilde{\mathbf{p}}_n^{b,-}(z_s) = \tilde{\mathbf{p}}_n^{a,-}(z_s) + \tilde{\mathbf{b}}^-(z_s), \quad (4-35)$$

together with the definitions for the global upgoing and downgoing reflection matrices,

$$\tilde{\mathbf{p}}_n^{b,-}(z_s) = \tilde{\mathbf{R}}_n^+(z_s) \tilde{\mathbf{p}}_n^{b,+}(z_s), \quad (4-36)$$

$$\tilde{\mathbf{p}}_n^{a,+}(z_s) = \tilde{\mathbf{R}}_n^-(z_s) \tilde{\mathbf{p}}_n^{a,-}(z_s). \quad (4-37)$$

We defined  $\tilde{\mathbf{R}}_n^+$  and  $\tilde{\mathbf{R}}_n^-$  under and above the source level, respectively, they cannot be extrapolated across the source level using equations 4-9 and 4-10. We can solve this system for  $\tilde{\mathbf{p}}_n^{b,-}$ ,  $\tilde{\mathbf{p}}_n^{b,+}$ ,  $\tilde{\mathbf{p}}_n^{a,-}$  and  $\tilde{\mathbf{p}}_n^{a,+}$ , this gives

$$\tilde{\mathbf{p}}_n^{b,-}(z_s) = \left[ \mathbf{I} - \tilde{\mathbf{R}}_n^+(z_s)\tilde{\mathbf{R}}_n^-(z_s) \right]^{-1} \left[ \tilde{\mathbf{R}}_n^+(z_s)\tilde{\mathbf{b}}^+ - \tilde{\mathbf{R}}_n^+(z_s)\tilde{\mathbf{R}}_n^-(z_s)\tilde{\mathbf{b}}^- \right], \quad (4-38)$$

$$\tilde{\mathbf{p}}_n^{b,+}(z_s) = \left[ \mathbf{I} - \tilde{\mathbf{R}}_n^-(z_s)\tilde{\mathbf{R}}_n^+(z_s) \right]^{-1} \left[ \tilde{\mathbf{b}}^+ - \tilde{\mathbf{R}}_n^-(z_s)\tilde{\mathbf{b}}^- \right], \quad (4-39)$$

$$\tilde{\mathbf{p}}_n^{a,-}(z_s) = \left[ \mathbf{I} - \tilde{\mathbf{R}}_n^+(z_s)\tilde{\mathbf{R}}_n^-(z_s) \right]^{-1} \left[ \tilde{\mathbf{R}}_n^+(z_s)\tilde{\mathbf{b}}^+ - \tilde{\mathbf{b}}^- \right], \quad (4-40)$$

$$\tilde{\mathbf{p}}_n^{a,+}(z_s) = \left[ \mathbf{I} - \tilde{\mathbf{R}}_n^-(z_s)\tilde{\mathbf{R}}_n^+(z_s) \right]^{-1} \left[ \tilde{\mathbf{R}}_n^-(z_s)\tilde{\mathbf{R}}_n^+(z_s)\tilde{\mathbf{b}}^+ - \tilde{\mathbf{R}}_n^-(z_s)\tilde{\mathbf{b}}^- \right]. \quad (4-41)$$

Note that equations 4-38 and 4-39 satisfy equation 4-36 and equations 4-40 and 4-41 satisfy equation 4-37. This set provides the basis of our modeling schemes that incorporate multiple scattering.

#### 4-4 Determination of the wave fields outside the source layer

We need an equation that relates the upgoing and downgoing wave field amplitudes in two adjacent layers  $n$  and  $n+1$  that can be used to propagate known wave field amplitudes in layer  $n$  across interface  $n$  to layer  $n+1$ . Following the same procedure as in previous Section 4-2, we start from the boundary condition at a source-free interface below the source level,

$$\lim_{z \downarrow z_n} \tilde{\mathbf{q}}_{n+1}(z) - \lim_{z \uparrow z_n} \tilde{\mathbf{q}}_n(z) = \mathbf{0}. \quad (4-42)$$

Again we substitute  $\tilde{\mathbf{q}}_n = \tilde{\mathbf{L}}\tilde{\mathbf{p}}_n$  into the boundary condition, and we evaluate the limits,

$$\tilde{\mathbf{L}}_{n+1}\tilde{\mathbf{p}}_{n+1}(z_n) = \tilde{\mathbf{L}}_n\tilde{\mathbf{p}}_n(z_n). \quad (4-43)$$

We reverse the left-hand and right-hand sides of this equation, and use the re-arranged composition matrix  $\tilde{\mathbf{L}}$  given in equation 4-19 to split the equation. We need only one of the resulting two equations,

$$\tilde{\mathbf{L}}'_n\tilde{\mathbf{p}}_n^+(z_n) + \tilde{\mathbf{L}}'_n\tilde{\mathbf{p}}_n^-(z_n) = \tilde{\mathbf{L}}'_{n+1}\tilde{\mathbf{p}}_{n+1}^+(z_n) + \tilde{\mathbf{L}}'_{n+1}\tilde{\mathbf{p}}_{n+1}^-(z_n). \quad (4-44)$$

We solve this equation for  $\tilde{\mathbf{p}}_{n+1}^+(z_n)$  making use of the definition of  $\tilde{\mathbf{L}}'_n$  in equation 4-27. We find

$$\tilde{\mathbf{p}}_{n+1}^+(z_n) = \left[ \mathbf{I} + \tilde{\mathbf{R}}_{n+1,N}^+(z_n) \right]^{-1} \left[ \tilde{\mathbf{L}}'_n \right]^{-1} \left[ \mathbf{I} + \tilde{\mathbf{R}}_{n,N}^+(z_n) \right] \tilde{\mathbf{p}}_n^+(z_n). \quad (4-45)$$

Note again that we have

$$\tilde{\mathbf{R}}_{n+1}^+(z_n) = \tilde{\mathbf{W}}^+(z_{n+1}, z_n)\tilde{\mathbf{R}}_{n+1}^+(z_{n+1})\tilde{\mathbf{W}}^+(z_{n+1}, z_n). \quad (4-46)$$

Equation 4-45 can be used to propagate a known downgoing wave field amplitude across an interface. To obtain the upgoing wave field in the next layer we simply use the global reflection matrix in that layer according to,

$$\tilde{\mathbf{p}}_{n+1}^-(z_n) = \tilde{\mathbf{R}}_{n+1}^+(z_n)\tilde{\mathbf{p}}_{n+1}^+(z_n), \quad (4-47)$$

with  $\tilde{\mathbf{R}}_{n+1,N}^+(z_n)$  defined in equation 4-46.

## 4-5 Scattering matrix against a pressure-free surface

We approximate the air in the upper half-space of our earths model with vacuum. Only electromagnetic waves propagate in vacuum and there are no seismic waves. Therefore we need a special scattering matrix for the pressure-free surface at  $z = z_0$ . There are two wave types in the vacuum  $\tilde{p}_{0,te}^+$  and  $\tilde{p}_{0,te}^-$ , in the subsurface there are four wave types  $\tilde{p}_{1,sh}^+$ ,  $\tilde{p}_{1,te}^+$ ,  $\tilde{p}_{1,sh}^-$  and  $\tilde{p}_{1,te}^-$ . The scattering matrix is  $3 \times 3$ ,

$$\begin{pmatrix} \tilde{p}_{0,te}^-(z_0) \\ \tilde{p}_{1,sh}^+(z_0) \\ \tilde{p}_{1,te}^+(z_0) \end{pmatrix} = \begin{pmatrix} \tilde{r}_{0,te-te}^+(z_0) & \tilde{t}_{te-sh}^-(z_0) & \tilde{t}_{te-te}^-(z_0) \\ \tilde{t}_{sh-te}^+(z_0) & \tilde{r}_{1,sh-sh}^-(z_0) & \tilde{r}_{1,sh-te}^-(z_0) \\ \tilde{t}_{te-te}^+(z_0) & \tilde{r}_{1,te-sh}^-(z_0) & \tilde{r}_{1,te-te}^-(z_0) \end{pmatrix} \begin{pmatrix} \tilde{p}_{0,te}^+(z_0) \\ \tilde{p}_{1,sh}^-(z_0) \\ \tilde{p}_{1,te}^-(z_0) \end{pmatrix}. \quad (4-48)$$

We ignore the definitions of transmission coefficients and follow [van der Burg \[2002\]](#) and [Shaw \[2004\]](#) to solve for the pressure-free surface local reflection matrix. From Section 2-3-1 we have at the interface of a pressure-free surface,

$$\begin{pmatrix} 0 \\ \tilde{E}_2 \\ -\tilde{H}_1 \end{pmatrix}_{air} = \begin{pmatrix} \tilde{\tau}_{23}^b \\ \tilde{E}_2 \\ -\tilde{H}_1 \end{pmatrix}_{subsurface}. \quad (4-49)$$

If we want to compose these from the one-way wave types that exist in the vacuum and in the subsurface we write,

$$\begin{pmatrix} 0 & 0 \\ \tilde{a}_{0,te,1}^+ & \tilde{a}_{0,te,1}^- \\ \tilde{a}_{0,te,2}^+ & \tilde{a}_{0,te,2}^- \end{pmatrix} \begin{pmatrix} \tilde{p}_{0,te}^+(z_0) \\ \tilde{p}_{0,te}^-(z_0) \end{pmatrix} = \begin{pmatrix} \tilde{a}_{1,sh,1}^+ & \tilde{a}_{1,te,1}^+ & \tilde{a}_{1,sh,1}^- & \tilde{a}_{1,te,1}^- \\ \tilde{a}_{1,sh,2}^+ & \tilde{a}_{1,te,2}^+ & \tilde{a}_{1,sh,2}^- & \tilde{a}_{1,te,2}^- \\ \tilde{a}_{1,sh,4}^+ & \tilde{a}_{1,te,4}^+ & \tilde{a}_{1,sh,4}^- & \tilde{a}_{1,te,4}^- \end{pmatrix} \begin{pmatrix} \tilde{p}_{1,sh}^+(z_0) \\ \tilde{p}_{1,te}^+(z_0) \\ \tilde{p}_{1,sh}^-(z_0) \\ \tilde{p}_{1,te}^-(z_0) \end{pmatrix}, \quad (4-50)$$

where  $\tilde{a}_{0,te,i}^\pm$  is given by  $\mathbf{a}_{te}^\pm$  in equation 3-69 and  $\tilde{a}_{1,w,i}^\pm$  is given by  $\mathbf{a}_w^\pm$  in equation 3-57. Equation 4-50 is rearranged to mimic equation 4-48,

$$\begin{pmatrix} 0 & \tilde{a}_{1,sh,1}^+ & \tilde{a}_{1,te,1}^+ \\ -\tilde{a}_{0,te,1}^- & \tilde{a}_{1,sh,2}^+ & \tilde{a}_{1,te,2}^+ \\ -\tilde{a}_{0,te,2}^- & \tilde{a}_{1,sh,4}^+ & \tilde{a}_{1,te,4}^+ \end{pmatrix} \begin{pmatrix} \tilde{p}_{0,te}^-(z_0) \\ \tilde{p}_{1,sh}^+(z_0) \\ \tilde{p}_{1,te}^+(z_0) \end{pmatrix} = \begin{pmatrix} 0 & -\tilde{a}_{1,sh,1}^- & -\tilde{a}_{1,te,1}^- \\ \tilde{a}_{0,te,1}^+ & -\tilde{a}_{1,sh,2}^- & -\tilde{a}_{1,te,2}^- \\ \tilde{a}_{0,te,2}^+ & -\tilde{a}_{1,sh,4}^- & -\tilde{a}_{1,te,4}^- \end{pmatrix} \begin{pmatrix} \tilde{p}_{0,te}^+(z_0) \\ \tilde{p}_{1,sh}^-(z_0) \\ \tilde{p}_{1,te}^-(z_0) \end{pmatrix}. \quad (4-51)$$

Using the results of [van der Burg \[2002\]](#), we perform a division with the matrix in the left-hand side of equation 4-51, we find for the upgoing reflection matrix

$$\tilde{r}_{0,sh-sh}^- = \frac{1}{\underline{\Lambda}} \left( \tilde{\mathcal{H}}_{1,sh} \left( \tilde{\mathcal{H}}_{1,te} + \tilde{\mathcal{H}}_{0,te} \right) \hat{\xi}_{te} - \tilde{\mathcal{H}}_{1,te} \left( \tilde{\mathcal{H}}_{1,sh} - \tilde{\mathcal{H}}_{0,te} \right) \hat{\xi}_{sh} \right), \quad (4-52)$$

$$\tilde{r}_{0,sh-te}^- = \frac{1}{\underline{\Lambda}} \left( \tilde{\mathcal{H}}_{1,te} \left( \tilde{\mathcal{H}}_{1,te} + \tilde{\mathcal{H}}_{0,te} \right) \hat{\xi}_{te} - \tilde{\mathcal{H}}_{1,te} \left( \tilde{\mathcal{H}}_{1,te} - \tilde{\mathcal{H}}_{0,te} \right) \hat{\xi}_{te} \right), \quad (4-53)$$

$$\tilde{r}_{0,te-sh}^- = \frac{1}{\underline{\Lambda}} \left( \tilde{\mathcal{H}}_{1,sh} \left( \tilde{\mathcal{H}}_{1,sh} - \tilde{\mathcal{H}}_{0,te} \right) \hat{\xi}_{sh} - \tilde{\mathcal{H}}_{1,sh} \left( \tilde{\mathcal{H}}_{1,sh} + \tilde{\mathcal{H}}_{0,te} \right) \hat{\xi}_{sh} \right), \quad (4-54)$$

$$\tilde{r}_{0,te-te}^- = \frac{1}{\underline{\Lambda}} \left( \tilde{\mathcal{H}}_{1,sh} \left( \tilde{\mathcal{H}}_{1,te} - \tilde{\mathcal{H}}_{0,te} \right) \hat{\xi}_{te} - \tilde{\mathcal{H}}_{1,te} \left( \tilde{\mathcal{H}}_{1,sh} + \tilde{\mathcal{H}}_{0,te} \right) \hat{\xi}_{sh} \right), \quad (4-55)$$

where

$$\underline{\Lambda} = \tilde{\mathcal{H}}_{1,sh}\hat{\xi}_{te} \left( \tilde{\mathcal{H}}_{1,sh} + \tilde{\mathcal{H}}_{0,te} \right) - \tilde{\mathcal{H}}_{1,te}\hat{\xi}_{sh} \left( \tilde{\mathcal{H}}_{1,sh} + \tilde{\mathcal{H}}_{0,te} \right). \quad (4-56)$$

The first subscript of the operator  $\tilde{\mathcal{H}}$  denotes the layer under consideration. For example,  $\tilde{\mathcal{H}}_{1,w}$  is the square root operator for wavetype  $w$  in the first subsurface layer, while  $\tilde{\mathcal{H}}_{0,w}$  is the square root operator for wavetype  $w$  in the vacuum. The upgoing local reflection matrix at the pressure-free surface that initializes the recursive scheme for upgoing global reflection matrices in the stack of layers is given in equations 4-55, 4-54, 4-53 and 4-52.

## 4-6 Seismoelectric modeling scheme

Our seismoelectric simulation scheme is based upon the building blocks derived in this chapter. The first step is to calculate the global reflection matrices at the boundaries of the source layer. This is done iteratively, using equation 4-26 or 4-31, starting from the local reflection matrices at the outer interfaces. For the scattering matrix of the pressure-free surface we use the equations of Section 4-5. In step two we use equation 4-39 or 4-40 in Section 4-3 to calculate the wavefield in the source layer. We need the wavefield in the direction of the receiver, at the same side of the source level as the receiver level. Step three is to propagate the wavefield across the interfaces until we reach the receiver layer, this is done as a function of the global reflection matrices that we have already calculated in step one. The wavefield in the receiver layer is completely determined by reflecting the wavefield once, such that we have both upgoing and downgoing components. A schematic overview of the path of calculation is given in Figure 4-2.

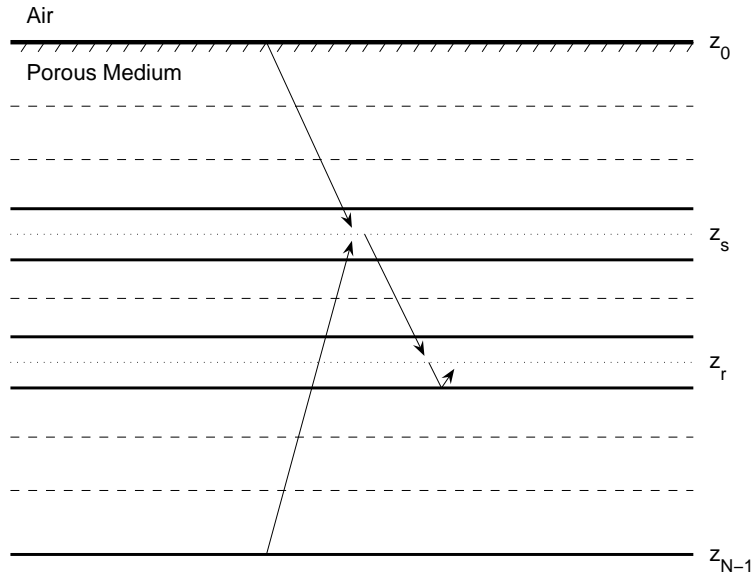


**Figure 4-2:** Calculation scheme of the seismoelectric responses of a source buried in a layered medium. Step 1; iteratively calculate the global reflection matrices, from the outer interfaces up to the source layer. Step 2; solve the wavefield inside the source layer. Step 3; iteratively propagate the known field from the source layer to the receiver layer. Step 4; solve the field inside the receiver layer.

# Examples of seismoelectric simulations in 2D

In this chapter we give several examples of seismoelectric simulations using the one-way wave equations of Chapter 3 and the reflection formalism of Chapter 4. We have an exact solution in the frequency-wavenumber domain, that we compute on a discretised grid and transform numerically to the time-space domain. When we discretise the wavenumber-frequency grid, we discretise the source, and introduce a periodicity in the time-space solution. After describing how we use Matlab's  $[\mathbf{X}] = \text{fft}(\mathbf{x})$  and  $[\mathbf{x}] = \text{ifft}(\mathbf{X})$  functions to perform discrete Fourier transformations, we describe the causality trick that damps the introduced periodicity in time. In the next section we introduce the media types used throughout this thesis. In the last section we show the results of a transmission experiment in a homogeneous medium. The results of a reflection and transmission experiment in a more complex medium containing two interfaces, the upper half-space being air approximated by vacuum and the lower half-space being a porous medium.

## 5-1 Numerical implementation

### 5-1-1 Discrete Fourier transformations

We start from exact relations in the horizontal wavenumber frequency domain as defined by equations 1-2 and 1-4. To transform back to the space-time domain we need to employ equations 1-3 and 1-5. However, we compute the solution along a discrete time and space axes defined by,

$$\mathbf{t} = [-NT : NT - 1] \Delta t, \quad (5-1)$$

$$\mathbf{x} = [-NX : NX - 1] \Delta x. \quad (5-2)$$

Correspondingly, the angular frequency and wavenumber axes are also discretised,

$$\underline{\omega} = [-NT : NT - 1] \Delta\omega, \quad (5-3)$$

$$\underline{\mathbf{k}} = [-NX : NX - 1] \Delta x. \quad (5-4)$$

If we substitute equations 5-1, 5-2, 5-3 and 5-4 into our definitions of the Fourier transformations 1-2 and 1-3 and replace the integrals by summations over frequencies and times,  $t_n = n\Delta t$ ,  $\omega_m = m\Delta\omega$ ,  $\hat{f}(\mathbf{x}, f) \rightarrow \hat{\underline{\mathbf{f}}}_m(\mathbf{x})$  and  $f(\mathbf{x}, t) \rightarrow \underline{\mathbf{f}}_n(\mathbf{x})$  we arrive at

$$\hat{\underline{\mathbf{f}}}_m(\mathbf{x}) = \sum_{n=-NT}^{NT-1} \underline{\mathbf{f}}_n(\mathbf{x}) e^{-i(\Delta\omega\Delta t n m) \Delta t}, \quad (5-5)$$

$$\underline{\mathbf{f}}_n(\mathbf{x}) = \frac{1}{2\pi} \sum_{m=-NT}^{NT-1} \hat{\underline{\mathbf{f}}}_m(\mathbf{x}) e^{i(\Delta\omega\Delta t n m) \Delta\omega}. \quad (5-6)$$

Note that we only discretise the time and frequency axes at this point. It is easy to see that the periodicity of the Fourier kernel is  $\Delta\omega\Delta t = \frac{2\pi}{2NT}$ . We also have that the angular frequency is linked to the frequency through  $\omega = 2\pi f$  (with  $f$  the frequency in Hz), so we have  $\Delta\omega = 2\pi\Delta f$ . In Matlab, we cannot use an index to an array that is negative or zero. We first rearrange the summation to run from 0 to  $2\pi$ , in stead of from  $-\pi$  to  $\pi$  used in 5-5 and 5-6, by replacing the negative counters with  $m = 2NT + [-NT : -1 : -1]$  and then we add one to the index counters. Changing the range from  $-\pi$  to  $\pi$  into 0 to  $2\pi$ , and the reverse, is performed by the standard Matlab functions  $[\mathbf{X}] = \text{fftshift}(\mathbf{x})$  and  $[\mathbf{x}] = \text{ifftshift}(\mathbf{X})$ . We arrive at

$$\hat{\underline{\mathbf{f}}}_m(\mathbf{x}) = \Delta t \sum_{n=1}^{2NT} \underline{\mathbf{f}}_n(\mathbf{x}) e^{-i\frac{2\pi}{2NT}(n-1)(m-1)}, \quad (5-7)$$

$$\underline{\mathbf{f}}_n(\mathbf{x}) = \Delta f \sum_{m=1}^{2NT} \hat{\underline{\mathbf{f}}}_m(\mathbf{x}) e^{i\frac{2\pi}{2NT}(n-1)(m-1)}. \quad (5-8)$$

We employ Matlab's  $[\mathbf{X}] = \text{fft}(\mathbf{x})$  and  $[\mathbf{x}] = \text{ifft}(\mathbf{X})$  functions, they perform a transformation of vectors with length  $N$  of the form

$$X(k) = \sum_{j=1}^N x(j) e^{(-2\pi i/N)(j-1)(k-1)}, \quad (5-9)$$

$$x(j) = \frac{1}{N} \sum_{k=1}^N X(k) e^{(2\pi i/N)(j-1)(k-1)}. \quad (5-10)$$

If we apply the  $[\mathbf{x}] = \text{ifft}(\mathbf{X})$  transformation to our exact solution in the frequency domain, we have  $N_t = 2NT = \frac{1}{\Delta t \Delta f}$  and we need to apply an amplitude correction to the function output. We match the temporal Fourier transformation 5-7 to the transformation performed by  $[\mathbf{x}] = \text{ifft}(\mathbf{X})$  by defining  $\hat{\underline{\mathbf{f}}}' = \frac{\hat{\underline{\mathbf{f}}}}{\Delta t}$ . This means we have to scale the function return by  $\frac{1}{\Delta t}$ . Since we use only positive frequencies, we have to padd our array with zeros in the negative frequencies and multiply the return of  $\text{ifft}(\mathbf{X})$  by 2 according to equation 1-6. A similar argument can be made for the spatial Fourier transformation. However, because of the different sign convention we employ  $[\mathbf{x}] = \text{fft}(\mathbf{X})$  to transform back to the space domain. Hence we need to perform an amplitude correction  $\frac{\Delta k}{2\pi}$ .

### 5-1-2 Causality trick

If we discretise the solution in the wavenumber-frequency domain, we introduce a periodicity in the source position in the space-time domain window. This means that events leaving at the maximum positive recording times return in the solution after traveling through the negative times. Events leaving the window at maximum offset continue in the negative offsets. This wrapping effect can be seen in Figure 5-1(a), where we see the response of a  $f_2^b$  source recorded by a  $v_2^s$  receiver-line after it is propagated over a distance of 150 m. There exists an exact trick that damps the anti-causal events in our space-time window. We add a small

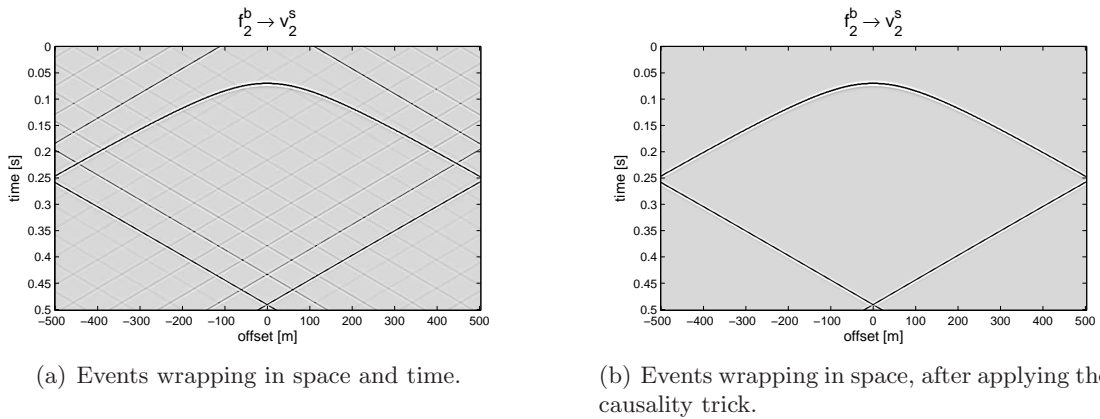


**Figure 5-1:** Wrapping effects in (a) and the results of applying the causality trick in (b).

negative imaginary number to our real frequency array. Using complex frequencies means that we have a Fourier transformed equivalent of a time function multiplied with a damping exponential in time (black curve in Figure 5-2). The damping factor is equal to the imaginary frequency value. The anti-causal events are damped twice, before they reoccur in the positive time window. We multiply our time domain return of the discrete Fourier transformation by a growing exponential (blue curve in Figure 5-2) that undoes the effect of the damping that we introduced in the frequency domain on the causal events (red curve in Figure 5-2). Note that the curves in Figure 5-2 only show the first order wrap around, the higher order wrap arounds are damped even stronger. We can get rid of the wrapping in space by choosing a space interval large enough to encompass the first arrivals in the time interval.

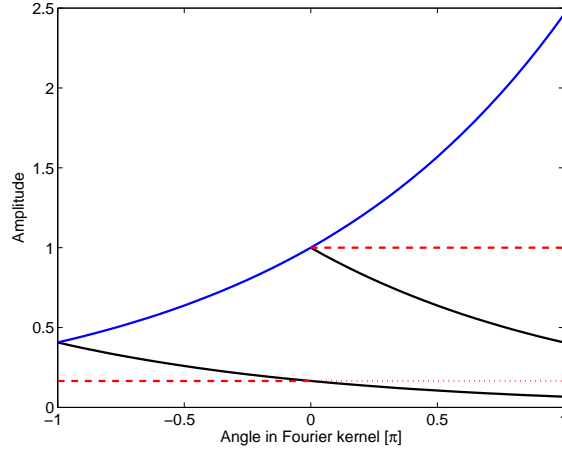


**Figure 5-2:** Exponentials in the causality trick: Black curve: damped exact solution in the frequency domain. Blue curve: growing exponential to correct for the damping. Red Curve: result after correcting for the damping.

## 5-2 Medium parameters for medium type A and B

Throughout this thesis we make use of two sets of medium parameters, sets A and B. These are the same two media types as used by Shaw [2004]. In both media the seismoelectric coupling is present, but in medium B this coupling is considerably higher than in medium A. In Table 5-1 we list the properties of the two medium types.

**Table 5-1:** Medium characteristics of two porous media.

Parameters	Symbol	Medium A	Medium B
Porosity	$\phi$	40 %	20 %
Fluid density	$\rho^f$	1000 kg m <sup>-3</sup>	1000 kg m <sup>-3</sup>
Solid density	$\rho^s$	2700 kg m <sup>-3</sup>	2700 kg m <sup>-3</sup>
Bulk Modulus of the solid	$K^s$	4 · 10 <sup>10</sup> N m <sup>-2</sup>	4 · 10 <sup>10</sup> N m <sup>-2</sup>
Bulk Modulus of the fluid	$K^f$	2.2 · 10 <sup>9</sup> N m <sup>-2</sup>	2.2 · 10 <sup>9</sup> N m <sup>-2</sup>
Bulk Modulus of the framework	$K^{fr}$	4 · 10 <sup>9</sup> N m <sup>-2</sup>	4 · 10 <sup>9</sup> N m <sup>-2</sup>
Shear Modulus of the framework	N	9 · 10 <sup>9</sup> N m <sup>-2</sup>	9 · 10 <sup>9</sup> N m <sup>-2</sup>
Viscosity	$\eta$	10 <sup>-3</sup> N s m <sup>-2</sup>	10 <sup>-3</sup> N s m <sup>-2</sup>
Relative permittivity of the solid	$\epsilon^s$	4 F m <sup>-1</sup>	4 F m <sup>-1</sup>
Relative permittivity of the fluid	$\epsilon^f$	80 F m <sup>-1</sup>	80 F m <sup>-1</sup>
Tortuosity	$\alpha_\infty$	3	3
Similarity parameter	m	8	8
Electrolyte concentration	C	10 <sup>-6</sup> Mol l <sup>-1</sup>	10 <sup>-2</sup> Mol l <sup>-1</sup>
Electrolyte		NaCl	NaCl
Ion mobility <sup>1</sup>	$b_l$	$Na^+$ 5.2 · 10 <sup>-8</sup> m s <sup>-1</sup> N <sup>-1</sup>	$Cl^-$ 7.9 · 10 <sup>-8</sup> m s <sup>-1</sup> N <sup>-1</sup>

<sup>1</sup>from Nabighian and Corbett [1987]

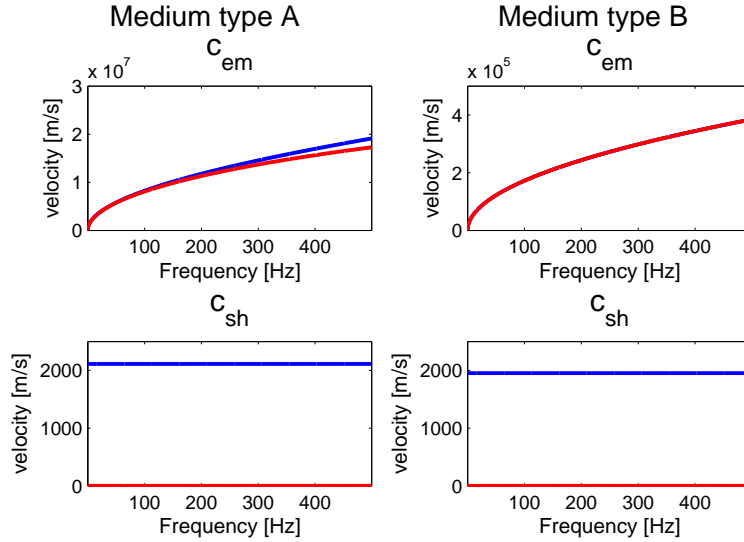


**Figure 5-3:** Real (blue curves) and imaginary (red curves) parts of the wave velocities. The real and imaginary parts of the electromagnetic wave speed in medium B overlap.

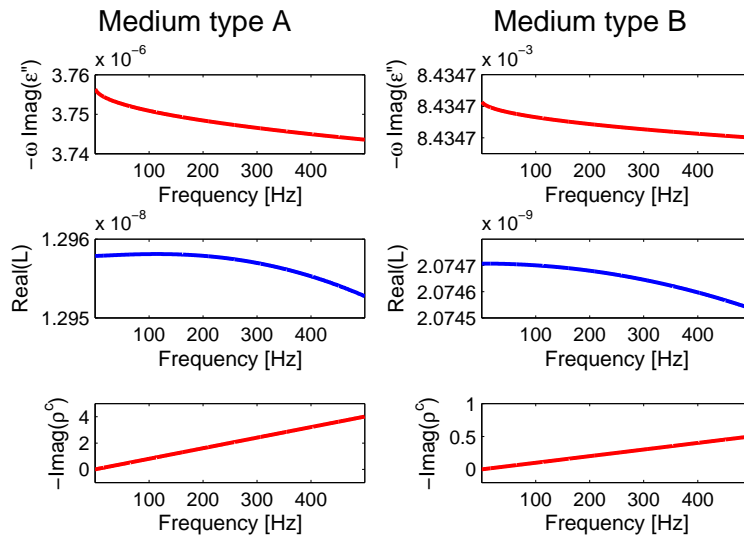


**Figure 5-4:** Loss functions appearing in Sections 7-4 and 7-8; imaginary parts of  $\hat{\epsilon}$  and  $\hat{\rho}^c$ , real part of  $\hat{\mathcal{L}}$ .

Medium type A corresponds to a clean sandstone, with 40% porosity, containing clean water with a very low salinity. Medium type B corresponds to the same type of sandstone, but with a porosity of 20% containing a *NaCl* brine of  $10^{-2}$  [Mol/l] (a concentration of 584 [mg/l]). We use equation 3-55 to compute the wave velocities of electromagnetic waves and seismic waves. In Figure 5-3 we plot the real (in blue) and imaginary parts (in red). Note how the shear waves have a small imaginary part, but the electromagnetic waves have comparable real and imaginary parts, implying the strong diffusive character of the electromagnetic field.

The dispersion of shear waves is a little higher in medium type A than in medium type B. In Figure 5-4 we plot the loss terms in the SH-TE system that appear in the interferometric Green's function representations of Sections 7-4 and 7-8. We only plot the parts that act as losses in the volume integrals 7-15 and 7-43, the imaginary parts of  $\hat{\epsilon}$  and  $\hat{\rho}^c$  and the real part of  $\hat{\mathcal{L}}$ .

### 5-2-1 Reflection matrices

To complete the characteristics of the medium parameters we show the reflection matrices that occur for the geometries of this thesis, using equation 4-30 to compute the local reflection matrix. In figures 5-5 and 5-6 we give the reflection matrices of the interface between medium type A and medium type B approached from both sides.

The amplitude of the reflection coefficient is plotted versus the ray parameter times the absolute wave velocity of the incident wave. There exists a very simple relationship between ray parameter and horizontal wavenumber, given by  $k_1 = \omega p_1$ . The ray parameter is the measure for the direction of propagation of a plane wave, according to

$$p_1 = \frac{\sin(\theta)}{c}, \quad (5-11)$$

where  $\theta$  is the propagation angle and  $c$  is the wave propagation velocity. Note in Figures 5-5 and 5-6 how the conversion from an incident shear wave to an outgoing electromagnetic wave only takes place for very high angles of incidence. While the conversion from an incident electromagnetic wave to an outgoing shear wave takes place for a wide angle of incidents. This effect is even stronger for the reflection against the pressure-free surface interface from below, see figure 5-7. We use the equations of van der Burg [2002] given in Section 4-5 to compute the local upgoing reflection matrix of the pressure-free surface using porous medium type A.

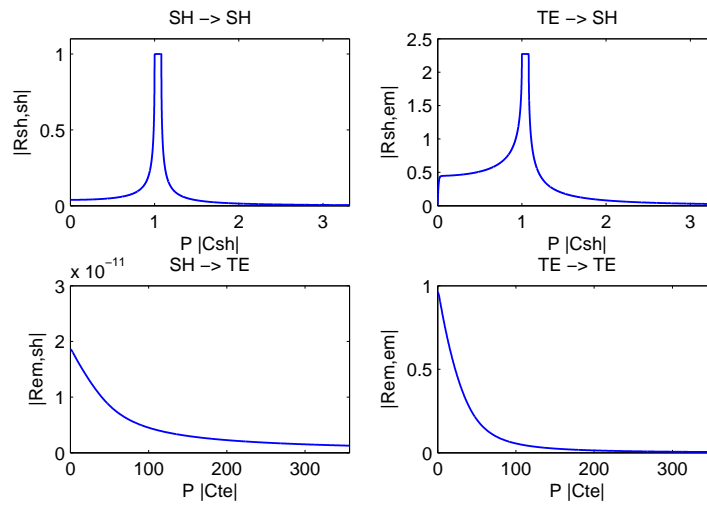


**Figure 5-5:** Reflection matrix, from layer type A against B. Horizontal axis is the ray parameter times the absolute wave velocity of the incident wave, in medium type A.

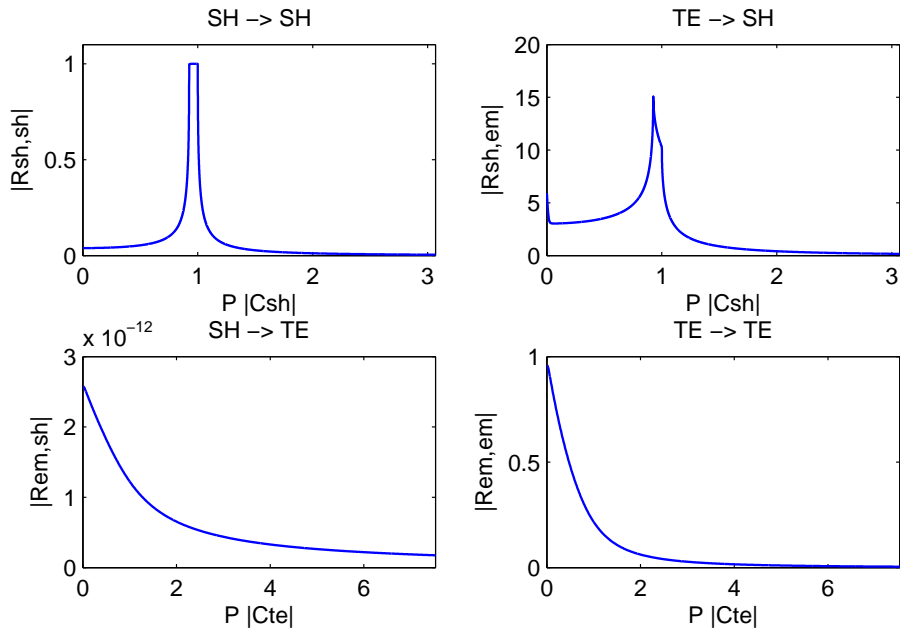


**Figure 5-6:** Reflection matrix, from layer type B against A. Horizontal axis is the ray parameter times the absolute wave velocity of the incident wave, in medium type B.

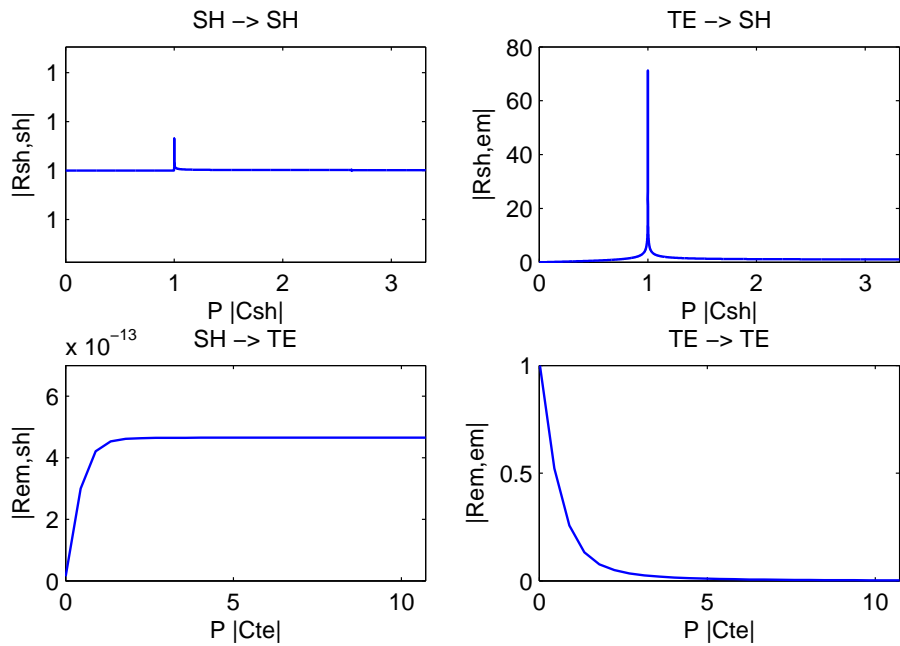


**Figure 5-7:** Pressure-free surface scattering matrix, from layer type A against vacuum.

### 5-3 Reflection and transmission experiments

In this section we show examples of a seismoelectrical experiment to familiarize the reader with the interpretation of electroseismograms. The first example is the simplest case possible; a transmission experiment in a homogeneous medium. We have one source and at a distance of 150 meter we place a line of receivers, see Figure 5-8. Blue rays are shear waves and red rays are electromagnetic waves. We always record two events, event number one, labeled 1, travels with the shear velocity, while event number two, labeled 2, travels with the electromagnetic wave velocity. This means that both electromagnetic and seismic sources emit electromagnetic and shear waves. We use a source that emits a Ricker wavelet  $S^{rw}$ , see equation 5-12, with center angular frequency  $\omega_0$  of 800 Radians, corresponding to approximately 127 Hz. In Figure 5-9 we see the  $x_2$  component of the electric field,  $\hat{E}_2$ , recording as a response of a force source in the  $x_2$  direction,  $\hat{f}_2$ . In Figure 5-10 we see a recording of the  $x_2$  component of the particle velocity in the solid,  $\hat{v}_2^s$ , as a response to an electric current source acting in the  $x_2$  direction,  $\hat{j}_2^e$ . Both events are hyperbolic, however the hyperbolicity of the electromagnetic event is very small due to the velocity of the electromagnetic wave. Thus we see a nearly flat electromagnetic event and a hyperbolic shear wave event.

$$\hat{S}^{rw} = \frac{2}{\sqrt{\pi}} \frac{\omega^2}{\omega_0^3} \exp\left(\frac{-\omega^2}{\omega_0^2}\right). \quad (5-12)$$

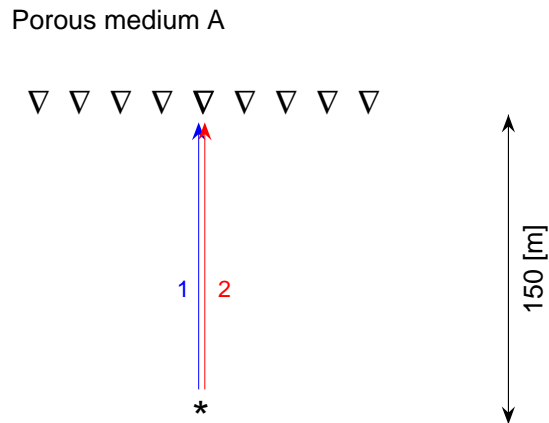


**Figure 5-8:** Experiment geometry of a transmission experiment in a homogeneous medium, 2 events, see text.

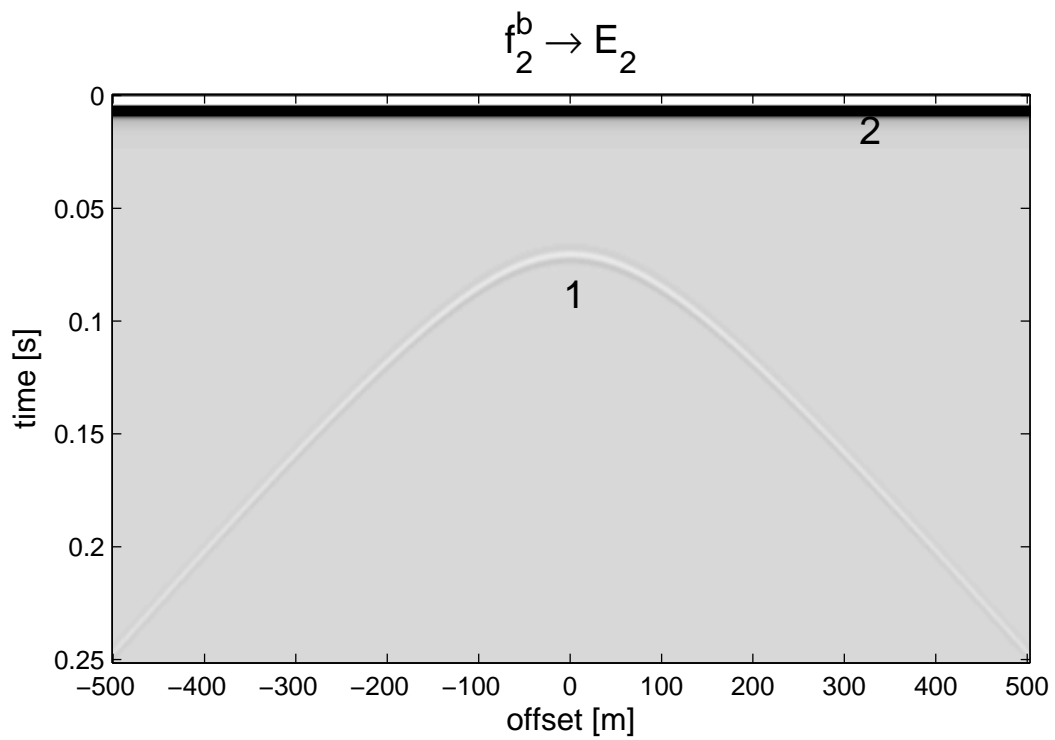


**Figure 5-9:** Transmission experiment in a homogeneous medium  $f_2 \rightarrow E_2$ ; 1: shear wave or co-seismic event, 2: electromagnetic wave event.

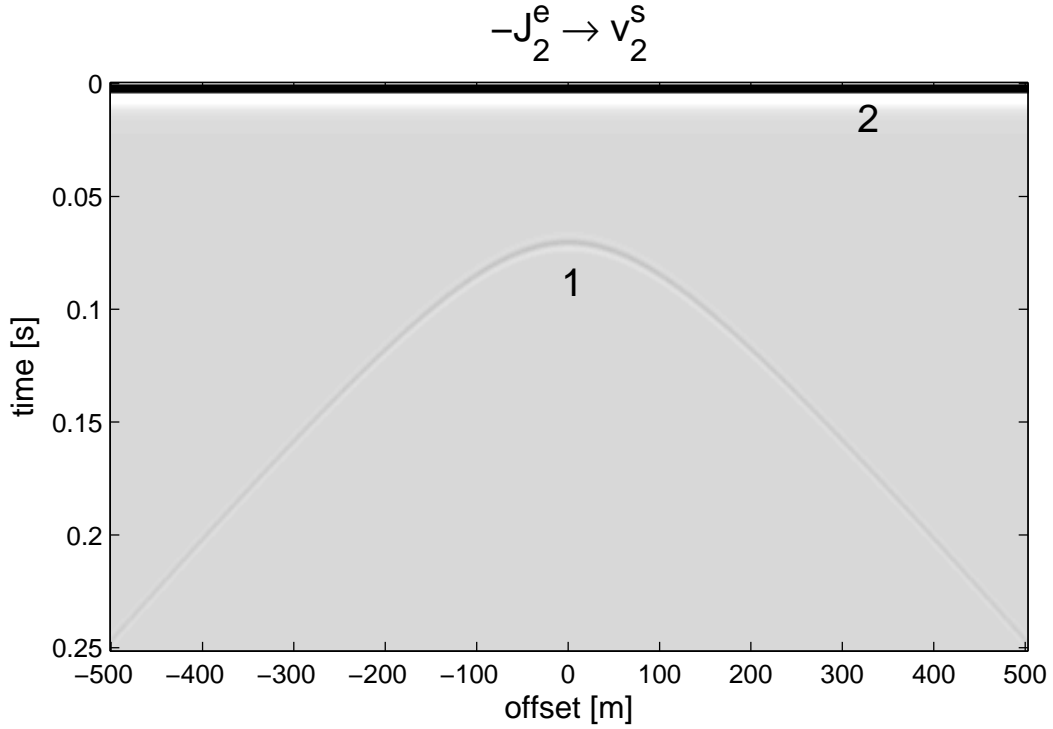


**Figure 5-10:** Transmission experiment in a homogeneous medium  $-J_2^{s,e} \rightarrow v_2^s$ ; 1: shear wave event, 2: electromagnetic wave event.

Note the similarity between Figure 5-9 and 5-10, they are equal except for a sign switch. This is a manifestation of source-receiver reciprocity, see Section 7-6,  $G^{v^s, J^e}(\mathbf{x}_A, \mathbf{x}_B) = -G^{E, f}(\mathbf{x}_B, \mathbf{x}_A)$ .

The second example is a more realistic geometry corresponding to an aquifer with a brine 100 [m] beneath the pressure-free surface, see Figure 5-11. There are two interfaces in the geometry, thus we have multiple arrivals. The receivers are placed infinitively close to, but under the pressure-free surface. In the first simulation the source is at an infinitesimal distance below the receivers. The source and receiver ghosts of the pressure-free surface are indistinguishable from their primaries. Figure 5-11 shows the geometry and the primary arrivals, blue rays are shear waves and red rays are electromagnetic waves, at each interface there is a conversion and the number of possible rays paths double. Figure 5-12 shows the simulation of a reflection experiment using a current source,  $-J_2^{s,e}$ , in the  $x_2$  direction and we measure the  $x_2$  component of the velocity in the solid,  $v_2^s$ .

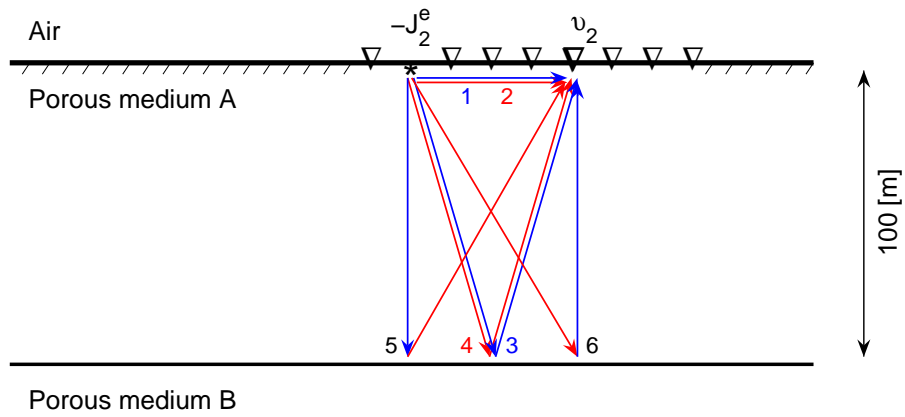


Figure 5-11: Experiment geometry of a reflection experiment above an aquifer.

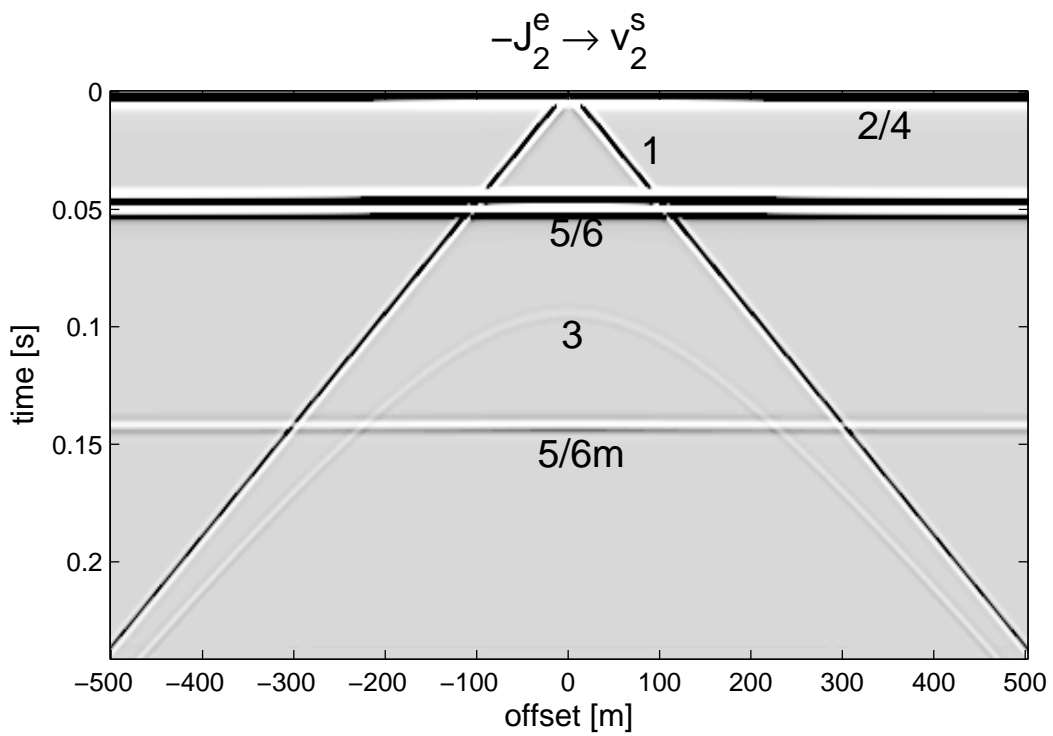


Figure 5-12: Reflection experiment above an aquifer, 5 events see text.

In figure 5-12 we see 5 events, the labels correspond to the ray paths in figure 5-11. Flat event labeled '2/4' is the combination of all rays that only traveled as an electromagnetic wave. Event '1' is the direct shear wave emitted by the electrical source that travels along the surface. Event '5/6' is the combination of the converted waves at the interface. The strongest component leaves the source as an electromagnetic wave and converts at the subsurface interface everywhere simultaneously, the result is a vertically upgoing almost plane wave. It arrives at the one-way travel time of the subsurface interface. If we write travel-time, we mean shear wave travel time really. Because the travel time associated with the propagation of an electromagnetic wave is negligible on this time scale. Event '3' is a shear wave emitted from the electrical source and reflecting at the subsurface interface. It arrives at two-way travel time of the subsurface interface. Event '5/6m' is the multiple of event '5/6', it made a full shear wave multiple between the two interfaces, and therefore arrived at two-way travel time after event '5/6'.

For the second simulation we place the source 50 meter beneath the subsurface interface. In figure 5-13 we show the geometry together with the primaries. In figure 5-14 we see 7 events, the labels correspond to the ray paths in figure 5-13. Event '2' is the combination of all the rays that travel purely as an electromagnetic wave. Event '3' is the arrival of the transmitted conversion on the subsurface interface. Event '1' is the co-seismic electrical field of the direct shear wave. Event '1m<sup>1</sup>' is the manifestation of the electromagnetic wave that is created when the direct shear wave hits the pressure-free surface. It is really a multiple of event '1', and at zero offset it coincides with its primary. Event '3m<sup>1</sup>' is the multiple of event '3', it arrives at two-way shear wave travel time of the subsurface interface. Event '1m<sup>2</sup>' is another multiple of event '1', it made a full shear wave multiple between the two interfaces. Event '3m<sup>2</sup>' is the second order multiple of event '3'.

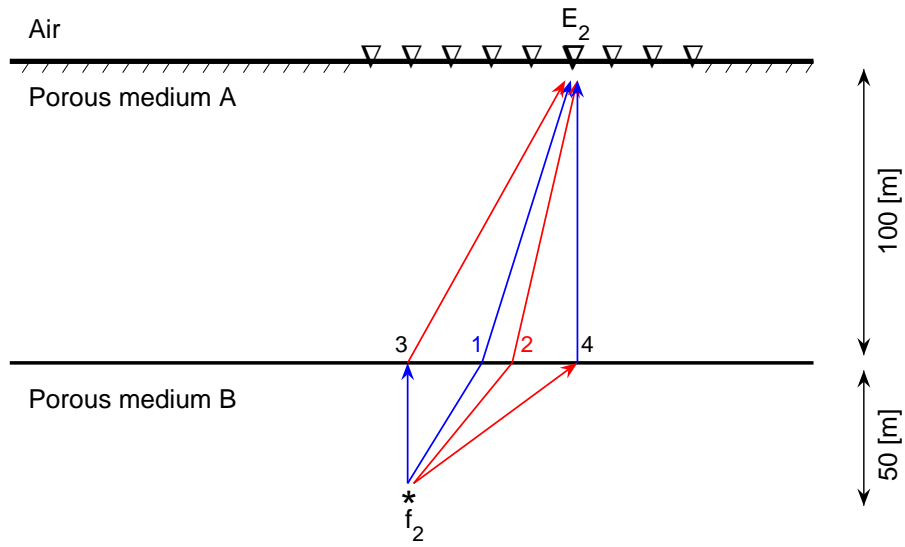


Figure 5-13: Experiment geometry of a transmission experiment in an aquifer.

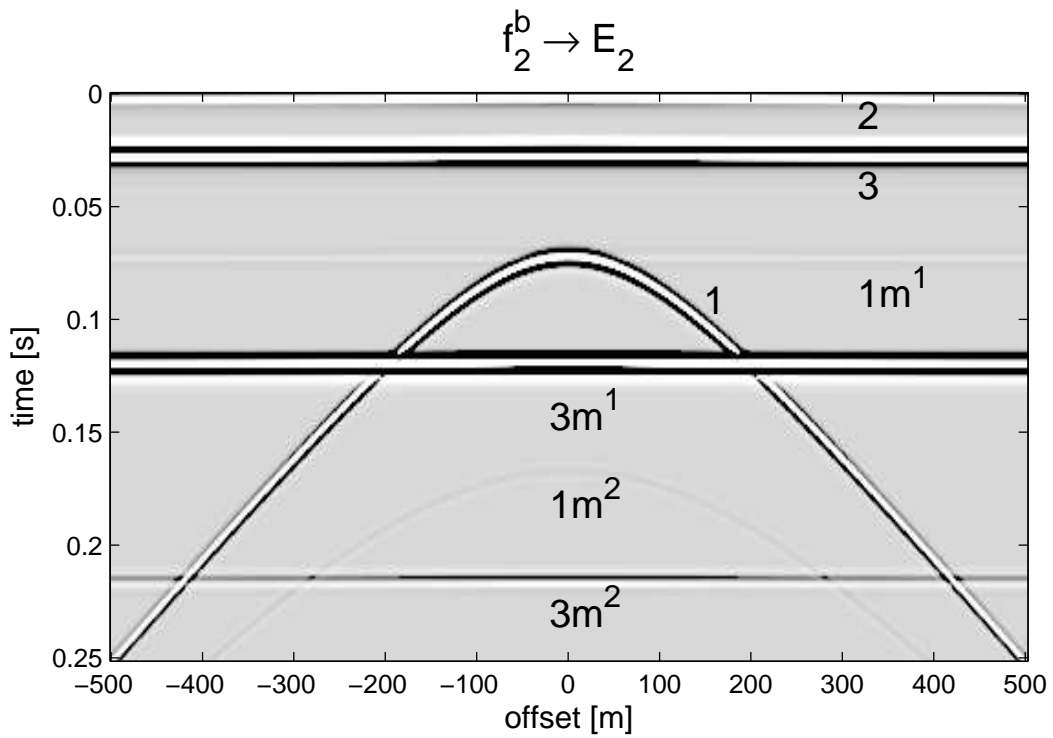


Figure 5-14: Transmission experiment in an aquifer, 7 events see text.



## **Part II**

# **Interferometric Seismoelectric Green's Function Recovery**



# Theory of interferometric Green's function recovery

In this chapter we introduce the interferometric Green's function representation for the general flow, diffusion and wave equation as derived by [Wapenaar et al. \[2006\]](#) from the reciprocity theorems of [Wapenaar and Fokkema \[2004\]](#). By writing the interferometric Green's function representations for the general flow, diffusion and wave equation, it went beyond the scope of elastodynamic wave fields by [Wapenaar and Fokkema \[2006\]](#). It validated the representations for the electromagnetic wave field [[Slob et al., 2007](#)] and representations for a diffusive system [[Snieder et al., 2006](#)]. Moreover, it provided interferometric Green's function representations for the coupled elastodynamic and electromagnetic wave-fields, that are the subject of Chapter 7. For simplicity, we only consider the theory for non-flowing media, but by [Wapenaar et al. \[2006\]](#) it has also been derived for flowing media.

A reciprocity theorem interrelates two independent states in one and the same domain [[de Hoop, 1966](#)], [[Fokkema and van den Berg, 1993](#)], the basis for reciprocity theorems is the theorem of Gauss. In Section 6-1 the scalar theorem of Gauss is modified to apply to vectorial systems of arbitrary lengths. The results are used to derive a convolution-type reciprocity theorem in Section 6-2 and a correlation-type reciprocity theorem in Section 6-3. The convolution-type reciprocity theorem leads to the well-known source-receiver reciprocity relation, for the special case in which both states have the same medium parameters. The correlation-type reciprocity theorem is modified using the source-receiver reciprocity to find an interferometric Green's function matrix representation.

### 6-1 Matrix vector representation of the divergence theorem of Gauss

Reciprocity theorems are derived using the theorem of Gauss. For a scalar field  $a = a(\mathbf{x})$  in domain  $\mathbb{D}$  bounded by a boundary  $\partial\mathbb{D}$  with outward pointing normal vector  $\mathbf{n}$ , see Figure 6-1,

the divergence theorem of Gauss reads

$$\int_{\mathbb{D}} \partial_i a d^3 \mathbf{x} = \oint_{\partial \mathbb{D}} a n_i d^2 \mathbf{x}. \quad (6-1)$$

In the derivations of reciprocity theorems we need a divergence theorem for the matrix  $\mathbf{D}_{\mathbf{x}}$

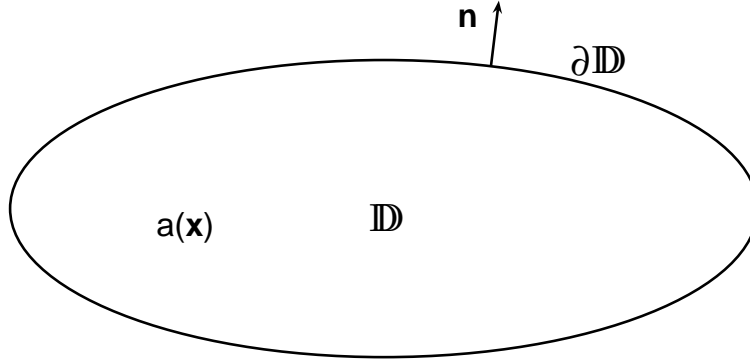


**Figure 6-1:** Scalar field  $a = a(\mathbf{x})$  in domain  $\mathbb{D}$  bounded by  $\partial \mathbb{D}$  with outward pointing normal vector  $\mathbf{n}$ .

appearing in the general diffusion, flow and wave equation 2-34 instead of the operator  $\partial_i$  in equation 6-1. Let  $D_{IJ}$  denote the  $I^{th}$  element from the  $J^{th}$  column of the matrix  $\mathbf{D}_{\mathbf{x}}$ , from symmetry relation 2-47 we have  $D_{IJ} = D_{JI}$ . We define a matrix  $\mathbf{N}_{\mathbf{x}}$  that contains the components of a normal vector  $n_i$  arranged in the same way as the partial spatial derivatives  $\partial_i$  in the matrix  $\mathbf{D}_{\mathbf{x}}$ . We replace the scalar field  $a$ , by a matrix field formed by the dyadic product of two vectors  $a_I(\mathbf{x})$  and  $b_J(\mathbf{x})$ . This generalizes equation 6-1 to

$$\int_{\mathbb{D}} D_{IJ} (a_I b_J) d^3 \mathbf{x} = \oint_{\partial \mathbb{D}} a_I b_J N_{IJ} d^2 \mathbf{x}. \quad (6-2)$$

The left hand-side contains the inner product of  $\mathbf{D}_{\mathbf{x}}$  with the matrix formed by the dyadic product of the vectors  $\mathbf{a}$  and  $\mathbf{b}$ , written as  $\mathbf{D}_{\mathbf{x}} \cdot (\mathbf{a} \mathbf{b}^t)$ . We evaluate the left-hand side of equation 6-2 using the product rule of  $D_{IJ} (a_I b_J)$  and the symmetry property of  $D_{IJ}$ . We obtain

$$\begin{aligned} D_{IJ} (a_I b_J) &= a_I D_{IJ} b_J + (D_{JI} a_I) b_J \\ \mathbf{D}_{\mathbf{x}} \cdot (\mathbf{a} \mathbf{b}^t) &= \mathbf{a}^t \mathbf{D}_{\mathbf{x}} \mathbf{b} + (\mathbf{D}_{\mathbf{x}} \mathbf{a})^t \mathbf{b}. \end{aligned} \quad (6-3)$$

When we rewrite the subscript notation on the left-hand side of equation 6-2 to a matrix-vector product we obtain the divergence theorem of Gauss in matrix-vector form, see also Figure 6-2,

$$\int_{\mathbb{D}} \mathbf{D}_{\mathbf{x}} \cdot (\mathbf{a} \mathbf{b}^t) d^3 \mathbf{x} = \int_{\mathbb{D}} \mathbf{a}^t \mathbf{D}_{\mathbf{x}} \mathbf{b} + (\mathbf{D}_{\mathbf{x}} \mathbf{a})^t \mathbf{b} d^3 \mathbf{x} = \oint_{\partial \mathbb{D}} \mathbf{a}^t \mathbf{N}_{\mathbf{x}} \mathbf{b} d^2 \mathbf{x}. \quad (6-4)$$

This equation is used in the derivation of the reciprocity theorem of the correlation type in Section 6-3. We consider a variant of equation 6-4 which we use in the derivation of the reciprocity theorem of the convolution type in Section 6-2. We replace  $\mathbf{a}$  by  $\mathbf{K}_0 \mathbf{a}$ , where  $\mathbf{K}_0$  is the real-valued diagonal matrix introduced in equation 2-46. Using equation 2-47 we obtain

$$\int_{\mathbb{D}} \mathbf{D}_{\mathbf{x}} \cdot (\mathbf{K}_0 \mathbf{a} \mathbf{b}^t) d^3 \mathbf{x} = \int_{\mathbb{D}} \mathbf{a}^t \mathbf{K}_0 \mathbf{D}_{\mathbf{x}} \mathbf{b} + (\mathbf{D}_{\mathbf{x}} \mathbf{a})^t \mathbf{K}_0 \mathbf{b} d^3 \mathbf{x} = \oint_{\partial \mathbb{D}} \mathbf{a}^t \mathbf{K}_0 \mathbf{N}_{\mathbf{x}} \mathbf{b} d^2 \mathbf{x}. \quad (6-5)$$

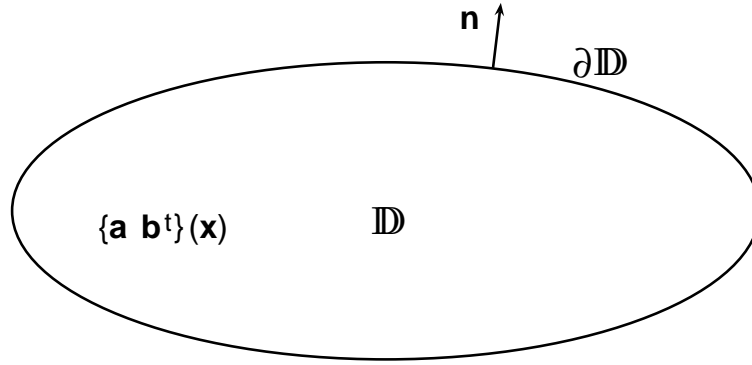


Figure 6-2: Matrix field  $\{\mathbf{a} \mathbf{b}^t\}(\mathbf{x})$  in domain  $\mathbb{D}$  bounded by  $\partial\mathbb{D}$  with normal vector  $\mathbf{n}$ .

## 6-2 Reciprocity theorem of the convolution type

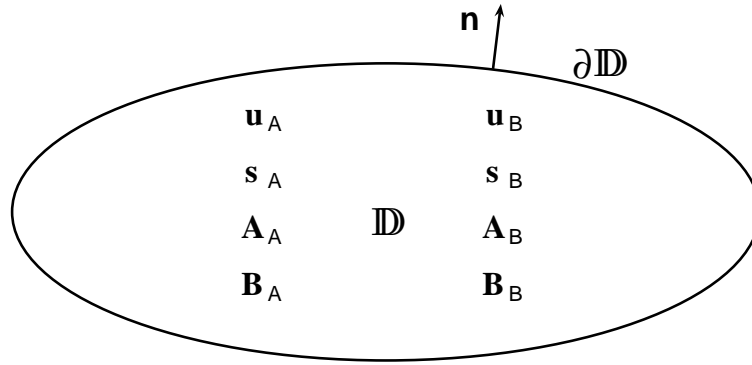


Figure 6-3: The general character of two physical states  $A$  and  $B$  for the reciprocity theorem of the convolution type in domain  $\mathbb{D}$ .

We consider two physical states in domain  $\mathbb{D}$ , they are distinguished with subscripts  $A$  and  $B$ . The material parameters and the source functions may be different in both states but for simplicity we consider non-flowing media, see Figure 6-3. We consider the interaction quantity  $\mathbf{D}_{\mathbf{x}} \cdot (\mathbf{K}_0 \mathbf{u}_A \mathbf{u}_B^t)$ , using equation 6-5 and the general flow, diffusion and wave equation 2-34 together with the symmetry properties for the system matrices 2-45 and 2-47 to expand the products. We find

$$\oint_{\partial\mathbb{D}} \hat{\mathbf{u}}_A^t \mathbf{K}_0 \mathbf{N}_{\mathbf{x}} \hat{\mathbf{u}}_B d^2\mathbf{x} = \int_{\mathbb{D}} [\hat{\mathbf{u}}_A^t \mathbf{K}_0 \hat{\mathbf{s}}_B - \hat{\mathbf{s}}_A^t \mathbf{K}_0 \hat{\mathbf{u}}_B] d^3\mathbf{x} + \int_{\mathbb{D}} \hat{\mathbf{u}}_A^t \mathbf{K}_0 \left[ i\omega (\hat{\mathbf{A}}_A - \hat{\mathbf{A}}_B) + (\hat{\mathbf{B}}_A - \hat{\mathbf{B}}_B) \right] \hat{\mathbf{u}}_B d^3\mathbf{x}. \quad (6-6)$$

This is the unified reciprocity theorem of the convolution type.

### 6-2-1 Source-receiver reciprocity

We consider a special case of the reciprocity theorem of the convolution type, when we have equal medium parameters in both states  $\hat{\mathbf{A}}_A = \hat{\mathbf{A}}_B = \hat{\mathbf{A}}$  and  $\hat{\mathbf{B}}_A = \hat{\mathbf{B}}_B = \hat{\mathbf{B}}$ . We choose point

$\mathbf{x}_A$  and  $\mathbf{x}_B$  both within  $\mathbb{D}$ . And we substitute the source vectors in both states by a frequency-independent point-source matrix  $\hat{\mathbf{s}}_{A,B} \rightarrow \mathbf{I}\delta(\mathbf{x} - \mathbf{x}_{A,B})$ . We consequentially have to replace the field vectors in both states by Green's function matrices  $\hat{\mathbf{u}}(\mathbf{x}, \mathbf{x}_{A,B}, \omega) \rightarrow \hat{\mathbf{G}}(\mathbf{x}, \mathbf{x}_{A,B}, \omega)$ . The diagonal of this Green's function matrix corresponds to the Green's function of the equivalent source field, while the off-diagonal elements are conversions of a certain emitted field type to another field type. See Section 7-1 equation 7-27 for the Green's function matrix of the SH-TE system. With these replacements, equation 6-6 becomes a reciprocity relation for the Green's function matrix of the convolution type. If we integrate over the whole space,  $r_{\mathbb{D}} \rightarrow \infty$ , the boundary integral on the left-hand side of equation 6-6 disappears on account of the radiation condition [Bleistein, 1984], more generally, since this boundary integral is a propagation invariant, as long as  $\mathbb{D}$  includes  $\mathbf{x}_A$  and  $\mathbf{x}_B$ , it vanishes for any  $\partial\mathbb{D}$ . The result is

$$\mathbf{K}_0 \hat{\mathbf{G}}^t(\mathbf{x}_A, \mathbf{x}_B, \omega) \mathbf{K}_0 = \hat{\mathbf{G}}(\mathbf{x}_B, \mathbf{x}_A, \omega). \quad (6-7)$$

From equation 6-7, we see that  $\mathbf{G}(\mathbf{x}_A, \mathbf{x}_B, \omega)$  commutes to  $\mathbf{G}(\mathbf{x}_B, \mathbf{x}_A, \omega)$  if we switch source and receiver positions *and types*. There is a possible sign switch modulated by  $\mathbf{K}_0$ . See Sections 7-2 and 7-6 for the specific source-receiver reciprocity relations of the SH-TE seismoelectric system in 1D and 2D.

### 6-3 Reciprocity theorem of the correlation type

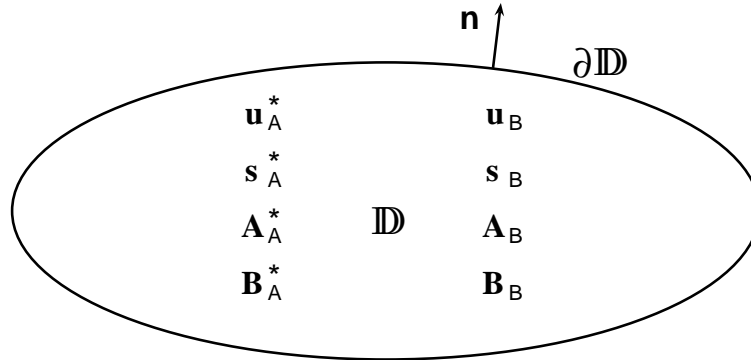


**Figure 6-4:** The general character of two physical states  $A$  and  $B$  for the reciprocity theorem of the correlation type in domain  $\mathbb{D}$ .

For the reciprocity theorem of the correlation type we consider two independent states  $A$  and  $B$  in the domain  $\mathbb{D}$ , but take the time-reversed state in  $A$ , see Figure 6-4. We consider the interaction quantity  $\mathbf{D}_{\mathbf{x}} \cdot (\mathbf{u}_A^* \mathbf{u}_B^t)$  and use the general flow, diffusion and wave equation 2-34 together with the symmetry properties for the system matrices 2-45 and 2-47 to expand the products. We find

$$\int_{\partial\mathbb{D}} \hat{\mathbf{u}}_A^\dagger \mathbf{N}_{\mathbf{x}} \hat{\mathbf{u}}_B d^2\mathbf{x} = \int_{\mathbb{D}} \left[ \hat{\mathbf{u}}_A^\dagger \hat{\mathbf{s}}_B + \hat{\mathbf{s}}_A^\dagger \hat{\mathbf{u}}_B \right] d^3\mathbf{x} - \int_{\mathbb{D}} \hat{\mathbf{u}}_A^\dagger \left[ i\omega \left( \hat{\mathbf{A}}_B - \hat{\mathbf{A}}_A^\dagger \right) + \left( \hat{\mathbf{B}}_B + \hat{\mathbf{B}}_A^\dagger \right) \right] \hat{\mathbf{u}}_B d^3\mathbf{x}. \quad (6-8)$$

This is the unified reciprocity theorem of the correlation type. The right-hand side of equation 6-8 contains a volume integral that does not disappear when we choose equal medium

parameters. This is an important different property of the correlation type reciprocity theorem with the convolution type reciprocity theorem. When we consider the situation in which the wave-fields, medium parameters and source functions in both states are identical we find the power balance for the general flow, diffusion and wave equation. Therefore the correlation-type reciprocity theorem is also referred to as the power reciprocity theorem.

## 6-4 Interferometric Green's function representations in 3D

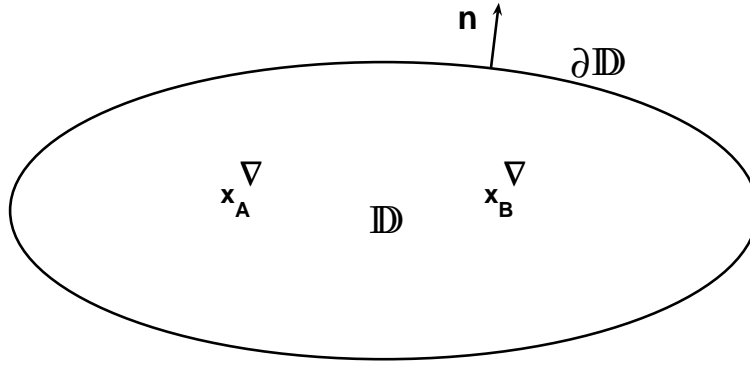


**Figure 6-5:** Geometry for the 3D interferometric Green's function representation.

We now modify the reciprocity theorem of the correlation type such that it can be used for interferometric recovery of the Green's function matrix. We start by introducing the same source matrix and Green's function matrix of Section 6-2-1 into equation 6-8. We choose points  $\mathbf{x}_A$  and  $\mathbf{x}_B$ , where  $\mathbf{x} = (x_1, x_2, x_3)$ , both within  $\mathbb{D}$  and define both states  $A$  and  $B$  with the same medium parameters, thus  $\hat{\mathbf{A}}_A = \hat{\mathbf{A}}_B = \hat{\mathbf{A}}$  and  $\hat{\mathbf{B}}_A = \hat{\mathbf{B}}_B = \hat{\mathbf{B}}$ . We find

$$\begin{aligned} \hat{\mathbf{G}}(\mathbf{x}_A, \mathbf{x}_B, \omega) + \hat{\mathbf{G}}^\dagger(\mathbf{x}_B, \mathbf{x}_A, \omega) = & \\ & \oint_{\partial\mathbb{D}} \hat{\mathbf{G}}^\dagger(\mathbf{x}, \mathbf{x}_A, \omega) \mathbf{N}_x \hat{\mathbf{G}}(\mathbf{x}, \mathbf{x}_B, \omega) d^2\mathbf{x} \\ & + \int_{\mathbb{D}} \hat{\mathbf{G}}^\dagger(\mathbf{x}, \mathbf{x}_A, \omega) \left[ i\omega \left( \hat{\mathbf{A}}_B - \hat{\mathbf{A}}_A^\dagger \right) + \left( \hat{\mathbf{B}}_B + \hat{\mathbf{B}}_A^\dagger \right) \right] \hat{\mathbf{G}}(\mathbf{x}, \mathbf{x}_B, \omega) d^3\mathbf{x}. \end{aligned} \quad (6-9)$$

The first integral on the right-hand side of equation 6-9 is over crosscorrelations of Green's functions from sources at  $\mathbf{x}_A$  and  $\mathbf{x}_B$  measured at the boundary  $\partial\mathbb{D}$  and the second integral on the right-hand side of equation 6-9 is over crosscorrelations of Green's functions from sources at  $\mathbf{x}_A$  and  $\mathbf{x}_B$  measured throughout the domain  $\mathbb{D}$ . We transpose both sides of equation 6-9 and use the source-receiver reciprocity relation 6-7 together with the symmetry properties for the system matrices  $\mathbf{A}$  and  $\mathbf{B}$  in equation 2-45. The result is

$$\begin{aligned} \hat{\mathbf{G}}(\mathbf{x}_B, \mathbf{x}_A, \omega) + \hat{\mathbf{G}}^\dagger(\mathbf{x}_A, \mathbf{x}_B, \omega) = & \\ & - \oint_{\partial\mathbb{D}} \hat{\mathbf{G}}(\mathbf{x}_B, \mathbf{x}, \omega) \mathbf{N}_x \hat{\mathbf{G}}^\dagger(\mathbf{x}_A, \mathbf{x}, \omega) d^2\mathbf{x} \\ & + \int_{\mathbb{D}} \hat{\mathbf{G}}(\mathbf{x}_B, \mathbf{x}, \omega) \left[ i\omega \left( \hat{\mathbf{A}}_B - \hat{\mathbf{A}}_A^\dagger \right) + \left( \hat{\mathbf{B}}_B + \hat{\mathbf{B}}_A^\dagger \right) \right] \hat{\mathbf{G}}^\dagger(\mathbf{x}_A, \mathbf{x}, \omega) d^3\mathbf{x}. \end{aligned} \quad (6-10)$$

The integrations on the right-hand side of equation 6-10 are of Green's functions of sources on the boundary  $\partial\mathbb{D}$  and throughout the volume  $\mathbb{D}$  measured at  $\mathbf{x}_A$  and  $\mathbf{x}_B$ . This step is the key to the modification of the reciprocity theorems to a relation that can be applied for interferometric Green's function recovery. Equation 6-10 tells us that we can retrieve a component of the Green's function matrix and the time-reversed of its reciprocal counterpart, if we cross-correlate observations of certain sources throughout the domain  $\mathbb{D}$  and on its boundary  $\partial\mathbb{D}$ , with appropriate weighting functions. The specific relationship between the two retrieved Green's functions is given by the source-receiver reciprocity relation 6-7. The importance of the different integrals are studied in Chapter 8. We call equation 6-10 an interferometric Green's function representation, because it represents the Green's function between  $\mathbf{x}_A$  and  $\mathbf{x}_B$  as an integral of cross-correlations of observed green's functions at point  $\mathbf{x}_A$  and  $\mathbf{x}_B$ .

## 6-5 Interferometric Green's function representations in 2D and 1D

To evaluate the interferometric Green's function representation for the SH-TE mode of propagation, we need to rewrite the representation in 2D. The volume domain  $\mathbb{D}$  reduces to a surface domain  $\mathbb{S}$ . Again we choose point  $\mathbf{x}_A$  and  $\mathbf{x}_B$ , where  $\mathbf{x} = (x_1, x_3)$ , both in  $\mathbb{S}$ . Equation 6-10 reduces to

$$\begin{aligned} \hat{\mathbf{G}}(\mathbf{x}_B, \mathbf{x}_A, \omega) + \hat{\mathbf{G}}^\dagger(\mathbf{x}_A, \mathbf{x}_B, \omega) = & \\ & - \oint_{\partial\mathbb{S}} \hat{\mathbf{G}}(\mathbf{x}_B, \mathbf{x}, \omega) \mathbf{N}_{\mathbf{x}} \hat{\mathbf{G}}^\dagger(\mathbf{x}_A, \mathbf{x}, \omega) d\mathbf{x} \\ & + \int_{\mathbb{S}} \hat{\mathbf{G}}(\mathbf{x}_B, \mathbf{x}, \omega) \left[ i\omega \left( \hat{\mathbf{A}}_B - \hat{\mathbf{A}}_A^\dagger \right) + \left( \hat{\mathbf{B}}_B + \hat{\mathbf{B}}_A^\dagger \right) \right] \hat{\mathbf{G}}^\dagger(\mathbf{x}_A, \mathbf{x}, \omega) d^2\mathbf{x}, \end{aligned} \quad (6-11)$$

where  $\mathbf{N}_{\mathbf{x}}$  contains the components of the normal vector  $\mathbf{n} = (n_1, n_3)$  on the line  $\partial\mathbb{S}$ . According to equation 6-11, we can retrieve a component of the Green's function matrix and the time-reversed of its reciprocal counterpart, if we crosscorrelate observations of certain sources all over the domain  $\mathbb{S}$  and on its boundary  $\partial\mathbb{S}$ , with appropriate weighting functions.

We can simplify the representation even further by going to a 1D system. We choose

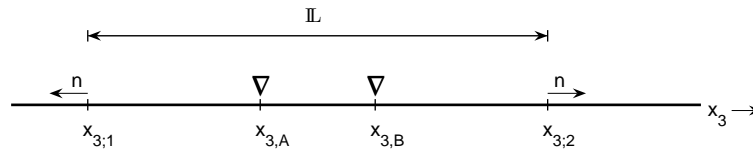


**Figure 6-6:** Geometry for the 1D interferometric Green's function representation.

$x_{3,1} < x_{3,A/B} < x_{3,2}$ , see Figure 6-6. The surface domain  $\mathbb{S}$  reduces to a line domain  $\mathbb{L}$  and the boundary integral reduces to a sum over two points on the edges of  $\mathbb{L}$ . We take the

$x_3$ -coordinate as the remaining coordinate. Equation 6-11 reduces to

$$\begin{aligned} & \hat{\mathbf{G}}(x_{3,B}, x_{3,A}, \omega) + \hat{\mathbf{G}}^\dagger(x_{3,A}, x_{3,B}, \omega) = \\ & - \sum_{k=1}^2 \left[ \hat{\mathbf{G}}(x_{3,B}, x_{3;k}, \omega) \mathbf{N}_{3,k} \hat{\mathbf{G}}^\dagger(x_{3,A}, x_{3;k}, \omega) \right] \\ & + \int_{x_{3,1}}^{x_{3,2}} \hat{\mathbf{G}}(x_{3,B}, x_3, \omega) \left[ i\omega \left( \hat{\mathbf{A}}_B - \hat{\mathbf{A}}_A^\dagger \right) + \left( \hat{\mathbf{B}}_B + \hat{\mathbf{B}}_A^\dagger \right) \right] \hat{\mathbf{G}}^\dagger(x_{3,A}, \mathbf{x}, \omega) dx_3, \end{aligned} \quad (6-12)$$

where  $\mathbf{N}_{3,k}$  is a matrix containing zeros and ones, we have  $\mathbf{N}_{3,1} = -\mathbf{N}_{3,1}$ . According to equation 6-12, we can retrieve a component of the Green's function matrix and the time-reversed of its reciprocal counterpart, if we crosscorrelate observations of certain sources all along the domain  $\mathbb{L}$  and on the domain boundary edge points, with appropriate weighting functions.



## SH-TE interferometric Green's function representations in 1D and 2D

In this section we derive interferometric Green's function representations for the SH-TE system in 1D and 2D. There is a high degree of similarity in the equations and both derivations follow the same line and can be read independently. We start writing the SH-TE system equations in a matrix form, such that the equations of the Chapter 7 can be applied to the separate systems. In what follows we generalize the system equations by assuming that there are elastic and magnetic losses, i.e.  $\hat{N}$  and  $\hat{\mu}$  are frequency dependent. We briefly discuss the contributions of the separate integrals in the interferometric representations, a more extensive discussion follows in the next chapter with numerical examples.

### 7-1 SH-TE seismoelectric coupling in 1D

Starting from the 22 equations in the matrices in chapter 2 we drop the  $x_1$  and  $x_2$  dependence, see derivations in Appendix C-2. The SH-TE system in 1D is governed by the fields  $\hat{E}_2$ ,  $\hat{H}_1$ ,  $\hat{v}_2^s$  and  $\hat{\tau}_{23}^b$ . The field  $\hat{w}_2$  does not obey an independent differential equation, therefore we eliminated  $\hat{w}_2$  from the system. The SH-TE system in 1D can be captured in the general flow, diffusion and wave equation as

$$i\omega \begin{pmatrix} \hat{\epsilon} & 0 & -\rho^f \hat{\mathcal{L}} & 0 \\ 0 & \hat{\mu} & 0 & 0 \\ \rho^f \hat{\mathcal{L}} & 0 & \hat{\rho}^c & 0 \\ 0 & 0 & 0 & \hat{N}^{-1} \end{pmatrix} \begin{pmatrix} \hat{E}_2 \\ \hat{H}_1 \\ \hat{v}_2^s \\ -\hat{\tau}_{23}^b \end{pmatrix} + \begin{pmatrix} 0 & -\partial_3 & 0 & 0 \\ -\partial_3 & 0 & 0 & 0 \\ 0 & 0 & 0 & \partial_3 \\ 0 & 0 & \partial_3 & 0 \end{pmatrix} \begin{pmatrix} \hat{E}_2 \\ \hat{H}_1 \\ \hat{v}_2^s \\ -\hat{\tau}_{23}^b \end{pmatrix} = \begin{pmatrix} -\hat{j}_2^{s,e} \\ -\hat{j}_1^{s,m} \\ \hat{f}_2^b \\ \hat{h}_3^b \end{pmatrix}, \quad (7-1)$$

where we combined the matrices  $\hat{\mathbf{A}}$  and  $\hat{\mathbf{B}}$ , by defining  $\hat{\epsilon} = \epsilon + \frac{1}{i\omega} \hat{\sigma}^e$  and  $\hat{\mu} = \mu + \frac{1}{i\omega} \hat{\sigma}^m$ . The system matrices of the SH-TE system obey the same symmetry properties as those of the

complete seismoelectric system matrices, see Section 2-2-1. We have

$$\mathbf{K}_0 \hat{\mathbf{A}}^t \mathbf{K}_0 = \mathbf{A}, \quad (7-2)$$

with

$$\mathbf{K}_0 = \text{diag}(-1, 1, 1, -1). \quad (7-3)$$

The field and source vectors are

$$\hat{\mathbf{u}} = \begin{pmatrix} \hat{E}_2 \\ \hat{H}_1 \\ \hat{v}_2^s \\ -\hat{\tau}_{23}^b \end{pmatrix} \quad \text{and} \quad \hat{\mathbf{s}} = \begin{pmatrix} -\hat{J}_2^{\mathbf{s},e} \\ -\hat{J}_1^{\mathbf{s},m} \\ \hat{f}_2^f \\ \hat{h}_3^b \end{pmatrix}. \quad (7-4)$$

We defined new electrical  $-\hat{J}_2^{\mathbf{s},e}$ , force  $\hat{f}_2^f$  and deformation rate  $\hat{h}_3^b$  sources, according to  $\hat{J}_2^{\mathbf{s},e} = \hat{J}_2^{\mathbf{s},e} + \hat{\mathcal{L}} \hat{f}_2^f$ ,  $\hat{f}_2^f = \hat{f}_2^b - \frac{\rho^f}{\rho^E} \hat{f}_2^b$  and  $\hat{h}_3^b = \hat{h}_{32}^b + \hat{h}_{23}^b$ . The force on the fluid phase  $\hat{f}^f$  is not an independent source type in the SH-TE system, see Section C-1, because there are no waves traveling only through the fluid phase.

We replace the source vector  $\hat{\mathbf{s}}$  by a  $4 \times 4$  point-source matrix  $\mathbf{I} \delta(x_3 - x_{3,s})$  and correspondingly, the field vector  $\mathbf{u}$  observed at  $x_{3,r}$  is replaced by a  $4 \times 4$  Green's function matrix,

$$\hat{\mathbf{G}}(x_{3,r}, x_{3,s}, \omega) = \begin{pmatrix} \hat{G}^{E,\underline{J}^e} & \hat{G}^{E,J^m} & \hat{G}^{E,\underline{f}} & \hat{G}^{E,\underline{h}} \\ \hat{G}^{H,\underline{J}^e} & \hat{G}^{H,J^m} & \hat{G}^{H,\underline{f}} & \hat{G}^{H,\underline{h}} \\ \hat{G}^{v,\underline{J}^e} & \hat{G}^{v,J^m} & \hat{G}^{v,\underline{f}} & \hat{G}^{v,\underline{h}} \\ \hat{G}^{\tau,\underline{J}^e} & \hat{G}^{\tau,J^m} & \hat{G}^{\tau,\underline{f}} & \hat{G}^{\tau,\underline{h}} \end{pmatrix} (x_{3,r}, x_{3,s}, \omega). \quad (7-5)$$

We omitted all unnecessary superscripts and directional subscripts of the fields and sources. In the notation of subsequent sections we will also omit the  $\omega$  dependence. Solutions for the SH-TE seismoelectric Green's functions in 1D in a homogeneous domain are given in Appendix C-3.

## 7-2 Convolution-type reciprocity theorem for SH-TE in 1D

In this section, we use the equations of Section 6-2 to find a convolution-type reciprocity theorem for SH-TE waves in 1D in the frequency domain. If we substitute the field vector from equation 7-4 for the two different states A and B into the interaction quantity  $\mathbf{D}_x \cdot (\mathbf{K}_0 \mathbf{u}_A \mathbf{u}_B^t)$  we find

$$\partial_3 \left[ \hat{E}_{2,A} \hat{H}_{1,B} - \hat{H}_{1,A} \hat{E}_{2,B} + \hat{\tau}_{23,A}^b \hat{v}_{2,B}^s - \hat{v}_{2,A}^s \hat{\tau}_{23,B}^b \right]. \quad (7-6)$$

We apply the product rule to equation 7-6 and substitute the differential equations 7-1, after integration over the domain  $\mathbb{L}$  from  $x_{3,1}$  to  $x_{3,2}$ , we apply the theorem of Gauss to the sum

containing the differential operator  $\partial_3$  and we find

$$\begin{aligned}
& \sum_{k=1}^2 \left[ \hat{E}_{2,A} \hat{H}_{1,B} - \hat{H}_{1,A} \hat{E}_{2,B} + \hat{\tau}_{23,A}^b \hat{v}_{2,B}^s - \hat{v}_{2,A}^s \hat{\tau}_{23,B}^b \right] n_{3;k} = \\
& \int_{x_{3;1}}^{x_{3;2}} \left[ \hat{E}_{2,A} \hat{J}_{2,B}^{s,e} - \hat{J}_{2,A}^{s,e} \hat{E}_{2,B} + \hat{J}_{1,A}^{s,m} \hat{H}_{1,B} - \hat{H}_{1,A} \hat{J}_{1,B}^{s,m} \right. \\
& \quad \left. + \hat{v}_{2,A}^s \hat{f}_{2,B} - \hat{f}_{2,A} \hat{v}_{2,B}^s + \hat{\tau}_{23,A}^b \hat{h}_{3,B} - \hat{h}_{3,A} \hat{\tau}_{23,B}^b \right] dx_3 \\
& + i\omega \int_{x_{3;1}}^{x_{3;2}} \left[ -\hat{E}_{2,A} (\hat{\varepsilon}_A - \hat{\varepsilon}_B) \hat{E}_{2,B} + \hat{E}_{2,A} \left( \rho_A^f \hat{\mathcal{L}}_A - \rho_B^f \hat{\mathcal{L}}_B \right) \hat{v}_{2,B}^s + \hat{H}_{1,A} (\hat{\mu}_A - \hat{\mu}_B) \hat{H}_{1,B} \right. \\
& \quad \left. + \hat{v}_{2,A} \left( \rho_A^f \hat{\mathcal{L}}_A - \rho_B^f \hat{\mathcal{L}}_B \right) \hat{E}_{2,B} + \hat{v}_{2,A}^s (\hat{\rho}_A^c - \hat{\rho}_B^c) \hat{v}_{2,B}^s - \hat{\tau}_{23,A}^b \left( \hat{N}_A^{-1} - \hat{N}_B^{-1} \right) \hat{\tau}_{23,B}^b \right] dx_3.
\end{aligned} \tag{7-7}$$

This is the convolution-type reciprocity theorem for 1D SH-TE seismoelectric waves. We substitute the SH-TE Green's function matrix 7-5 in 1D and the symmetry matrix 7-3 into the source-receiver relation for the Green's matrix equation 6-7, to we find the source-receiver reciprocity relations as

$$\hat{G}^{E,\underline{J}^e}(x_{3,A}, x_{3,B}) = \hat{G}^{E,\underline{J}^e}(x_{3,B}, x_{3,A}) \quad , \quad \hat{G}^{H,\underline{J}^e}(x_{3,A}, x_{3,B}) = -\hat{G}^{E,J^m}(x_{3,B}, x_{3,A}), \tag{7-8}$$

$$\hat{G}^{v,\underline{J}^e}(x_{3,A}, x_{3,B}) = -\hat{G}^{E,\underline{f}}(x_{3,B}, x_{3,A}) \quad , \quad \hat{G}^{\tau,\underline{J}^e}(x_{3,A}, x_{3,B}) = \hat{G}^{E,\underline{h}}(x_{3,B}, x_{3,A}), \tag{7-9}$$

$$\hat{G}^{H,J^m}(x_{3,A}, x_{3,B}) = \hat{G}^{H,J^m}(x_{3,B}, x_{3,A}) \quad , \quad \hat{G}^{v,\underline{f}}(x_{3,A}, x_{3,B}) = \hat{G}^{v,\underline{f}}(x_{3,B}, x_{3,A}), \tag{7-10}$$

$$\hat{G}^{\tau,\underline{h}}(x_{3,A}, x_{3,B}) = \hat{G}^{\tau,\underline{h}}(x_{3,B}, x_{3,A}) \quad , \quad \hat{G}^{v,J^m}(x_{3,A}, x_{3,B}) = \hat{G}^{H,\underline{f}}(x_{3,B}, x_{3,A}), \tag{7-11}$$

$$\hat{G}^{\tau,J^m}(x_{3,A}, x_{3,B}) = -\hat{G}^{H,\underline{h}}(x_{3,B}, x_{3,A}) \quad , \quad \hat{G}^{\tau,\underline{f}}(x_{3,A}, x_{3,B}) = -\hat{G}^{v,\underline{h}}(x_{3,B}, x_{3,A}). \tag{7-12}$$

### 7-3 Correlation-type reciprocity theorem for SH-TE in 1D

In this section, we use the equations of Section 6-3 to find a correlation-type reciprocity theorem for 1D SH-TE waves in the frequency domain. If we substitute the field vector from equation 7-4 for the two different states A and B into the interaction quantity  $\mathbf{D}_x \cdot (\mathbf{u}_A \mathbf{u}_B^t)$  we find

$$-\partial_3 \left[ \hat{E}_{2,A}^* \hat{H}_{1,B} + \hat{H}_{1,A}^* \hat{E}_{2,B} + \hat{\tau}_{23,A}^{b*} \hat{v}_{2,B}^s + \hat{v}_{2,A}^{s*} \hat{\tau}_{23,B}^b \right]. \tag{7-13}$$

We apply the product rule to equation 7-13 and substitute the differential equations 7-1, after integration along the length of  $\mathbb{L}$  from  $x_{3;1}$  to  $x_{3;2}$ , we apply the theorem of Gauss to the sum

containing the differential operator  $\partial_3$  and we find

$$\begin{aligned}
& - \sum_{k=1}^2 \left[ \hat{E}_{2,A}^* \hat{H}_{1,B} + \hat{H}_{1,A}^* \hat{E}_{2,B} + \hat{\tau}_{23,A}^{b*} \hat{v}_{2,B}^s + \hat{v}_{2,A}^{s*} \hat{\tau}_{23,B}^b \right] n_{3;k} = \\
& \int_{x_{3;1}}^{x_{3;2}} \left[ -\hat{J}_{2,A}^{s,e*} \hat{E}_{2,B} \quad - \quad \hat{E}_{2,A}^* \hat{J}_{2,B}^{s,e} \quad - \quad \hat{J}_{1,A}^{s,m*} \hat{H}_{1,B} \quad - \quad \hat{H}_{1,A}^* \hat{J}_{1,B}^{s,m} \right. \\
& \quad \left. + \hat{v}_{2,A}^{s*} \hat{f}_{2,B} \quad + \quad \hat{f}_{2,A}^* \hat{v}_{2,B}^s \quad - \quad \hat{h}_{3,A}^* \hat{\tau}_{23,B}^b \quad - \quad \hat{\tau}_{23,A}^{b*} \hat{h}_{3,B} \right] dx_3 \\
& - i\omega \int_{x_{3;1}}^{x_{3;2}} \left[ \hat{E}_{2,A}^* (\hat{\varepsilon}_B - \hat{\varepsilon}_A^*) \hat{E}_{2,B} - \hat{E}_{2,A}^* \left( \rho_B^f \hat{\mathcal{L}}_B + \rho_A^f \hat{\mathcal{L}}_A^* \right) \hat{v}_{2,B}^s + \hat{H}_{1,A}^* (\hat{\mu}_B - \hat{\mu}_A^*) \hat{H}_{1,B} \right. \\
& \left. + \hat{v}_{2,A}^* \left( \rho_B^f \hat{\mathcal{L}}_B + \rho_A^f \hat{\mathcal{L}}_A^* \right) \hat{E}_{2,B} + \hat{v}_{2,A}^{s*} (\hat{\rho}_B^c - \hat{\rho}_A^{c*}) \hat{v}_{2,B}^s + \hat{\tau}_{23,A}^{b*} \left( \hat{N}_B^{-1} - \hat{N}_A^{-1*} \right) \hat{\tau}_{23,B}^b \right] dx_3.
\end{aligned} \tag{7-14}$$

This is the correlation-type reciprocity theorem for SH-TE seismoelectric waves in 1D. Note that the domain integral on the right-hand side of equation 7-14 does not disappear if we choose equal medium parameters in both states. This domain integral is over the loss functions of the system and over the coupling coefficient, that governs the conversion of electromagnetic energy to elastodynamic energy and vice versa.

## 7-4 Seismoelectric interferometric Green's function recovery in 1D

From equation 6-12 we can derive an interferometric representation of the SH-TE Green's function matrix in 1D. We substitute the Green's function matrix 7-5 and medium parameter matrix of equation 7-1 into equation 6-12, to find

$$\begin{aligned}
& \hat{G}_{IJ}(x_{3,B}, x_{3,A}) + \hat{G}_{JI}^*(x_{3,A}, x_{3,B}) = \\
& \sum_{k=1}^2 n_{3;k} \left[ \hat{G}_{I2}^{Jm}(x_{3,B}, x_{3;k}) \hat{G}_{J1}^{Je*}(x_{3,A}, x_{3;k}) + \hat{G}_{I1}^{Je}(x_{3,B}, x_{3;k}) \hat{G}_{J2}^{Jm*}(x_{3,A}, x_{3;k}) \right. \\
& \quad \left. - \hat{G}_{I4}^h(x_{3,B}, x_{3;k}) \hat{G}_{J3}^{f*}(x_{3,A}, x_{3;k}) - \hat{G}_{I3}^f(x_{3,B}, x_{3;k}) \hat{G}_{J4}^{h*}(x_{3,A}, x_{3;k}) \right] \\
& + i\omega 2 \int_{x_{3;1}}^{x_{3;2}} \left[ \hat{G}_{I1}^{Je}(x_{3,B}, x_3) i\Im\{\hat{\varepsilon}\} \hat{G}_{J1}^{Je*}(x_{3,A}, x_3) - \hat{G}_{I1}^{Je}(x_{3,B}, x_3) \Re\{\rho^f \hat{\mathcal{L}}\} \hat{G}_{J3}^{f*}(x_{3,A}, x_3) \right. \\
& \quad + \hat{G}_{I3}^f(x_{3,B}, x_3) \Re\{\rho^f \hat{\mathcal{L}}\} \hat{G}_{J1}^{Je*}(x_{3,A}, x_3) + \hat{G}_{I3}^f(x_{3,B}, x_3) i\Im\{\hat{\rho}^c\} \hat{G}_{J3}^{f*}(x_{3,A}, x_3) \\
& \quad \left. + \hat{G}_{I2}^{Jm}(x_{3,B}, x_3) i\Im\{\hat{\mu}\} \hat{G}_{J2}^{Jm*}(x_{3,A}, x_3) + \hat{G}_{I4}^h(x_{3,B}, x_3) i\Im\{\hat{N}^{-1}\} \hat{G}_{J4}^{h*}(x_{3,A}, x_3) \right] dx_3,
\end{aligned} \tag{7-15}$$

in which  $\hat{G}_{IJ}(x_{3,A}, x_{3,B})$  denotes the  $I^{th}$  element of the  $J^{th}$  column of the Green's function matrix 7-5 at  $x_{3,B}$  yielding a response due to a point-source at  $x_{3,A}$ . The domain integral on the right-hand sides of equation 7-15 is a sum of crosscorrelations of observed responses of sources weighted by the loss and seismoelectric coupling functions. This integral not only compensates for the losses in  $\mathbb{L}$ , but also contributes to the seismoelectric coupling in  $\mathbb{L}$ . The summation of crosscorrelations of responses of sources on the end points of  $\mathbb{L}$  accounts for the contributions to the Green's functions from losses and seismoelectric coupling outside

the domain  $\mathbb{L}$ .

We can use 7-15 for an interferometric expression for every element of the Green's function matrix  $\hat{\mathbf{G}}(x_{3,B}, x_{3,A})$ . For example, for the particle velocity  $\hat{v}_2^s$  in the solid at observation location  $x_{3,B}$  due to an electrical current source  $-\underline{J}_2^{s,e}$  at observation location  $x_{3,A}$ , we have

$$\begin{aligned}
& \hat{G}^{v^s, \underline{J}^e}(x_{3,B}, x_{3,A}) + \hat{G}^{E, \underline{f}^*}(x_{3,A}, x_{3,B}) = \\
& \sum_{k=1}^2 n_{3;k} \left[ \hat{G}^{v, J^m}(x_{3,B}, x_{3;k}) \hat{G}^{E, \underline{J}^{e*}}(x_{3,A}, x_{3;k}) + \hat{G}^{v, \underline{J}^e}(x_{3,B}, x_{3;k}) \hat{G}^{E, J^{m*}}(x_{3,A}, x_{3;k}) \right. \\
& \quad \left. - \hat{G}^{v, \underline{h}}(x_{3,B}, x_{3;k}) \hat{G}^{E, \underline{f}^*}(x_{3,A}, x_{3;k}) - \hat{G}^{v, \underline{f}}(x_{3,B}, x_{3;k}) \hat{G}^{E, \underline{h}^*}(x_{3,A}, x_{3;k}) \right] \\
& + i\omega 2 \int_{x_{3,1}}^{x_{3,2}} \left[ \hat{G}^{v, \underline{J}^e}(x_{3,B}, x_3) i\mathfrak{Im}\{\hat{\varepsilon}\} \hat{G}^{E, \underline{J}^{e*}}(x_{3,A}, x_3) - \hat{G}^{v, \underline{J}^e}(x_{3,B}, x_3) \Re\{\rho^f \hat{\mathcal{L}}\} \hat{G}^{E, \underline{f}^*}(x_{3,A}, x_3) \right. \\
& \quad + \hat{G}^{v, \underline{f}}(x_{3,B}, x_3) \Re\{\rho^f \hat{\mathcal{L}}\} \hat{G}^{E, \underline{J}^{e*}}(x_{3,A}, x_3) + \hat{G}^{v, \underline{f}}(x_{3,B}, x_3) i\mathfrak{Im}\{\hat{\rho}^c\} \hat{G}^{E, \underline{f}^*}(x_{3,A}, x_3) \\
& \quad \left. + \hat{G}^{v, \underline{J}^m}(x_{3,B}, x_3) i\mathfrak{Im}\{\hat{\mu}\} \hat{G}^{E, \underline{J}^{m*}}(x_{3,A}, x_3) + \hat{G}^{v, \underline{h}}(x_{3,B}, x_3) i\mathfrak{Im}\{\hat{N}^{-1}\} \hat{G}^{E, \underline{h}^*}(x_{3,A}, x_3) \right] dx_3.
\end{aligned} \tag{7-16}$$

### 7-4-1 Interferometric representation in medium type A and B

We simplify equation 7-15 for the porous medium types A and B of Chapter 5 that have  $\hat{\mu} = \mu_0$  and obey perfect elasticity  $\hat{N} = N$ . The volume integral over the magnetic and elastic loss functions disappears. We consider all the sources to emit a Ricker wavelet  $\hat{s}^{rw}(\omega)$  with a power spectrum  $\hat{S}^{rw}(\omega)$ , thus we replaced the source vector  $\hat{s}$  of equation 7-4 by a  $4 \times 4$  point-source matrix  $\mathbf{I}\delta(x_3 - x_{3,s})\hat{s}^{rw}$ . We would find for the particle velocity  $\hat{v}_2^s$  at  $x_{3,B}$  due to a current source  $-\underline{J}_2^{s,e}$  at  $x_{3,A}$ ,

$$\begin{aligned}
& \left\{ \hat{G}^{v^s, \underline{J}^e}(x_{3,B}, x_{3,A}) + \hat{G}^{E, \underline{f}^*}(x_{3,A}, x_{3,B}) \right\} \hat{S}^{rw} = \\
& \sum_{k=1}^2 n_{3;k} \left[ \hat{G}^{v, J^m}(x_{3,B}, x_{3;k}) \hat{G}^{E, \underline{J}^{e*}}(x_{3,A}, x_{3;k}) + \hat{G}^{v, \underline{J}^e}(x_{3,B}, x_{3;k}) \hat{G}^{E, J^{m*}}(x_{3,A}, x_{3;k}) \right. \\
& \quad \left. - \hat{G}^{v, \underline{h}}(x_{3,B}, x_{3;k}) \hat{G}^{E, \underline{f}^*}(x_{3,A}, x_{3;k}) - \hat{G}^{v, \underline{f}}(x_{3,B}, x_{3;k}) \hat{G}^{E, \underline{h}^*}(x_{3,A}, x_{3;k}) \right] \hat{S}^{rw} \\
& + i\omega 2 \int_{x_{3,1}}^{x_{3,2}} \left[ \hat{G}^{v, \underline{J}^e}(x_{3,B}, x_3) i\mathfrak{Im}\{\hat{\varepsilon}\} \hat{G}^{E, \underline{J}^{e*}}(x_{3,A}, x_3) - \hat{G}^{v, \underline{J}^e}(x_{3,B}, x_3) \Re\{\rho^f \hat{\mathcal{L}}\} \hat{G}^{E, \underline{f}^*}(x_{3,A}, x_3) \right. \\
& \quad \left. + \hat{G}^{v, \underline{f}}(x_{3,B}, x_3) \Re\{\rho^f \hat{\mathcal{L}}\} \hat{G}^{E, \underline{J}^{e*}}(x_{3,A}, x_3, \omega) + \hat{G}^{v, \underline{f}}(x_{3,B}, x_3) i\mathfrak{Im}\{\hat{\rho}^c\} \hat{G}^{E, \underline{f}^*}(x_{3,A}, x_3) \right] \hat{S}^{rw} dx_3.
\end{aligned} \tag{7-17}$$

In Chapter 8 we use this equation to create an example of the SH-TE seismoelectric interferometric representation in 1D.

### 7-4-2 Relation between the two retrieved Green's function matrices

The left-hand side of equation 7-15 is a sum of the causal Green's function matrix and the time reversed of it's reciprocal Green's function matrix. Using the source-receiver reciprocity

relations 7-8 to 7-12, we can explore the left-hand side of equation 7-15 in the frequency domain. If there is a sign switch between  $\hat{G}_{IJ}(x_{3,B}, x_{3,A})$  and  $\hat{G}_{JI}^*(x_{3,A}, x_{3,B})$  we retrieve an imaginary signal, this means that the retrieved signal is asymmetric in the time domain. While if there is no sign switch between  $\hat{G}_{IJ}(x_{3,B}, x_{3,A})$  and  $\hat{G}_{JI}^*(x_{3,A}, x_{3,B})$ , we retrieve a purely real signal, which means that in the time domain we have a symmetric function. Applying the source-receiver relations 7-8 to 7-12 to the left-hand of equation 7-15, yields

$$\hat{\mathbf{G}}(x_{3,B}, x_{3,A}) + \hat{\mathbf{G}}^\dagger(x_{3,A}, x_{3,B}) = 2 \begin{pmatrix} \Re\{\hat{G}^{E,\underline{J}^e}\} & i\Im\{\hat{G}^{E,J^m}\} & i\Im\{\hat{G}^{E,\underline{f}}\} & \Re\{\hat{G}^{E,\underline{h}}\} \\ i\Im\{\hat{G}^{H,\underline{J}^e}\} & \Re\{\hat{G}^{H,J^m}\} & \Re\{\hat{G}^{H,\underline{f}}\} & i\Im\{\hat{G}^{H,\underline{h}}\} \\ i\Im\{\hat{G}^{v,\underline{J}^e}\} & \Re\{\hat{G}^{v,J^m}\} & \Re\{\hat{G}^{v,\underline{f}}\} & i\Im\{\hat{G}^{v,\underline{h}}\} \\ \Re\{\hat{G}^{\tau,\underline{J}^e}\} & i\Im\{\hat{G}^{\tau,J^m}\} & i\Im\{\hat{G}^{\tau,\underline{f}}\} & \Re\{\hat{G}^{\tau,\underline{h}}\} \end{pmatrix} (x_{3,B}, x_{3,A}). \quad (7-18)$$

## 7-5 SH-TE seismoelectric coupling in 2D

In Chapter 3 we have seen that in 2D the seismoelectric system decouples into the SH-TE and P-SV-TM modes of propagation. The SH-TE mode is governed by the fields  $E_2$ ,  $H_1$ ,  $H_3$ ,  $v_2^s$ ,  $-\hat{\tau}_{21}^b$ , and  $-\hat{\tau}_{23}^b$ . The coupling coefficient in the 3D seismoelectric system is incorporated in the equations for  $\mathbf{w}$ , the differential velocity of the solid and fluid phases,  $\mathbf{w}$ . In Appendix C-1 we see that in 2D the field  $w_2$  does not obey an independent differential equation. We eliminated  $w_2$  from the system of equations and defined new source functions that incorporate the force on the fluid phase. The SH-TE system in 2D can be captured in the general flow, diffusion and wave equation as

$$i\omega \hat{\mathbf{A}}\hat{\mathbf{u}} + \hat{\mathbf{B}}\hat{\mathbf{u}} + \mathbf{D}_x\hat{\mathbf{u}} = \hat{\mathbf{s}}. \quad (7-19)$$

Where the field  $\hat{\mathbf{u}}$  and source vectors  $\hat{\mathbf{s}}$  are defined by

$$\hat{\mathbf{u}}^t = (\hat{E}_2, \hat{H}_1, \hat{H}_3, \hat{v}_2^s, -\hat{\tau}_{21}^b, -\hat{\tau}_{23}^b) \quad (7-20)$$

$$\hat{\mathbf{s}}^t = (-\hat{J}_2^e, -\hat{J}_1^m, -\hat{J}_1^m, \hat{f}_2, \hat{h}_1^b, \hat{h}_3^b) \quad (7-21)$$

With the new source types  $\hat{J}_2^{s,e} = \hat{J}_2^{s,e} + \hat{\mathcal{L}}\hat{f}_2^f$ ,  $\hat{f}_2 = \hat{f}_2 - \frac{\rho^f}{\rho^E}\hat{f}_2^f$ ,  $\hat{h}_3^b = \hat{h}_{32}^b + \hat{h}_{23}^b$  and  $\hat{h}_1^b = \hat{h}_{12}^b + \hat{h}_{21}^b$ . The system matrices  $\hat{\mathbf{A}}$ ,  $\hat{\mathbf{B}}$  and  $\mathbf{D}_x$  are given by

$$\mathbf{A} = \begin{pmatrix} \epsilon & 0 & 0 & -\rho^f \hat{\mathcal{L}} & 0 & 0 \\ 0 & \mu & 0 & 0 & 0 & 0 \\ 0 & 0 & \mu & 0 & 0 & 0 \\ \rho^f \hat{\mathcal{L}} & 0 & 0 & \hat{\rho}^t & 0 & 0 \\ 0 & 0 & 0 & 0 & \frac{1}{N} & 0 \\ 0 & 0 & 0 & 0 & 0 & \frac{1}{N} \end{pmatrix}, \quad \mathbf{B} = \begin{pmatrix} \hat{\sigma}^e & 0 & 0 & 0 & 0 & 0 \\ 0 & \hat{\sigma}^m & 0 & 0 & 0 & 0 \\ 0 & 0 & \hat{\sigma}^m & 0 & 0 & 0 \\ 0 & 0 & 0 & 0 & 0 & 0 \\ 0 & 0 & 0 & 0 & 0 & 0 \\ 0 & 0 & 0 & 0 & 0 & 0 \end{pmatrix} \quad (7-22)$$

$$\text{and } \mathbf{D}_x = \begin{pmatrix} 0 & -\partial_3 & \partial_1 & 0 & 0 & 0 \\ -\partial_3 & 0 & 0 & 0 & 0 & 0 \\ \partial_1 & 0 & 0 & 0 & 0 & 0 \\ 0 & 0 & 0 & 0 & \partial_1 & \partial_3 \\ 0 & 0 & 0 & \partial_1 & 0 & 0 \\ 0 & 0 & 0 & \partial_3 & 0 & 0 \end{pmatrix}. \quad (7-23)$$

The system matrices of the SH-TE system obey the same symmetry properties as those of the entire seismoelectric system, see Section 2-2-1. We have

$$\mathbf{K}_0 \hat{\mathbf{A}} \mathbf{K}_0 = \hat{\mathbf{A}} \quad \text{and} \quad \mathbf{K}_0 \hat{\mathbf{B}} \mathbf{K}_0 = \hat{\mathbf{B}}. \quad (7-24)$$

The matrix  $\mathbf{D}_x$ , containing spatial derivatives, obeys

$$\mathbf{K}_0 \mathbf{D}_x \mathbf{K}_0 = -\mathbf{D}_x = -\mathbf{D}_x^t, \quad (7-25)$$

where  $\mathbf{K}_0$  is defined by

$$\mathbf{K}_0 = \text{diag}(-1, 1, 1, 1, -1, -1). \quad (7-26)$$

We replace the source vector  $\mathbf{s}$  by a  $6 \times 6$  point-source matrix  $\mathbf{I}\delta(\mathbf{x} - \mathbf{x}_s)$  and correspondingly replace the field vector  $\mathbf{u}$  observed at  $\mathbf{x}_r$  by a  $6 \times 6$  Green's function matrix,

$$\hat{\mathbf{G}}(\mathbf{x}_r, \mathbf{x}_s, \omega) = \begin{pmatrix} \hat{G}^{E, \underline{J}^e} & \hat{G}^{E, J_1^m} & \hat{G}^{E, J_3^m} & \hat{G}^{E, \underline{f}} & \hat{G}^{E, \underline{h}_1} & \hat{G}^{E, \underline{h}_3} \\ \hat{G}^{H_1, \underline{J}^e} & \hat{G}^{H_1, J_1^m} & \hat{G}^{H_1, J_3^m} & \hat{G}^{H_1, \underline{f}} & \hat{G}^{H_1, \underline{h}_1} & \hat{G}^{H_1, \underline{h}_3} \\ \hat{G}^{H_3, \underline{J}^e} & \hat{G}^{H_3, J_1^m} & \hat{G}^{H_3, J_3^m} & \hat{G}^{H_3, \underline{f}} & \hat{G}^{H_3, \underline{h}_1} & \hat{G}^{H_3, \underline{h}_3} \\ \hat{G}^{v, \underline{J}^e} & \hat{G}^{v, J_1^m} & \hat{G}^{v, J_3^m} & \hat{G}^{v, \underline{f}} & \hat{G}^{v, \underline{h}_1} & \hat{G}^{v, \underline{h}_3} \\ \hat{G}^{\tau_{21}, \underline{J}^e} & \hat{G}^{\tau_{21}, J_1^m} & \hat{G}^{\tau_{21}, J_3^m} & \hat{G}^{\tau_{21}, \underline{f}} & \hat{G}^{\tau_{21}, \underline{h}_1} & \hat{G}^{\tau_{21}, \underline{h}_3} \\ \hat{G}^{\tau_{23}, \underline{J}^e} & \hat{G}^{\tau_{23}, J_1^m} & \hat{G}^{\tau_{23}, J_3^m} & \hat{G}^{\tau_{23}, \underline{f}} & \hat{G}^{\tau_{23}, \underline{h}_1} & \hat{G}^{\tau_{23}, \underline{h}_3} \end{pmatrix} (\mathbf{x}_r, \mathbf{x}_s, \omega). \quad (7-27)$$

Where we omitted all unnecessary directional subscripts of the fields in the superscripts. In the notation of subsequent sections we will also omit the  $\omega$  dependence. In part I of this thesis, we further reduced this set by eliminating the fields  $H_3$  and  $\tau_{21}^b$  from the field vector  $\mathbf{u}$ . This way we obtained the two-way wave equation that we used to construct seismoelectric Green's functions for the SH-TE system in 2D in horizontally-stratified media.

## 7-6 Convolution-type reciprocity theorem for SH-TE in 2D

In this section we use the equations of Section 6-2 to find a convolution-type reciprocity theorem for SH-TE waves in 2D in the frequency domain. If we substitute the field vector from equation 7-21 for the two different states A and B into the interaction quantity  $\mathbf{D}_x \cdot (\mathbf{K}_0 \mathbf{u}_A \mathbf{u}_B^t)$ , we find

$$\begin{aligned} \partial_3 \left[ \hat{E}_{2,A} \hat{H}_{1,B} - \hat{H}_{1,A} \hat{E}_{2,B} + \hat{\tau} b_{23,A} \hat{v}_{2,B}^s - \hat{v}_{2,A}^s \hat{\tau}_{23,B}^b \right] \\ + \partial_1 \left[ \hat{H}_{3,A} \hat{E}_{2,B} - \hat{E}_{2,A} \hat{H}_{3,B} + \hat{\tau}_{21,A}^b \hat{v}_{2,B}^s - \hat{v}_{s2,A} \hat{\tau}_{21,B}^b \right]. \end{aligned} \quad (7-28)$$

We apply the product rule to equation 7-28 and substitute the differential equations 7-22 and 7-23, after integration over the domain  $\mathbb{S}$ , we apply the theorem of Gauss to the integral

containing the differential operators  $\partial_3$  and  $\partial_1$  and we find

$$\begin{aligned}
& \oint_{\partial\mathbb{S}} \left[ \left\{ \hat{E}_{2,A} \hat{H}_{1,B} - \hat{H}_{1,A} \hat{E}_{2,B} + \hat{\tau}_{23,A}^b \hat{v}_{2,B}^s - \hat{v}_{2,A}^s \hat{\tau}_{23,B}^b \right\} n_3 \right. \\
& \quad \left. + \left\{ \hat{H}_{3,A} \hat{E}_{2,B} - \hat{E}_{2,A} \hat{H}_{3,B} + \hat{\tau}_{21,A}^b \hat{v}_{2,B}^s - \hat{v}_{2,A}^s \hat{\tau}_{21,B}^b \right\} n_1 \right] d\mathbf{x} = \\
& \int_{\mathbb{S}} \left[ \hat{E}_{2,A} \hat{J}_{2,B}^{s,e} - \hat{J}_{2,A}^{s,e} \hat{E}_{2,B} + \hat{J}_{1,A}^{s,m} \hat{H}_{1,B} - \hat{H}_{1,A} \hat{J}_{1,B}^{s,m} + \hat{J}_{3,A}^{s,m} \hat{H}_{3,B} - \hat{H}_{3,A} \hat{J}_{3,B}^{s,m} \right. \\
& \quad \left. + \hat{v}_{2,A}^s \hat{f}_{2,B} - \hat{f}_{2,A} \hat{v}_{2,B} + \hat{\tau}_{23,A}^b \hat{h}_{3,B} - \hat{h}_{3,A} \hat{\tau}_{23,B}^b + \hat{\tau}_{21,A}^b \hat{h}_{1,B} - \hat{h}_{1,A} \hat{\tau}_{21,B}^b \right] d^2\mathbf{x} \\
& + i\omega \int_{\mathbb{S}} \left[ -\hat{E}_{2,A} (\hat{\varepsilon}_A - \hat{\varepsilon}_B) \hat{E}_{2,B} + \hat{E}_{2,A} \left( \rho_A^f \hat{\mathcal{L}}_A - \rho_B^f \hat{\mathcal{L}}_B \right) \hat{v}_{2,B}^s \right. \\
& \quad \left. + \hat{H}_{1,A} (\hat{\mu}_A - \hat{\mu}_B) \hat{H}_{1,B} + \hat{H}_{3,A} (\hat{\mu}_A - \hat{\mu}_B) \hat{H}_{3,B} \right. \\
& \quad \left. + \hat{v}_{2,A}^s \left( \rho_A^f \hat{\mathcal{L}}_A - \rho_B^f \hat{\mathcal{L}}_B \right) \hat{E}_{2,B} + \hat{v}_{2,A}^s (\hat{\rho}_A^c - \hat{\rho}_B^c) \hat{v}_{2,B}^s \right. \\
& \quad \left. - \hat{\tau}_{23,A}^b \left( \hat{N}_A^{-1} - \hat{N}_B^{-1} \right) \hat{\tau}_{23,B}^b - \hat{\tau}_{21,A}^b \left( \hat{N}_A^{-1} - \hat{N}_B^{-1} \right) \hat{\tau}_{21,B}^b \right] d^2\mathbf{x}. \tag{7-29}
\end{aligned}$$

This is the convolution-type reciprocity theorem for 2D SH-TE seismoelectric waves. We substitute the SH-TE Green's function matrix 7-27 in 2D and the symmetry matrix 7-26 into the source-receiver relation for the Green's matrix equation 6-7, to we find the source-receiver reciprocity relations as

$$\hat{G}^{E,\underline{J}^e}(\mathbf{x}_A, \mathbf{x}_B) = \hat{G}^{E,\underline{J}^e}(\mathbf{x}_B, \mathbf{x}_A) \quad , \quad \hat{G}^{H_1, J_1^m}(\mathbf{x}_A, \mathbf{x}_B) = \hat{G}^{H_1, J_1^m}(\mathbf{x}_B, \mathbf{x}_A), \tag{7-30}$$

$$\hat{G}^{H_3, J_3^m}(\mathbf{x}_A, \mathbf{x}_B) = \hat{G}^{H_3, J_3^m}(\mathbf{x}_B, \mathbf{x}_A) \quad , \quad \hat{G}^{H_1, J_3^m}(\mathbf{x}_A, \mathbf{x}_B) = \hat{G}^{H_3, J_1^m}(\mathbf{x}_B, \mathbf{x}_A), \tag{7-31}$$

$$\hat{G}^{H_1, \underline{J}^e}(\mathbf{x}_A, \mathbf{x}_B) = -\hat{G}^{E, J_1^m}(\mathbf{x}_B, \mathbf{x}_A) \quad , \quad \hat{G}^{H_3, \underline{J}^e}(\mathbf{x}_A, \mathbf{x}_B) = -\hat{G}^{E, J_3^m}(\mathbf{x}_B, \mathbf{x}_A), \tag{7-32}$$

$$\hat{G}^{v^s, J_1^m}(\mathbf{x}_A, \mathbf{x}_B) = \hat{G}^{H_1, \underline{f}}(\mathbf{x}_B, \mathbf{x}_A) \quad , \quad \hat{G}^{v^s, J_3^m}(\mathbf{x}_A, \mathbf{x}_B) = \hat{G}^{H_3, \underline{f}}(\mathbf{x}_B, \mathbf{x}_A), \tag{7-33}$$

$$\hat{G}^{\tau_{23}, \underline{J}^e}(\mathbf{x}_A, \mathbf{x}_B) = \hat{G}^{E, h_3}(\mathbf{x}_B, \mathbf{x}_A) \quad , \quad \hat{G}^{\tau_{21}, \underline{J}^e}(\mathbf{x}_A, \mathbf{x}_B) = \hat{G}^{E, h_1}(\mathbf{x}_B, \mathbf{x}_A), \tag{7-34}$$

$$\hat{G}^{\tau_{23}, J_3^m}(\mathbf{x}_A, \mathbf{x}_B) = -\hat{G}^{H, h_3}(\mathbf{x}_B, \mathbf{x}_A) \quad , \quad \hat{G}^{\tau_{21}, J_3^m}(\mathbf{x}_A, \mathbf{x}_B) = -\hat{G}^{H, h_1}(\mathbf{x}_B, \mathbf{x}_A), \tag{7-35}$$

$$\hat{G}^{\tau_{23}, J_3^m}(\mathbf{x}_A, \mathbf{x}_B) = -\hat{G}_3^{H, h_3}(\mathbf{x}_B, \mathbf{x}_A) \quad , \quad \hat{G}^{\tau_{21}, J_3^m}(\mathbf{x}_A, \mathbf{x}_B) = -\hat{G}_3^{H, h_1}(\mathbf{x}_B, \mathbf{x}_A), \tag{7-36}$$

$$\hat{G}^{v, \underline{f}}(\mathbf{x}_A, \mathbf{x}_B) = \hat{G}^{v, \underline{f}}(\mathbf{x}_B, \mathbf{x}_A) \quad , \quad \hat{G}^{\tau_{23}, h_3}(\mathbf{x}_A, \mathbf{x}_B) = \hat{G}^{\tau_{23}, h_3}(\mathbf{x}_B, \mathbf{x}_A), \tag{7-37}$$

$$\hat{G}^{\tau_{21}, h_1}(\mathbf{x}_A, \mathbf{x}_B) = \hat{G}^{\tau_{21}, h_1}(\mathbf{x}_B, \mathbf{x}_A) \quad , \quad \hat{G}^{\tau_{23}, h_1}(\mathbf{x}_A, \mathbf{x}_B) = \hat{G}^{\tau_{21}, h_3}(\mathbf{x}_B, \mathbf{x}_A), \tag{7-38}$$

$$\hat{G}^{\tau_{23}, \underline{f}}(\mathbf{x}_A, \mathbf{x}_B) = -\hat{G}^{v, h_3}(\mathbf{x}_B, \mathbf{x}_A) \quad , \quad \hat{G}^{\tau_{21}, \underline{f}}(\mathbf{x}_A, \mathbf{x}_B) = -\hat{G}^{v, h_1}(\mathbf{x}_B, \mathbf{x}_A), \tag{7-39}$$

$$\hat{G}^{v, \underline{J}^e}(\mathbf{x}_A, \mathbf{x}_B) = -\hat{G}^{E, \underline{f}}(\mathbf{x}_B, \mathbf{x}_A). \tag{7-40}$$

## 7-7 Correlation-type reciprocity theorem for SH-TE in 2D

In this section we use the equations of Section 6-3 to find a correlation-type reciprocity theorem for SH-TE waves in 2D in the frequency domain. We substitute the field vector from equation 7-21 for two different states A and B into the interaction quantity  $\mathbf{D}_\mathbf{x} \cdot (\mathbf{u}_A \mathbf{u}_B^t)$ , to find

$$\begin{aligned}
& -\partial_3 \left[ \hat{E}_{2,A}^* \hat{H}_{1,B} + \hat{H}_{1,A}^* \hat{E}_{2,B} + \hat{\tau}_{23,A}^{b*} \hat{v}_{2,B}^s + \hat{v}_{2,A}^{s*} \hat{\tau}_{23,B}^b \right] \\
& \quad + \partial_1 \left[ \hat{H}_{3,A}^* \hat{E}_{2,B} + \hat{E}_{2,A}^* \hat{H}_{3,B} - \hat{\tau}_{21,A}^{b*} \hat{v}_{2,B}^s - \hat{v}_{2,A}^{s*} \hat{\tau}_{21,B}^b \right]. \tag{7-41}
\end{aligned}$$

We apply the product rule and substitute the differential equations equations 7-22 and 7-23, after integration over the domain  $\mathbb{S}$ , we apply the theorem of Gauss to the integral containing the differential operators  $\partial_3$  and  $\partial_1$  and we find

$$\begin{aligned}
& \oint_{\partial\mathbb{S}} \left[ - \left\{ \hat{E}_{2,A}^* \hat{H}_{1,B} + \hat{H}_{1,A}^* \hat{E}_{2,B} + \hat{\tau}_{23,A}^{b*} \hat{v}_{2,B}^s + \hat{v}_{2,A}^{s*} \hat{\tau}_{23,B}^b \right\} n_3 \right. \\
& \quad \left. + \left\{ \hat{H}_{3,A}^* \hat{E}_{2,B} + \hat{E}_{2,A}^* \hat{H}_{3,B} - \hat{\tau}_{21,A}^{b*} \hat{v}_{2,B}^{s*} - \hat{v}_{2,A}^{s*} \hat{\tau}_{21,B}^b \right\} n_1 \right] d\mathbf{x} = \\
& \int_{\mathbb{S}} \left[ -\hat{J}_{2,A}^{s,e*} \hat{E}_{2,B} - \hat{E}_{2,A}^* \hat{J}_{2,B}^{s,e} - \hat{J}_{1,A}^{s,m*} \hat{H}_{1,B} - \hat{H}_{1,A}^* \hat{J}_{1,B}^{s,m} - \hat{J}_{3,A}^{s,m*} \hat{H}_{3,B} - \hat{H}_{3,A}^* \hat{J}_{3,B}^{s,m} \right. \\
& \quad \left. + \hat{v}_{2,A}^s \hat{f}_{2,B} + \hat{f}_{2,A}^* \hat{v}_{2,B} - \hat{\tau}_{23,A}^{b*} \hat{h}_{3,B}^b - \hat{h}_{3,A}^{b*} \hat{\tau}_{23,B}^b - \hat{\tau}_{21,A}^{b*} \hat{h}_{1,B}^b - \hat{h}_{1,A}^{b*} \hat{\tau}_{21,B}^b \right] d^2\mathbf{x} \\
& -i\omega \int_{\mathbb{S}} \left[ \hat{E}_{2,A}^* (\hat{\varepsilon}_B - \hat{\varepsilon}_A^*) \hat{E}_{2,B} - \hat{E}_{2,A}^* \left( \rho_B^f \hat{\mathcal{L}}_B + \rho_A^{f*} \hat{\mathcal{L}}_A^* \right) \hat{v}_{2,B}^s \right. \\
& \quad \left. + \hat{H}_{1,A}^* (\hat{\mu}_B - \hat{\mu}_A^*) \hat{H}_{1,B} + \hat{H}_{3,A}^* (\hat{\mu}_B - \hat{\mu}_A^*) \hat{H}_{3,B} \right. \\
& \quad \left. + \hat{v}_{2,A}^{s*} \left( \rho_B^f \hat{\mathcal{L}}_B + \rho_A^{f*} \hat{\mathcal{L}}_A^* \right) \hat{E}_{2,B} + \hat{v}_{2,A}^{s*} (\hat{\rho}_B^c - \hat{\rho}_A^{c*}) \hat{v}_{2,B}^s \right. \\
& \quad \left. + \hat{\tau}_{23,A}^{b*} \left( \hat{N}_B^{-1} - \hat{N}_A^{-1*} \right) \hat{\tau}_{23,B}^b + \hat{\tau}_{21,A}^{b*} \left( \hat{N}_B^{-1} - \hat{N}_A^{-1*} \right) \hat{\tau}_{21,B}^b \right] d^2\mathbf{x}. \tag{7-42}
\end{aligned}$$

This is the correlation-type reciprocity theorem for SH-TE seismoelectric waves in 2D. Note that the right-hand side of equation 7-42 does not disappear if we choose equal medium parameters in both states. The right-hand side of equation 7-42 contains a volume integral over the loss functions of the system and over the coupling coefficient, that governs the conversion of electromagnetic energy to elastodynamic energy and vice versa.

## 7-8 Seismoelectric interferometric Green's function recovery in 2D

From equation 6-11 we can derive an interferometric representation of the SH-TE Green's function matrix in 2D. We substitute the Green's function matrix 7-27 and the medium

parameter matrices 7-23 into equation 6-11, to find

$$\begin{aligned}
& \hat{G}_{IJ}(\mathbf{x}_B, \mathbf{x}_A) + \hat{G}_{JI}^*(\mathbf{x}_A, \mathbf{x}_B) = \\
& - \oint_{\partial\mathbb{S}} \left[ -\hat{G}_{I2}^{Jm}(\mathbf{x}_B, \mathbf{x}) n_3 \hat{G}_{J1}^{Je*}(\mathbf{x}_A, \mathbf{x}) - \hat{G}_{I1}^{Je}(\mathbf{x}_B, \mathbf{x}) n_3 \hat{G}_{J2}^{Jm*}(\mathbf{x}_A, \mathbf{x}) \right. \\
& \quad + \hat{G}_{I6}^{h3}(\mathbf{x}_B, \mathbf{x}) n_3 \hat{G}_{J4}^{f*}(\mathbf{x}_A, \mathbf{x}) + \hat{G}_{I4}^f(\mathbf{x}_B, \mathbf{x}) n_3 \hat{G}_{J6}^{h3*}(\mathbf{x}_A, \mathbf{x}) \\
& \quad + \hat{G}_{I1}^{Je}(\mathbf{x}_B, \mathbf{x}) n_1 \hat{G}_{J3}^{Jm*}(\mathbf{x}_A, \mathbf{x}) + \hat{G}_{I3}^{Jm}(\mathbf{x}_B, \mathbf{x}) n_1 \hat{G}_{J1}^{Je*}(\mathbf{x}_A, \mathbf{x}) \\
& \quad \left. + \hat{G}_{I4}^f(\mathbf{x}_B, \mathbf{x}) n_1 \hat{G}_{J5}^{h1*}(\mathbf{x}_A, \mathbf{x}) + \hat{G}_{I5}^{h1}(\mathbf{x}_B, \mathbf{x}) n_1 \hat{G}_{J4}^{f*}(\mathbf{x}_A, \mathbf{x}) \right] d\mathbf{x} \\
& + i\omega 2 \int_{\mathbb{S}} \left[ \hat{G}_{I1}^{Je}(\mathbf{x}_B, \mathbf{x}) i\Im\{\hat{\varepsilon}\} \hat{G}_{J1}^{Je*}(\mathbf{x}_A, \mathbf{x}) - \hat{G}_{I1}^{Je}(\mathbf{x}_B, \mathbf{x}) \Re\{\rho^f \hat{\mathcal{L}}\} \hat{G}_{J4}^{f*}(\mathbf{x}_A, \mathbf{x}) \right. \\
& \quad + \hat{G}_{I4}^f(\mathbf{x}_B, \mathbf{x}) \Re\{\rho^f \hat{\mathcal{L}}\} \hat{G}_{J1}^{Je*}(\mathbf{x}_A, \mathbf{x}) + \hat{G}_{I4}^f(\mathbf{x}_B, \mathbf{x}) i\Im\{\hat{\rho}^c\} \hat{G}_{J4}^{f*}(\mathbf{x}_A, \mathbf{x}) \\
& \quad + \hat{G}_{I2}^{Jm}(\mathbf{x}_B, \mathbf{x}) i\Im\{\hat{\mu}\} \hat{G}_{J2}^{Jm*}(\mathbf{x}_A, \mathbf{x}) + \hat{G}_{I3}^{Jm}(\mathbf{x}_B, \mathbf{x}) i\Im\{\hat{\mu}\} \hat{G}_{J3}^{Jm*}(\mathbf{x}_A, \mathbf{x}) \\
& \quad \left. + \hat{G}_{I5}^{h1}(\mathbf{x}_B, \mathbf{x}) i\Im\{\hat{N}^{-1}\} \hat{G}_{J5}^{h1*}(\mathbf{x}_A, \mathbf{x}) + \hat{G}_{I6}^{h3}(\mathbf{x}_B, \mathbf{x}) i\Im\{\hat{N}^{-1}\} \hat{G}_{J6}^{h3*}(\mathbf{x}_A, \mathbf{x}) \right] d^2\mathbf{x}.
\end{aligned} \tag{7-43}$$

In which  $\hat{G}_{IJ}(x_A, x_B)$  denotes the  $I^{th}$  element of the  $J^{th}$  column of the Green's function matrix 7-27 at  $x_B$  yielding a response due to a point-source at  $x_A$ . The domain integral over  $\mathbb{S}$  on the right-hand side of equation 7-43 is a sum of crosscorrelations of observed responses of sources weighted by the loss and seismoelectric coupling functions. This integral not only compensates for the losses inside  $\mathbb{S}$ , but also contributes to the seismoelectric coupling inside  $\mathbb{S}$ . The crosscorrelations of responses of sources on the boundary  $\partial\mathbb{S}$  accounts for the contributions to the Green's functions from losses and seismoelectric coupling outside  $\mathbb{S}$ .

We can use equation 7-43 for an interferometric expression for every element of the Green's function matrix  $\hat{\mathbf{G}}(x_B, x_A)$ . For example, for the particle velocity  $\hat{v}_2^s$  in the solid at observation location  $x_B$  due to an electrical current source  $-\underline{J}_2^{s,e}$  at observation location  $x_A$ , we have

$$\begin{aligned}
& \hat{G}^{v,J^e}(\mathbf{x}_B, \mathbf{x}_A) + \hat{G}^{E,f*}(\mathbf{x}_A, \mathbf{x}_B) = \\
& \oint_{\partial\mathbb{S}} \left[ \hat{G}^{v,J^m}(\mathbf{x}_B, \mathbf{x}) n_3 \hat{G}^{E,J^e*}(\mathbf{x}_A, \mathbf{x}) + \hat{G}^{v,J^e}(\mathbf{x}_B, \mathbf{x}) n_3 \hat{G}^{E,J^m*}(\mathbf{x}_A, \mathbf{x}) \right. \\
& \quad - \hat{G}^{v,h3}(\mathbf{x}_B, \mathbf{x}) n_3 \hat{G}^{E,f*}(\mathbf{x}_A, \mathbf{x}) - \hat{G}^{v,f}(\mathbf{x}_B, \mathbf{x}) n_3 \hat{G}^{E,h3*}(\mathbf{x}_A, \mathbf{x}) \\
& \quad - \hat{G}^{v,J^e}(\mathbf{x}_B, \mathbf{x}) n_1 \hat{G}^{E,J^m*}(\mathbf{x}_A, \mathbf{x}) - \hat{G}^{v,J^m}(\mathbf{x}_B, \mathbf{x}) n_1 \hat{G}^{E,J^e*}(\mathbf{x}_A, \mathbf{x}) \\
& \quad \left. - \hat{G}^{v,f}(\mathbf{x}_B, \mathbf{x}) n_1 \hat{G}^{E,h1*}(\mathbf{x}_A, \mathbf{x}) - \hat{G}^{v,h1}(\mathbf{x}_B, \mathbf{x}) n_1 \hat{G}^{E,f*}(\mathbf{x}_A, \mathbf{x}) \right] d\mathbf{x} \\
& + i\omega 2 \int_{\mathbb{S}} \left[ \hat{G}^{v,J^e}(\mathbf{x}_B, \mathbf{x}) i\Im\{\hat{\varepsilon}\} \hat{G}^{E,J^e*}(\mathbf{x}_A, \mathbf{x}) - \hat{G}^{v,J^e}(\mathbf{x}_B, \mathbf{x}) \Re\{\rho^f \hat{\mathcal{L}}\} \hat{G}^{E,f*}(\mathbf{x}_A, \mathbf{x}) \right. \\
& \quad + \hat{G}^{v,f}(\mathbf{x}_B, \mathbf{x}) \Re\{\rho^f \hat{\mathcal{L}}\} \hat{G}^{E,J^e*}(\mathbf{x}_A, \mathbf{x}) + \hat{G}^{v,f}(\mathbf{x}_B, \mathbf{x}) i\Im\{\hat{\rho}^c\} \hat{G}^{E,f*}(\mathbf{x}_A, \mathbf{x}) \\
& \quad + \hat{G}^{v,J^m}(\mathbf{x}_B, \mathbf{x}) i\Im\{\hat{\mu}\} \hat{G}^{E,J^m*}(\mathbf{x}_A, \mathbf{x}) + \hat{G}^{v,J^m}(\mathbf{x}_B, \mathbf{x}) i\Im\{\hat{\mu}\} \hat{G}^{E,J^m*}(\mathbf{x}_A, \mathbf{x}) \\
& \quad \left. + \hat{G}^{v,h3}(\mathbf{x}_B, \mathbf{x}) i\Im\{\hat{N}^{-1}\} \hat{G}^{E,h3*}(\mathbf{x}_A, \mathbf{x}) + \hat{G}^{v,h1}(\mathbf{x}_B, \mathbf{x}) i\Im\{\hat{N}^{-1}\} \hat{G}^{E,h1*}(\mathbf{x}_A, \mathbf{x}) \right] d^2\mathbf{x}.
\end{aligned} \tag{7-44}$$

### 7-8-1 Interferometric representation in medium type A and B

We simplify equation 7-15 this for porous medium types A and B of Chapter 5 that have  $\hat{\mu} = \mu_0$  and obey perfect elasticity  $\hat{N} = N$ . The volume integral over the magnetic and elastic loss functions disappears. We separate the boundary integral into a horizontal part  $\mathbb{S}_3$  and vertical part  $\mathbb{S}_1$ . The horizontal boundaries have normal vector  $n_3 = 1$  for the lower boundary and  $n_3 = -1$  for the upper boundary. The vertical boundaries have normal vector  $n_1 = -1$  for the left side and  $n_1 = 1$  for the right side boundary. We consider all the sources to emit a Ricker wavelet  $\hat{s}^{rw}(\omega)$  with a power spectrum  $\hat{S}^{rw}(\omega)$ , thus we replaced the source vector  $\hat{\mathbf{s}}$  of equation 7-21 by a  $6 \times 6$  point-source matrix  $\mathbf{I}\delta(\mathbf{x} - \mathbf{x}_s)\hat{s}^{rw}$ . We would find for the particle velocity  $\hat{v}_2^s$  at  $x_{3,B}$  due to a current source  $-\hat{J}_2^{s,e}$  at  $x_{3,A}$ ,

$$\begin{aligned}
& \left\{ \hat{G}^{v,\underline{J}^e}(\mathbf{x}_B, \mathbf{x}_A) + \hat{G}^{E,\underline{f}^*}(\mathbf{x}_A, \mathbf{x}_B) \right\} \hat{S}^{rw} = \\
& \oint_{\partial\mathbb{S}_3} \left[ \hat{G}^{v,J_1^m}(\mathbf{x}_B, \mathbf{x})n_3\hat{G}^{E,\underline{J}^{e*}}(\mathbf{x}_A, \mathbf{x}) + \hat{G}^{v,\underline{J}^e}(\mathbf{x}_B, \mathbf{x})n_3\hat{G}^{E,J_1^{m*}}(\mathbf{x}_A, \mathbf{x}) \right. \\
& \quad \left. - \hat{G}^{v,\underline{h}_3}(\mathbf{x}_B, \mathbf{x})n_3\hat{G}^{E,\underline{f}^*}(\mathbf{x}_A, \mathbf{x}) - \hat{G}^{v,\underline{f}}(\mathbf{x}_B, \mathbf{x})n_3\hat{G}^{E,\underline{h}_3^*}(\mathbf{x}_A, \mathbf{x}) \right] \hat{S}^{rw} d\mathbf{x} \\
& - \oint_{\partial\mathbb{S}_1} \left[ \hat{G}^{v,\underline{J}^e}(\mathbf{x}_B, \mathbf{x})n_1\hat{G}^{E,J_3^{m*}}(\mathbf{x}_A, \mathbf{x}) + \hat{G}^{v^s,J_3^m}(\mathbf{x}_B, \mathbf{x})n_1\hat{G}^{E,\underline{J}^{e*}}(\mathbf{x}_A, \mathbf{x}) \right. \\
& \quad \left. + \hat{G}^{v,\underline{f}}(\mathbf{x}_B, \mathbf{x})n_1\hat{G}^{E,\underline{h}_1^*}(\mathbf{x}_A, \mathbf{x}) + \hat{G}^{v,\underline{h}_1}(\mathbf{x}_B, \mathbf{x})n_1\hat{G}^{E,\underline{f}^*}(\mathbf{x}_A, \mathbf{x}) \right] \hat{S}^{rw} d\mathbf{x} \\
& + i\omega 2 \int_{\mathbb{S}} \left[ \hat{G}^{v,\underline{J}^e}(\mathbf{x}_B, \mathbf{x})i\mathfrak{Im}\{\hat{\varepsilon}\}\hat{G}^{E,\underline{J}^{e*}}(\mathbf{x}_A, \mathbf{x}) - \hat{G}^{v,\underline{J}^e}(\mathbf{x}_B, \mathbf{x})\mathfrak{Re}\{\rho^f\hat{\mathcal{L}}\}\hat{G}^{E,\underline{f}^*}(\mathbf{x}_A, \mathbf{x}) \right. \\
& \quad \left. + \hat{G}^{v,\underline{f}}(\mathbf{x}_B, \mathbf{x})\mathfrak{Re}\{\rho^f\hat{\mathcal{L}}\}\hat{G}^{E,\underline{J}^{e*}}(\mathbf{x}_A, \mathbf{x}) + \hat{G}^{v,\underline{f}}(\mathbf{x}_B, \mathbf{x})i\mathfrak{Im}\{\hat{\rho}^c\}\hat{G}^{E,\underline{f}^*}(\mathbf{x}_A, \mathbf{x}) \right] \hat{S}^{rw} d^2\mathbf{x}.
\end{aligned} \tag{7-45}$$

In Chapter 8 we use this equation to recover the SH-TE seismoelectric Green's function in 2D in homogeneous media.

### 7-8-2 Relation between the two retrieved Green's function matrices

The left-hand side of equation 7-43 is a sum of the causal Green's function matrix and the time reversed of it's reciprocal Green's function matrix. Using the source-receiver reciprocity relations 7-30 to 7-40, we can explore the left-hand side of equation 7-43 in the frequency domain. If there is a sign switch between  $\hat{G}_{IJ}(x_{3,B}, x_{3,A})$  and  $\hat{G}_{JI}^*(x_{3,A}, x_{3,B})$  we retrieve an imaginary signal, this means that the retrieved signal is asymmetric in the time domain. While if there is no sign switch between  $\hat{G}_{IJ}(x_{3,B}, x_{3,A})$  and  $\hat{G}_{JI}^*(x_{3,A}, x_{3,B})$ , we retrieve a purely real signal, which means that in the time domain we have a symmetric function.

Applying the source-receiver relations 7-30 to 7-40 to the left-hand of equation 7-43, yields

$$\begin{aligned}
 & \hat{\mathbf{G}}(\mathbf{x}_B, \mathbf{x}_A) + \hat{\mathbf{G}}^\dagger(\mathbf{x}_A, \mathbf{x}_B) = \\
 & 2 \left( \begin{array}{cccccc}
 \Re\{\hat{G}^{E,\underline{J}^e}\} & i\Im\{\hat{G}^{E,J_1^m}\} & i\Im\{\hat{G}^{E,J_3^m}\} & i\Im\{\hat{G}^{E,\underline{f}}\} & \Re\{\hat{G}^{E,\underline{h}_1}\} & \Re\{\hat{G}^{E,\underline{h}_3}\} \\
 i\Im\{\hat{G}^{H_1,\underline{J}^e}\} & \Re\{\hat{G}^{H_1,J_1^m}\} & \Re\{\hat{G}^{H_1,J_3^m}\} & \Re\{\hat{G}^{H_1,\underline{f}}\} & i\Im\{\hat{G}^{H_1,\underline{h}_1}\} & i\Im\{\hat{G}^{H_1,\underline{h}_3}\} \\
 i\Im\{\hat{G}^{H_3,\underline{J}^e}\} & \Re\{\hat{G}^{H_3,J_1^m}\} & \Re\{\hat{G}^{H_3,J_3^m}\} & \Re\{\hat{G}^{H_3,\underline{f}}\} & i\Im\{\hat{G}^{H_3,\underline{h}_1}\} & i\Im\{\hat{G}^{H_3,\underline{h}_3}\} \\
 i\Im\{\hat{G}^{v,\underline{J}^e}\} & \Re\{\hat{G}^{v,J_1^m}\} & \Re\{\hat{G}^{v,J_3^m}\} & \Re\{\hat{G}^{v,\underline{f}}\} & i\Im\{\hat{G}^{v,\underline{h}_1}\} & i\Im\{\hat{G}^{v,\underline{h}_3}\} \\
 \Re\{\hat{G}^{\tau_{21},\underline{J}^e}\} & i\Im\{\hat{G}^{\tau_{21},J_1^m}\} & i\Im\{\hat{G}^{\tau_{21},J_3^m}\} & i\Im\{\hat{G}^{\tau_{21},\underline{f}}\} & \Re\{\hat{G}^{\tau_{21},\underline{h}_1}\} & \Re\{\hat{G}^{\tau_{21},\underline{h}_3}\} \\
 \Re\{\hat{G}^{\tau_{23},\underline{J}^e}\} & i\Im\{\hat{G}^{\tau_{23},J_1^m}\} & i\Im\{\hat{G}^{\tau_{23},J_3^m}\} & i\Im\{\hat{G}^{\tau_{23},\underline{f}}\} & \Re\{\hat{G}^{\tau_{23},\underline{h}_1}\} & \Re\{\hat{G}^{\tau_{23},\underline{h}_3}\}
 \end{array} \right) \\
 & \hspace{20em} (\mathbf{x}_B, \mathbf{x}_A).
 \end{aligned}
 \tag{7-46}$$

# Simulation of interferometric seismoelectric Green's function recovery

This chapter contains several examples of the interferometric representations of Chapter 7. We consider a homogeneous world and perform the experiments separately in the two media types introduced in Chapter 5. The 1D examples have been created using the Green's functions of Appendix C-3. The 2D example is created using the one-way wave equations of Chapter 3. We describe the observations of our experiments, paying particular attention to the role of the different integrals of interferometric representations. All events in the 1D and 2D correlations have been consistently labeled. There are two physical events, see Section 5-3, the first arrives with the electromagnetic wave velocity and is labeled *a*. The second event arrives with the shear wave velocity and is labeled *b*. There is a spurious event in the separate contributions of the domain and boundary integrals, this event is labeled *c*. The events are not always continuous in the figures, in that case they have been assigned an extra subscript that is explained in the text.

### 8-1 1D Seismoelectric interferometry in homogeneous media.

We consider the situation of 2 receivers, labeled A and B, at a distance of 150 meter, see Figure 8-1. The domain  $\mathbb{L}$  is chosen to extend 325 meter away from the receivers. We place two source types at 8000 source positions evenly spaced by 10 cm, between the end points of  $\mathbb{L}$ , thus performing a middle Riemann sum to evaluate the domain integral. Each source is weighted as prescribed in the 1D interferometric representation equation 7-17. At each of the end points we place 8 sources. At receiver A we measure the electrical field and at receiver B we measure the particle velocity, evaluating the interferometric representation for  $G^{v,\underline{J}^e}(\mathbf{x}_B, \mathbf{x}_A, t) + G^{E,\underline{f}}(\mathbf{x}_A, \mathbf{x}_B, -t)$  in 1D given by equation 7-17. Thus we should recover the sum of two Green's functions, the causal response of the particle velocity at B due to a

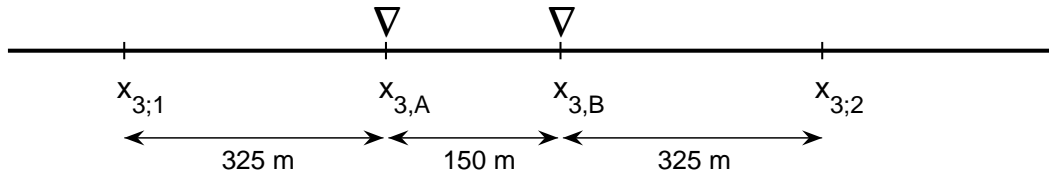


**Figure 8-1:** Symmetric position of receivers and boundary points for 1D interferometry; receiver distance is 150 m, the boundary points are 325 meter away from the receivers. Examples are shown in Figures 8-2, 8-3, 8-4 and 8-5.

electrical current source at B plus the time-reversed response of the electrical field at A as a result of a force source at B. All sources emit a Ricker wavelet, equation 5-12, with a central radial frequency of  $\omega_0 = 800$  radians. Thus the recovered Green's functions are convolved with the autocorrelation of the source function, see equation 7-17. The Green's functions were calculated using a time sampling of  $\Delta t = 0.001$  seconds.

### 8-1-1 Results in medium type A

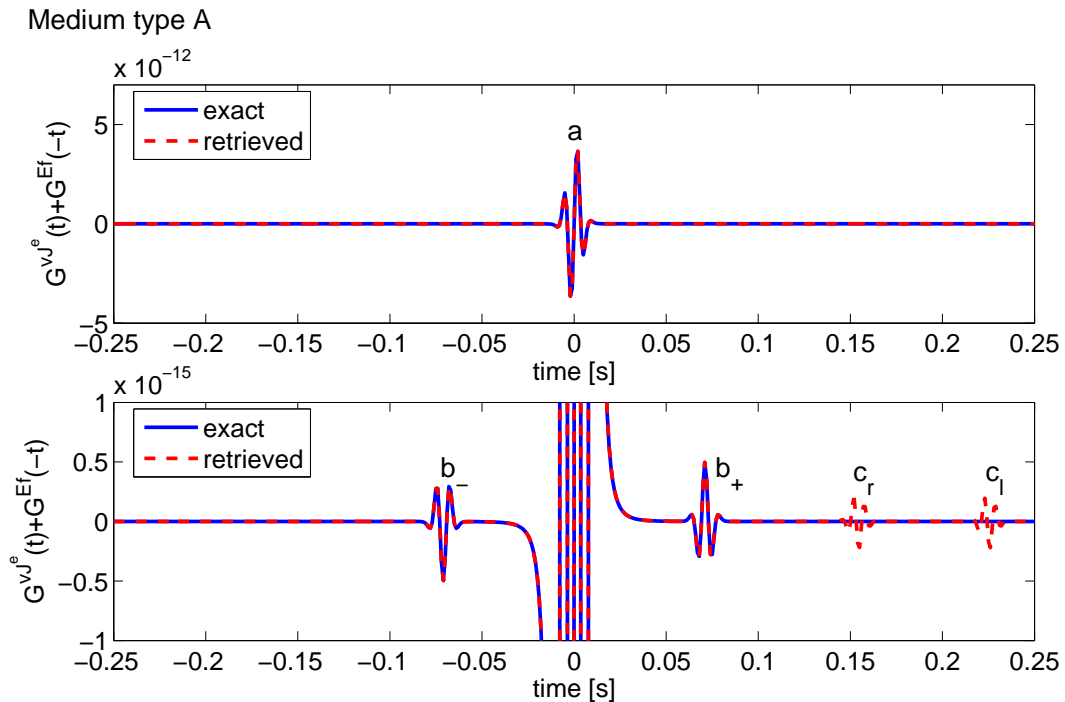


**Figure 8-2:** Exact and retrieved superposition of  $G^{v,j^e}(\mathbf{x}_B, \mathbf{x}_A, t)$  and  $G^{E,f}(\mathbf{x}_A, \mathbf{x}_B, -t)$  in medium type A, using two source types at 8000 source positions evenly spaced over 800 meter. Receiver offset is 150 meter as indicated in Figure 8-1.

We perform the computations using the medium parameters as described for medium type A in Section 5-2. We recover the Green's functions reasonably well and find two physical events in each Green's function, see Figure 8-2. The second event, labeled  $b$ , arrives at  $t = \pm 0.07$

seconds and is three orders of magnitude smaller than the first event, labeled  $a$ , that arrives around  $t = 0$  seconds. Event  $a$  is actually the superposition of the electromagnetic arrivals in  $G^{v,J^e}(\mathbf{x}_B, \mathbf{x}_A, t)$  and  $G^{E,f}(\mathbf{x}_A, \mathbf{x}_B, -t)$ . There are two visible spurious events, labeled  $c_r$  and  $c_l$  in positive times at  $t = 0.15$  seconds and  $t = 0.22$  seconds, they are about half as strong as event  $b$ , see Section 8-1-3 for their origin. In Figure 8-3 we see the separate contributions of the boundary points and the domain integral. We can see in the top panel of Figure 8-3 that the amplitudes of both integrals are strong for event  $a$  but they are reversed in polarity. The contribution from the domain integral is stronger than the desired event, hence the contribution of the boundary is subtracted, this results in the perfect reconstruction of event  $a$ . Event  $b_+$  in  $G^{v,J^e}(\mathbf{x}_B, \mathbf{x}_A, t)$  is reconstructed in a similar way. The contribution of the domain integral is stronger than that of the boundary points and has the correct phase as event  $b_+$  of the exact Green's function. The contribution of the boundary integral is weaker and reversed in polarity with respect to the contribution of the domain integral, they subtract and perfectly reconstruct the shear wave event in positive times. Event  $b_-$  in  $G^{E,f}(\mathbf{x}_A, \mathbf{x}_B, -t)$

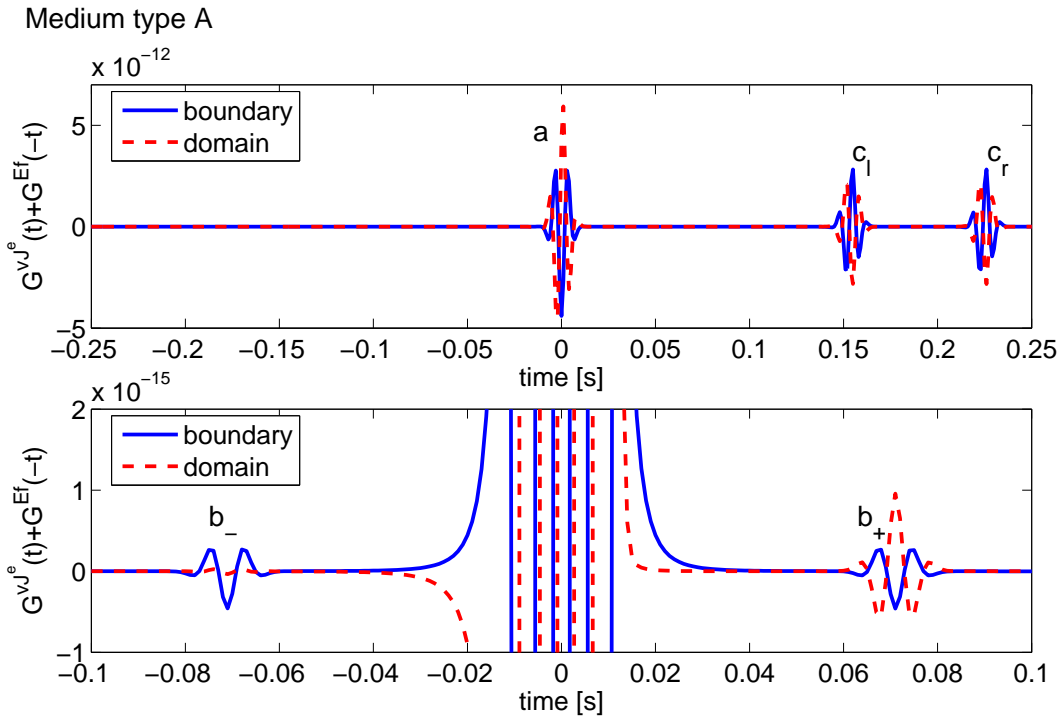


**Figure 8-3:** Separate contributions of the domain integral (red dashed curve) and the boundary points (blue continuous curve) to the reconstruction of the Green's functions in Figure 8-2.

is reconstructed differently. The contribution of the boundary points seem to be equal (on eyesight) to the contribution of the boundary to event  $b_+$  in  $G^{v,J^e}(\mathbf{x}_B, \mathbf{x}_A, t)$ . However, the total contribution of the domain integral is a lot smaller to  $b_-$  than to  $b_+$  in Figure 8-3. But the contributions of the domain and boundary integrals add constructively to reconstruct the event  $b_-$  in  $G^{E,f}(\mathbf{x}_A, \mathbf{x}_B, -t)$ , which is anti-symmetric to the event  $b_+$  in  $G^{v,J^e}(\mathbf{x}_B, \mathbf{x}_A, t)$ .

### 8-1-2 Results in medium type B

We perform the same computations as above, in the medium with characteristics described as medium type B in Section 5-2. We recover the Green's functions even better than in medium type A using the same geometry, see Figure 8-1. Events  $b_+$  and  $b_-$  have slightly larger arrival times than the second events in medium type A, they are two orders of magnitude smaller than event  $a$ . Spurious events  $c_r$  and  $c_l$  are three orders of magnitude smaller than events  $b_-$  and  $b_+$ . In Figure 8-5 we see the separate contributions of the boundary points and the domain integral. We see that the contributions to the reconstructed Green's functions behave similarly as in medium type A. But we do notice that the relative contribution of the boundary points to event,  $a$ , is clearly smaller than the relative contribution of the domain integral. It can also be observed that event  $a$  is three orders of magnitude smaller in medium type B than in medium type A, while the seismic event is only one order of magnitude smaller. But we see that the relative contribution of the domain integral to event  $b_-$  in  $G^{E,f}(\mathbf{x}_A, \mathbf{x}_B, -t)$  is smaller than it was in medium type A.

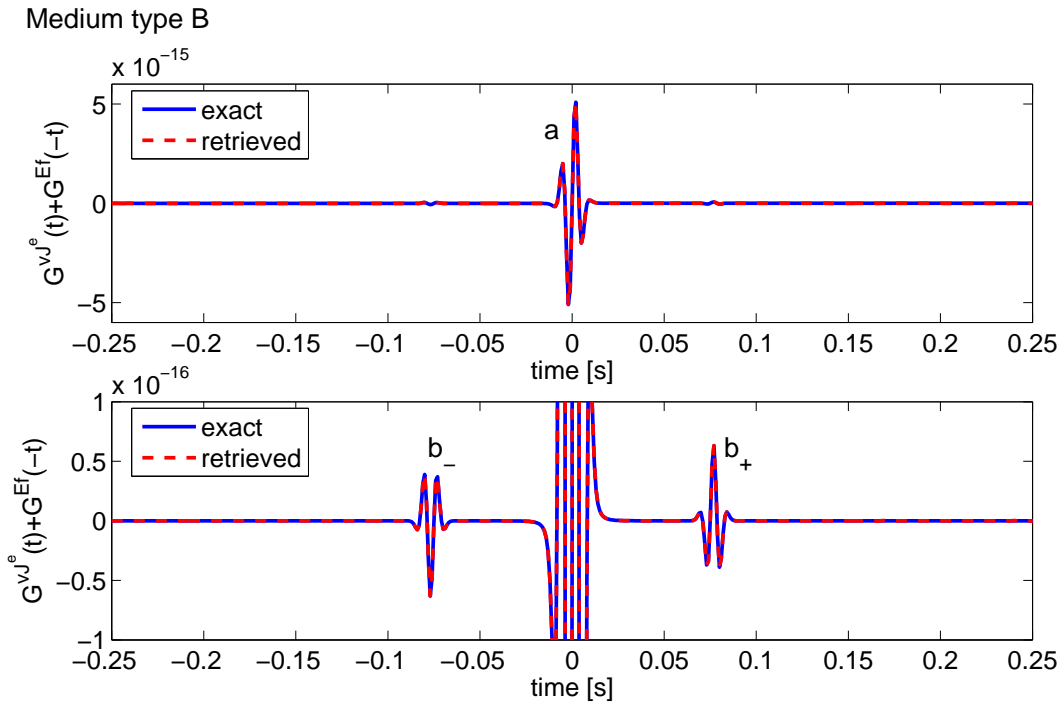


**Figure 8-4:** Exact and retrieved superposition of  $G^{v,j^e}(\mathbf{x}_B, \mathbf{x}_A, t)$  and  $G^{E,f}(\mathbf{x}_A, \mathbf{x}_B, -t)$  in medium type B, using two source types at 8000 source positions evenly spaced over 800 meter. Receiver offset 150 meter as indicated in Figure 8-1.

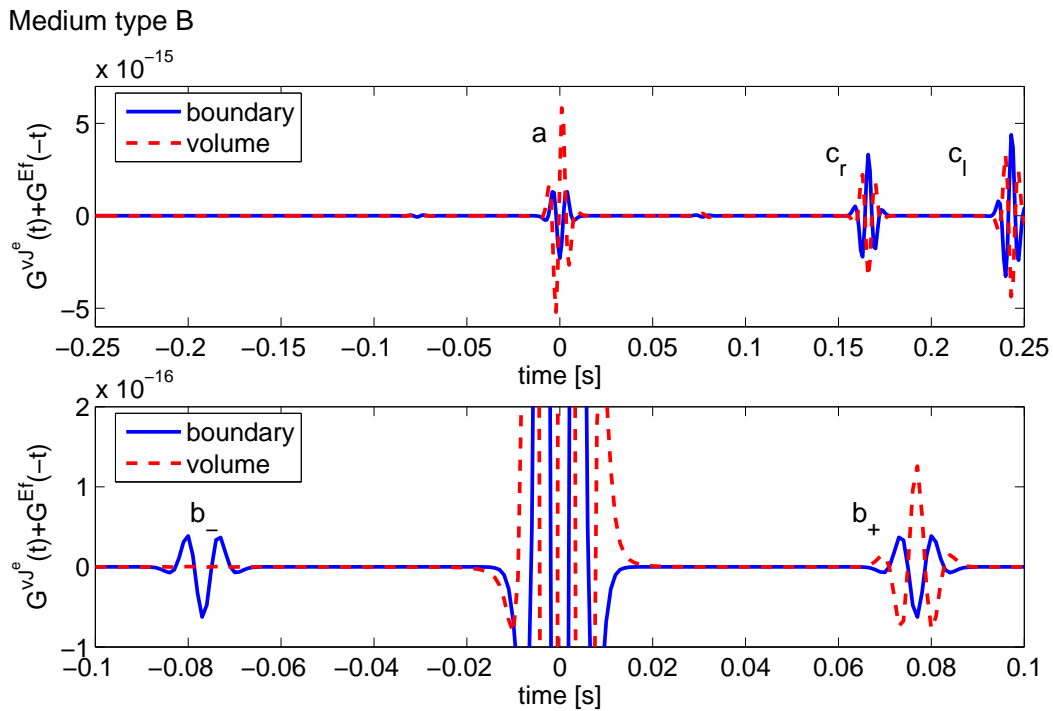


**Figure 8-5:** Separate contributions of the domain integral (red dashed curve) and the boundary points (blue continuous curve) to the reconstruction of the Green's functions in Figure 8-4.

### 8-1-3 Middle Riemann sum

The spurious events in the contributions of the domain integral and the boundary points should cancel out exactly when combined. In these simulations they do so only approximately, because we evaluated the domain integral by performing a middle Riemann sum. The middle Riemann sum divides the integrand in equally spaced regions, the value of the integrand over that region is approximated by the exact value in the middle of that region weighted by the size of the region. The smaller the regions are, the more exact the Riemann sum is. In Figure 8-6 we choose three different source spacings; 1.0 meter, 0.5 meter and 0.1 meter and evaluate the 1D interferometric integral equation 7-17 for both media types. We show the exact result with a blue continuous line, there are no physical events at times later than  $t = 0.1$  seconds. However, there are two visible remainders of the imperfect cancellation of spurious events  $c_r$  and  $c_l$  arriving at times later than  $t = 0.1$  seconds. This remainder is larger in medium type A than in medium type B in absolute sense and relative to event,  $b_+$ , near 0.07 seconds.

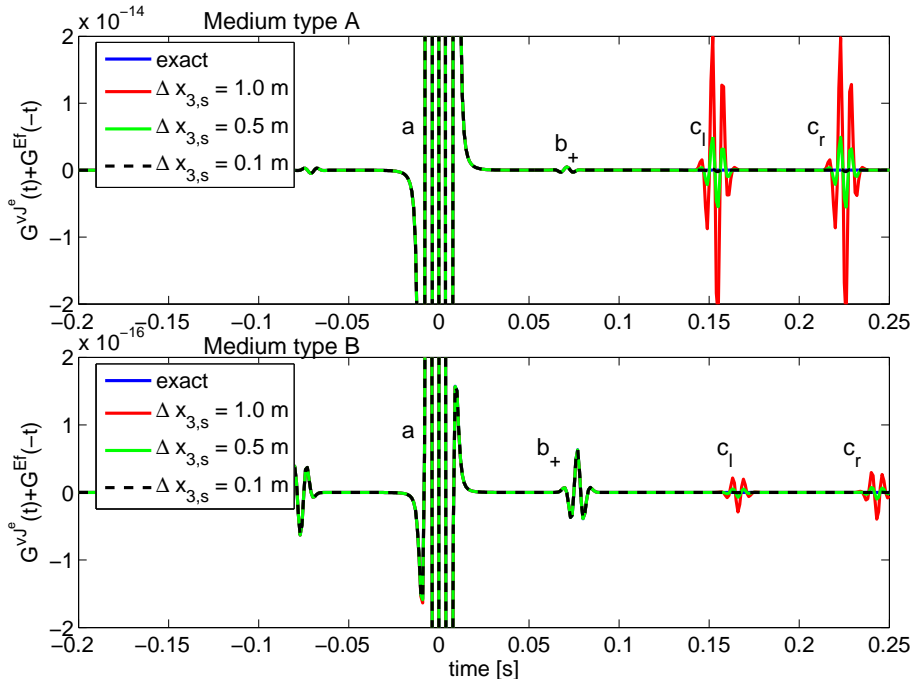


**Figure 8-6:** Recovered signal using three different sample densities of the Riemann sum;  $\Delta_s = 1$  meter,  $\Delta_s = .5$  meter,  $\Delta_s = 0.1$  meter.

## 8-2 Dissecting the 1D interferometric representation

In this section, we take a closer look to the different contributions from the boundary points and different parts of the domain integral, to the reconstruction of  $G^{v,l^e}(\mathbf{x}_B, \mathbf{x}_A, t) + G^{E,f}(\mathbf{x}_A, \mathbf{x}_B, -t)$  in medium type A. We distinguish between the contributions of the different sides of the boundary contribution, from  $x_{3,1}$  and from  $x_{3,2}$ . The domain integral can be dissected in three contributions, from the segment left of receiver A, the segment between the two receivers and the segment part on the right side of receiver B, see Figure 8-7.

In Figure 8-8 we see the contribution of the sources at  $x_{3;1}$  (blue continuous curve) and at  $x_{3;2}$  (red dashed curve). We see how they each contribute equally to event,  $a$ . Each of the boundary points creates its own spurious event,  $c_r$  and  $c_l$ , both in positive times. Event  $c_l$  is constructed by the sources at the left boundary point,  $x_{3;1}$ . Event  $c_r$  is constructed by sources at the right boundary point,  $x_{3;2}$ . The contribution from the sources at  $x_{3;1}$  (continuous blue curve) ends up in the Green's function of waves traveling in the same direction from  $G^{v,\mathcal{J}^e}(\mathbf{x}_B, \mathbf{x}_A, t)$  and vice versa for the contribution of  $x_{3;2}$  (dashed red curve) to the Green's function  $G^{E,\mathcal{J}^f}(\mathbf{x}_A, \mathbf{x}_B, -t)$ . Lastly, we notice how the significant contributions from  $x_{3;1}$  seem to be all causal with a zero-phase wavelet, but the contributions from  $x_{3;2}$  are both causal and anti-causal.

The contributions of the three segments of the domain integral are shown in Figure 8-9. From each segment we can distinguish three events. Segment labeled 2 has both causal and anti-causal contributions, but it only contributes to physical events. Its contribution to event  $b_-$ , in  $G^{E,\mathcal{J}^f}(\mathbf{x}_A, \mathbf{x}_B, -t)$  is two orders of magnitude smaller than the contribution made by segment 3, which is still an order of magnitude smaller than the contribution of the boundary points, see Figures 8-8 and 8-5. In  $G^{E,\mathcal{J}^f}(\mathbf{x}_A, \mathbf{x}_B, -t)$  the domain and boundary contributions have equal polarity. The contribution of segment 2 to event  $b_+$  in  $G^{v,\mathcal{J}^e}(\mathbf{x}_B, \mathbf{x}_A, t)$  is almost equal to the contribution by segment 1, but reversed in polarity. Therefore they nearly cancel, the result is an event *three* orders of magnitude smaller, that still contributes strongly to the total reconstructed event  $b_+$ , see Figures 8-2 and 8-3. All three segments contribute to event  $a$ , but the contribution of segment 1 is at least an order of magnitude smaller than the contributions of segments 2 and 3, which are approximately equal, all three segments contribute with the same polarity to event  $a$ . The spurious events  $c_r$  and  $c_l$ , come from the two outer segments. The arrivals from segment 1, within the first 7 to 8 orders, are all causal with a zero-phase wavelet, while the contributions from segment 3 are both causal and anti-causal.

### 8-2-1 Main contributions in crosscorrelations of the interferometric representation.

In this subsection we analyse the contributions of the different terms in the boundary and domain integrals. The interferometric representation, equation 7-17, contains 8 different crosscorrelations of Green's functions. The arrivals of shear or electromagnetic waves in the Green's functions are stronger or weaker for different source types. The crosscorrelations

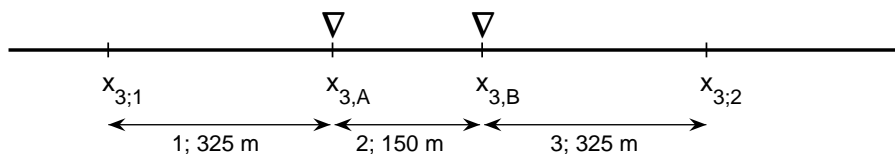


**Figure 8-7:** Three different segments of the domain integral. The first segment (labeled 1) is located left of receiver A and is 325 meter long, the second segment (labeled 2) lies in between the two receivers and is 150 meter long, the third segment (labeled 3) is located right of receiver B and is 325 meter long.

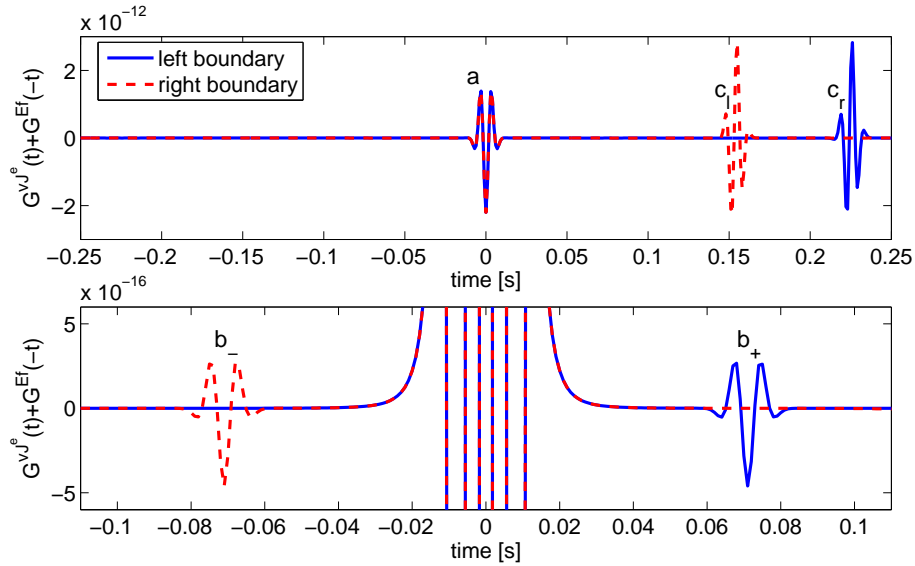


**Figure 8-8:** The separate contributions of the sources at  $x_{3;1}$  (blue continuous curve) and the sources at  $x_{3;2}$  (red dashed curve) to the total boundary contribution in Figure 8-3.

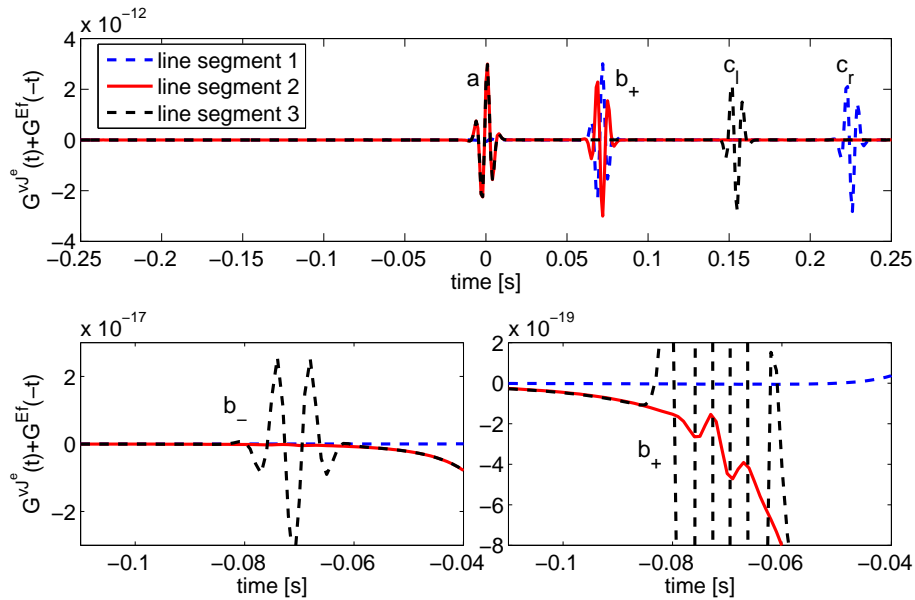


**Figure 8-9:** The contributions of the three segments to the total domain contribution in Figure 8-3.

in the domain integral are also weighted by the loss functions and the coupling coefficient. Therefore certain terms in the representation contribute stronger to the reconstruction of certain events than others terms do. The contributions of each of the four crosscorrelation terms, equation 8-1 to 8-4, from the left boundary point,  $x_{3;1}$ , are shown in Figure 8-10. The contributions of each of the four crosscorrelation terms, equation 8-1 to 8-4, from the left boundary point,  $x_{3;2}$ , are shown in Figure 8-11.

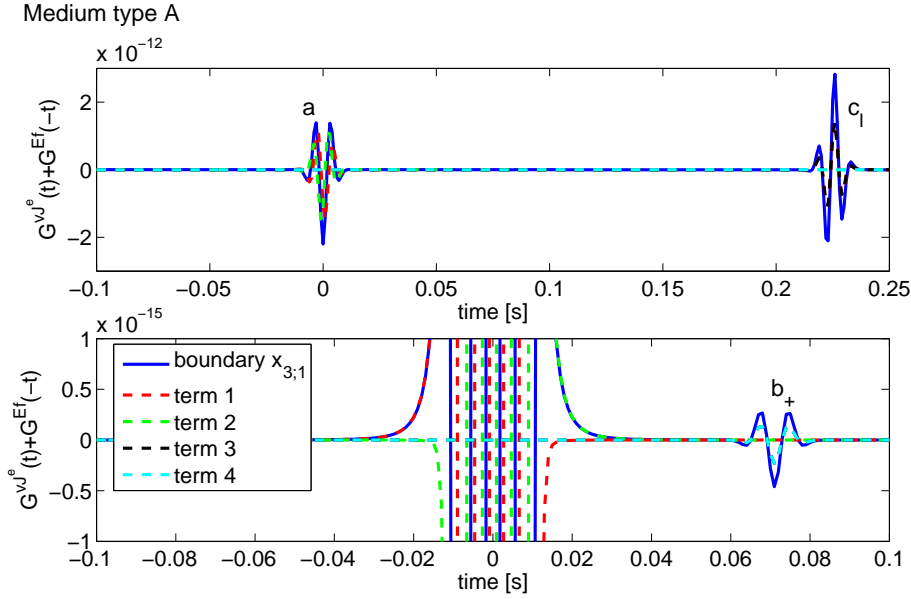


**Figure 8-10:** Contributions from the different crosscorrelation terms at the boundary point  $x_{3;1}$ , to the total contribution coming from the boundary point  $x_{3;1}$ . The crosscorrelation terms are defined in equations 8-1 to 8-4.

The terms of Figures 8-10 and 8-11 are given by;

$$term1 : \hat{G}^{v,J^m}(x_{3,B}, x_{3;k}) \hat{G}^{E,J^e*}(x_{3,A}, x_{3;k}), \quad (8-1)$$

$$term2 : \hat{G}^{v,J^e}(x_{3,B}, x_{3;k}) \hat{G}^{E,J^m*}(x_{3,A}, x_{3;k}), \quad (8-2)$$

$$term3 : -\hat{G}^{v,h}(x_{3,B}, x_{3;k}) \hat{G}^{E,f*}(x_{3,A}, x_{3;k}), \quad (8-3)$$

$$term4 : -\hat{G}^{v,f}(x_{3,B}, x_{3;k}) \hat{G}^{E,h*}(x_{3,A}, x_{3;k}). \quad (8-4)$$

We see in Figures 8-10 and 8-11 that terms 2 and 3 contribute equally to the spurious events  $c_r$  and  $c_l$ , terms 1 and 2 contribute equally to event  $a$ , terms 3 and 4 contribute equally to event  $b_+$  and  $b_-$ . In Figure 8-12 we display the contributions of each of the four crosscorrelation terms, equation 8-5 to 8-8, to the total contribution coming from the domain integral.

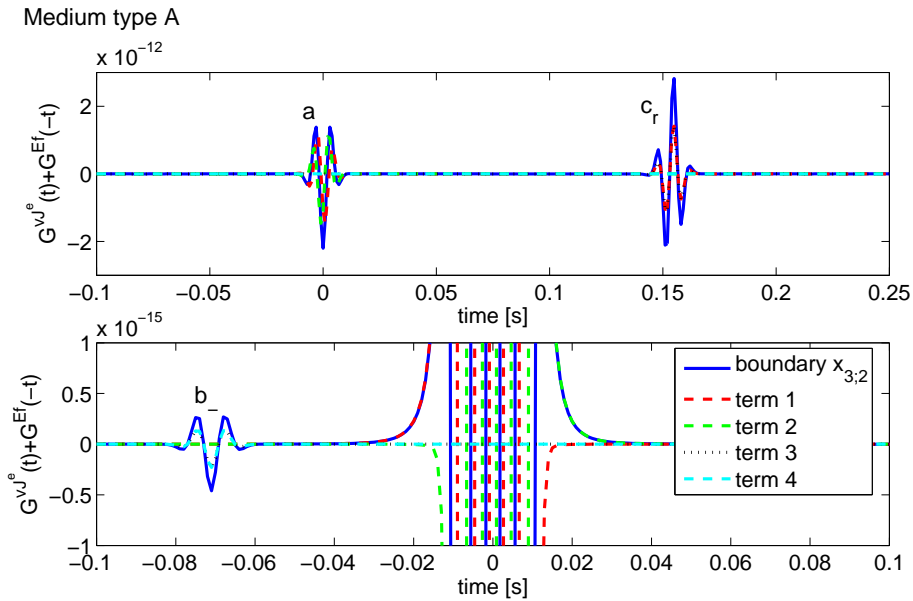


**Figure 8-11:** Contributions from the different crosscorrelation terms at the boundary point  $x_{3,2}$ , to the total contribution coming from the boundary point  $x_{3,2}$ . The crosscorrelation terms are defined in equations 8-1 to 8-4.

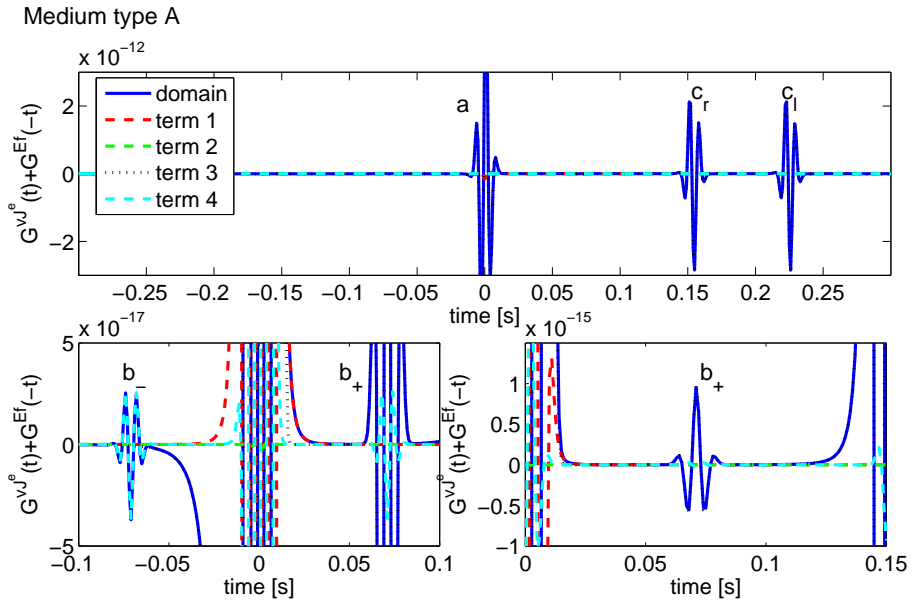


**Figure 8-12:** Contributions from the different crosscorrelations in the domain integral, to the total contribution of the domain integral. The crosscorrelation terms are defined in equations 8-5 to 8-8.

The terms of Figure 8-12 are given by

$$1 : \hat{G}^{v,\underline{J}^e}(x_{3,B}, x_3) i\mathcal{I}\mathfrak{m}\{\hat{\varepsilon}\} \hat{G}^{E,\underline{J}^e*}(x_{3,A}, x_3), \quad (8-5)$$

$$2 : -\hat{G}^{v,\underline{J}^e}(x_{3,B}, x_3) \Re\{\rho^f \hat{\mathcal{L}}\} \hat{G}^{E,\underline{J}^e*}(x_{3,A}, x_3), \quad (8-6)$$

$$3 : \hat{G}^{v,\underline{J}^e}(x_{3,B}, x_3) \Re\{\rho^f \hat{\mathcal{L}}\} \hat{G}^{E,\underline{J}^e*}(x_{3,A}, x_3), \quad (8-7)$$

$$4 : \hat{G}^{v,\underline{J}^e}(x_{3,B}, x_3) i\mathcal{I}\mathfrak{m}\{\hat{\rho}^c\} \hat{G}^{E,\underline{J}^e*}(x_{3,A}, x_3). \quad (8-8)$$

The 4<sup>th</sup> term almost completely reconstructs event  $b_-$ , while the 3<sup>rd</sup> term almost completely accounts for event  $b_+$ . Event  $a$  is also dominantly constructed from the contribution of term 3.

### 8-2-2 Correlation gather of the domain integral

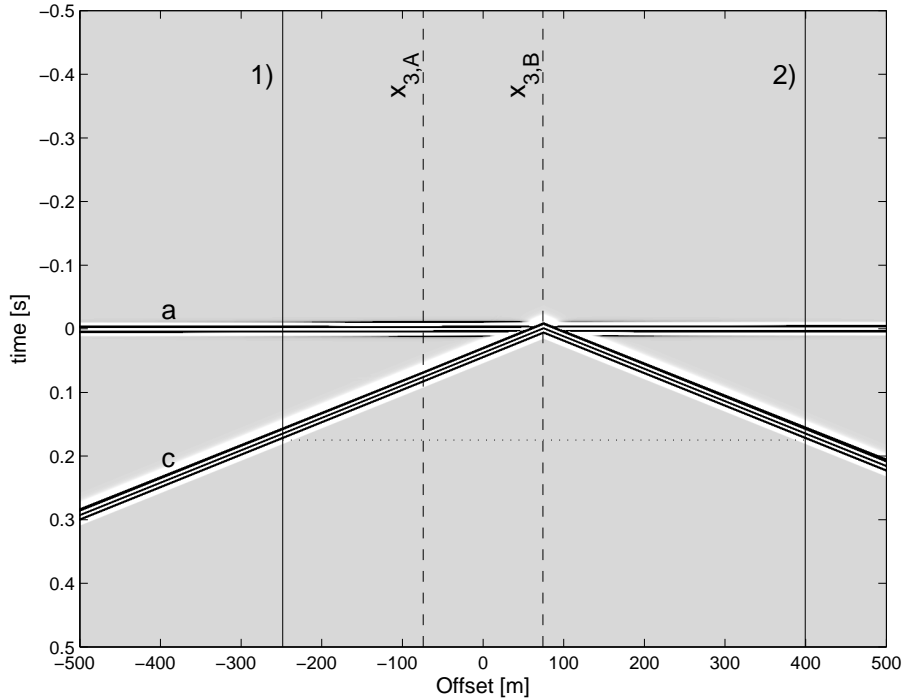


**Figure 8-13:** Correlation gather for seismoelectric interferometry compiled for 10000 source positions in a domain stretching from  $-500$  meter to  $500$  meter. The receiver locations at  $-75$  meter and  $75$  meter are indicated by dashed lines, and labeled  $x_{3,A}$  and  $x_{3,B}$ . Two events can be distinguished, events  $a$  and  $c$ , see text. Two alternative boundary points can be take such that event  $b$  hits both boundaries simultaneously. One possible choice is levels labeled 1 and 2, see Figure 8-16.

It is very useful to study a correlation gather, because it gives visual insight on stationary phases and contributions from different regions of the source coverage. Usually the correlation gather is created from the sources on the boundary only, but since we deal with a seismoelectric diffusive system in 1D we can collect a gather of the sources in the domain integral. The receivers are  $150$  meter apart from each other in medium type B, the correlation gather covers a total length of  $1000$  meter and is compiled for  $10000$  source positions. In Figure 8-13

the gather is shown on a linear gray scale with a clip value of 0.0001 of the maximum value. We can only distinguish two events. Event *a*, is nearly stationary for all offsets, see Section 9-4-2, and arrives around  $t = 0$  seconds. Event *b*, is not visible in Figure 8-13. Event *c*, is non-stationary for all offsets except for sources near receiver B it gives a strong contribution at  $t = 0$  seconds. This event resides in positive times but is not symmetric around the midpoint of the receivers, it intersects with the contribution from the boundaries at different times for symmetrically positioned boundaries. The further away we choose the boundary positions from receiver B, the later the arrival times of the strong spurious events in the separate contributions from the domain and boundary integrals.

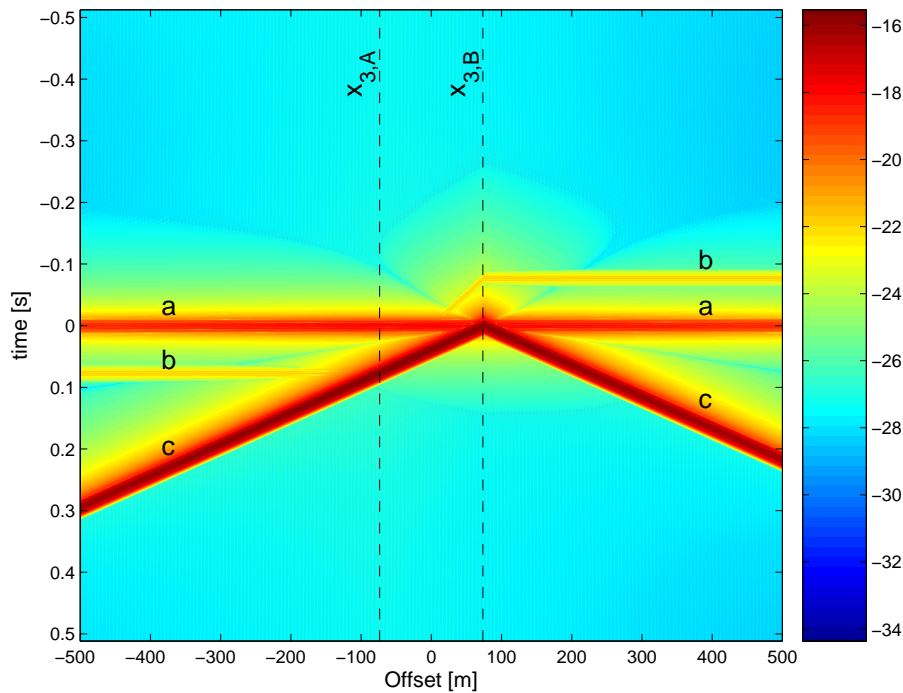


**Figure 8-14:** Logarithm of the absolute value of the Correlation gather in Figure 8-13. We can now distinguish three events, labeled *a*, *b* and *c*, see text.

In Figure 8-14 we see the logarithmic value of the absolute amplitude of the correlation gather in Figure 8-13. We can see a third event labeled, *b*, that is several orders of magnitude smaller than events *a* and *c*. This event is stationary for the parts of the domain that lay outside of the receivers span. It is non-stationary in between the two receivers and arrives at causal times if we are at  $x_3 < x_{3,A}$  and at anti-causal times for  $x_3 > x_{3,B}$ .

### 8-2-3 Alternative boundary positions

There are two distinct boundary positions that give a special alignment of physical and spurious events. The first has been proposed in the correlation gather Figure 8-13. If we choose our boundaries at equal distances from receiver B, for example as in Figure 8-15, we would find that the two strong spurious events in positive times overlap, see top panel of Figure 8-16. The other choice is to place the boundary points just outside the receivers, it can

easily be seen in Figures 8-13 and 8-14 that the spurious events would arrive simultaneously with the two physical events, see bottom panel of Figure 8-16. Remember that we have to include both receivers inside  $\mathbb{L}$  for the interferometric representation to hold, see Section 6-5.

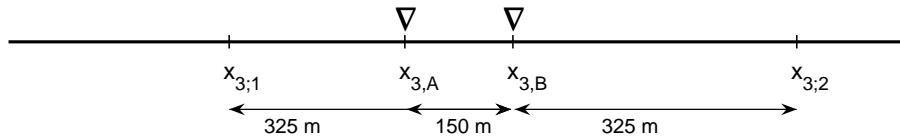


**Figure 8-15:** Alternative position of receivers and boundary points for 1D interferometry; boundary points are taken symmetrically around receiver B at a distance of 325 meter. Example is shown in Figure 8-16.

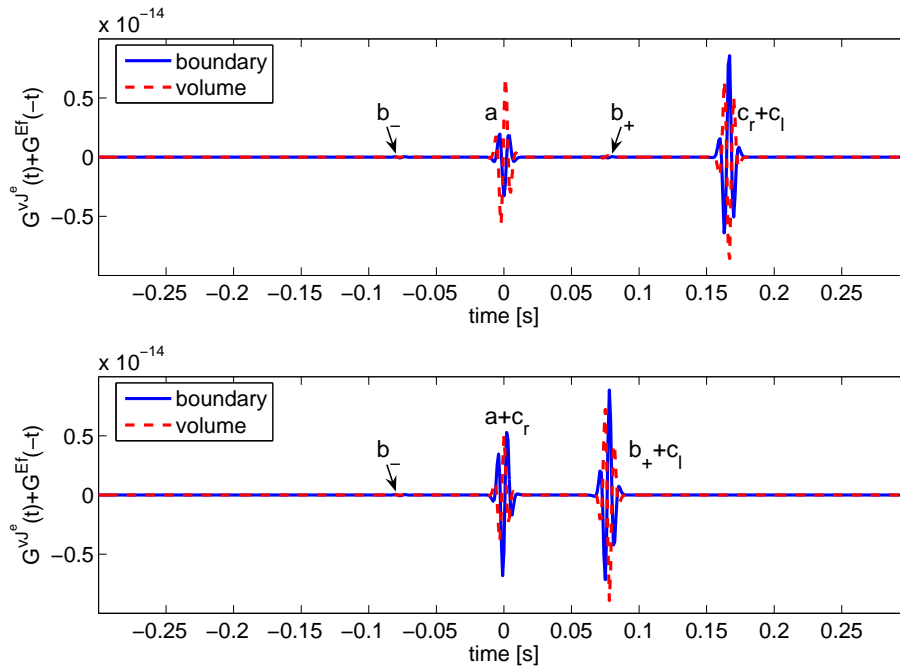


**Figure 8-16:** Reconstructed signal using two alternative positions of the boundaries. Top panel; boundary points are both at a distance of 325 meter from receiver B. Bottom panel; boundary points are just besides the receivers.

### 8-3 2D Seismoelectric interferometry in a homogeneous medium

We consider the situation of two receivers in a homogeneous world. The  $x_1$  and  $x_3$  axes being the horizontal distance and depth. We position receiver A at a depth of 225 meter below the upper domain boundary and receiver B positioned 150 meter directly below receiver A. The lower domain boundary is located 600 meter below the upper boundary. See Figure 8-17 for the experimental setup. We use the modeling method as described in Part I of this thesis, but deal with a rather simplified case because there are no heterogeneities. We evaluate the interferometric representation for  $G^{v,\underline{J}^e}(\mathbf{x}_B, \mathbf{x}_A, t) + G^{E,\underline{f}}(\mathbf{x}_A, \mathbf{x}_B, -t)$  in 2D given by equation 7-45. We place sources spaced as 1 per squared meter on an area of  $1794 \times 600$  squared meters. All sources emit a Ricker wavelet, equation 5-12, with a central angular frequency of  $\omega = 800$  radians, the recovered Green's functions are convolved with the autocorrelation of the source wavelet. The Green's functions were calculated using a time sampling of  $\Delta t = 0.001$  seconds. We omitted the side boundary  $\partial\mathcal{S}_1$  for the calculations in this section. We used the medium parameters of medium type B, see Section 5-2.

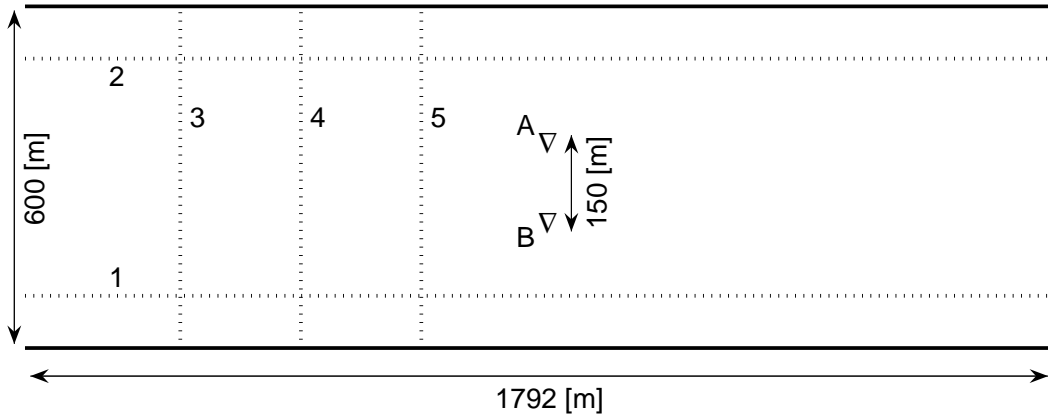


**Figure 8-17:** Geometry for 2D seismoelectric interferometric experiment. The dotted lines labeled 1, 2, 3, 4 and 5, denote the locations of the correlation gathers in Figures 8-24, 8-25, 8-26, 8-27 and 8-28, respectively.

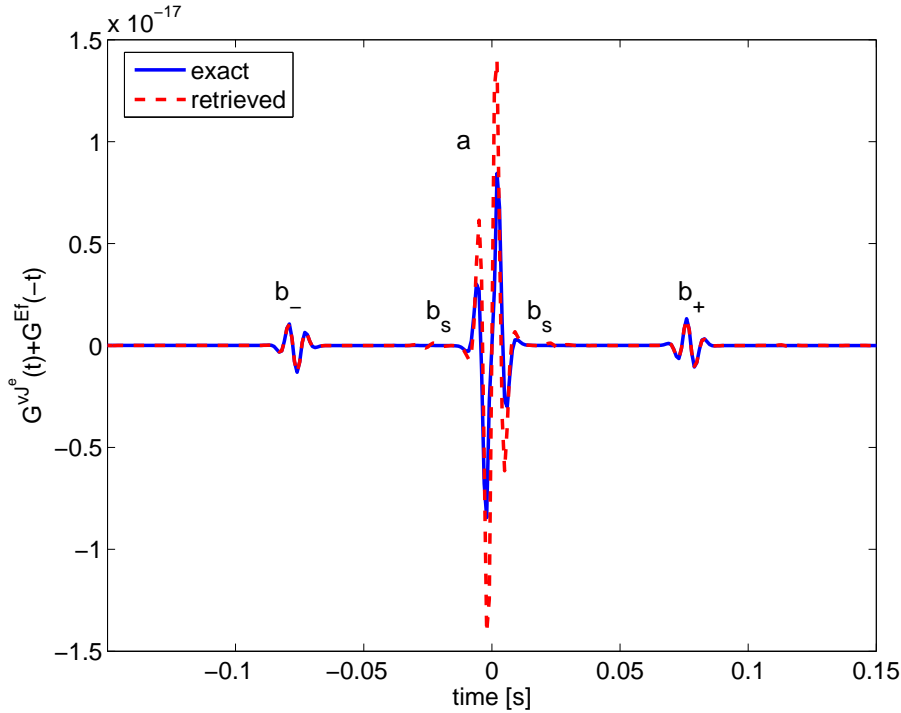


**Figure 8-18:** Exact and retrieved superposition of  $G^{v,J^e}(t)$  and  $G^{E,f}(-t)$  in medium type B in 2D.

In Figure 8-18 we see the exact and retrieved superposition of  $G^{v,J^e}(\mathbf{x}_B, \mathbf{x}_A, t) + G^{E,f}(\mathbf{x}_A, \mathbf{x}_B, -t)$ . We recover the second physical events, labeled  $b_-$  and  $b_+$ , arriving near  $t = \pm 0.07$  seconds, very well. But we do not recover the first event, labeled  $a$ , so well. In addition to that, we see two small spurious events, labeled  $b_s$ , arriving at early times  $t = \pm 0.02$  seconds. In Figure 8-19 we plotted the separate contributions from the boundary integral and the domain integral. We see strong spurious events in the separate contributions from the domain and boundary integrals that cancel each other after combination. The cancellation is imperfect, as in the 1D computations, and some spurious events remain in the end result. In Figures 8-20 and 8-21 we can see the contribution from each source level with depth. Figure 8-20 is a 2D version of Figure 8-13, but it is a correlation gather in the sense that it is a compilation of summed horizontal correlation gathers. In 2D we encounter some additional spurious events with respect to the 1D results due to the limited source aperture in horizontal direction. Event  $a$  in Figures 8-20 and 8-21 form the first arrival, event  $b$  forms the second physical arrival. Event  $c$  is canceled by the boundary contributions from the upper and lower boundaries. Events  $b_s$  and  $c_s$  are spurious events, whose origin we can see later in Figures 8-24 and 8-25.

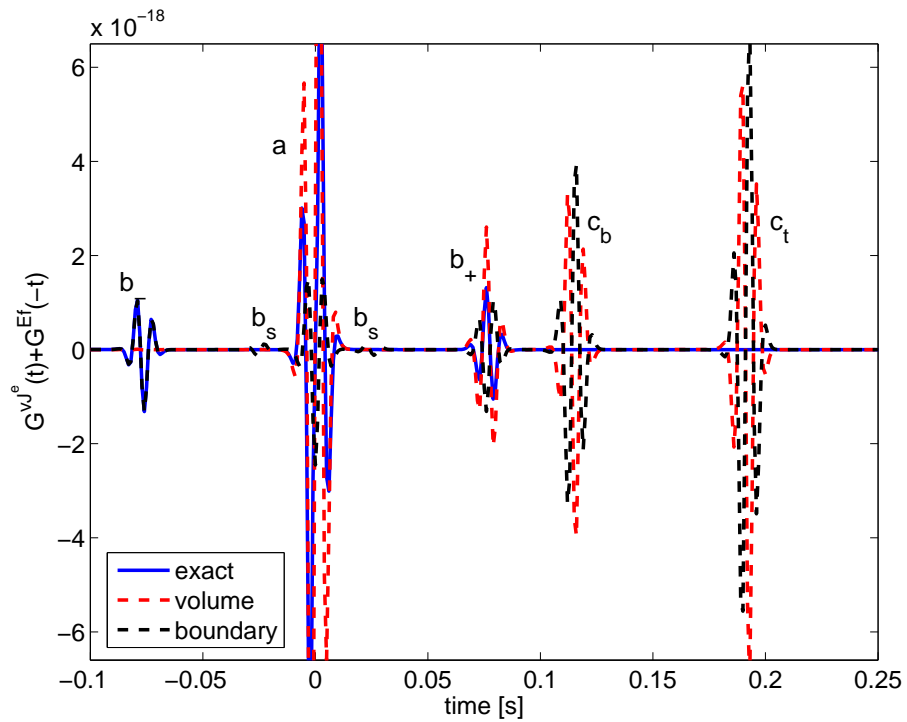


**Figure 8-19:** Boundary integral, domain integral contributions to the exact retrieved signal.

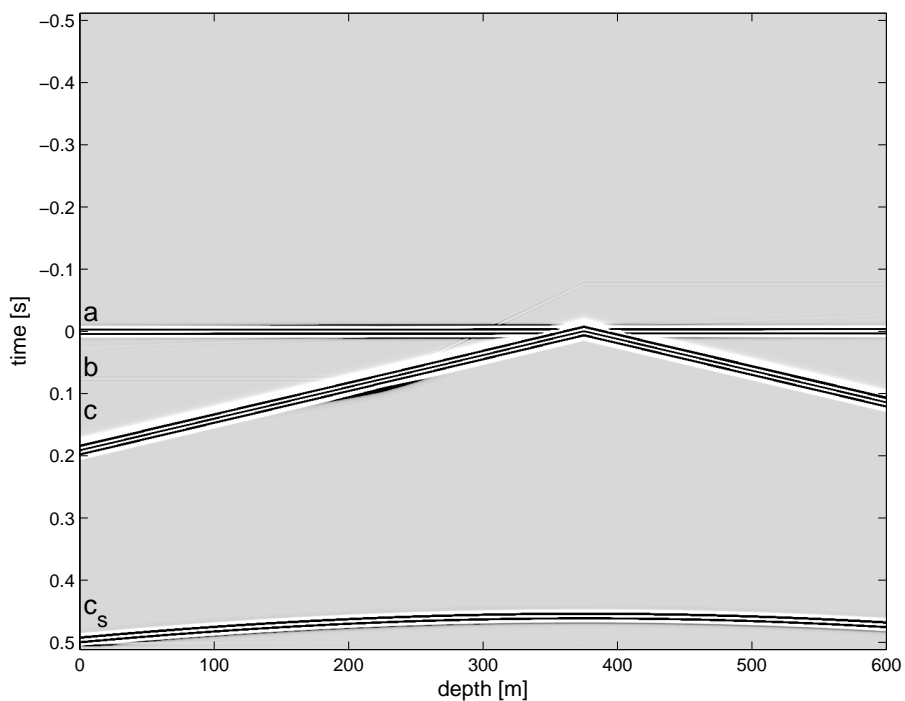


**Figure 8-20:** Source contributions with depth to the recovered signal in Figure 8-18; the domain integral crosscorrelations have been summed in the horizontal direction for each depth level, creating one trace for each depth level. Annotations see text.

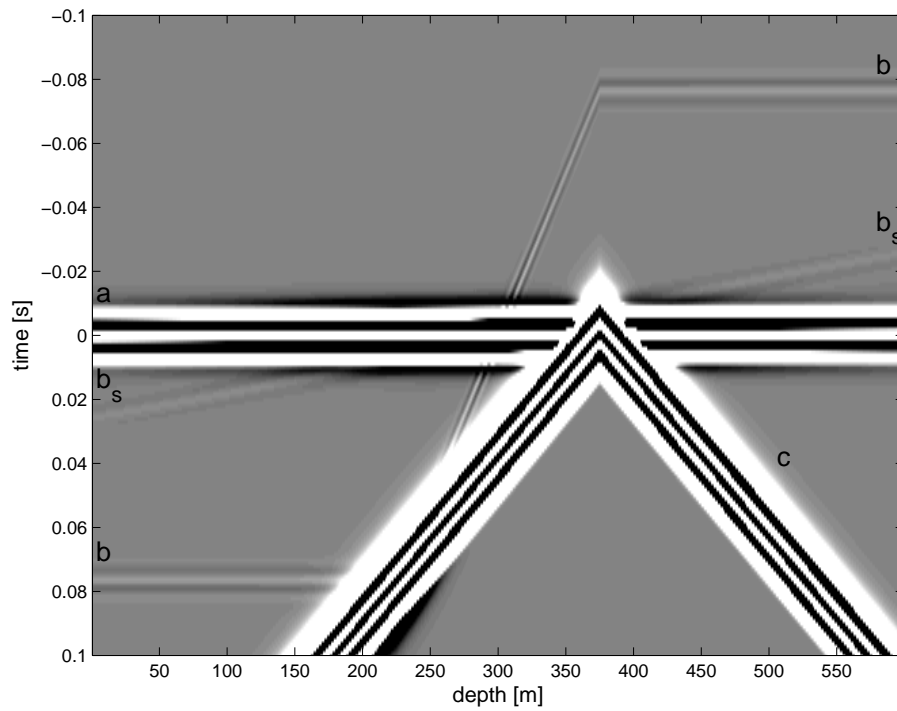


**Figure 8-21:** A close look at the time window  $t = -0.1$  to  $t = 0.1$  seconds of Figure 8-20, brightening has been adjusted to enhance arrivals  $b$  and  $b_s$ . Annotations see text.

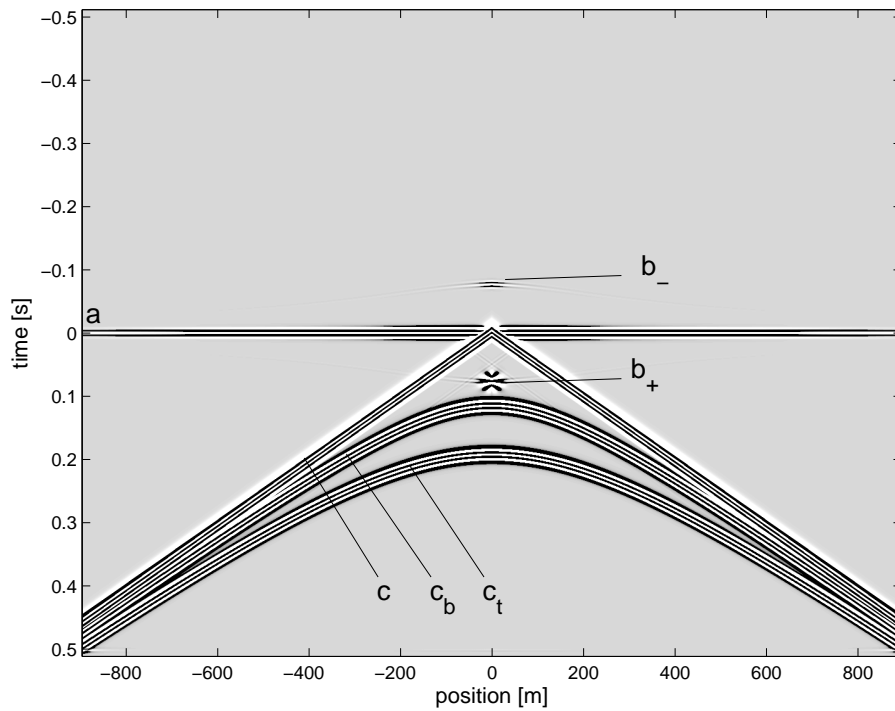


**Figure 8-22:** Source contributions with horizontal distance to the recovered signal in Figure 8-18; the domain integral crosscorrelations have been summed in the vertical direction for each horizontal position, creating one trace for each horizontal position. Annotations see text.

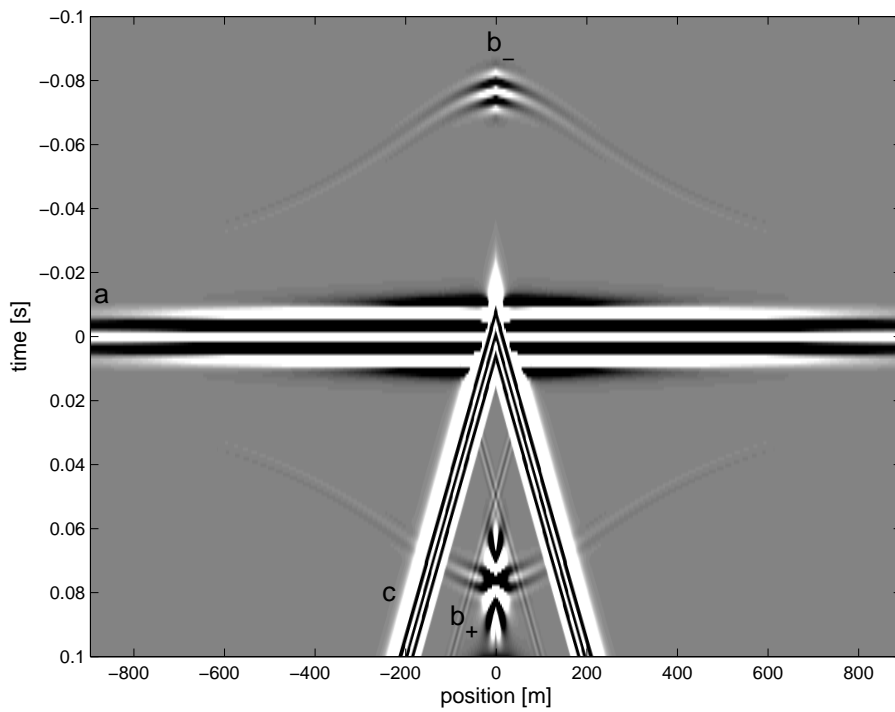


**Figure 8-23:** A close look at the time window  $t = -0.1$  to  $t = 0.1$  seconds of Figure 8-22, brightening has been adjusted to enhance arrivals  $b_1$  and  $b_2$ . Annotations see text.

In Figures 8-22 and 8-23 we show the contributions per horizontal distance, we compiled summed vertical correlation gathers. Events  $b_-$  and  $b_+$ , are clearly constructed by sources with a lateral position close to the line crossing both receivers. This is not the case for event  $a$ , that has contributions from sources outside the considered domain. Events  $c$ ,  $c_t$  and  $c_b$  are appearances of the spurious event in the domain integral that is canceled by the boundary integral. Event  $c$  is the stationary phase in the vertical correlation gathers, of the spurious event in the separate contribution from the domain integral. Events  $c_t$  and  $c_b$  are the spurious events in the separate domain contribution that arise that the top and bottom of the domain. We can see that the spurious event caused by neglecting the boundary integral over  $\partial\mathbb{S}_1$  arrives even later than the window shown in Figure 8-19. There is an additional spurious event clearly visible in Figure 8-23, this ‘cross’ is caused by cross-correlations remnants of the spatial and temporal wrap arounds in the calculations of the 2D Green’s functions.

Finally, we show five cross sections from the cube of crosscorrelation traces through the domain. Their locations are shown in Figure 8-17. The horizontal correlation gathers are chosen above and below the receivers, respectively. Note how event  $b$  is located in positive times for the sources above the receivers and in negative times for sources below the receivers. We can also see that event  $a$  is stationary with respect to horizontal position. Event  $b$  becomes stationary with respect to horizontal position, for sources near the line crossing both receivers. Spurious event  $c$ , arrives at increasingly later times for the sources away from the receivers. Figures 8-26, 8-27 8-28 are three vertical correlation gathers, they have been chosen at one side of the receivers because the behavior of the correlations is symmetric in  $x_1$  as can be seen in Figure 8-22. Events  $a$ ,  $b$  and  $c$  can be seen, but only event  $a$  is stationary with respect to depth. We can see how event  $b$  gradually moves from positive times for sources above the receivers to negative times for sources below the receivers.

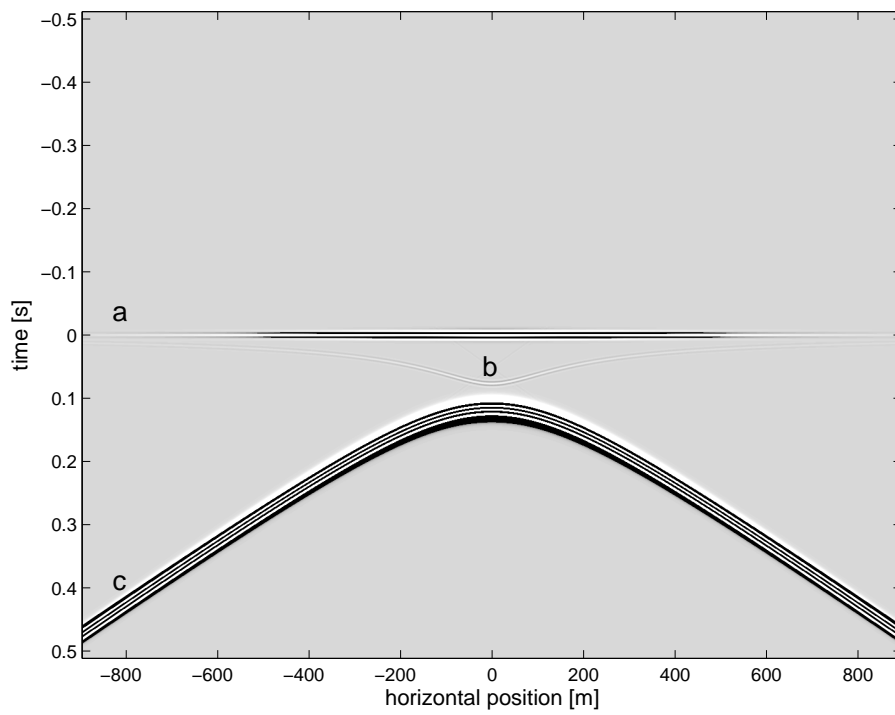


**Figure 8-24:** Correlation gather of horizontal surface of sources at  $x_3 = 150$  meter. Annotations see text.

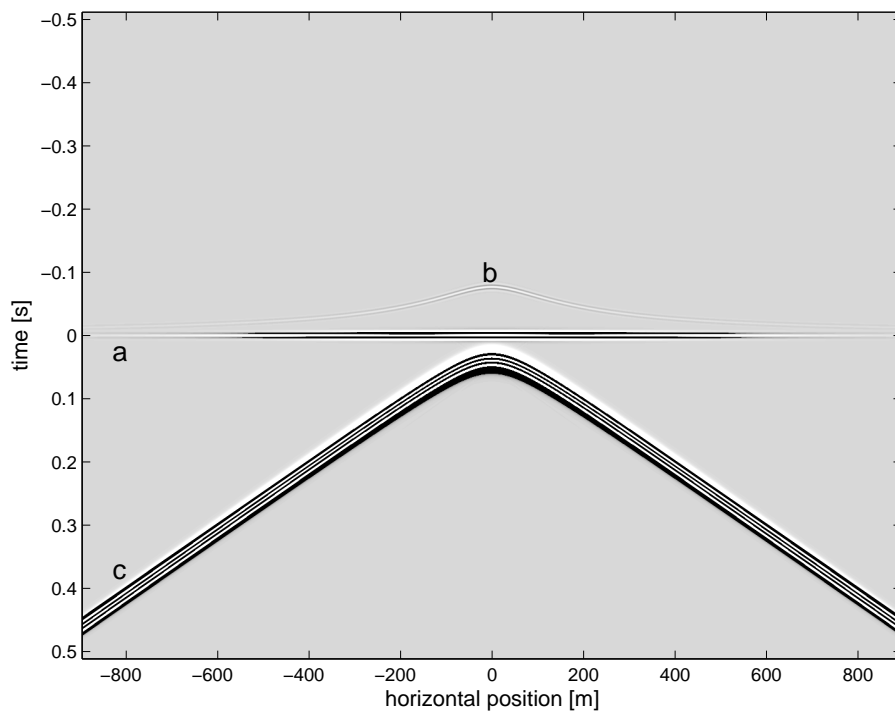


**Figure 8-25:** Correlation gather of horizontal surface of sources at  $x_3 = 450$  meter. Annotations see text.

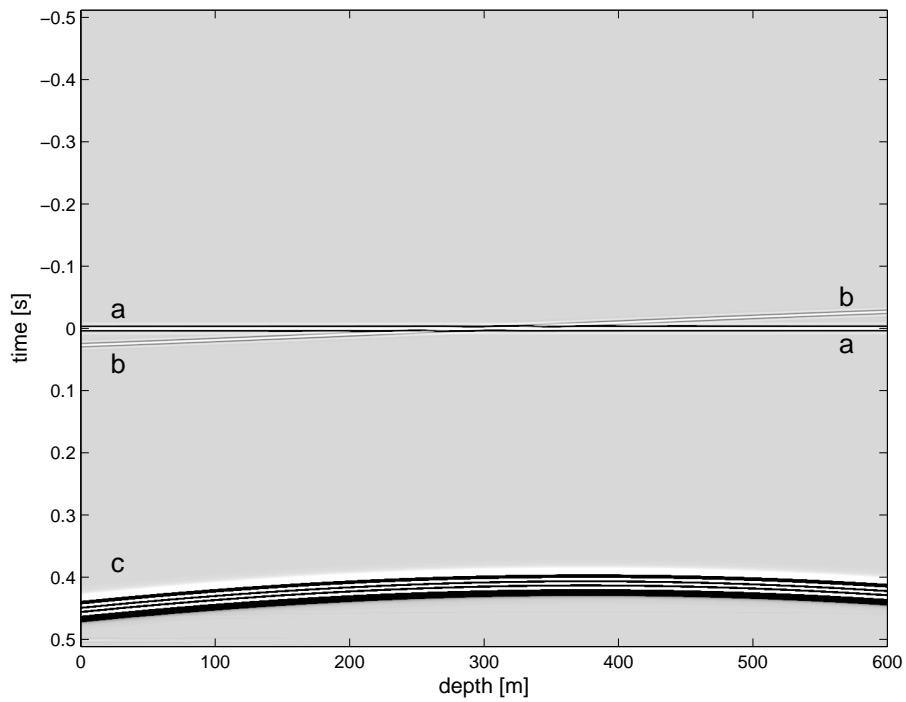


**Figure 8-26:** Correlation gather of a vertical surface of sources at  $x_1 = -800$  meter. Annotations see text.

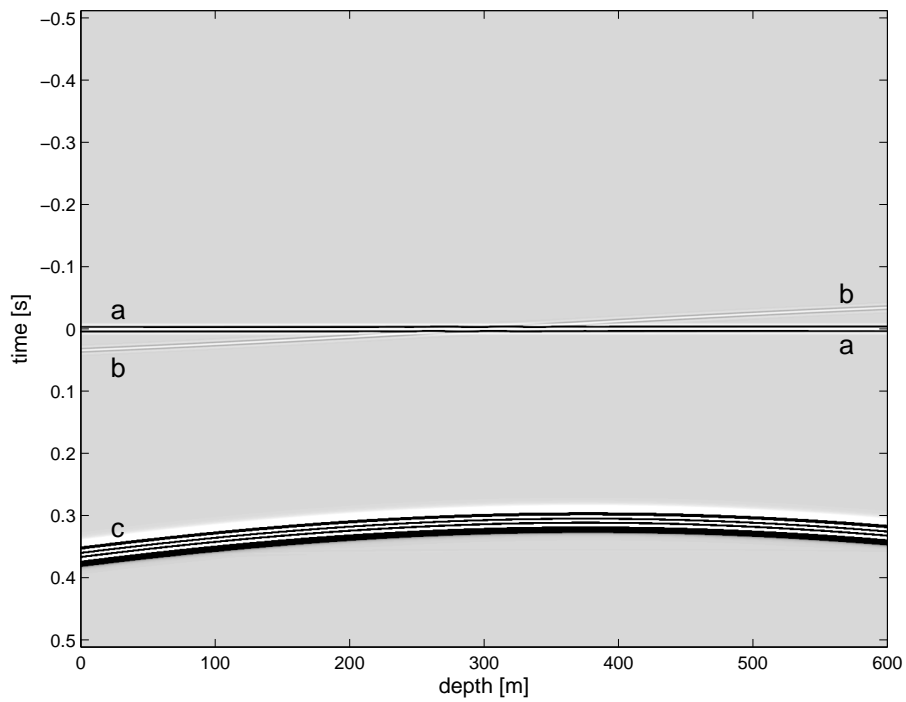


**Figure 8-27:** Correlation gather of a vertical surface of sources at  $x_1 = -600$  meter. Annotations see text.

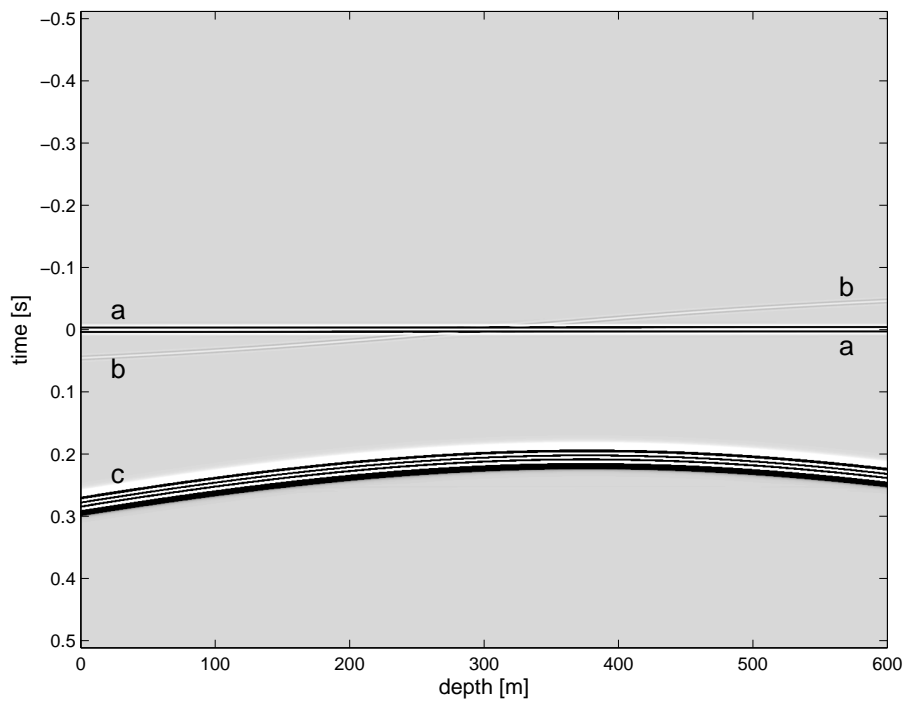


**Figure 8-28:** Correlation gather of a vertical surface of sources at  $x_1 = -400$  meter. Annotations see text.

# Discussion and conclusions

We discuss the results of Part I only briefly, because the results are relatively straightforward. The 1D results of Part II are discussed with particular attention to how the events were created by the interferometric representation. We discuss the relative contributions of different parts of the boundary and domain integrals. The relative contribution of the different terms under the integrations of both the domain and the boundary are discussed. Finally we explain the 2D results using the concepts we have learned from the 1D simulations.

### 9-1 Forward modeling in 2D

The derivation of the two-way wave equation was already performed by previous researchers [White and Zhou, 2006], [Wapenaar, 2007, in preparation], in this work we included a small but valuable extension by including deformation rate sources. This completes the two-way wave equation and enables us to evaluate the 2D interferometric representations in Part II. The causality trick has been applied to successfully minimize temporal wrapping caused by the improper discretisation of the solution. Spatial wrap around can be avoided choosing an appropriate space-time window as already discussed by Haartsen and Pride [1997]. However they did not note that the 'flat' arrivals, i.e. with a very small hyperbolicity due to the relatively fast electromagnetic speed, also wrap around. Events that are even in space, see the flat arrivals in Figures 5-12, 5-14, would become enhanced, while flat events that are uneven in space, for example in  $G^{v,J_3^m}$ , would become faded, especially on the flanks.

### 9-2 Seismoelectric interferometric Green's function representation

In Chapter 7 we derived specific representations of Green's functions between two receivers, as a function of sources in and on a domain and its boundary that encloses both receivers. The boundary integral in equation 6-10 is a summation of 4 different source types, simplify parameters and source functions, we drop the subscripts A and B and the reciprocity theorem of the

correlation-type reduces to Poynting's theorem. The domain integral over the term containing the coupling coefficient reduces a domain integral over  $2\Im\{\hat{v}_{2,r}^{s*}\hat{E}_{2,r}\}\Re\{\rho^f\hat{\mathcal{L}}\}$ . In words this term constitutes the energy that is transferred to heat in the coupling of electromagnetic and seismic fields. It is interesting to see that this term is weighted by the conservative strength of the coupling coefficient, so this term is only as strong as the coupling between the seismic and electromagnetic fields.

### 9-3 Numerical evaluation of the Seismoelectric interferometric Green's function representation

The interferometric representation of  $G^{v,\mathcal{J}^e}(\mathbf{x}_B, \mathbf{x}_A, t) + G^{E,\mathcal{I}}(\mathbf{x}_A, \mathbf{x}_B, -t)$  has been shown valid for the bandwidth of the source function, in both 1D and 2D, see Figures 8-2, 8-4 and 8-18. But we can safely say that it is valid for the entire bandwidth for which the seismoelectric system of equations is valid. Our numerical simulations of the interferometric representations carried additional spurious events besides the physical events that are predicted by the exact direct modeled Green's functions. All those spurious events can easily be attributed to either a numerical artifact or an artifact arising from the approximations made in the discrete interferometric representations. With numerical artifacts we mean events that were caused purely by the way we calculate the responses at the receivers. For example the weak remnant of temporal wrapping caused when using a discrete Fourier transformation. Artifacts caused by approximations of the interferometric representations include those of ignoring the sides  $\partial\mathbb{S}_1$  and of the finite sampling of the Riemann sum that we use to approximate the domain and boundary integrations. The most obvious observation is that both the domain integral and the boundary integral contain a very strong spurious event that interfere destructively. In Figure 8-6 we see that for this destructive interference to lead to a spurious event smaller than the second physical event, the Riemann sum has to be sampled quite dense. Definitely with  $\Delta\mathbf{x}_s \leq 1$  meter for the media types as defined in section 5-2. But this will depend on the receiver offset and the distance to the boundaries. There are two such strong events, one associated with each boundary. They both arrive in positive times for the interferometric representation for  $G^{v,\mathcal{J}^e}(\mathbf{x}_B, \mathbf{x}_A, t) + G^{E,\mathcal{I}}(\mathbf{x}_A, \mathbf{x}_B, -t)$ . Since the left-hand side of the interferometric representations in matrix form, see equation 6-10, is Hermitian the right-hand side also is. If we evaluate  $G^{E,\mathcal{I}}(\mathbf{x}_B, \mathbf{x}_A, t) + G^{v,\mathcal{J}^e}(\mathbf{x}_A, \mathbf{x}_B, -t)$ , both *strong* spurious events would reside in the negative time window. This is good news, we can use this knowledge to interpret spurious events arising when we ignore the domain or boundary integral.

### 9-4 Domain versus boundary integral

For common seismic interferometry, the domain integral can be ignored because the losses are low. The effect of ignoring the losses would only affect the amplitudes of the arrivals, and not create any additional spurious events [Snieder, 2007]. The same has been concluded for mildly diffusive electromagnetic systems [Slob et al., 2006], with the provision that ignoring the surface integral did not lead to more spurious events than those that had been created by simplifying the surface integral under a far field approximation. We did not perform a far field

approximation of the boundary integral, so this cannot yet be concluded for seismoelectric interferometry.

In a homogeneous medium the surface integral disappears if our domain covers the entire infinite medium, provided the medium has one or more non-zero loss terms. Then, even when the domain only covers part of the infinite medium, the contribution of the boundary integral decreases with distance due to the losses in the system. If the boundary is far away with respect to the receiver offset and the losses in the domain are high enough, the spurious events that remain after neglecting the boundary integral are negligible.

In Figures 8-3 and 8-5 we can see that the contribution of the domain integral to the second physical event in positive times has the correct phase but the amplitude is too strong, while the contribution to the second physical event in negative times is too weak. The segments of the domain integral outside the receiver span complement the contribution of the receiver span. If the domain integral does not extend over all space, the boundary integral complements the domain integral. We recover an asymmetric signal, see Section 7-4-2, the contributions of the domain segments outside the receiver span and additional contributions of the boundary integral to have equal polarity for both second physical events, see Figure 8-7. This cannot easily be extended for inhomogeneous media, because separation of the domain in three segments is no longer valid due to reflections and transmissions. The sensitivity of the amplitude errors introduced when we omit the contributions of the domain integral depend on the wave-type of the arrival. We can see in Figures 8-3 and 8-5 how the contributions of the boundary integral, relatively to the domain integral, is of larger contribution in medium type B than in medium type A. But the domain integral contribution is of higher importance to the first physical events around  $t = 0$  second in medium type B than in medium type A. In Section 5-3 we discussed how the second event travels as a shear wave and the first event travels as an electromagnetic wave. The shear wave losses are concluded to be higher in medium type A than in medium type B, see Section 5-2, while the electromagnetic losses are higher in medium type B than in medium type A. The conclusion is that the amplitude errors arising from ignoring the domain and or boundary integral contribution will in general be different for all events. Depending on the wave-type and of the receivers to the boundaries. However, this does not mean that ignoring the domain integral will cause the amplitude of the second physical events in both positive and negative times to decrease. In fact for  $G^{v,\underline{J}^e}(\mathbf{x}_B, \mathbf{x}_A, t) + G^{E,\underline{f}}(\mathbf{x}_A, \mathbf{x}_B, -t)$  the amplitude of the second event in  $G^{v,\underline{J}^e}(\mathbf{x}_B, \mathbf{x}_A, t)$  will increase, while the amplitude of the second event in  $G^{E,\underline{f}}(\mathbf{x}_A, \mathbf{x}_B, -t)$  will decrease.

### 9-4-1 Main contributions to the retrieved result

Even though we need the entire representation to retrieve the exact Green's functions, there are certain parts of the representation that contribute significantly less than other parts. In Figures 8-10 and 8-11, we see how terms 3 and 4 create the second physical events in  $G^{v,\underline{J}^e}(\mathbf{x}_B, \mathbf{x}_A, t) + G^{E,\underline{f}}(\mathbf{x}_A, \mathbf{x}_B, -t)$  and how term 1 and 2 create the first physical events that arrive around  $t = 0$  second. Terms 1 and 2 are boundary integrals over electromagnetic sources (see equations 8-1 and 8-2), they create the event that arrived with the electromagnetic wave speed. While the seismic sources (see equations 8-3 and 8-4) create the event arriving with shear wave velocity. Ignoring one type of boundary sources would inevitably lead to missing either electromagnetic arrivals or seismic arrivals in the contribution of the boundary integral.

The contribution of the domain integral is almost completely given by the 3<sup>rd</sup> term,  $\hat{G}^{v,f}(\mathbf{x}_{3,B}, \mathbf{x}_3) \Re\{\rho^f \hat{\mathcal{L}}\} \hat{G}^{E,J^e*}(\mathbf{x}_{3,A}, \mathbf{x}_3)$ . This term contains recordings of two different fields at two different receiver positions of two different source types at the same source position acting simultaneously. These Green's functions are each very strong, because they measure the field type associated with the source type, i.e.  $E_2$  response of  $J_2^e$  and  $v_2^s$  response of  $f_2$ . The weakest contribution comes from the 2<sup>nd</sup> term, that contains recordings of two different fields at two different receiver positions of two different source types at the same source position acting simultaneously. But each recorded field is the response of the other source type, i.e.  $E_2$  response of  $f_2$  and  $v_2^s$  response of  $J_2^e$ . Some events that arise in these crosscorrelations are too weak to be visible in the figures of Chapter 7. The third term has no significant contribution to the second event in negative times. The total but weak contribution of the domain integral to reconstructing the second event in negative times comes completely from the 4<sup>th</sup> term. The 4<sup>th</sup> term most dominantly compensates for the shear wave losses inside the domain and is the most important contribution to events  $b_+$  and  $b_-$ . The 1<sup>st</sup> term most dominantly compensates for electromagnetic losses inside the domain, it is the most important contribution to event  $a$ . There will be a loss of amplitudes and imperfect destructive interference of spurious events, but judging from the small contributions of the 1<sup>st</sup> and 4<sup>th</sup> terms in the domain integral, they can probably be ignored if the boundary integral is close enough. The 2<sup>nd</sup> and 3<sup>rd</sup> term cannot be ignored. Although the 2<sup>nd</sup> term is very weak, it is closely associated with the 3<sup>rd</sup> term. This can be seen when we complex conjugate the entire expression, the 2<sup>nd</sup> term transforms in the 3<sup>rd</sup> term and vice versa. This is the key to the Hermitian property of equations 7-15 and 7-43. The condition set by Wapenaar [2004] that the loss matrix should be diagonal for the interferometric representation to become a direct crosscorrelation of two Green's functions seems to be hard to realise. Simply ignoring the off diagonal terms would seriously affect the amplitude and phase of the recovered events, the spurious event  $c$  would also remain in the recovered result.

## 9-4-2 Stationary phases

A stationary phase in the context of seismic interferometry has been used to refer to positions of sources on the boundary integral for which the phase of certain events in the correlation gather becomes stationary [Snieder, 2004a], [Snieder, 2006], crosscorrelations of recordings due to these sources have stationary arrival times. In 1D the boundary integral consists of just two points, that logically are at the stationary phase for all events. But since we deal with a domain integral over the loss functions, we see that both physical events are stationary for line segments 1 and 3. In Figure 8-14, we can see that event labeled  $b$ , corresponding to the second physical event in positive and negative times, has stationary contributions from the line segments outside the receiver span. The same can be said for event labeled  $a$  in Figures 8-13 or 8-14, corresponding to the first physical event, but since its arrival time is almost zero seconds, the non-stationary behavior for line segment 2 is not visible. It is interesting to note that the spurious event, labeled  $c$  is non-stationary in the entire domain. Choosing a larger domain would not only decrease the amplitude of the spurious events in the separate boundary and domain integrals, but also increase the arrival time.

## 9-5 2D versus 1D

An important step toward real situations is to understand the interferometric representation in 2D. Fortunately, the results are very similar to 1D, but because we omitted the boundary integral over  $\partial\mathbb{S}_1$  we expect some spurious events. In Figure 8-18 we see that we reconstruct the second physical events very well, but reconstruct the first event with a too strong amplitude. In Figures 8-22 and 8-23 it is simple to see the consequences of modeling in 2D. Firstly, we see how the vertical line with  $x_1 = 0$  meter contains all stationary phases, see also Figures 8-24 and 8-25, outside this line all phases are non-stationary. This is a direct consequence of the positioning of both receivers on a vertical line. However, sources positioned in the limits  $x_1 \rightarrow \pm\infty$  are at stationary phases for all physical events. However, source contributions decrease with distance because of the losses in the system, if we extend our domain in horizontal distances far enough we can exclude the sides of the boundary. We see how event *a* in Figures 8-22 and 8-23 is clearly cut-off due to the limited horizontal aperture. Event *c* has a very strong contribution to the reconstruction of the first arrival. The amplitude of the contribution of event *c* is decreased by event *a*, since event *a* was not reconstructed perfectly, the combination with *c* will lead to an event that is too strong. We can also see two small spurious events at  $t = \pm 0.02$  seconds in Figure 8-18, these are spurious events due to the limited horizontal aperture, see Figures 8-23 and 8-24 or 8-25. Figure 8-23 also gives us a good insight on the reconstruction of event  $b_+$ . We can see the strong event, labeled  $b_+$ , that in 1D is created by the sources in the segment of the receiver span. We see a very strong event that will be decreased by the contributions of sources outside the receiver span and on the boundary integral. The spurious event *c* is also non-stationary in the  $x_1$  direction, these should be canceled by destructive interference with the contributions from the  $\partial\mathbb{S}_1$  boundary. The stationary contributions to the physical events remain stationary lines, they lie in a vertical line with  $x_1 = 0$  meter. We can conclude from Figure 8-23, that the line segments outside the receiver span are the stationary lines for events *a* and *b*. The boundary integral contains stationary phases for the physical events, where the stationary line of the domain intersects the boundary.

## 9-6 Conclusions

We validated the interferometric Greens function representation for  $G^{v,\underline{J}^e}(\mathbf{x}_B, \mathbf{x}_A, t) + G^{E,\underline{f}}(\mathbf{x}_A, \mathbf{x}_B, -t)$ . We have shown that we need a dense distribution of sources throughout a domain and on its boundary to obtain exact reconstruction. The electromagnetic sources of the representation contribute dominantly to the reconstruction of the diffusive EM field. The seismic sources contribute dominantly to the reconstruction of the shear wave field. Sources near receivers cannot be neglected for the reconstruction of  $G^{v,\underline{J}^e}$ . A strong non-stationary event is identified in the domain integral and boundary integral contribution to  $G^{v,\underline{J}^e}(\mathbf{x}_B, \mathbf{x}_A, t)$ , it is absent in the reciprocal Green's function  $G^{E,\underline{f}}(\mathbf{x}_A, \mathbf{x}_B, -t)$ . A numerical study should be conducted to generalize these conclusions to inhomogeneous media.



---

## References

- Airy, G. B. (1833). On the phaenomena of newton's rings when formed between two transparent substances of different refractive powers. *The London and Edinburgh Philosophical Magazine and Journal of Science*, 2:20–30.
- Biot, M. A. (1956). Theory of propagation of elastic waves in a fluid-saturated porous solid. i. low-frequency range. *J. Acoust. Soc. Am.*, 28(2):168–178.
- Bleistein, N. (1984). *Mathematical methods for wave phenomena*. Academic Press Inc., Orlando.
- Bourbié, T., Coussy, O., and Zinszner, B. (1987). *Acoustics of porous media*. Institut Francais du Pétrole. Institut Francais du Pétrole publications, Paris. Translated from French, 'Acoustique des milieux poreux'.
- Bracewell, R. N. (2000). *The Fourier Transform and Its Applications*. McGraw-Hill, Boston, third edition.
- Claerbout, J. F. (1968). Synthesis of a layered medium from its acoustic transmission response. *Geophysics*, 33(2):264–269.
- de Hoop, A. T. (1966). An elastodynamic reciprocity theorem for linear, viscoelastic media. *Appl. Sci. Res.*, 16:3945.
- Deresiewicz, H. and Skalak, R. (1963). On uniqueness in dynamic poroelasticity. *Bull. Seism. Soc. Am.*, 53(4):783–788.
- Fokkema, J. T. and van den Berg, P. M. (1993). *Seismic applications of acoustic reciprocity*. Elsevier, Amsterdam.
- Fokkema, J. T. and Ziolkowski, A. (1987). The critical reflection theorem. *Geophysics*, 52(7):965–972.
- Frenkel, J. (1944). On the theory of seismic and seismoelectric phenomena in a moist soil. *J. Physics (Soviet)*, 8(4):230–241.

- Grimbergen, J. L. T., Dessing, F. J., and Wapenaar, C. P. A. (1998). Modal expansion of one-way operators in laterally varying media. *Geophysics*, 63(3):995–1005.
- Haartsen, M. W. (1995). *Coupled Electromagnetic and Acoustic Wavefield Modeling in Poro-Elastic Media and its Applications in Geophysical Exploration*. PhD thesis, Massachusetts Institute of Technology.
- Haartsen, M. W. and Pride, S. R. (1997). Electro seismic waves from point sources in layered media. *J. Geophys. Res.*, 102(B11):24745–24784.
- Ivanov, A. (1939). Effect of electrization of earth layers by elastic waves passing through them. *Dokl. Adad. Nauk. SSSR*, 24(1):41–45.
- Johnson, D. L. (1989). Scaling function for dynamic permeability in porous media. *Phys. Rev. Lett.*, 63(5):580.
- Johnson, D. L., Koplik, J., and Dashen, R. (1987). Theory of dynamic permeability and tortuosity in fluid-saturated porous media. *J. Fluid Mech.*, 176:379–402.
- Nabighian, M. N. and Corbett, J. D. (1987). *Electromagnetic methods in applied geophysics - theory. Volume 1*. Investigations in Geophysics. Society of Exploration Geophysicists, Tulsa.
- Pride, S. (1994). Governing equations for the coupled electromagnetics and acoustics of porous media. *Phys. Rev. B*, 50(21):15678–15696.
- Pride, S. R. and Haartsen, M. W. (1996). Electro seismic wave properties. *J. Acoust. Soc. Am.*, 100(3):1301–1315.
- Pride, S. R. and Morgan, F. D. (1991). Electrokinetic dissipation induced by seismic waves. *Geophysics*, 56(7):914–925.
- Schoenberg, M. and Sen, P. N. (1983). Properties of a periodically stratified acoustic half-space and its relation to a biot fluid. *J. Acoust. Soc. Am.*, 73:61–67.
- Shaw, A. R. (2004). *The seismo-electric method and its sensitivity to subsurface contrasts*. PhD thesis, Delft University of Technology.
- Slob, E., Draganov, D., and Wapenaar, K. (2006). GPR without a source. In *Proceedings of the Eleventh International Conference on Ground Penetrating Radar*.
- Slob, E., Draganov, D., and Wapenaar, K. (2007). Interferometric electromagnetic greens functions representations using propagation invariants. *Geophys. J. Int.*, 169:60–80.
- Snieder, R. (2004a). Extracting the green’s function from the correlation of coda waves: A derivation based on stationary phase. *Phys. Rev. Lett.*, 69(4):046610–1–046610–8.
- Snieder, R. (2006). Retrieving the greens function of the diffusion equation from the response to a random forcing. *Phys. Rev. E*, 74:046620–1 – 046620–4.
- Snieder, R. (2007). Extracting the greens function of attenuating heterogeneous acoustic media from uncorrelated waves. *J. Acoust. Soc. Am.*, 121(5):2637 – 2643.

- Snieder, R., Wapenaar, K., and Larner, K. (2006). Spurious multiples in seismic interferometry of primaries. *Geophysics*, 71(4):SI111SI124.
- Snieder, R. K. (2004b). Extracting the green's function from the correlation of coda waves: A derivation based on stationary phase. *Phys. Rev. E*, 69:046610–1 – 046620–8.
- Thompson, R. R. (1936). The seismic electric effect. *Geophysics*, 1(3):327–335.
- Thompson, R. R. (1939). A note on the seismic-electric effect. *Geophysics*, 4(2):102–105.
- Ursin, B. (1983). Review of elastic and electromagnetic wave propagation in horizontally layered media. *Geophysics*, 48(8):1063–1081.
- van der Burg, D. W. (2002). Source decomposition and receiver composition for electro-kinetic measurements. Master's thesis, Delft University of Technology.
- Wapenaar, C. P. A. (1996). Reciprocity theorems for two-way and one-way wave vectors: A comparison. *J. Acoust. Soc. Am.*, 100(6):3508–3518.
- Wapenaar, C. P. A. and Berkhout, A. J. (1989). *Elastic wave field extrapolation; redatuming of single- and multi-component seismic data*. Advances in exploration geophysics II. Elsevier, Amsterdam.
- Wapenaar, K. (2004). Retrieving the elastodynamic greens function of an arbitrary inhomogeneous medium by cross correlation. *Phys. Rev. Lett.*, 93(25):254301–1 – 254301–4.
- Wapenaar, K. (2007). Seismic wave theory; representations, decomposition and applications. in preparation.
- Wapenaar, K. and Fokkema, J. (2004). Reciprocity theorems for diffusion, flow, and waves. *J. Appl. Mech.*, 71:145–150.
- Wapenaar, K. and Fokkema, J. (2006). Greens function representations for seismic interferometry. *Geophysics*, 71(4):SI33SI46.
- Wapenaar, K., Slob, E., and Snieder, R. (2006). Unified greens function retrieval by cross correlation. *Phys. Rev. Lett.*, 97(23):234301–1 – 234301–4.
- Weaver, R. and Lobkis, O. (2002). On the emergence of the greens function in the correlations of a diffuse field: pulse-echo using thermal phonons. *Ultrasonics*, 40:435439.
- White, B. S. and Zhou, M. (2006). Electro seismic prospecting in layered media. *SIAM Journal on Applied Mathematics*, 67(1):69–98.



---

## Appendix A

---

# Derivation of the seismoelectric two-way wave equation

In this appendix we will derive the seismoelectric two-way wave equation of chapter 3 following [Wapenaar, 2007, in preparation], prepublished by Shaw [2004]. The two-way wave equation 3-1, A-1 equates the vertical variation of the continuous field quantities as a function of the horizontal derivatives of the continuous field quantities and a source vector,

$$\partial_z \hat{\mathbf{q}} = \hat{\mathcal{A}} \hat{\mathbf{q}} + \hat{\mathbf{d}}. \quad (\text{A-1})$$

The field quantities that are continuous over a horizontal source free interface are captured in the vector  $\mathbf{q}$ , see section 2-3. The two-way wave equation equates the vertical variations in  $\hat{\mathbf{q}}$  as a function of the horizontal derivatives of  $\hat{\mathbf{q}}$  in  $\hat{\mathcal{A}}$  and a two way source-vector  $\hat{\mathbf{d}}$ . We consider an isotropic medium, in addition to the parameters given in section 2-1-3 and 2-1-5 we define  $\hat{\rho}^E = \frac{\eta}{i\omega \mathbf{k}}$ ,  $\hat{\epsilon} = \epsilon + \frac{1}{i\omega} \hat{\sigma}^e$  and  $\hat{\epsilon}_{\mathcal{L}} = \hat{\epsilon} - \hat{\rho}_E \hat{\mathcal{L}}^2$ , and in isotropic media we have  $\hat{\rho}_{ij}^E = \hat{\rho}^E \delta_{ij}$ ,  $\hat{\epsilon}_{ij} = \hat{\epsilon} \delta_{ij}$  and  $\hat{\epsilon}_{\mathcal{L},ij} = \hat{\epsilon}_{\mathcal{L}} \delta_{ij}$ .

We rewrite the equations of motion 2-9 and 2-10 as

$$i\omega \rho^b \hat{\mathbf{v}}^s + i\omega \rho^f \boldsymbol{\delta}_j \hat{w}_j - \partial_j \hat{\tau}_j^b = \hat{\mathbf{f}}^b, \quad (\text{A-2})$$

$$i\omega \rho^f \boldsymbol{\delta}_i^t \hat{\mathbf{v}}^s + \frac{\eta}{\hat{k}} \left( \hat{w}_i - \hat{\mathcal{L}} \left( \gamma_i^t \hat{\mathbf{E}}_0 + \delta_{3i} \hat{E}_3 \right) \right) + \partial_i \hat{p} = \hat{f}_i^f, \quad (\text{A-3})$$

where the vectors  $\hat{\mathbf{v}}^s$ ,  $\hat{\tau}_j^b$ ,  $\hat{\mathbf{E}}_0$ ,  $\hat{\mathbf{f}}^b$ ,  $\delta_i$  and  $\gamma_i$  are defined as

$$\hat{\mathbf{v}}^s = \begin{pmatrix} \hat{v}_1^s \\ \hat{v}_2^s \\ \hat{v}_3^s \end{pmatrix}, \hat{\tau}_j^b = \begin{pmatrix} \hat{\tau}_{1j}^b \\ \hat{\tau}_{2j}^b \\ \hat{\tau}_{3j}^b \end{pmatrix}, \hat{\mathbf{E}}_0 = \begin{pmatrix} \hat{E}_1 \\ \hat{E}_2 \end{pmatrix}, \hat{\mathbf{f}}^b = \begin{pmatrix} \hat{f}_1^b \\ \hat{f}_2^b \\ \hat{f}_3^b \end{pmatrix}, \boldsymbol{\delta}_i = \begin{pmatrix} \delta_{1i} \\ \delta_{2i} \\ \delta_{3i} \end{pmatrix}, \gamma_i = \begin{pmatrix} \delta_{1i} \\ \delta_{2i} \end{pmatrix}. \quad (\text{A-4})$$

Before we rewrite the stress-strain relations 2-11 and 2-12 in a similar form, we eliminate the term  $\partial_k \hat{w}_k$  from equation 2-11, using equation 2-12. This yields

$$-i\omega \hat{\tau}_{ij}^b + e_{ijkl} \partial_l \hat{v}_k^s - i\omega \frac{d}{M} \delta_{ij} \hat{p} = e_{ijkl} \hat{h}_{kl}^b, \quad (\text{A-5})$$

with  $e_{ijkl}$  defined as

$$e_{ijkl} = c_{ijkl} - \frac{d^2}{M} \delta_{ij} \delta_{kl}. \quad (\text{A-6})$$

The stress-strain relations A-5 and 2-12 are now written as

$$-i\omega \hat{\tau}_j^b + \mathbf{e}_{jl} \partial_l \hat{\mathbf{v}}^s - i\omega \frac{d}{M} \delta_j \hat{p} = \mathbf{e}_{jl} \hat{\mathbf{h}}_l^b, \quad (\text{A-7})$$

$$i\omega \hat{p} + d \delta_k^t \partial_k \hat{\mathbf{v}}^s + M \partial_k \hat{w}_k = \hat{\mathbf{d}}_l^T \hat{\mathbf{h}}_l^b + \hat{M} \hat{q}^i, \quad (\text{A-8})$$

with matrix  $\mathbf{e}_{jl}$  and vector  $\mathbf{0}$  defined as

$$\mathbf{e}_{ij} = \begin{pmatrix} e_{1i1j} & e_{1i2j} & e_{1i3j} \\ e_{2i1j} & e_{2i2j} & e_{2i3j} \\ e_{3i1j} & e_{3i2j} & e_{3i3j} \end{pmatrix}. \quad (\text{A-9})$$

Note that

$$\mathbf{e}_{ij}^t = \mathbf{e}_{ji}. \quad (\text{A-10})$$

The electromagnetic field equations 2-35 and 2-36 are rewritten as

$$i\omega \hat{\varepsilon}_{\mathcal{L}} \hat{\mathbf{E}}_0 + \frac{\eta}{k} \hat{\mathcal{L}} \gamma_{\alpha} \hat{w}_{\alpha} + \partial_3 \hat{\mathbf{H}}_0 - \begin{pmatrix} \partial_2 \\ -\partial_1 \end{pmatrix} \hat{H}_3 = -\hat{\mathbf{J}}_0^{\text{s},e}, \quad (\text{A-11})$$

$$i\omega \hat{\varepsilon}_{\mathcal{L}} + \frac{\eta}{k} \hat{\mathcal{L}} \hat{w}_3 - (\partial_1 \partial_2) \hat{\mathbf{H}}_0 = -\hat{J}_3^{\text{s},e}, \quad (\text{A-12})$$

$$i\omega \mu_0 \hat{\mathbf{H}}_0 + \partial_3 \hat{\mathbf{E}}_0 - \begin{pmatrix} \partial_1 \\ \partial_2 \end{pmatrix} \hat{E}_3 = -\hat{\mathbf{J}}_0^{\text{s},m}, \quad (\text{A-13})$$

$$i\omega \mu_0 \hat{H}_3 - \partial_3 \hat{\mathbf{E}}_0 - (\partial_1 \partial_2) \hat{\mathbf{E}}_0 = -\hat{J}_3^{\text{s},m}, \quad (\text{A-14})$$

were the vectors  $\hat{\mathbf{H}}_0$ ,  $\hat{\mathbf{J}}_0^{\text{s},e}$ ,  $\hat{\mathbf{J}}_0^{\text{s},m}$  are defined as

$$\hat{\mathbf{H}}_0 = \begin{pmatrix} \hat{H}_2 \\ -\hat{H}_1 \end{pmatrix}, \hat{\mathbf{J}}_0^{\text{s},e} = \begin{pmatrix} \hat{J}_1^{\text{s},e} \\ \hat{J}_2^{\text{s},e} \end{pmatrix}, \hat{\mathbf{J}}_0^{\text{s},m} = \begin{pmatrix} \hat{J}_2^{\text{s},m} \\ -\hat{J}_1^{\text{s},m} \end{pmatrix}. \quad (\text{A-15})$$

Next we separate the vertical derivatives in from the lateral derivatives, according to

$$-\partial_3 \hat{\tau}_3^b = -i\omega \rho^b \mathbf{v}^s - i\omega \rho^f (\delta_{\alpha} \hat{w}_{\alpha} + \delta_3 \hat{w}_3) + \partial_{\alpha} \hat{\tau}_{\alpha}^b + \hat{\mathbf{f}}^b, \quad (\text{A-16})$$

$$\partial_3 \hat{p} = -\omega \rho^f \delta_3^t \hat{\mathbf{v}}^s - \frac{\eta}{k} (\hat{w}_3 - \hat{\mathcal{L}} \hat{E}_3) + \hat{f}_3^f, \quad (\text{A-17})$$

$$\partial_3 \hat{\mathbf{v}}^s = \mathbf{e}_{33}^{-1} \left( i\omega \hat{\tau}_3^b + i\omega \frac{d}{M} \delta_3 \hat{p} - \mathbf{e}_{3\beta} \partial_{\beta} \hat{\mathbf{v}}^s \right) + \mathbf{e}_{33}^{-1} \mathbf{e}_{3l} \hat{\mathbf{h}}_l^b, \quad (\text{A-18})$$

$$\partial_3 \hat{w}_3 = -\frac{i\omega}{M} \hat{p} - \frac{d}{M} \left( \delta_{\beta}^t \partial_{\beta} \hat{\mathbf{v}}^s + \delta_3^t \partial_3 \hat{\mathbf{v}}^s \right) - \partial_{\beta} \hat{w}_{\beta} + \hat{\mathbf{d}}_l^T \hat{\mathbf{h}}_l^b + \hat{M} \hat{q}^i, \quad (\text{A-19})$$

$$\partial_3 \hat{\mathbf{E}}_0 = -\omega \mu_0 \hat{\mathbf{H}}_0 + \begin{pmatrix} \partial_1 \\ \partial_2 \end{pmatrix} \hat{E}_3 - \hat{\mathbf{J}}_0^{\text{s},m}, \quad (\text{A-20})$$

$$\partial \hat{\mathbf{H}}_0 = -i\omega \hat{\varepsilon}_{\mathcal{L}} \hat{\mathbf{E}}_0 - \frac{\eta}{k} \hat{\mathcal{L}} \gamma_{\alpha} \hat{w}_{\alpha} + \begin{pmatrix} \partial_2 \\ -\partial_1 \end{pmatrix} \hat{H}_3 - \hat{\mathbf{J}}_0^{\text{s},e}. \quad (\text{A-21})$$

Using equations A-3 and A-7, we can eliminate the terms  $\delta_\alpha \hat{w}_\alpha$  and  $\partial_\alpha \hat{\tau}_\alpha$  from equation A-16, yielding

$$\begin{aligned} -\partial_3 \hat{\tau}_3^b &= -i\omega \rho^b \hat{v}^s + i\omega \rho^f \delta_\alpha \left( i\omega \rho^f \frac{\eta}{\hat{k}} \delta_\alpha^t \hat{v}^s + \frac{\hat{k}}{\eta} \partial_\alpha \hat{p} - \hat{\mathcal{L}} \gamma_\alpha^t \hat{\mathbf{E}}_0 \right) - i\omega \rho^f \delta_3 \hat{w}_3 \\ &\quad + \frac{1}{i\omega} \partial_\alpha \left( \mathbf{e}_{\alpha\beta} \partial_\beta \hat{v}^s + \mathbf{e}_{\alpha 3} \partial_3 \hat{v}^s - i\omega \frac{d}{M} \delta_\alpha \hat{p} \right) + \hat{\mathbf{f}}^b - i\omega \rho^f \frac{\hat{k}}{\eta} \delta_\alpha^f \hat{f}_\alpha^f \\ &\quad + \frac{1}{i\omega} \partial_\alpha \mathbf{e}_{\alpha l} \hat{\mathbf{h}}_l^b, \end{aligned} \quad (\text{A-22})$$

or upon substitution of equation A-18

$$\begin{aligned} -\partial_3 \hat{\tau}_3^b &= \partial_\alpha \left( \mathbf{e}_{\alpha 3} \mathbf{e}_{33}^{-1} \hat{\tau}_3^b \right) + i\omega \rho^f \frac{\hat{k}}{\eta} \delta_\alpha \partial_\alpha \hat{p} - \frac{1}{i\omega} \partial_\alpha \left( i\omega \frac{d}{M} \mathbf{r}_\alpha \hat{p} - \mathbf{R}_{\alpha\beta} \partial_\beta \hat{v}^s \right) \\ &\quad - i\omega \left( \rho^b \mathbf{I}_3 - i\omega (\rho^f)^2 \frac{\hat{k}}{\eta} \delta_\alpha \delta_\alpha^t \right) \hat{v}^s - i\omega \rho^f \delta_3 \hat{w}_3 - i\omega \rho^f \hat{\mathcal{L}} \delta_\alpha \gamma_\alpha^t \hat{\mathbf{E}}_0 \\ &\quad + \hat{\mathbf{f}}^b - i\omega \rho^f \frac{\hat{k}}{\eta} \delta_\alpha^f \hat{f}_\alpha^f + \frac{1}{i\omega} \partial_\alpha \mathbf{R}_{\alpha\beta} \hat{\mathbf{h}}_\beta^b, \end{aligned} \quad (\text{A-23})$$

where  $\mathbf{I}_3$  is a  $3 \times 3$  identity matrix and

$$\mathbf{R}_{\alpha\beta} = \mathbf{e}_{\alpha\beta} - \mathbf{e}_{\alpha 3} \mathbf{e}_{33}^{-1} \mathbf{e}_{3\beta}, \quad (\text{A-24})$$

$$\mathbf{r}_\alpha = \delta_\alpha - \mathbf{e}_{\alpha 3} \mathbf{e}_{33}^{-1} \delta_3. \quad (\text{A-25})$$

Note that  $\mathbf{R}_{\alpha\beta}^t = \mathbf{R}_{\beta\alpha}$ . On account of equation A-10, Using equation A-12, we eliminate  $\hat{E}_3$  from equation A-17, yielding

$$\partial_3 \hat{p} = -i\omega \rho^f \delta_3^t \hat{v}^s - \frac{\eta}{\hat{k}} \left( 1 + \frac{1}{i\omega \hat{\varepsilon}_\mathcal{L}} \frac{\eta}{\hat{k}} \hat{\mathcal{L}}^2 \right) \hat{w}_3 + \frac{1}{i\omega \hat{\varepsilon}_\mathcal{L}} \frac{\eta}{\hat{k}} \hat{\mathcal{L}} (\partial_1 \partial_2) \hat{\mathbf{H}}_0 - \frac{1}{i\omega \hat{\varepsilon}_\mathcal{L}} \frac{\eta}{\hat{k}} \hat{\mathcal{L}} \hat{\mathbf{J}}_3^{s,e} + \hat{f}_3^f. \quad (\text{A-26})$$

Using equations A-18 and A-3, we eliminate the terms  $\partial_3 \hat{v}^s$  and  $\partial_\beta \hat{w}_\beta$  from equation A-19, according to

$$\begin{aligned} \partial_3 \hat{w}_3 &= -\frac{d}{M} \delta_3^t \mathbf{e}_{33}^{-1} \left( i\omega \hat{\tau}_3^b + i\omega \frac{d}{M} \delta_3 \hat{p} \right) - \frac{i\omega}{M} \hat{p} + \partial_\beta \left( \frac{\hat{k}}{\eta} \partial_\beta \hat{p} + i\omega \rho^f \frac{\hat{k}}{\eta} \delta_\beta^t \hat{v}^s - \hat{\mathcal{L}} \gamma_\beta^t \hat{\mathbf{E}}_0 \right) \\ &\quad - \frac{d}{M} \mathbf{r}_\beta^t \partial_\beta \hat{v}^s - \partial_\beta \frac{\hat{k}}{\eta} \hat{f}_\beta^f + \frac{d}{M} \mathbf{r}_\beta^t \hat{\mathbf{h}}_\beta + \hat{q}^i. \end{aligned} \quad (\text{A-27})$$

Using equation A-12, we can eliminate  $\hat{E}_3$  from equation A-21, yielding

$$\begin{aligned} \partial_3 \hat{\mathbf{E}}_0 &= -i\omega \mu_0 \hat{\mathbf{H}}_0 + \left( \frac{\partial_1}{\partial_2} \right) \frac{1}{i\omega \hat{\varepsilon}_\mathcal{L}} (\partial_1 \partial_2) \hat{\mathbf{H}}_0 \\ &\quad - \left( \frac{\partial_1}{\partial_2} \right) \frac{1}{i\omega \hat{\varepsilon}_\mathcal{L}} \frac{\eta}{\hat{k}} \hat{\mathcal{L}} \hat{w}_3 - \hat{\mathbf{J}}_0^{s,m} - \left( \frac{\partial_1}{\partial_2} \right) \frac{1}{i\omega \hat{\varepsilon}_\mathcal{L}} \hat{\mathbf{J}}_3^{s,e}. \end{aligned} \quad (\text{A-28})$$

Using equations A-14 and A-3, we eliminate  $\hat{H}_3$  and  $\hat{w}_\alpha$  from equation A-21, yielding

$$\begin{aligned} \partial_3 \hat{\mathbf{H}}_0 &= -i\omega \hat{\varepsilon}_\mathcal{L} \hat{\mathbf{E}}_0 + \frac{\eta}{\hat{k}} \hat{\mathcal{L}} \gamma_\alpha \left( i\omega \rho^f \frac{\hat{k}}{\eta} \delta_\alpha^t \hat{v}^s + \frac{\hat{k}}{\eta} (\partial_\alpha \hat{p} - \hat{f}_\alpha^f) - \hat{\mathcal{L}} \gamma_\alpha^t \hat{\mathbf{E}}_0 \right) - \hat{\mathbf{J}}_0^{s,e} \\ &\quad + \left( \frac{\partial_2}{-\partial_1} \right) \frac{1}{i\omega \mu_0} (\partial_2 - \partial_1) \hat{\mathbf{E}}_0 - \left( \frac{\partial_2}{-\partial_1} \right) \frac{1}{i\omega \mu_0} \hat{\mathbf{J}}_0^{s,m}. \end{aligned} \quad (\text{A-29})$$

Equations A-23, A-26, A-28, A-18, A-27 and A-29 are now combined into the seismoelectric two-way wave equation, according to

$$\partial_z \hat{\mathbf{q}} = \hat{\mathcal{A}} \hat{\mathbf{q}} + \hat{\mathbf{d}}, \quad (\text{A-30})$$

where the wave vector  $\hat{\mathbf{q}}$  and the source vector  $\hat{\mathbf{d}}$  are defined as

$$\hat{\mathbf{q}} = \begin{pmatrix} -\hat{\tau}_3^b \\ \hat{p} \\ \hat{\mathbf{E}}_0 \\ \hat{\mathbf{v}}^s \\ \hat{w}_3 \\ \hat{\mathbf{H}}_0 \end{pmatrix}, \quad \hat{\mathbf{d}} = \begin{pmatrix} \hat{\mathbf{f}}^b - i\omega\rho^f \frac{\hat{k}}{\eta} \boldsymbol{\delta}_\alpha \hat{f}_\alpha^f + \frac{1}{i\omega} \partial_\alpha \mathbf{R}_{\alpha\beta} \hat{\mathbf{h}}_\beta^b \\ \hat{f}_3^f - \frac{1}{i\omega\hat{\varepsilon}_\mathcal{L}} \hat{\mathcal{L}} \frac{\eta}{k} \hat{J}_3^{\text{s},e} \\ -\hat{\mathbf{J}}_0^{\text{s},m} - \begin{pmatrix} \partial_1 \\ \partial_2 \end{pmatrix} \frac{1}{i\omega\hat{\varepsilon}_\mathcal{L}} \hat{J}_3^{\text{s},e} \\ \hat{\mathbf{h}}_3^b + \mathbf{e}_{33}^{-1} \mathbf{e}_{3\alpha} \hat{\mathbf{h}}_\alpha^b \\ \hat{q}^i - \partial_\beta \frac{\hat{k}}{\eta} \hat{f}_\beta^f + \frac{\mathbf{d}}{M} \mathbf{r}_\beta^t \hat{\mathbf{h}}_\beta \\ -\hat{\mathbf{J}}_0^{\text{s},e} - \hat{\mathcal{L}} \gamma_\alpha \hat{f}_\alpha^f - \begin{pmatrix} \partial_2 \\ -\partial_1 \end{pmatrix} \frac{1}{i\omega\mu_0} \hat{J}_3^{\text{s},m} \end{pmatrix}, \quad (\text{A-31})$$

and the operator matrix  $\hat{\mathcal{A}}$  as

$$\hat{\mathcal{A}} = \begin{pmatrix} \hat{\mathcal{A}}_{11} & \hat{\mathcal{A}}_{12} \\ \hat{\mathcal{A}}_{21} & \hat{\mathcal{A}}_{22} \end{pmatrix}, \quad (\text{A-32})$$

with

$$\hat{\mathcal{A}}_{11} = \begin{pmatrix} \hat{\mathcal{A}}_{11}^{11} & \hat{\mathcal{A}}_{11}^{12} & \hat{\mathcal{A}}_{11}^{13} \\ \hat{\mathcal{A}}_{11}^{21} & \hat{\mathcal{A}}_{11}^{22} & \hat{\mathcal{A}}_{11}^{23} \\ \hat{\mathcal{A}}_{11}^{31} & \hat{\mathcal{A}}_{11}^{32} & \hat{\mathcal{A}}_{11}^{33} \\ \hat{\mathcal{A}}_{11}^{41} & \hat{\mathcal{A}}_{11}^{42} & \hat{\mathcal{A}}_{11}^{43} \end{pmatrix}, \quad \hat{\mathcal{A}}_{12} = \begin{pmatrix} \hat{\mathcal{A}}_{12}^{11} & \hat{\mathcal{A}}_{12}^{12} & \hat{\mathcal{A}}_{12}^{13} \\ \hat{\mathcal{A}}_{12}^{21} & \hat{\mathcal{A}}_{12}^{22} & \hat{\mathcal{A}}_{12}^{23} \\ \hat{\mathcal{A}}_{12}^{31} & \hat{\mathcal{A}}_{12}^{32} & \hat{\mathcal{A}}_{12}^{33} \\ \hat{\mathcal{A}}_{12}^{41} & \hat{\mathcal{A}}_{12}^{42} & \hat{\mathcal{A}}_{12}^{43} \end{pmatrix}, \quad (\text{A-33})$$

$$\hat{\mathcal{A}}_{21} = \begin{pmatrix} \hat{\mathcal{A}}_{21}^{11} & \hat{\mathcal{A}}_{21}^{12} & \hat{\mathcal{A}}_{21}^{13} \\ \hat{\mathcal{A}}_{21}^{21} & \hat{\mathcal{A}}_{21}^{22} & \hat{\mathcal{A}}_{21}^{23} \\ \hat{\mathcal{A}}_{21}^{31} & \hat{\mathcal{A}}_{21}^{32} & \hat{\mathcal{A}}_{21}^{33} \\ \hat{\mathcal{A}}_{21}^{41} & \hat{\mathcal{A}}_{21}^{42} & \hat{\mathcal{A}}_{21}^{43} \end{pmatrix}, \quad \hat{\mathcal{A}}_{22} = \begin{pmatrix} \hat{\mathcal{A}}_{22}^{11} & \hat{\mathcal{A}}_{22}^{12} & \hat{\mathcal{A}}_{22}^{13} \\ \hat{\mathcal{A}}_{22}^{21} & \hat{\mathcal{A}}_{22}^{22} & \hat{\mathcal{A}}_{22}^{23} \\ \hat{\mathcal{A}}_{22}^{31} & \hat{\mathcal{A}}_{22}^{32} & \hat{\mathcal{A}}_{22}^{33} \\ \hat{\mathcal{A}}_{22}^{41} & \hat{\mathcal{A}}_{22}^{42} & \hat{\mathcal{A}}_{22}^{43} \end{pmatrix}.$$

Where

$$\hat{\mathcal{A}}_{11}^{11} = -\partial_\alpha (\mathbf{e}_{\alpha 3} \mathbf{e}_{33}^{-1}), \quad (\text{A-34})$$

$$\hat{\mathcal{A}}_{11}^{12} = i\omega \rho^f \frac{\hat{k}}{\eta} \boldsymbol{\delta}_\alpha \partial_\alpha - \partial_\alpha \left( \frac{\text{d}}{M} \mathbf{r}_\alpha \right), \quad (\text{A-35})$$

$$\hat{\mathcal{A}}_{11}^{13} = -i\omega \rho^f \hat{\mathcal{L}} \boldsymbol{\delta}_\alpha \gamma_\alpha^t, \quad (\text{A-36})$$

$$\hat{\mathcal{A}}_{12}^{11} = \frac{1}{i\omega} \partial_\alpha (\mathbf{R}_{\alpha\beta} \partial_\beta) - i\omega \left( \rho^b \mathbf{I}_3 - i\omega (\rho^f)^2 \frac{\hat{k}}{\eta} \boldsymbol{\delta}_\alpha \boldsymbol{\delta}_\alpha^t \right), \quad (\text{A-37})$$

$$\hat{\mathcal{A}}_{12}^{12} = -i\omega \rho^f \boldsymbol{\delta}_3, \quad (\text{A-38})$$

$$\hat{\mathcal{A}}_{12}^{21} = -i\omega \rho^f \boldsymbol{\delta}_3^t, \quad (\text{A-39})$$

$$\hat{\mathcal{A}}_{12}^{22} = -\frac{\eta}{\hat{k}} \left( 1 + \frac{1}{i\omega \hat{\varepsilon}_\mathcal{L}} \frac{\eta}{\hat{k}} \hat{\mathcal{L}}^2 \right), \quad (\text{A-40})$$

$$\hat{\mathcal{A}}_{12}^{23} = \frac{1}{i\omega \hat{\varepsilon}_\mathcal{L}} \frac{\eta}{\hat{k}} \hat{\mathcal{L}} (\partial_1 \partial_2), \quad (\text{A-41})$$

$$\hat{\mathcal{A}}_{12}^{32} = -\begin{pmatrix} \partial_1 \\ \partial_2 \end{pmatrix} \frac{1}{i\omega \hat{\varepsilon}_\mathcal{L}} \frac{\eta}{\hat{k}} \hat{\mathcal{L}}, \quad (\text{A-42})$$

$$\hat{\mathcal{A}}_{12}^{33} = -i\omega \mu_0 \mathbf{I}_2 + \begin{pmatrix} \partial_1 \\ \partial_2 \end{pmatrix} \frac{1}{i\omega \hat{\varepsilon}_\mathcal{L}} (\partial_1 \partial_2), \quad (\text{A-43})$$

$$\hat{\mathcal{A}}_{21}^{11} = -i\omega \mathbf{e}_{33}^{-1}, \quad (\text{A-44})$$

$$\hat{\mathcal{A}}_{21}^{12} = i\omega \frac{\text{d}}{M} \mathbf{e}_{33}^{-1} \boldsymbol{\delta}_3, \quad (\text{A-45})$$

$$\hat{\mathcal{A}}_{21}^{21} = i\omega \frac{\text{d}}{M} \boldsymbol{\delta}_3^t \mathbf{e}_{33}^{-1}, \quad (\text{A-46})$$

$$\hat{\mathcal{A}}_{21}^{22} = -i\omega \frac{\text{d}^2}{M^2} \boldsymbol{\delta}_3^t \mathbf{e}_{33}^{-1} \boldsymbol{\delta}_3^t - \frac{i\omega}{M} + \partial_\beta \left( \frac{\hat{k}}{\eta} \partial_\beta \right), \quad (\text{A-47})$$

$$\hat{\mathcal{A}}_{21}^{23} = -\partial_\beta \hat{\mathcal{L}} \gamma_\beta^t, \quad (\text{A-48})$$

$$\hat{\mathcal{A}}_{21}^{32} = \hat{\mathcal{L}} \gamma_\alpha \partial_\alpha, \quad (\text{A-49})$$

$$\hat{\mathcal{A}}_{21}^{33} = -i\omega \hat{\varepsilon}_\mathcal{L} \mathbf{I}_2 + \begin{pmatrix} \partial_2 \\ -\partial_1 \end{pmatrix} \frac{1}{i\omega \mu_0} (\partial_2 - \partial_1) - \frac{\eta}{\hat{k}} \hat{\mathcal{L}}^2 \gamma_\alpha \gamma_\alpha^t, \quad (\text{A-50})$$

$$\hat{\mathcal{A}}_{22}^{11} = -\mathbf{e}_{33}^{-1} \mathbf{e}_{3\beta} \partial_\beta, \quad (\text{A-51})$$

$$\hat{\mathcal{A}}_{22}^{21} = \partial_\beta \left( i\omega \rho^f \frac{\hat{k}}{\eta} \boldsymbol{\delta}_\beta^t \right) - \frac{\text{d}}{M} \mathbf{r}_\beta^t \partial_\beta, \quad (\text{A-52})$$

$$\hat{\mathcal{A}}_{22}^{31} = i\omega \rho^f \hat{\mathcal{L}} \gamma_\alpha \boldsymbol{\delta}_\alpha^t, \quad (\text{A-53})$$

where  $\mathbf{I}_2$  is a  $2 \times 2$  identity matrix. The submatrices that have not been listed are zero. The stiffness matrix  $\mathbf{e}_{jl}$  reads, according to equations A-6, A-9 and 2-16

$$(\mathbf{e}_{jl})_{kl} = e_{ijkl} = S \delta_{ij} \delta_{kl} + N (\delta_{ik} \delta_{jl} + \delta_{il} \delta_{jk}), \quad (\text{A-54})$$

with

$$S = K_G - \frac{2}{3} N - \frac{\text{d}^2}{M}. \quad (\text{A-55})$$

We have eliminated the fields  $\boldsymbol{\tau}_1^b, \boldsymbol{\tau}_2^b, \mathbf{E}_3, \mathbf{H}_3, w_1$  and  $w_2$ . The source quantities  $J_3^{s,e}, J_3^{s,m}, f_1^f, f_2^f, \mathbf{h}_1^b$  and  $\mathbf{h}_2^b$  are still contained in the source vector  $\mathbf{d}$ . The eliminated field quantities can simply be calculated, using equations 2-22, 2-23, 2-10 and A-7, from quantities in  $\mathbf{q}$  according to

$$\hat{E}_3 = \frac{1}{i\omega\hat{\varepsilon}_{\mathcal{L}}} \left( \partial_2 \hat{H}_1 - \partial_1 \hat{H}_2 - \hat{\mathcal{L}} \frac{\eta}{k} \hat{w}_3 - \hat{J}_3^{s,e} \right), \quad (\text{A-56})$$

$$\hat{H}_3 = \frac{1}{i\omega\mu_0} \left( \partial_2 \hat{E}_1 - \partial_1 \hat{E}_2 - \hat{J}_3^{s,m} \right), \quad (\text{A-57})$$

$$\hat{w}_1 = \frac{k}{\eta} \left( \hat{f}_1^f - \partial_1 \hat{p}^f - i\omega\rho^f \hat{v}_1^s \right) + \hat{\mathcal{L}} \hat{E}_1, \quad (\text{A-58})$$

$$\hat{w}_2 = \frac{k}{\eta} \left( \hat{f}_2^f - \partial_2 \hat{p}^f - i\omega\rho^f \hat{v}_2^s \right) + \hat{\mathcal{L}} \hat{E}_2, \quad (\text{A-59})$$

$$-\hat{\boldsymbol{\tau}}_1^b = \frac{1}{i\omega} \left( \mathbf{e}_{1l} \hat{\mathbf{h}}_l^b + i\omega \frac{d}{M} \delta_1 \hat{p}^f - \mathbf{e}_{1l} \partial_l \hat{\mathbf{v}}^s \right), \quad (\text{A-60})$$

$$-\hat{\boldsymbol{\tau}}_2^b = \frac{1}{i\omega} \left( \mathbf{e}_{2l} \hat{\mathbf{h}}_l^b + i\omega \frac{d}{M} \delta_2 \hat{p}^f - \mathbf{e}_{2l} \partial_l \hat{\mathbf{v}}^s \right). \quad (\text{A-61})$$

---

## Appendix B

---

# SH-TE Decomposition

### B-1 Velocities

We start from the matrix  $\mathcal{A}_{shte}$  of the SH-TE mode 3-33 in the horizontal-wavenumber frequency domain it is given by

$$\tilde{\mathcal{A}}_{shte} = \begin{pmatrix} 0 & -i\omega\rho^f\hat{\mathcal{L}} & -i\omega\hat{\rho}^c + \frac{ik_1^2}{\omega}N & 0 \\ 0 & 0 & 0 & -i\omega\mu_0 \\ -i\omega\frac{1}{N} & 0 & 0 & 0 \\ 0 & -i\omega\hat{\varepsilon} + \frac{ik_1^2}{\omega}\frac{1}{\mu_0} & i\omega\rho^f\hat{\mathcal{L}} & 0 \end{pmatrix}. \quad (\text{B-1})$$

When we omit the subscript  $shte$ , by default we mean the SH-TE system in this appendix.

To solve for upgoing and downgoing waves, we determine the eigenvalues of the system matrix  $|\tilde{\mathcal{A}} - \lambda\mathbf{I}| = 0$ . The trivial solution of a zero-eigenvalue gives the velocity for a wave traveling purely in the horizontal direction. Hence the velocity in a layer is found solving  $|\tilde{\mathcal{A}}| = 0$ ,

$$\begin{vmatrix} 0 & -i\omega\rho^f\hat{\mathcal{L}} & -i\omega\hat{\rho}^c + \frac{ik_1^2}{\omega}N & 0 \\ 0 & 0 & 0 & -i\omega\mu_0 \\ -i\omega\frac{1}{N} & 0 & 0 & 0 \\ 0 & -i\omega\hat{\varepsilon} + \frac{ik_1^2}{\omega}\frac{1}{\mu_0} & i\omega\rho^f\hat{\mathcal{L}} & 0 \end{vmatrix} = 0. \quad (\text{B-2})$$

We perform Laplace development over the first and last columns, this leads to

$$\left(\omega^2\frac{\mu_0}{N}\right) \begin{vmatrix} -i\omega\rho^f\hat{\mathcal{L}} & -i\omega\hat{\rho}^c + \frac{ik_1^2}{\omega}N \\ -i\omega\hat{\varepsilon} + \frac{ik_1^2}{\omega}\frac{1}{\mu_0} & i\omega\rho^f\hat{\mathcal{L}} \end{vmatrix} = 0, \quad (\text{B-3})$$

since for  $\omega \neq 0$  the factor  $\omega^2\frac{\mu_0}{N} \neq 0$ , we have

$$\begin{vmatrix} -i\omega\rho^f\hat{\mathcal{L}} & -i\omega\hat{\rho}^c + \frac{ik_1^2}{\omega}N \\ -i\omega\hat{\varepsilon} + \frac{ik_1^2}{\omega}\frac{1}{\mu_0} & i\omega\rho^f\hat{\mathcal{L}} \end{vmatrix} = 0, \quad (\text{B-4})$$

thus

$$\omega^2 (\rho^f)^2 \hat{\mathcal{L}}^2 - \left[ \left( -i\omega \hat{\rho}^c + \frac{ik_1^2}{\omega} N \right) \left( -i\omega \hat{\varepsilon} + \frac{ik_1^2}{\omega} \frac{1}{\mu_0} \right) \right] = 0 \quad (\text{B-5})$$

or as quadratic in  $\frac{k_1^2}{\omega^2}$ ,

$$\left( \frac{N}{\mu_0} \right) \frac{k_1^4}{\omega^4} + \left[ - \left( \frac{1}{\mu_0} \hat{\rho}^c + \hat{\varepsilon} N \right) \right] \frac{k_1^2}{\omega^2} + \left( \rho^{f2} \hat{\mathcal{L}}^2 + (\hat{\rho}^c)^2 \hat{\varepsilon} \right) = 0. \quad (\text{B-6})$$

The general solution to a quadratic equation  $ax^2 + bx + c = 0$  is given as  $x = \frac{-b \pm \sqrt{b^2 - 4ac}}{2a}$ . Using this to solve for  $\frac{k_1^2}{\omega^2}$  in equation B-6 gives

$$2 \frac{k_1^2}{\omega^2} = \frac{\hat{\rho}^c}{N} + \hat{\varepsilon} \mu_0 \pm \sqrt{\left( \frac{\hat{\rho}^c}{N} - \hat{\varepsilon} \mu_0 \right)^2 - 4 \frac{\mu_0}{N} \left( \rho^f \hat{\mathcal{L}} \right)^2}. \quad (\text{B-7})$$

For horizontally propagating plane waves we have  $\frac{k_1^2}{\omega^2} = \frac{1}{c^2}$ , hence for the velocities of SH-TE seismoelectric waves we have

$$\frac{2}{c^2} = \frac{\hat{\rho}^c}{N} + \hat{\varepsilon} \mu_0 \pm \sqrt{\left( \frac{\hat{\rho}^c}{N} - \hat{\varepsilon} \mu_0 \right)^2 - 4 \frac{\mu_0}{N} \left( \rho^f \hat{\mathcal{L}} \right)^2}. \quad (\text{B-8})$$

The plus sign is associated with the velocity of the SH-wave  $c_{sh}$  and the minus sign with the velocity of the  $c_{te}$  wave, as can be seen when the coupling coefficient is set to zero  $\mathcal{L} = 0$ . These velocities are a function of the medium parameters of the layer under consideration.

## B-2 Non-zero eigenvalues

We look for non-zero solutions of the equation  $|\tilde{\mathcal{A}} - \lambda \mathbf{I}| = 0$ . Thus we solve for

$$\begin{vmatrix} -\lambda & -i\omega \rho^f \hat{\mathcal{L}} & -i\omega \hat{\rho}^c + \frac{ik_1^2}{\omega} N & 0 \\ 0 & -\lambda & 0 & -i\omega \mu_0 \\ -i\omega \frac{1}{N} & 0 & -\lambda & 0 \\ 0 & -i\omega \hat{\varepsilon} + \frac{ik_1^2}{\omega} \frac{1}{\mu_0} & i\omega \rho^f \hat{\mathcal{L}} & -\lambda \end{vmatrix} = 0, \quad (\text{B-9})$$

performing Laplace development over the 4<sup>th</sup> column leads to

$$\begin{aligned} -i\omega \mu_0 & \begin{vmatrix} -\lambda & -i\omega \rho^f \hat{\mathcal{L}} & -i\omega \hat{\rho}^c + \frac{ik_1^2}{\omega} N \\ -i\omega \frac{1}{N} & 0 & -\lambda \end{vmatrix} \\ -\lambda & \begin{vmatrix} -\lambda & -i\omega \rho^f \hat{\mathcal{L}} & -i\omega \hat{\rho}^c + \frac{ik_1^2}{\omega} N \\ 0 & -i\omega \hat{\varepsilon} + \frac{ik_1^2}{\omega} \frac{1}{\mu_0} & i\omega \rho^f \hat{\mathcal{L}} \\ -i\omega \frac{1}{N} & 0 & -\lambda \end{vmatrix} = 0. \end{aligned} \quad (\text{B-10})$$

In the first determinant of equation B-11 we perform Laplace development over the middle column, and in the second determinant we perform Laplace development over the first column

$$\begin{aligned} \omega^2 \mu_0 \rho^f \hat{\mathcal{L}} \begin{vmatrix} -i\omega \frac{1}{N} & -\lambda \\ 0 & i\omega \rho^f \hat{\mathcal{L}} \end{vmatrix} - (-i\omega \mu_0) \begin{vmatrix} -i\omega \hat{\varepsilon} + \frac{ik_1^2}{\omega} \frac{1}{\mu_0} \\ -i\omega \frac{1}{N} \end{vmatrix} \begin{vmatrix} -\lambda & -i\omega \hat{\rho}^c + \frac{ik_1^2}{\omega} N \\ -i\omega \frac{1}{N} & -\lambda \end{vmatrix} \\ + \lambda^2 \begin{vmatrix} -\lambda & 0 \\ 0 & -\lambda \end{vmatrix} - \lambda \begin{vmatrix} -i\omega \frac{1}{N} \\ -i\omega \rho^f \hat{\mathcal{L}} \end{vmatrix} \begin{vmatrix} -i\omega \hat{\rho}^c + \frac{ik_1^2}{\omega} N \\ -\lambda \end{vmatrix} = 0 \end{aligned} \quad (\text{B-11})$$

or

$$\begin{aligned} -\omega^4 \frac{\mu_0}{N} (\rho^f \hat{\mathcal{L}})^2 - (-i\omega \mu_0) \left( -i\omega \hat{\varepsilon} + \frac{ik_1^2}{\omega} \frac{1}{\mu_0} \right) \lambda^2 \\ + (-i\omega \mu_0) \left( -i\omega \hat{\varepsilon} + \frac{ik_1^2}{\omega} \frac{1}{\mu_0} \right) \left( -i\omega \hat{\rho}^c + \frac{ik_1^2}{\omega} N \right) \left( -i\omega \frac{1}{N} \right) \\ + \lambda^4 - \lambda^2 \left( -i\omega \frac{1}{N} \right) \left( -i\omega \hat{\rho}^c + \frac{ik_1^2}{\omega} N \right) = 0. \end{aligned} \quad (\text{B-12})$$

From equation B-12 which we extract a quadratic function in  $\lambda^2$

$$\begin{aligned} \lambda^4 + \left[ (\omega^2 \mu_0 \hat{\varepsilon} - k_1^2) + \left( \omega^2 \frac{\hat{\rho}^c}{N} - k_1^2 \right) \right] \lambda^2 \\ + \left[ \omega^4 \frac{\mu_0}{N} (\rho^f \hat{\mathcal{L}})^2 + (\omega^2 \mu_0 \hat{\varepsilon} - k_1^2) + \left( \omega^2 \frac{\hat{\rho}^c}{N} - k_1^2 \right) \right] = 0, \end{aligned} \quad (\text{B-13})$$

which we solve again as a quadratic function;

$$2\lambda^2 = -\omega^2 \left( \frac{\hat{\rho}^c}{N} + \hat{\varepsilon} \mu_0 \right) + 2k_1^2 \pm \omega^2 \sqrt{\left( \frac{\hat{\rho}^c}{N} - \hat{\varepsilon} \mu_0 \right)^2 - 4 \frac{\mu_0}{N} (\rho^f \hat{\mathcal{L}})^2}. \quad (\text{B-14})$$

Equation B-14 can be simplified using the expression B-8 for the seismoelectric velocities, this leads to

$$k_1^2 - \lambda_w^2 = \frac{\omega^2}{\hat{c}_w^2}. \quad (\text{B-15})$$

We define an operator  $\tilde{\mathcal{H}} = \sqrt{\frac{\omega^2}{\hat{c}_w^2} - k_1^2}$ , such that our eigenvalues are

$$i\tilde{\mathcal{H}}_{sh}, \quad i\tilde{\mathcal{H}}_{te}, \quad -i\tilde{\mathcal{H}}_{sh} \text{ and } -i\tilde{\mathcal{H}}_{te}. \quad (\text{B-16})$$

In what follows we will use a generalized eigenvalue  $i\tilde{\mathcal{H}}_w^\pm = \mp i \sqrt{\frac{\omega^2}{\hat{c}_w^2} - k_1^2} = \mp i\tilde{\mathcal{H}}_w$ . In which the superscript  $\pm$  denotes upgoing or downgoing waves ( $+$  denotes down) according to the choice of the sign of the square root operator made in section 3-4 and the subscript  $w$  denotes the wavetype. We have diagonalized the matrix  $\tilde{\mathcal{A}}$  and find  $\tilde{\mathcal{H}}$ , where

$$\tilde{\mathcal{H}} = \begin{pmatrix} i\tilde{\mathcal{H}}_{sh}^+ & 0 & 0 & 0 \\ 0 & i\tilde{\mathcal{H}}_{te}^+ & 0 & 0 \\ 0 & 0 & i\tilde{\mathcal{H}}_{sh}^- & 0 \\ 0 & 0 & 0 & i\tilde{\mathcal{H}}_{te}^- \end{pmatrix}. \quad (\text{B-17})$$

### B-3 Eigenvectors of SH-TE system

We need the eigenvectors to diagonalize the system matrix  $\tilde{\mathcal{A}}$  and decompose the SHTE fields  $-\tilde{\tau}_{23}^b$ ,  $\tilde{E}_2$ ,  $\tilde{v}_2^s$  and  $-\tilde{H}_1$  in upgoing and downgoing waves. We start from a general eigenvalue  $i\tilde{\mathcal{H}}_w^\pm$  and derive a general eigenvector  $\mathbf{a}_w^\pm$ . From the eigenvector problem  $(\tilde{\mathcal{A}} - \tilde{\mathcal{H}})\mathbf{a}_w^\pm = 0$  we have four equations for each eigenvalue,

$$-i\tilde{\mathcal{H}}_w^\pm a_{1,w}^\pm - i\omega\rho^f \hat{\mathcal{L}} a_{2,w}^\pm + \left(-i\omega\hat{\rho}^c + \frac{ik_1^2}{\omega}N\right) a_{3,w}^\pm = 0, \quad (\text{B-18})$$

$$-i\tilde{\mathcal{H}}_w^\pm a_{2,w}^\pm - i\omega\mu_0 a_{4,w}^\pm = 0, \quad (\text{B-19})$$

$$-i\omega\frac{1}{N}a_{1,w}^\pm - i\tilde{\mathcal{H}}_w^\pm a_{3,w}^\pm = 0, \quad (\text{B-20})$$

$$\left(-i\omega\hat{\varepsilon} + \frac{ik_1^2}{\omega}\frac{1}{\mu_0}\right) a_{2,w}^\pm + i\omega\rho^f \hat{\mathcal{L}} a_{3,w}^\pm - i\tilde{\mathcal{H}}_w^\pm a_{4,w}^\pm = 0. \quad (\text{B-21})$$

We solve this set of equations, normalizing to  $a_{3,n}^\pm = 1$ , from equation B-20 we find

$$a_{1,w}^\pm = -\left(\frac{\tilde{\mathcal{H}}_w^\pm}{\omega}\right) N, \quad (\text{B-22})$$

using equation B-19 we find

$$a_{4,w}^\pm = -\frac{\tilde{\mathcal{H}}_w^\pm}{\omega}\frac{1}{\mu_0}a_{2,w}^\pm. \quad (\text{B-23})$$

Finally, substituting equations B-22 and B-23 into equation B-18 we find

$$a_{2,w}^\pm = \frac{\left(\frac{1}{\hat{\varepsilon}_w^2} - \frac{\hat{\rho}^c}{N}\right)}{\frac{1}{N}\rho^f \hat{\mathcal{L}}}. \quad (\text{B-24})$$

Summarizing, we have

$$\mathbf{a}_w^\pm = \begin{pmatrix} \pm \frac{\tilde{\mathcal{H}}_w^\pm}{\omega} N \\ \hat{\xi}_w^1 \\ 1 \\ \pm \frac{\tilde{\mathcal{H}}_w^\pm}{\omega} \frac{1}{\mu_0} \hat{\xi}_w^1 \end{pmatrix}, \quad (\text{B-25})$$

where

$$\hat{\xi}_w^1 = \frac{\left(\frac{1}{\hat{\varepsilon}_w^2} - \frac{\hat{\rho}^c}{N}\right)}{\frac{1}{N}\rho^f \hat{\mathcal{L}}}. \quad (\text{B-26})$$

There is another expression for the scaling term  $\hat{\xi}$ . Which we find when we substitute equation B-23 in equation B-21

$$\left(-i\omega\hat{\varepsilon} + \frac{ik_1^2}{\omega}\frac{1}{\mu_0}\right) a_{3,w}^\pm + i\omega\rho^f \hat{\mathcal{L}} - i\tilde{\mathcal{H}}_w^\pm \left(-\frac{\tilde{\mathcal{H}}_w^\pm}{\mu_0\omega} a_{2,w}^\pm\right) = 0. \quad (\text{B-27})$$

Again normalize to  $a_{3,w}^\pm = 1$ , we find

$$a_{2,w}^\pm = \frac{\mu_0 \rho^f \hat{\mathcal{L}}}{\hat{\varepsilon} \mu_0 - \frac{1}{\hat{c}_w^2}}. \quad (\text{B-28})$$

This choice leads to

$$\mathbf{a}_w^\pm = \begin{pmatrix} \pm \frac{\tilde{\mathcal{H}}_w}{\omega} N \\ \hat{\xi}_w^2 \\ 1 \\ \pm \frac{\tilde{\mathcal{H}}_w}{\omega} \frac{1}{\mu_0} \hat{\xi}_w^2 \end{pmatrix}, \quad (\text{B-29})$$

where

$$\hat{\xi}_w^2 = \frac{\mu_0 \rho^f \hat{\mathcal{L}}}{\left( \hat{\varepsilon} \mu_0 - \frac{1}{\hat{c}_w^2} \right)}. \quad (\text{B-30})$$

If we equate B-26 and B-30 we obtain B-8.

There is an expression for  $\mathbf{a}_n^\pm$  from Haartsen [1995], Pride and Haartsen [1996], Haartsen and Pride [1997]. This one was previously also used by Shaw [2004], van der Burg [2002] and White and Zhou [2006], rearranging and rewriting for the fields in our SH-TE two-way field vector  $\tilde{\mathbf{q}}$  gives

$$\mathbf{a}_w^\pm = \begin{pmatrix} \pm \frac{\tilde{\mathcal{H}}_w}{\omega} N \\ \hat{\xi}_w^3 \\ 1 \\ \pm \frac{\tilde{\mathcal{H}}_w}{\omega} \frac{1}{\mu_0} \hat{\xi}_w^3 \end{pmatrix}, \quad (\text{B-31})$$

where

$$\hat{\xi}_w^3 = \frac{\mu_0 \hat{\mathcal{L}} \hat{\rho}^E (N - \rho^b \hat{c}_w^2)}{\hat{\varepsilon}_{\mathcal{L}} \mu_0 \rho^f \hat{c}_w^2 - \rho^f}. \quad (\text{B-32})$$

We now equate  $\hat{\xi}_w^1$  and  $\hat{\xi}_w^3$ , this is a little tedious,

$$\frac{\frac{N}{\hat{c}_w^2} - \hat{\rho}^c}{\rho^f \hat{\mathcal{L}}} = \frac{\mu_0 \hat{\mathcal{L}} \hat{\rho}^E (\rho^b \hat{c}_w^2 - N)}{\hat{\varepsilon}_{\mathcal{L}} \mu_0 \rho^f \hat{c}_w^2 - \rho^f}, \quad (\text{B-33})$$

with

$$\hat{\rho}^c = \left( \rho^b - \frac{(\rho^f)^2}{\hat{\rho}^E} \right) \quad \text{and} \quad \hat{\varepsilon}_{\mathcal{L}} = \hat{\varepsilon} - \hat{\rho}^E \hat{\mathcal{L}}^2. \quad (\text{B-34})$$

Cross-multiplying the denominators gives

$$\left( \frac{N}{\hat{c}_w^2} - \hat{\rho}^c \right) \left( \left( \hat{\varepsilon} - \hat{\rho}^E \hat{\mathcal{L}}^2 \right) \mu_0 \rho^f \hat{c}_w^2 - \rho^f \right) = \left( \mu_0 \hat{\mathcal{L}} \hat{\rho}^E \rho^b \hat{c}_w^2 - N \right) \left( \rho^f \hat{\mathcal{L}} \right). \quad (\text{B-35})$$

We divide by  $\rho^f$  and develop all multiplication terms

$$\begin{aligned} N \hat{\varepsilon} \mu_0 - \hat{\rho}^c \hat{\varepsilon} \mu_0 \hat{c}_w^2 - N \hat{\rho}^E \hat{\mathcal{L}}^2 \mu_0 + \hat{\rho}^c \hat{\rho}^E \hat{\mathcal{L}}^2 \mu_0 \hat{c}_w^2 - \frac{N}{\hat{c}_w^2} + \hat{\rho}^c = \\ \mu_0 \hat{\mathcal{L}}^2 \hat{\rho}^E \rho^b \hat{c}_w^2 - N \mu_0 \hat{\mathcal{L}}^2 \hat{\rho}^E, \end{aligned} \quad (\text{B-36})$$

summing out the  $N\mu_0\hat{\mathcal{L}}^2\hat{\rho}^E$  term, dividing by  $\hat{c}_w^2$  and rearranging gives

$$N\frac{1}{\hat{c}_w^4} - (\hat{\rho}^c + \hat{\varepsilon}\mu_0N)\frac{1}{\hat{c}_w^2} - \left(\hat{\varepsilon}\mu_0\hat{\rho}^c + \rho^b\hat{\rho}^E\hat{\mathcal{L}}^2\mu_0 - \hat{\rho}^c\hat{\rho}^E\hat{\mathcal{L}}^2\mu_0\right) = 0. \quad (\text{B-37})$$

Now we replace the  $\hat{\rho}^c$  in the last term with  $\rho^b - \frac{(\rho^f)^2}{\hat{\rho}^E}$  and we find

$$N\frac{1}{\hat{c}_w^4} - (\hat{\rho}^c + \hat{\varepsilon}\mu_0N)\frac{1}{\hat{c}_w^2} - \hat{\varepsilon}\mu_0\hat{\rho}^c + \mu_0\left(\rho^f\hat{\mathcal{L}}\right)^2 = 0. \quad (\text{B-38})$$

Which is again the quadratic function in  $\frac{1}{\hat{c}_w}$  found in section B-1 deriving the seismoelectric wave velocities  $\hat{c}_w$ , thus  $\hat{\xi}_w^1 = \hat{\xi}_w^3$ .

### B-3-1 Stability of the scaling terms

We have shown that all three scaling terms B-26, B-30 and B-32 are equal. However, this does not mean that they can all be applied for seismoelectric modeling. The third expression for the eigenvectors using  $\hat{\xi}_w^3$ , see equation B-32 has been used successfully by previous authors [Haartsen, 1995], [Pride and Haartsen, 1996], [Haartsen and Pride, 1997], [van der Burg, 2002], [Shaw, 2004], [White and Zhou, 2006]. The first two expressions for the eigenvectors using  $\hat{\xi}_w^1$  or  $\hat{\xi}_w^2$ , see equations B-26 and B-30, are both esthetically preferred above the one one used by previous authors. However the terms  $\hat{\xi}_w^1$  and  $\hat{\xi}_w^2$  exhibit numerical instabilities. Through trial and error we found that if we combine  $\hat{\xi}_{te}^1$  and  $\hat{\xi}_{sh}^2$  we can construct stable composition and decomposition matrices. In figure B-1 we plot  $\hat{\xi}_{sh}^1$ ,  $\hat{\xi}_{te}^1$ ,  $\hat{\xi}_{sh}^2$ ,  $\hat{\xi}_{te}^2$ ,  $\hat{\xi}_{sh}^3$  and  $\hat{\xi}_{te}^3$  in the first subsurface layer and see the instability issues.

## B-4 The decoupled SH-TE systems

The seismoelectric SH-TE system consist of a SH polarized shear wave traveling through in the solid part of the porous medium and a TE polarized electromagnetic wave. They are coupled the terms  $\pm i\omega\rho^f\hat{\mathcal{L}}$  in the SH-TE system matrix  $\tilde{\mathcal{A}}_{sh\text{te}}$ . If we set the coupling coefficient zero, we see how the matrix  $\tilde{\mathcal{A}}_{sh\text{te}}$  decouples into a SH system and a TE system with matrices  $\tilde{\mathcal{A}}_{sh}$  and  $\tilde{\mathcal{A}}_{te}$ . matrices  $\tilde{\mathcal{A}}_{sh}$  and  $\tilde{\mathcal{A}}_{te}$ .

### B-4-1 Decoupled SH waves in porous media

The two-way wave equation of the SH system in porous media is given by

$$\partial_3\tilde{\mathbf{q}} = \tilde{\mathcal{A}}\tilde{\mathbf{q}} + \tilde{\mathbf{d}}, \quad (\text{B-39})$$

with

$$\tilde{\mathcal{A}} = \begin{pmatrix} 0 & -i\omega\hat{\rho}^c + \frac{ik_1^2}{\omega}N \\ -i\omega\frac{1}{N} & 0 \end{pmatrix}, \quad (\text{B-40})$$

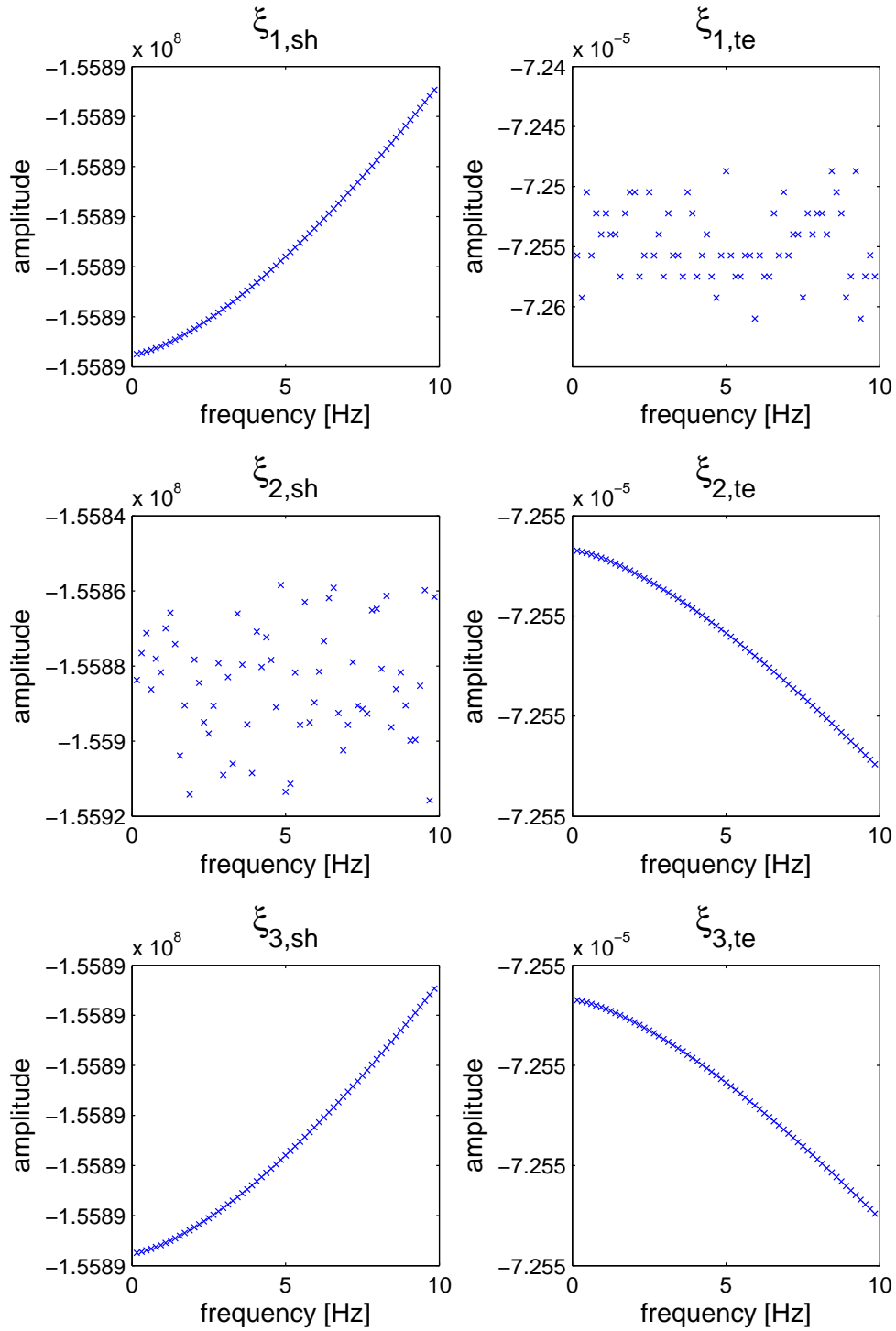


**Figure B-1:** Overview of the numerical behavior of the three different  $\xi$  terms, calculated from 0 Hz to 10 Hz using the media parameters of the layer type A.

$$\tilde{\mathbf{q}} = \begin{pmatrix} -\tilde{\gamma}_{23}^b \\ \tilde{v}_2^s \end{pmatrix} \quad \text{and} \quad \tilde{\mathbf{d}} = \begin{pmatrix} \tilde{f}_2^b - \frac{\rho^f}{\hat{\rho}^E} \tilde{f}_2^f + \frac{k_1}{\omega} N (\hat{h}_{12} + \hat{h}_{12}) \\ h_{23} + h_{32} \end{pmatrix}. \quad (\text{B-41})$$

The velocities of SH waves  $c_{sh}$  is found evaluating  $|\tilde{\mathcal{A}}| = 0$  for horizontally propagating waves ( $\frac{1}{c^2} = \frac{k_1^2}{\omega^2}$ ), we find

$$\frac{1}{c_{sh}^2} = \frac{k_1^2}{\omega^2} = \frac{\hat{\rho}^c}{N}. \quad (\text{B-42})$$

We solve the eigenvalue problem  $|\tilde{\mathcal{A}} - \mathbf{I}\lambda| = 0$  and find

$$\lambda^2 + \omega^2 \frac{\hat{\rho}^c}{N} - k_1^2 = 0, \quad (\text{B-43})$$

or using B-42 we write

$$-\lambda^2 = \frac{\omega^2}{c_{sh}} - k_1^2 \quad (\text{B-44})$$

Thus we have two eigenvalues  $i\mathcal{H}$  and  $-i\mathcal{H}$ , which we collect as  $i\tilde{\mathcal{H}}^\pm = \mp i\sqrt{\frac{\omega^2}{c_{sh}^2} - k_1^2}$ .

Substituting the eigenvalue  $i\tilde{\mathcal{H}}^\pm$  in the eigenvector problem  $(\tilde{\mathcal{A}} - \mathcal{H})\mathbf{a}^\pm = 0$  we find two equations

$$-i\tilde{\mathcal{H}}^\pm a_1^\pm + \left(-i\omega\hat{\rho}^c + \frac{ik_1^2}{\omega}N\right)a_2^\pm = 0, \quad (\text{B-45})$$

$$-i\omega\frac{1}{N}a_1^\pm - i\tilde{\mathcal{H}}^\pm = 0. \quad (\text{B-46})$$

we these two equations normalizing to  $a_2^\pm = 1$ , and find

$$\mathbf{a}^\pm = \begin{pmatrix} \pm \frac{\tilde{\mathcal{H}}}{\omega} N \\ 1 \end{pmatrix}. \quad (\text{B-47})$$

To complete these equations we also give the composition and decomposition matrices, although we do not use these in our modeling scheme. We arrange the eigenvectors into the columns of  $\tilde{\mathbf{L}}$  as  $\tilde{\mathbf{L}} = (\tilde{\mathbf{a}}^+, \tilde{\mathbf{a}}^-)$ . We have  $\tilde{\mathbf{L}}$  and  $\tilde{\mathbf{L}}^{-1}$  given by

$$\tilde{\mathbf{L}} = \begin{pmatrix} \frac{\tilde{\mathcal{H}}}{\omega} N & -\frac{\tilde{\mathcal{H}}}{\omega} N \\ 1 & 1 \end{pmatrix} \quad \text{and} \quad \tilde{\mathbf{L}}^{-1} = \frac{1}{2} \begin{pmatrix} \frac{\omega}{\tilde{\mathcal{H}}} \frac{1}{N} & 1 \\ -\frac{\omega}{\tilde{\mathcal{H}}} \frac{1}{N} & 1 \end{pmatrix}. \quad (\text{B-48})$$

#### B-4-2 Decoupled TE waves in vacuum

The other seismoelectric wave type TE also propagates independently when the coupling coefficient is set to zero. For simplicity we will evaluate this wave in vacuum. This in

addition to  $\hat{\mathcal{L}} = 0$  we also have  $\hat{\epsilon} = \epsilon_0$ ,  $\hat{\mu} = \mu_0$  and  $\hat{\sigma}^m = 0$ . The two-way wave equation for TE electromagnetic waves becomes

$$\tilde{\mathbf{q}} = \tilde{\mathcal{A}}\tilde{\mathbf{q}} + \tilde{\mathbf{d}}, \quad (\text{B-49})$$

with

$$\tilde{\mathcal{A}} = \begin{pmatrix} 0 & -i\omega\mu_0 \\ -i\omega\epsilon_0 + \frac{ik_1^2}{\omega} \frac{1}{\mu_0} & 0 \end{pmatrix}, \quad (\text{B-50})$$

$$\tilde{\mathbf{q}} = \begin{pmatrix} \tilde{E}_2 \\ -\tilde{H}_1 \end{pmatrix} \quad \text{and} \quad \tilde{\mathbf{d}} = \begin{pmatrix} \tilde{J}_1^{s,m} \\ -\tilde{J}_2^{s,e} \end{pmatrix}. \quad (\text{B-51})$$

We evaluate  $|\tilde{\mathcal{A}}| = 0$  for horizontally propagating plane waves  $\frac{1}{c_0^2} = \frac{k_1^2}{\omega^2}$  and find the electromagnetic wave velocity

$$(i\omega\mu_0) \left( -i\omega\epsilon_0 + \frac{ik_1^2}{\omega} \frac{1}{\mu_0} \right) = 0, \quad (\text{B-52})$$

$$\frac{1}{c_0^2} = \frac{k_1^2}{\omega^2} = \epsilon_0\mu_0. \quad (\text{B-53})$$

Following the same procedure as in above sections to find expressions for the eigenvalues, we again find

$$\lambda^2 + (i\omega\mu_0) \left( -i\omega\epsilon_0 + \frac{ik_1^2}{\omega} \frac{1}{\mu_0} \right) = 0, \quad (\text{B-54})$$

or

$$\frac{1}{c_0^2} = \frac{k_1^2}{\omega^2} - \frac{\lambda^2}{\omega^2}. \quad (\text{B-55})$$

We see again that we have two eigenvalues  $i\tilde{\mathcal{H}}$  and  $-i\tilde{\mathcal{H}}$ , which we collect as  $i\tilde{\mathcal{H}}^\pm = \mp i\sqrt{\frac{\omega^2}{c_0^2} - k_1^2}$ .

Substituting the general eigenvalue  $\tilde{\mathcal{H}}^\pm$  into the eigenvector problem we find two equations

$$-i\tilde{\mathcal{H}}^\pm - i\omega\mu_0 = 0 \quad (\text{B-56})$$

$$-i\omega\epsilon_0 + \frac{ik_1^2}{\omega} \frac{1}{\mu_0} - i\tilde{\mathcal{H}}^\pm = 0 \quad (\text{B-57})$$

We solve these equations normalizing for  $= 1$  and find

$$\mathbf{a}^\pm = \begin{pmatrix} 1 \\ \pm \frac{\tilde{\mathcal{H}}}{\omega} \frac{1}{\mu_0} \end{pmatrix} \quad (\text{B-58})$$

If we arrange the eigenvectors into the columns of  $\tilde{\mathbf{L}}$  as  $\tilde{\mathbf{L}} = (\tilde{\mathbf{a}}^+, \tilde{\mathbf{a}}^-)$ . We find for the composition and decomposition matrices

$$\tilde{\mathbf{L}} = \begin{pmatrix} 1 & 1 \\ \frac{\tilde{\mathcal{H}}}{\omega} \frac{1}{\mu_0} & -\frac{\tilde{\mathcal{H}}}{\omega} \frac{1}{\mu_0} \end{pmatrix} \quad \text{and} \quad \tilde{\mathbf{L}}^{-1} = \frac{1}{2} \begin{pmatrix} 1 & \frac{\omega}{\tilde{\mathcal{H}}}\mu_0 \\ 1 & -\frac{\omega}{\tilde{\mathcal{H}}}\mu_0 \end{pmatrix} \quad (\text{B-59})$$



---

## Appendix C

---

# SH-TE general diffusion, flow and wave equation in 2D and 1D

We start from the seismoelectric general diffusion, flow and wave equation matrices of section 2-2. In 2D and 1D the SH-TE system decoupled from the P-SV-TM system. We need a general diffusion, flow and wave equation for the SH-TE system to employ the general derivations of Wapenaar et al. [2006] to find interferometric Green's function representations.

### C-1 SH-TE general diffusion, flow and wave equation in 2D

Expanding the equations of Pride with  $\partial_2 = 0$  for the fields that govern the SH-TE system we find

$$i\omega\epsilon\hat{E}_2 + \left(\hat{\sigma}^e - \eta\hat{\mathcal{L}}^2\hat{k}^{-1}\right)\hat{E}_2 + \eta\hat{\mathcal{L}}\hat{k}^{-1}\hat{w}_2 - \partial_3\hat{H}_1 + \partial_1\hat{H}_3 = -\hat{J}_2^{s,e}, \quad (\text{C-1})$$

$$i\omega\mu\hat{H}_1 + \hat{\sigma}^m\hat{H}_1 - \partial_3\hat{E}_2 = -\hat{J}_1^{s,m}, \quad (\text{C-2})$$

$$i\omega\mu\hat{H}_3 + \hat{\sigma}^m\hat{H}_3 + \partial_1\hat{E}_2 = -\hat{J}_3^{s,m}, \quad (\text{C-3})$$

$$i\omega\rho^b\hat{v}_2^s + i\omega\rho^f\hat{w}_2 - \partial_1\hat{\tau}_{21} - \partial_3\hat{\tau}_{23} = \hat{f}_2^b, \quad (\text{C-4})$$

$$-i\omega\hat{\tau}_{12} + N\partial_1\hat{v}_2^s = N\hat{h}_{21}^b + N\hat{h}_{12}^b, \quad (\text{C-5})$$

$$-i\omega\hat{\tau}_{21} + N\partial_1\hat{v}_2^s = N\hat{h}_{12}^b + N\hat{h}_{21}^b, \quad (\text{C-6})$$

$$-i\omega\hat{\tau}_{23} + N\partial_3\hat{v}_2^s = N\hat{h}_{32}^b + N\hat{h}_{23}^b, \quad (\text{C-7})$$

$$-i\omega\hat{\tau}_{32} + N\partial_3\hat{v}_2^s = N\hat{h}_{23}^b + N\hat{h}_{32}^b, \quad (\text{C-8})$$

$$i\omega\rho^f\hat{v}_2^s + \eta k^{-1}\left(\hat{w}_2 - \hat{\mathcal{L}}\hat{E}_2\right) = \hat{f}_2^f. \quad (\text{C-9})$$

Equations C-5 and C-7 are equal to equations C-6 and C-8, therefore we omit equations C-5 and C-8. We rewrite equation C-9 as

$$\hat{w}_2 = \hat{\mathcal{L}}\hat{E}_2 - i\omega\frac{\hat{k}}{\eta}\rho^f\hat{v}_2^s + \frac{\hat{k}}{\eta}\hat{f}_2^f. \quad (\text{C-10})$$

We use equation C-10 to eliminate  $\hat{w}_2$  in equations C-1 and C-4. We normalize equations C-6 and C-7 by  $N$ . We find

$$i\omega\epsilon\hat{E}_2 + \hat{\sigma}^e\hat{E}_2 - i\omega\rho^f\hat{\mathcal{L}}\hat{v}_2^s - \partial_3\hat{H}_1 + \partial_1\hat{H}_3 = -\left(\hat{J}_2^{s,e} + \hat{\mathcal{L}}\hat{f}_2^f\right), \quad (\text{C-11})$$

$$i\omega\hat{\rho}^c\hat{v}_2^s + i\omega\rho^f\hat{\mathcal{L}}\hat{E}_2 - \partial_1\hat{\tau}_{21}^b - \partial_3\hat{\tau}_{23}^b = \hat{f}_2^b - \frac{\rho^f}{\hat{\rho}^E}\hat{f}_2^f, \quad (\text{C-12})$$

$$-i\omega\frac{1}{N}\hat{\tau}_{21} + \partial_1\hat{v}_2^s = \hat{h}_{12}^b + \hat{h}_{21}^b, \quad (\text{C-13})$$

$$-i\omega\frac{1}{N}\hat{\tau}_{23} + \partial_3\hat{v}_2^s = \hat{h}_{32}^b + \hat{h}_{23}^b, \quad (\text{C-14})$$

where  $\hat{\rho}^E = \frac{1}{i\omega}\frac{\eta}{k}$  and  $\hat{\rho}^c = \rho^b - \frac{(\rho^f)^2}{\hat{\rho}^E}$ .

We define 4 alternative source types, the force on the fluid phase is not an independent source type in the SH-TE system, therefore we include it in the electrical current density and the force on the bulk as:  $\hat{J}_2^{s,e} = \hat{J}_2^{s,e} + \hat{\mathcal{L}}\hat{f}_2^f$  and  $\hat{f}_2 = \hat{f}_2^b - \frac{\rho^f}{\hat{\rho}^E}\hat{f}_2^f$ . The deformation rate sources  $\hat{h}_1^b$  and  $\hat{h}_3^b$  have been defined for notational convenience as  $\hat{h}_1^b = \hat{h}_{12}^b + \hat{h}_{21}^b$  and  $\hat{h}_3^b = \hat{h}_{32}^b + \hat{h}_{23}^b$ . Equation C-11, C-12, C-3 C-3, C-13 and C-14 can now be captured into the general diffusion flow and wave equation as

$$i\omega\hat{\mathbf{A}}\hat{\mathbf{u}} + \hat{\mathbf{B}}\hat{\mathbf{u}} + \mathbf{D}_x\hat{\mathbf{u}} = \hat{\mathbf{s}}, \quad (\text{C-15})$$

where the field vector  $\hat{\mathbf{u}}$  and the source vector  $\hat{\mathbf{s}}$  are defined by

$$\hat{\mathbf{u}}^T = \left(\hat{E}_2, \hat{H}_1, \hat{H}_3, \hat{v}_2^s, -\hat{\tau}_{21}^b, -\hat{\tau}_{23}^b\right) \quad (\text{C-16})$$

and

$$\hat{\mathbf{s}}^T = \left(-\hat{J}_2^{s,e}, -\hat{J}_1^m, -\hat{J}_3^m, \hat{f}_2, \hat{h}_1^b, \hat{h}_3^b\right). \quad (\text{C-17})$$

The matrices  $\hat{\mathbf{A}}$ ,  $\hat{\mathbf{B}}$  and  $\mathbf{D}_x$  are defined by

$$\hat{\mathbf{A}} = \begin{pmatrix} \epsilon & 0 & 0 & -\rho^f\hat{\mathcal{L}} & 0 & 0 \\ 0 & \mu & 0 & 0 & 0 & 0 \\ 0 & 0 & \mu & 0 & 0 & 0 \\ \rho^f\hat{\mathcal{L}} & 0 & 0 & \hat{\rho}^c & 0 & 0 \\ 0 & 0 & 0 & 0 & \frac{1}{N} & 0 \\ 0 & 0 & 0 & 0 & 0 & \frac{1}{N} \end{pmatrix}, \quad \hat{\mathbf{B}} = \begin{pmatrix} \hat{\sigma}^e & 0 & 0 & 0 & 0 & 0 \\ 0 & \hat{\sigma}^m & 0 & 0 & 0 & 0 \\ 0 & 0 & \hat{\sigma}^m & 0 & 0 & 0 \\ 0 & 0 & 0 & 0 & 0 & 0 \\ 0 & 0 & 0 & 0 & 0 & 0 \\ 0 & 0 & 0 & 0 & 0 & 0 \end{pmatrix}$$

$$\text{and } \mathbf{D}_x = \begin{pmatrix} 0 & -\partial_3 & \partial_1 & 0 & 0 & 0 \\ -\partial_3 & 0 & 0 & 0 & 0 & 0 \\ \partial_1 & 0 & 0 & 0 & 0 & 0 \\ 0 & 0 & 0 & 0 & \partial_1 & \partial_3 \\ 0 & 0 & 0 & \partial_1 & 0 & 0 \\ 0 & 0 & 0 & \partial_3 & 0 & 0 \end{pmatrix}. \quad (\text{C-18})$$

## C-2 SH-TE general diffusion, flow and wave equation in 1D

We start from equations C-11, C-12, C-13 and C-14, setting  $\partial_1 = 0$  results to four equations

$$i\omega\epsilon\hat{E}_2 + \hat{\sigma}^e\hat{E}_2 - i\omega\rho^f\hat{\mathcal{L}}\hat{v}_2^s - \partial_3\hat{H}_1 = -\hat{J}_2^{s,e}, \quad (\text{C-19})$$

$$i\omega\mu\hat{H}_1 + \hat{\sigma}^m\hat{H}_1 - \partial_3\hat{E}_2 = -\hat{J}_1^{s,m}, \quad (\text{C-20})$$

$$i\omega\rho^c\hat{v}_2^s + i\omega\rho^f\hat{\mathcal{L}}\hat{E}_2 - \partial_3\hat{\tau}_{23}^b = \hat{f}_2, \quad (\text{C-21})$$

$$-i\omega\frac{1}{N}\hat{\tau}_{23}^b + \partial_3\hat{v}_2^s = \hat{h}_3^b. \quad (\text{C-22})$$

We capture equations C-19, C-20, C-21 and C-22 into the general flow, diffusion and wave equation C-15 with field and source vectors given by

$$\hat{\mathbf{u}} = \begin{pmatrix} \hat{E}_2 \\ \hat{H}_1 \\ \hat{v}_2^s \\ -\hat{\tau}_{23}^b \end{pmatrix} \quad \text{and} \quad \hat{\mathbf{s}} = \begin{pmatrix} -\hat{J}_2^{s,e} \\ -\hat{J}_1^{s,m} \\ \hat{f}_2 \\ \hat{h}_3^b \end{pmatrix}. \quad (\text{C-23})$$

And the matrices  $\hat{\mathbf{A}}$ ,  $\hat{\mathbf{B}}$  and  $\mathbf{D}_x$  by

$$\hat{\mathbf{A}} = \begin{pmatrix} \epsilon & 0 & -\rho^f\hat{\mathcal{L}} & 0 \\ 0 & \mu & 0 & 0 \\ \rho^f\hat{\mathcal{L}} & 0 & \rho^c & 0 \\ 0 & 0 & 0 & \frac{1}{N} \end{pmatrix}, \quad \hat{\mathbf{B}} = \begin{pmatrix} \hat{\sigma}^e & 0 & 0 & 0 \\ 0 & \hat{\sigma}^m & 0 & 0 \\ 0 & 0 & 0 & 0 \\ 0 & 0 & 0 & 0 \end{pmatrix} \quad (\text{C-24})$$

$$\text{and} \quad \mathbf{D}_x = \begin{pmatrix} 0 & -\partial_3 & 0 & 0 \\ -\partial_3 & 0 & 0 & 0 \\ 0 & 0 & 0 & \partial_3 \\ 0 & 0 & \partial_3 & 0 \end{pmatrix}. \quad (\text{C-25})$$

## C-3 Solution to the 1D SH-TE seismoelectric system in a homogeneous domain

We can solve equations C-19 to C-22 for the fields  $\hat{v}_2^s$ ,  $\hat{E}_2$ ,  $\hat{H}_1$  and  $\hat{\tau}_{23}^b$ . We find that all field quantities obey a fourth order ODE.

$$\begin{aligned} \partial_3^4\hat{E}_2 - \{i\omega\}^2 \left( \frac{\hat{\rho}^c}{N} + \hat{\epsilon}\hat{\mu} \right) \partial_3^2\hat{E}_2 + \{i\omega\}^4 \left( \frac{\hat{\rho}^c\hat{\mu}\hat{\epsilon}}{N} + \frac{\rho^f\hat{\mathcal{L}}\hat{\mu}}{N} \right) \hat{E}_2 = \\ \left[ i\omega^3 \frac{\hat{\rho}^c\hat{\mu}}{N} - i\omega\hat{\mu}\partial_3^2 \right] \left( -\hat{J}_2^{s,e} \right) + \left[ i\omega^2 \frac{\hat{\rho}^c}{N} \partial_3 - \partial_3^3 \right] \left( -\hat{J}_1^{s,m} \right) \\ + \left[ i\omega^3 \frac{\hat{\mu}\rho^f\hat{\mathcal{L}}}{N} \right] \left( \hat{f}_2 \right) - \left[ i\omega^2\rho^f\hat{\mathcal{L}}\hat{\mu}\partial_3 \right] \left( \hat{h}_3^b \right), \quad (\text{C-26}) \end{aligned}$$

$$\begin{aligned}
\partial_3^4 \hat{H}_1 - \{i\omega\}^2 \left( \frac{\hat{\rho}^c}{N} + \hat{\varepsilon}\hat{\mu} \right) \partial_3^2 \hat{H}_1 + \{i\omega\}^4 \left( \frac{\hat{\rho}^c \hat{\mu} \hat{\varepsilon}}{N} + \frac{\rho^f \hat{\mathcal{L}} \hat{\mu}}{N} \right) \hat{H}_1 = \\
\left[ i\omega^2 \frac{\hat{\rho}^c}{N} \partial_3 - \partial_3^3 \right] \left( -\hat{J}_2^{s,e} \right) - \left[ i\omega \hat{\varepsilon} \partial_3^2 - i\omega^3 \left( \frac{\hat{\rho}^c \hat{\varepsilon}}{N} + \frac{(\rho^f \hat{\mathcal{L}})^2}{N} \right) \right] \left( -\hat{J}_1^{s,m} \right) \\
+ \left[ i\omega^2 \frac{\rho^f \hat{\mathcal{L}}}{N} \partial_3 \right] \left( \hat{f}_2 \right) - \left[ i\omega \rho^f \hat{\mathcal{L}} \partial_3^2 \right] \left( \hat{h}_3^b \right), \quad (C-27)
\end{aligned}$$

$$\begin{aligned}
\partial_3^4 \hat{v}_2^s - \{i\omega\}^2 \left( \frac{\hat{\rho}^c}{N} + \hat{\varepsilon}\hat{\mu} \right) \partial_3^2 \hat{v}_2^s + \{i\omega\}^4 \left( \frac{\hat{\rho}^c \hat{\mu} \hat{\varepsilon}}{N} + \frac{\rho^f \hat{\mathcal{L}} \hat{\mu}}{N} \right) \hat{v}_2^s = \\
- \left[ i\omega^3 \frac{\rho^f \hat{\mathcal{L}} \hat{\mu}}{N} \right] \left( -\hat{J}_2^{s,e} \right) - \left[ i\omega^2 \frac{\rho^f \hat{\mathcal{L}}}{N} \partial_3 \right] \left( -\hat{J}_1^{s,m} \right) \\
+ \left[ i\omega^3 \frac{\hat{\varepsilon}\hat{\mu}}{N} - i\omega \frac{1}{N} \partial_3^2 \right] \left( \hat{f}_2 \right) + \left[ \partial_3^3 - i\omega^2 \hat{\varepsilon}\hat{\mu} \partial_3 \right] \left( \hat{h}_3^b \right), \quad (C-28)
\end{aligned}$$

$$\begin{aligned}
\partial_3^4 \hat{\tau}_{23}^b - \{i\omega\}^2 \left( \frac{\hat{\rho}^c}{N} + \hat{\varepsilon}\hat{\mu} \right) \partial_3^2 \hat{\tau}_{23}^b + \{i\omega\}^4 \left( \frac{\hat{\rho}^c \hat{\mu} \hat{\varepsilon}}{N} + \frac{\rho^f \hat{\mathcal{L}} \hat{\mu}}{N} \right) \hat{\tau}_{23}^b = \\
+ \left[ i\omega^2 \rho^f \hat{\mathcal{L}} \hat{\mu} \partial_3 \right] \left( -\hat{J}_2^{s,e} \right) + \left[ i\omega \rho^f \hat{\mathcal{L}} \partial_3^2 \right] \left( -\hat{J}_1^{s,m} \right) \\
+ \left[ \partial_3^3 - i\omega^2 \hat{\varepsilon}\hat{\mu} \partial_3 \right] \left( \hat{f}_2 \right) + \left[ -i\omega \hat{\rho}^c \partial_3^2 + i\omega^3 \left( \hat{\varepsilon}\hat{\mu} \hat{\rho}^c + (\rho^f \hat{\mathcal{L}})^2 \hat{\mu} \right) \right] \left( \hat{h}_3^b \right), \quad (C-29)
\end{aligned}$$

where  $\hat{\varepsilon} = \epsilon + \frac{1}{i\omega} \hat{\sigma}^e$  and  $\hat{\mu} = \mu + \frac{1}{i\omega} \hat{\sigma}^m$ . The left-hand sides of equations C-26 to C-29 can be simplified to

$$\left[ \partial_3 - \frac{i\omega}{\hat{c}_{sh}} \right] \left[ \partial_3 + \frac{i\omega}{\hat{c}_{sh}} \right] \left[ \partial_3 - \frac{i\omega}{\hat{c}_{te}} \right] \left[ \partial_3 + \frac{i\omega}{\hat{c}_{te}} \right] \hat{\mathbf{u}}. \quad (C-30)$$

Which is a 4<sup>th</sup> order wave equation for all the fields in the field vector  $\hat{\mathbf{u}}$ . And the wave velocities  $\hat{c}_{sh}$  and  $\hat{c}_{te}$  are given by

$$\frac{2}{\hat{c}_{sh}^2} = \frac{\hat{\rho}^c}{N} + \hat{\varepsilon}\hat{\mu} + \sqrt{\left( \frac{\hat{\rho}^c}{N} - \hat{\varepsilon}\hat{\mu} \right)^2 - 4 \frac{\mu_0}{N} (\rho^f \hat{\mathcal{L}})^2}, \quad (C-31)$$

$$\frac{2}{\hat{c}_{te}^2} = \frac{\hat{\rho}^c}{N} + \hat{\varepsilon}\hat{\mu} - \sqrt{\left( \frac{\hat{\rho}^c}{N} - \hat{\varepsilon}\hat{\mu} \right)^2 - 4 \frac{\mu_0}{N} (\rho^f \hat{\mathcal{L}})^2}. \quad (C-32)$$

### C-3-1 Green's matrix for the 1D SH-TE system in a homogeneous domain

We defined the Green's matrix in section 7-1 by replacing the  $4 \times 1$  source vector by a  $4 \times 4$  source matrix. From equations C-26 to C-29 we see that the solutions to the Green's functions are defined by a scalar part of the Green's function  $\hat{G}^s$  multiplied with the correct weighting

factor for each source type. The weighting factors are defined on the right-hand sides of equations C-26 to C-29. The Green's matrix elements are given by

$$\hat{G}_{2,2}^{E,J^e} = \left[ i\omega^3 \hat{\mu} \frac{\hat{\rho}^c}{N} - i\omega \hat{\mu} \partial_3^2 \right] \hat{G}^s, \quad (\text{C-33})$$

$$\hat{G}_{2,1}^{E,J^m} = \left[ i\omega^2 \frac{\hat{\rho}^c}{N} \partial_3 - \partial_3^3 \right] \hat{G}^s, \quad (\text{C-34})$$

$$\hat{G}_{2,2}^{E,f} = \left[ i\omega^3 \frac{\rho^f \hat{\mathcal{L}}}{N} \hat{\mu} \right] \hat{G}^s, \quad (\text{C-35})$$

$$\hat{G}_{2,23}^{E,h^b} = - \left[ i\omega^2 \rho^f \hat{\mathcal{L}} \hat{\mu} \partial_3 \right] \hat{G}^s, \quad (\text{C-36})$$

$$\hat{G}_{1,2}^{H,J^e} = \left[ i\omega^2 \frac{\hat{\rho}^c}{N} \partial_3 - \partial_3^3 \right] \hat{G}^s, \quad (\text{C-37})$$

$$\hat{G}_{1,1}^{H,J^m} = - \left[ i\omega \varepsilon \partial_3^2 - i\omega^3 \left( \frac{\hat{\rho}^c}{N} \hat{\varepsilon} + \frac{(\rho^f \hat{\mathcal{L}})^2}{N} \right) \right] \hat{G}^s, \quad (\text{C-38})$$

$$\hat{G}_{1,2}^{H,f} = \left[ i\omega^2 \frac{\rho^f \hat{\mathcal{L}}}{N} \partial_3 \right] \hat{G}^s, \quad (\text{C-39})$$

$$\hat{G}_{1,23}^{H,h^b} = - \left[ i\omega \rho^f \hat{\mathcal{L}} \partial_3^2 \right] \hat{G}^s, \quad (\text{C-40})$$

$$\hat{G}_{2,2}^{v^s,J^e} = - \left[ i\omega^3 \frac{\rho^f \hat{\mu} \hat{\mathcal{L}}}{N} \hat{\mu} \right] \hat{G}^s, \quad (\text{C-41})$$

$$\hat{G}_{2,1}^{v^s,J^m} = - \left[ i\omega^2 \frac{\rho^f \hat{\mathcal{L}}}{N} \partial_3 \right] \hat{G}^s, \quad (\text{C-42})$$

$$\hat{G}_{2,2}^{v^s,f} = \left[ i\omega^3 \frac{\hat{\varepsilon} \hat{\mu}}{N} - i\omega \frac{1}{N} \partial_3^2 \right] \hat{G}^s, \quad (\text{C-43})$$

$$\hat{G}_{2,23}^{v^s,h^b} = \left[ \partial_3^3 - i\omega^2 \hat{\varepsilon} \hat{\mu} \partial_3 \right] \hat{G}^s, \quad (\text{C-44})$$

$$\hat{G}_{23,2}^{\tau^b,J^e} = \left[ i\omega^2 \rho^f \hat{\mathcal{L}} \hat{\mu} \partial_3 \right] \hat{G}^s, \quad (\text{C-45})$$

$$\hat{G}_{23,1}^{\tau^b,J^m} = \left[ i\omega \rho^f \hat{\mathcal{L}} \partial_3^2 \right] \hat{G}^s, \quad (\text{C-46})$$

$$\hat{G}_{23,2}^{\tau^b,f} = \left[ \partial_3^3 - i\omega^2 \hat{\varepsilon} \hat{\mu} \partial_3 \right] \hat{G}^s, \quad (\text{C-47})$$

$$\hat{G}_{23,23}^{\tau^b,h^b} = - \left[ i\omega \hat{\rho}^c \partial_3^2 - i\omega^3 \left( \hat{\varepsilon} \hat{\mu} \hat{\rho}^c + (\rho^f \hat{\mathcal{L}})^2 \hat{\mu} \right) \right] \hat{G}^s. \quad (\text{C-48})$$

The scalar part of the Green's matrix is given by the inverse of the 4<sup>th</sup> order wave equation C-30. The scalar Green's function obeys

$$\left[ \partial_3^2 - \left( \frac{i\omega}{\hat{c}_{sh}} \right)^2 \right] \left[ \partial_3^2 - \left( \frac{i\omega}{\hat{c}_{te}} \right)^2 \right] \hat{G}^s(x_3, \omega) = \delta(x_3 - x_{3,s}). \quad (\text{C-49})$$

Equation C-49 can be algebraically manipulated in the vertical wavenumber-frequency manipulated to

$$\hat{G}^s(x_3, \omega) = \left[ \{ik_3\}^2 - \{i\omega \hat{s}_{sh}\}^2 \right]^{-1} \left[ \{ik_3\}^2 - \{i\omega \hat{s}_{te}\}^2 \right]^{-1} \delta(x_3 - x_{3,s}). \quad (\text{C-50})$$

Where we defined the slowness  $\hat{s}_{sh;te}$  as  $\hat{s}_{sh;te} = \hat{c}_{sh;te}^{-1}$ . Equation C-50 can also be written as

$$\hat{G}^s(x_3, \omega) = - \left[ \{i\omega\hat{s}_{sh}\}^2 - \{i\omega\hat{s}_{te}\}^2 \right]^{-1} \left[ \left( \{ik_3\}^2 - \{i\omega\hat{s}_{te}\}^2 \right)^{-1} - \left( \{ik_3\}^2 - \{i\omega\hat{s}_{sh}\}^2 \right)^{-1} \right] \delta(x_3 - x_{3,s}).$$

This implies that the scalar Green function is the sum of two Green functions, each satisfying a modified Helmholtz equation

$$\left[ \partial_3 \partial_3 - \{i\omega\hat{s}_{sh}\}^2 \right] \hat{G}_{sh;te}^s(x_3, \omega) = -\delta(x_3 - x_{3,s}). \quad (C-51)$$

The solution to this equation is well known,

$$\hat{G}_{sh;te}^s(x_3, \omega) = \frac{\exp(-i\omega\hat{s}_{sh;te}|x_3 - x_{3,s}|)}{2i\omega\hat{s}_{sh;te}}, \quad (C-52)$$

and the complete scalar Green function is given by,

$$\hat{G}^s(x_3, \omega) = \frac{\hat{G}_{te}^s(x_3, \omega) - \hat{G}_{sh}^s(x_3, \omega)}{\{i\omega\hat{s}_{sh}\}^2 - \{i\omega\hat{s}_{te}\}^2}. \quad (C-53)$$

The first two derivatives of the partial Green functions are given by

$$\partial_3 \hat{G}_{sh;te}^s(x_3, \omega) = -\frac{1}{2} \text{sign}(x_3 - x_{3,s}) \exp(-i\omega\hat{s}_{sh;te}|x_3 - x_{3,s}|), \quad (C-54)$$

$$\partial_3 \partial_3 \hat{G}_{sh;te}^s(x_3, \omega) = -\delta(x_3 - x_{3,s}) + \{i\omega\hat{s}_{sh;te}\}^2 \hat{G}_{sh;te}^s(x_3, \omega), \quad (C-55)$$

and hence the first three derivatives acting on the full scalar Green function are given by

$$\partial_3 \hat{G}^s(x_3, \omega) = -\text{sign}(x_3 - x_{3,s}) \frac{\{i\omega\hat{s}_{te}\} \hat{G}_{te} - \{i\omega\hat{s}_{sh}\} \hat{G}_{sh}}{\{i\omega\hat{s}_{sh}\}^2 - \{i\omega\hat{s}_{te}\}^2}, \quad (C-56)$$

$$\partial_3 \partial_3 \hat{G}^s(x_3, \omega) = \frac{\{i\omega\hat{s}_{te}\}^2 \hat{G}_{te} - \{i\omega\hat{s}_{sh}\}^2 \hat{G}_{sh}}{\{i\omega\hat{s}_{sh}\}^2 - \{i\omega\hat{s}_{te}\}^2}, \quad (C-57)$$

$$\partial_3 \partial_3 \partial_3 \hat{G}^s(x_3, \omega) = -\text{sign}(x_3 - x_{3,s}) \frac{\{i\omega\hat{s}_{te}\}^3 \hat{G}_{te} - \{i\omega\hat{s}_{sh}\}^3 \hat{G}_{sh}}{\{i\omega\hat{s}_{sh}\}^2 - \{i\omega\hat{s}_{te}\}^2}. \quad (C-58)$$

This completes the solution.